

The background of the cover is a photograph of an oil pumpjack (jack-o'-lantern) in silhouette against a dramatic sunset sky. The sun is a bright, glowing orb positioned directly behind the central vertical support of the pumpjack, creating a lens flare effect. The sky transitions from a deep orange near the horizon to a pale blue at the top, with wispy white clouds scattered throughout. The pumpjack's long, angled arm extends from the base towards the upper right corner of the frame.

Amir H. Mohammadi
Editor

PETROLEUM
SCIENCE AND
TECHNOLOGY

Heavy Oil

Characteristics, Production and
Emerging Technologies

NOVA

PETROLEUM SCIENCE AND TECHNOLOGY

HEAVY OIL

**CHARACTERISTICS, PRODUCTION
AND EMERGING TECHNOLOGIES**

No part of this digital document may be reproduced, stored in a retrieval system or transmitted in any form or by any means. The publisher has taken reasonable care in the preparation of this digital document, but makes no expressed or implied warranty of any kind and assumes no responsibility for any errors or omissions. No liability is assumed for incidental or consequential damages in connection with or arising out of information contained herein. This digital document is sold with the clear understanding that the publisher is not engaged in rendering legal, medical or any other professional services.

PETROLEUM SCIENCE AND TECHNOLOGY

Additional books in this series can be found on Nova's website under the Series tab.

Additional e-books in this series can be found on Nova's website under the e-book tab.

PETROLEUM SCIENCE AND TECHNOLOGY

HEAVY OIL
CHARACTERISTICS, PRODUCTION
AND EMERGING TECHNOLOGIES

AMIR H. MOHAMMADI
EDITOR

The logo for Nova Publishers features the word "nova" in a bold, lowercase serif font. The letter "o" is replaced by a stylized globe showing the Americas. To the left of the "nova" text is a decorative graphic of a semi-circle of dots of varying sizes, arranged in a pattern that suggests a sunburst or a molecular structure. Below "nova" is the word "publishers" in a smaller, lowercase serif font. At the bottom of the logo is the text "New York" in an italicized serif font.
nova
publishers
New York

Copyright © 2017 by Nova Science Publishers, Inc.

All rights reserved. No part of this book may be reproduced, stored in a retrieval system or transmitted in any form or by any means: electronic, electrostatic, magnetic, tape, mechanical photocopying, recording or otherwise without the written permission of the Publisher.

We have partnered with Copyright Clearance Center to make it easy for you to obtain permissions to reuse content from this publication. Simply navigate to this publication's page on Nova's website and locate the "Get Permission" button below the title description. This button is linked directly to the title's permission page on copyright.com. Alternatively, you can visit copyright.com and search by title, ISBN, or ISSN.

For further questions about using the service on copyright.com, please contact:

Copyright Clearance Center

Phone: +1-(978) 750-8400 Fax: +1-(978) 750-4470 E-mail: info@copyright.com.

NOTICE TO THE READER

The Publisher has taken reasonable care in the preparation of this book, but makes no expressed or implied warranty of any kind and assumes no responsibility for any errors or omissions. No liability is assumed for incidental or consequential damages in connection with or arising out of information contained in this book. The Publisher shall not be liable for any special, consequential, or exemplary damages resulting, in whole or in part, from the readers' use of, or reliance upon, this material. Any parts of this book based on government reports are so indicated and copyright is claimed for those parts to the extent applicable to compilations of such works.

Independent verification should be sought for any data, advice or recommendations contained in this book. In addition, no responsibility is assumed by the publisher for any injury and/or damage to persons or property arising from any methods, products, instructions, ideas or otherwise contained in this publication.

This publication is designed to provide accurate and authoritative information with regard to the subject matter covered herein. It is sold with the clear understanding that the Publisher is not engaged in rendering legal or any other professional services. If legal or any other expert assistance is required, the services of a competent person should be sought. FROM A DECLARATION OF PARTICIPANTS JOINTLY ADOPTED BY A COMMITTEE OF THE AMERICAN BAR ASSOCIATION AND A COMMITTEE OF PUBLISHERS.

Additional color graphics may be available in the e-book version of this book.

Library of Congress Cataloging-in-Publication Data

ISBN: ; 9: /3/75832/: 89/7 (eBook)

Published by Nova Science Publishers, Inc. † New York

CONTENTS

Preface		vii
Chapter 1	Modeling of Low-Salinity Waterflood with Temperature-Dependent Geochemical Reactions for Heavy Oil Carbonate Reservoirs <i>Ji Ho Lee, Moon Sik Jeong and Kun Sang Lee</i>	1
Chapter 2	SAGD History from Modeling Point of View <i>Aria Rahimbakhsh, Morteza Sabeti, Amir H Mohammadi and Khashayar Sharifi</i>	21
Chapter 3	Oil Production Optimization via Optimum Artificial Lift Design <i>Abbas Khaksar Manshad, Mehdi Jabbari and Amir H Mohammadi</i>	53
Chapter 4	Polyvinyl Alcohol (PVA) as an Emulsifying Agent for Viscosity Reduction of Heavy and Extra-Heavy Oils <i>Olalekan S. Alade, Kyuro Sasaki, Bayonile Ademodi, Adeniyi S. Ogunlaja, Yuichi Sugai and Ryo Ueda</i>	67
Chapter 5	An Introduction to Asphaltenes Chemistry <i>Jalil Bahman, Masoud Nasiri, Morteza Sabeti and Amir H. Mohammadi</i>	93
Chapter 6	Scaling Equations for Asphaltene Precipitation Modeling <i>Forough Ameli, Abdolhossein Hemmati-Sarapardeh, Sassan Hajirezaie, Amir H Mohammadi and Bahram Dabir</i>	127
Chapter 7	On the Estimation of Wax Deposition in Crude Oil Systems <i>Abbas Khaksar Manshad, Habib Rostami, Hojjat Rezaei, Seyed Moein Hosseini, Hasan Niknafs and Amir H Mohammadi</i>	161
Chapter 8	Efficient Estimation of Well Testing Parameters for Naturally Fractured Oil Reservoirs: Application in Reservoir Characterization <i>Abbas Khaksar Manshad, Habib Rostami, Seyed-Moein Hosseini and Amir H Mohammadi</i>	175
Chapter 9	On the Prediction of Well Productivity Index for Horizontal Oil Wells <i>Abbas Khaksar Manshad, Habib Rostami and Amir H. Mohammadi</i>	193

Chapter 10	Evaluation of Petro-Physical Properties (Porosity and Permeability) of Carbonate Oil Reservoirs <i>Abbas Khaksar Manshad, Habib Rostami, Peyman Torabideh and Amir H. Mohammadi</i>	203
Chapter 11	Prediction and Elimination of Drill String Sticking Using Artificial Intelligence Technique <i>Hojat Toreifi, Abbas Khaksar Manshad, Habib Rostami and Amir H. Mohammadi</i>	221
Chapter 12	Integrated Lost Circulation Prediction in Drilling Operation <i>Abbas Khaksar Manshad, Habib Rostami, Hasan Niknafe and Amir H Mohammadi</i>	243
Chapter 13	Optimization of Drilling Penetration Rate in Oil Fields Using Artificial Intelligence Technique <i>Abbas Khaksar Manshad, Habib Rostami, Hojjat Toreifi and Amir H. Mohammadi</i>	255
Chapter 14	Improvement of Drilling Penetration Rate in Oil Fields Using a PSO - GA - MLP Hybrid Network <i>Abbas Khaksar Manshad, Habib Rostami, Hojjat Toreifi and Amir H. Mohammadi</i>	271
Chapter 15	Estimating the Drilling Fluid Density in the Mud Technology: Application in High Temperature and High Pressure Petroleum Wells <i>Abbas Khaksar Manshad, Habib Rostami, Hojjat Toreifi and Amir H. Mohammadi</i>	287
Index		297

PREFACE

Chapter 1 presents modeling of low-salinity waterflood with temperature-dependent geochemical reactions for heavy oil carbonate reservoirs. It investigates the feasibility of thermal low-salinity waterflood in heavy oil reservoir. Sensitivity study has also been performed to capture the uncertainty originated from deployment of the process in a thermally-conductive reservoir. This study suggests careful evaluation of heat loss before deploying hot low-salinity waterflood process.

Chapter 2 presents SAGD (Steam Assisted Gravity Drainage) history from numerical modeling point of view. In this chapter, the path from its inchoate state to the present condition has been traced mentioning the more outstanding studies conducted. The application of a new technology has been stated in the SAGD process to both reduce the operational costs and improve the whole process's efficiency.

Chapter 3 evaluates oil production optimization via optimum artificial lift design. The results of this study enable us to compare the gas lift method with electric submersible pump (ESP) method and the optimum and the best option can be selected.

Chapter 4 presents the need and basic technical aspects of emulsification technology in reducing viscosity and flow property of heavy oil. Moreover, attractive properties of PolyVinyl Alcohol (PVA) and few research efforts on its suitability as an emulsifying agent in heavy and extra-heavy oil emulsification are reviewed.

In Chapters 5 and 6, asphaltene chemistry and scaling equations for asphaltene precipitation modeling are reviewed. The topic of asphaltene is too hard to be explained and reviewed in two chapters. Nevertheless, a big effort has been made to sum up all important aspects. It is expected that the latter two chapters provide better understanding of asphaltene precipitation associated with oil and heavy oil industry.

Chapters 7 to 15 report applications of artificial intelligence (AI) and data mining techniques in upstream of oil and heavy oil industry:

Chapter 7 presents an AI model for estimating wax deposition in crude oil system. The results are successfully compared with two previously reported models.

Chapter 8 presents three different AI models for prediction of well testing parameters (permeability, skin factor and reservoir initial pressure) for naturally fractured oil reservoirs. Well testing is an interpretation technique during which pressure of a well is recorded with respect to time to estimate reservoir and well parameters which are essential to reservoir characterization and management.

Chapter 9 examines the application of AI technique for predicting well productivity index (PI) for horizontal oil wells. Data obtained from flow and pressure unsteady tests nearly at insitu reservoir conditions can be used to determine the productivity index. Reservoir productivity index of wells can be considered as one of the most important parameters in determining the economic value of a reservoir. Productivity index of wells accompanying with certain reservoir parameters plays an important role in the evaluation of oil and heavy oil reserves.

Chapter 10 evaluates petro-physical properties (porosity and permeability) of carbonate oil reservoirs using various AI techniques. Accurate determination of petro-physical properties plays an important role in reservoir engineering calculations.

Chapters 11 to 15 report applications of AI and data mining in drilling engineering calculations:

Chapter 11 presents prediction and elimination of drill string sticking which is a frequently occurring and risk-prone problem during drilling operation that imposes rises to the drilling cost of operations. Developing reliable and new predictive tools for minimizing drill string stuck is therefore of great interest in drilling engineering and can be used in drilling operation design.

Chapter 12 presents an integrated lost circulation prediction in drilling operation as lost circulation is one of the most important issues that oil industry challenges with. Throughout drilling operation, cementing job or moving down the drilling pipes, great pressure of drilling fluid causes an over balance pressure on reservoir, hence the drilling fluid penetrates the reservoir and is wasted. When the total loss happens, drilling pipes may stuck and make some incredible issues. In this situation, it is better to know how drilling fluid moves and how much loss occurs, and then predict loss severity and add proper drilling fluid contents. Several obtainable factors affect circulation loss while drilling. In this chapter, operational parameters of an oilfield were used to predict the mud loss severity.

Chapters 13 and 14 present applications of AI methods in optimization and improvement of drilling penetration rate in oil fields. The advantage of the latter methods than the other drilling improvement methods is consideration of all effective parameters on drilling operation and being accurate, comprehensive, and easy application.

Chapter 15 reports a reliable method for estimating the drilling fluid density in the mud technology as accurate knowledge of the drilling fluid density is important in many drilling engineering calculations.

Chapter 1

**MODELING OF LOW-SALINITY WATERFLOOD
WITH TEMPERATURE-DEPENDENT
GEOCHEMICAL REACTIONS FOR HEAVY OIL
CARBONATE RESERVOIRS**

Ji Ho Lee¹, Moon Sik Jeong¹ and Kun Sang Lee^{1,}*

¹Department of Earth Resources and Environmental Engineering,
Hanyang University, Seoul, S. Korea

ABSTRACT

Enhancing oil mobility and drainage by thermal process in heavy oil reservoirs has been well understood for increased oil recovery. Carbonate reservoirs naturally tend to have high residual oil saturation due to wettability and heterogeneity. Combined with thermal process, low-salinity waterflood (LSWF) has become a promising EOR candidate for heavy oil carbonate reservoirs. The LSWF is cost-effective over tertiary EOR and has been reported to reduce residual oil saturation. The LSWF effect inherently involves thermal sensitivity because wettability modification effect behind LSWF mechanism is attributed to temperature-dependent geochemical reactions in oil-brine-mineral system.

Spatial and temporal variations of temperature in the reservoir provide various levels of mineral dissolution, aqueous reaction, and ion exchange determining various levels of wettability modification as well as oil mobility. In consideration of thermal effect on geochemical reactions, this study has investigated the feasibility of thermal LSWF in heavy oil reservoir. Sensitivity study has captured the uncertainty when the process has been deployed in a thermally-conductive reservoir.

* E-mail: kunslee@hanyang.ac.kr

INTRODUCTION

The most common enhanced oil recovery (EOR) technology subject to heavy oil reservoirs is thermal method. Thermal recovery produces oil by heating viscous-oil reservoir (Oseterloh and Jones 2003; Ramlal et al. 2004). The heat is transported into reservoir by the injection of hot fluids such as steam or hot water. Though most of thermal recovery methods provide heat through steam, the steam injection is not feasible or economical under certain conditions. Hot water flood is closer to conventional waterflood than any other thermal recoveries in its operation and is comparatively simple process (Farouq Ali 1974). Hot water generated on the surface is injected into reservoirs and enhances oil mobility to flow easily to producer. Messner and Stelling (1990) have provided the feasibility of hot waterflood combined with steam injection in the field. Goodyear et al. (1996) have assessed the application of hot waterflood in heavy oil (up to 400 cp) reservoir through numerical simulation. Hot waterflood process has lower energy injection rates than steam injection and energy transport to reservoir becomes less. The lower estimated ultimate recovery due to less transported energy into reservoir may be overcome through hybrid process with another EOR method.

One of possible EOR methods is low-salinity waterflood (LSWF) because of high potential to modify wettability alteration in carbonate reservoirs. Even though reservoir is in high temperature condition, LSWF has provided improved oil recovery through imbibition tests in chalk (Zhang et al. 2007). Advantages of LSWF have been recognized through substantial experiments. Zhang and Morrow (2006) have conducted a number of experiments to reveal mechanism responsible for LSWF effect. Lager et al. (2008) have suggested necessary condition to observe improved oil recovery in sandstone. However, an exact mechanism behind LSWF in sandstone is still controversial. Among hypothetical mechanisms, wettability modification toward water wetness has explained the observed LSWF effects through experimental studies (Jadhunandan and Morrow 1995; Tang and Morrow 1999). For carbonate reservoirs, the observation of modified water wetness due to cationic surfactants dissolved in seawater, which is catalyzed by sulfate ion presented in SW (Zhang et al. 2006). It has encouraged to investigate similar conceptual LSWF named smart water, modification of ion composition of the injected fluid (Standnes et al., 2002; Austad et al. 2008). Well-known successful case is the Ekofisk in the North Sea. The fractured chalk reservoir has been flooded by seawater for about 25 years with great success. Lager et al. (2008) and Austad et al. (2010) have illustrated the wettability alteration is originated from chemical reaction in crude oil-brine-rock system for both sandstone and carbonate reservoirs. It has triggered LSWF modeling to combine geochemistry covering mineral dissolution/precipitation, aqueous reaction, and ion exchange (Cuong et al. 2013). The geochemistry-coupled LSWF has been recognized as a great option to integrate with other EOR methods, hot waterflood in this study.

Investigations between thermal effect and wettability modification attributed to geochemistry have been conducted under various temperature conditions. Strand et al. (2006) has investigated seawater injection experiment in chalk and recorded effluent concentration of Ca^{2+} and SO_4^{2-} at various temperatures. As temperature increases, effluent of both components has been retarded. Another experiments (Zhang et al. 2007) have investigated temperature effect on effluent concentration of Ca^{2+} and Mg^{2+} . It has revealed Ca^{2+} has

stronger tendency to remain in chalk core over Mg^{2+} at $20^{\circ}C$ and vice versa at $130^{\circ}C$. Imbibition experiments were performed to investigate how Ca^{2+} , Mg^{2+} , and SO_4^{2-} influence oil production at different temperatures. Different oil productions have been resulted according to composition of injecting fluid at different temperatures. No matter what composition injection fluid has, higher temperature has provided increased oil recovery.

Despite of substantial experiments with respect to the influence of thermal energy n LSWF effects in carbonate reservoirs, the investigation of thermal low salinity waterflood or hot LSWF has not been thoroughly assessed for improving oil production. This study has assessed synergetic effects contributing to wettability modification and mobility control during hot LSWF in carbonate reservoirs. This study also covers the investigation of improved LSWF effects due to transported thermal energy and sensitivity study of the process in conductive reservoirs.

BASIC THEORY

Modeling hot LSWF covers multi-phase and multi-component transport involving non-isothermal condition as well as geochemical reactions. Geochemical reactions considered in this study are aqueous reaction, mineral dissolution/precipitation, and ion exchange. Hot waterflood requires the solution of energy balance equation to define temperature of reservoir at each time. The calculated equilibrium temperature at specific time influences geochemical reaction by controlling equilibrium constant of geochemical reactions as well as oil mobility.

In aqueous reactions, the composition of aqueous phase is determined to reach thermodynamic equilibrium state at specific temperature. This reaction is faster than mineral dissolution/precipitation explained later. At equilibrium, reaction quotient, aka ion activity product (IAP) becomes equal to equilibrium constant as follows:

$$Q_{\alpha} - K_{eq,\alpha} = 0 \quad (1)$$

$$K_{eq,\alpha} = \exp \left[-\frac{1}{RT} \sum_{k=1}^{n_{aq}} v_{k,\alpha} (\Delta G_f^o)_{k,\alpha} \right] \quad (2)$$

$$Q_{\alpha} = \prod_{k=1}^{n_{aq}} a_k^{v_{k,\alpha}} \quad (3)$$

where α represents aqueous reaction; $K_{eq,\alpha}$ the equilibrium constant at specific temperature; Q_{α} the IAP; k the component; R the gas constant; T the temperature; n_{aq} the number of aqueous components and gases components; ΔG_f^o the Gibbs free energy for each species; a_k the activity; $v_{k,\alpha}$ the stoichiometry coefficients of aqueous reaction.

The activity is the adjusted concentration of ions in solutions to consider electrostatics interacting between ions. It is the function of molality or molarity of ions using activity

coefficients. Commonly, three models covering Davies model, B-dot model, and Pitzer's model are applied to predict activity coefficients. These models account for temperature effect on ion activity as well. For diluted solution, first two models are more appropriate than Pitzer's model. In this study, B-dot model, modified Debye-Hückel model, is used as calculated below:

$$a_k = \gamma_k m_k \quad (4)$$

$$\log \gamma_k = -\frac{A_\gamma z_k^2 \sqrt{I}}{1 + \dot{a}_k B_\gamma \sqrt{I}} + \dot{B}I \quad (5)$$

$$I = \frac{1}{2} \sum_{k=1}^{n_{aq}} m_k z_k^2 \quad (6)$$

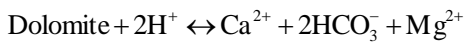
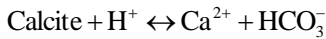
where γ_k is the activity coefficient; m_k the molality; A_γ , B_γ , and \dot{B} the temperature dependent coefficients; I the ionic strength; \dot{a}_k the ion-size parameter; z_k the charge number of ion.

In addition to temperature-dependent activity, temperature effect reflected in aqueous reaction has been introduced through equilibrium constant. It is calculated with analytical expression as follows:

$$\log K = A_1 + A_2 T + \frac{A_3}{T} + A_4 \log T + \frac{A_5}{T^2} \quad (7)$$

where A_1 , A_2 , A_3 , A_4 , and A_5 are the fitting parameters.

Participating minerals in target carbonate reservoirs are mainly comprised of calcite and dolomite. Calcite and dolomite dissolution and precipitation are heterogeneous and non-equilibrium reactions and represented in below:



The mineral reactions are relatively slow reactions, taking place at a significantly smaller rate than the transport processes that redistribute components. The kinetic reaction for dissolution or precipitation of minerals follows the rate law suggested by Bethke (1996):

$$r_{\beta} = \hat{A}_{\beta} k_{\beta} \left(1 - \frac{Q_{\beta}}{K_{eq,\beta}} \right) \quad (8)$$

where β represents mineral type, calcite or dolomite; r_{β} the reaction rate; k_{β} the reaction rate constant; \hat{A}_{β} the reactive surface area of mineral; $K_{eq,\beta}$ the solubility product constant at specific temperature; Q_{β} the ion activity product which is analogous to ion activity product in aqueous reaction and calculated as follows:

$$Q_{\beta} = \prod_{k=1}^{n_{aq}} a_k^{v_{k,\beta}} \quad (9)$$

where $v_{k,\beta}$ is the stoichiometric coefficients of mineral reaction.

Mineral dissolution/precipitation become the formation/consumption of aqueous species. The rate of mineral reactions is related to rate of aqueous species change. It is determined with reaction rate and stoichiometric coefficients as represented below:

$$\gamma_{k,\beta} = v_{k,\beta} r_{\beta} \quad (10)$$

where $\gamma_{k,\beta}$ is the reaction rate of formation/consumption of component.

In mineral dissolution/precipitation, temperature change affects solubility product constant, $K_{eq,\beta}$ as well as activity. The solubility product constant determined with polynomial equation, which is analogous to aqueous reaction. Kinetic reaction rate is also highly influenced by the temperature. This follows Arrhenius equation to adjust reaction rate constant as follows:

$$k_{\beta} = k_{o\beta} \exp \left[-\frac{E_{a\beta}}{R} \left(\frac{1}{T} - \frac{1}{T_o} \right) \right] \quad (11)$$

where $k_{o\beta}$ is reaction rate constant at reference temperature; $E_{a\beta}$ the activation energy; T_o the reference temperature.

Divalent cations and anions (Ca^{2+} , Mg^{2+} , and SO_4^{2-}) are observed to interact with carbonate rock surface through NMR experiments (Kwak et al. 2014).

It is modeled with reversible ion exchange reaction. Similar to aqueous and mineral reactions, chemical equilibrium constants define equilibrium composition in aqueous and solid phases. The chemical equilibrium constant in ion exchange widely referred to selectivity coefficient, which is function of activity. Related ion exchange reactions and selectivity coefficients are represented below:



$$K_{\text{Na}/\text{Ca}} = \frac{[\alpha(\text{Ca}^{2+})]^{0.5} \alpha(\text{Na} - \text{X})}{\alpha(\text{Na}^+) [\alpha(\text{Ca} - \text{X}_2)]^{0.5}} \quad (14)$$

$$K_{\text{Na}/\text{Mg}} = \frac{[\alpha(\text{Mg}^{2+})]^{0.5} \alpha(\text{Na} - \text{X})}{\alpha(\text{Na}^+) [\alpha(\text{Mg} - \text{X}_2)]^{0.5}} \quad (15)$$

where X represents carbonate rock surface; $K_{\text{Na}/\text{Ca}}$ and $K_{\text{Na}/\text{Mg}}$ the selectivity coefficients.

MODELING

Non-isothermal multi-phases and multi-components transport simulation has conducted with GEM developed by CMG. Oil property modeling is provided by WINPROP. To find unknown relative permeability curves before and after wettability modifications, history matching process has been conducted with CMOST. Sensitivity study to analyse uncertainty of hot LSWF has been also carried out with CMOST.

Description of Coreflood Experiment

Gachuz-Muro and Sohrabi (2014) have investigated the performance of smart water for heavy oil carbonate reservoir under high temperature (92°C). Smart water is 10 times diluted seawater, which comes from Gulf of Mexico. The experiments cover imbibition test for six cores and coreflood for four cores. Only limestone 6 coreflood experiment is considered in this study because it provides improved oil production due to smart water injection. Description of smart water, formation water and core are represented in Tables 1 and 2.

For oil modelling, Gachuz-Muro and Sohrabi (2013) provided data in a range of temperature. The oil viscosity data from 20°C to 115°C is represented in Figure 1. However, the density of oil is only evaluated at 20°C with 14.12°API. Because WINPROP hardly understands °API directly, reference water density is required. No information of water density is represented in a series of the referred studies.

Table 1. Brine composition

	Formation water (mg/l)	Seawater (mg/l)	10 times diluted seawater (mg/l)
Na ⁺	9,614.97	11,429.38	1,142.93
Ca ²⁺	320.36	429.60	42.96
Mg ²⁺	218.94	1,361.60	136.16
K ⁺	-	351.10	35.11
Ba ²⁺	-	0.01	-
Sr ²⁺	-	8.37	0.83
Cl ⁻	15,117.25	20,040.00	2,004.00
SO ₄ ²⁻	550.63	3,500.00	350.00
HCO ₃ ⁻	1,135.9	47.58	4.75
pH	8.01	7.80	7.20

Gachuz-Muro and Sohrabi, 2014.

Table 2. Core properties

Length (cm)	Diameter (cm)	Porosity	Pore volume (ml)	Permeability (mD)	Initial water saturation
15.2	2.52	0.2064	15.55	19.40	0.3213

Gachuz-Muro and Sohrabi, 2014.

GWB developed by The Geochemist's Workbench has calculated density of water with formation water composition and it is 1.025g/cm³. Despite of insufficient density data in reservoir temperature, one-dimensional coreflooding, neglecting gravity force, places importance on viscosity rather than density. After matching density data at only 20°C, modified-Pedersen model has been applied to match viscosity data in a range of temperature. To reduce matching error between modelling and experiment data, viscosity data from 65 to 115°C are covered, around mainly ambient reservoir temperature (92°C). Regressed viscosity data is represented in Figure 1.

RESULT

In LSWF experiment, 10 times diluted seawater injection follows seawater injection. To find unknown relative permeability curves, history matching process proceeds to match production data. Injection rate is assumed to be 0.0001525 m³/day, which is in the range of typical displacement rate (Gupta et al., 2011). Based on the injection rate, relative permeability curves before and after low salinity water injection are determined. Matching relative permeability curve has taken Corey type into account. History matching to oil production is represented to Figure 2.

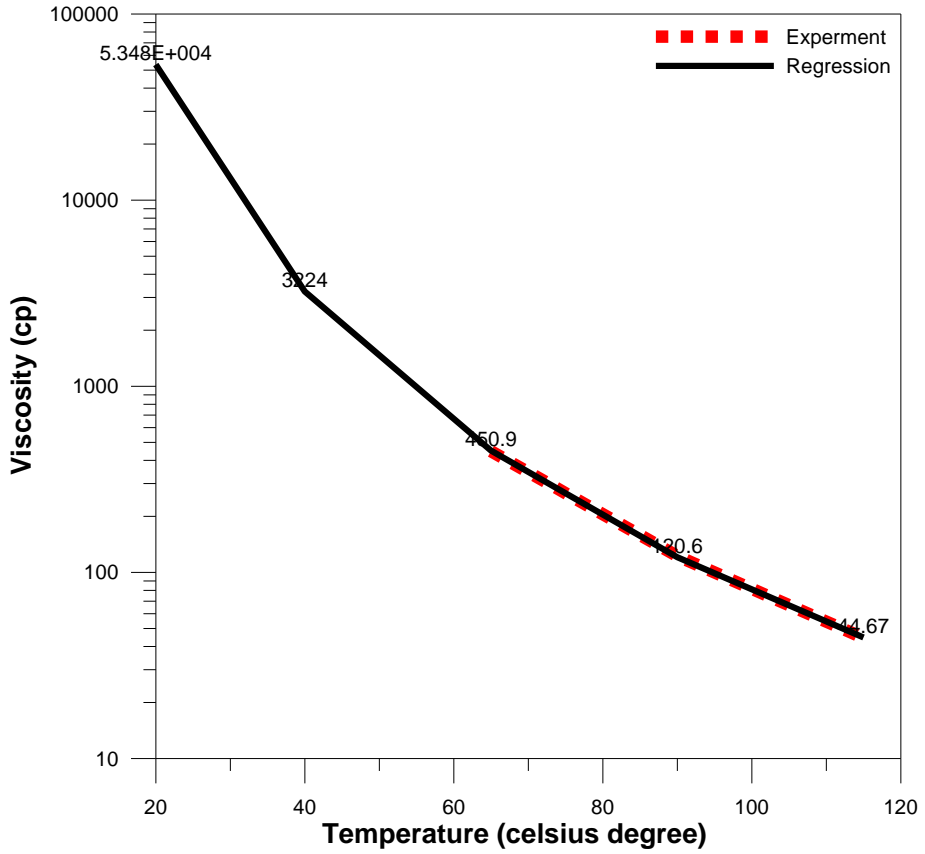


Figure 1. Experimental and regressed data of temperature-dependent oil viscosity (Gachuz-Muro and Sohrabi, 2013).

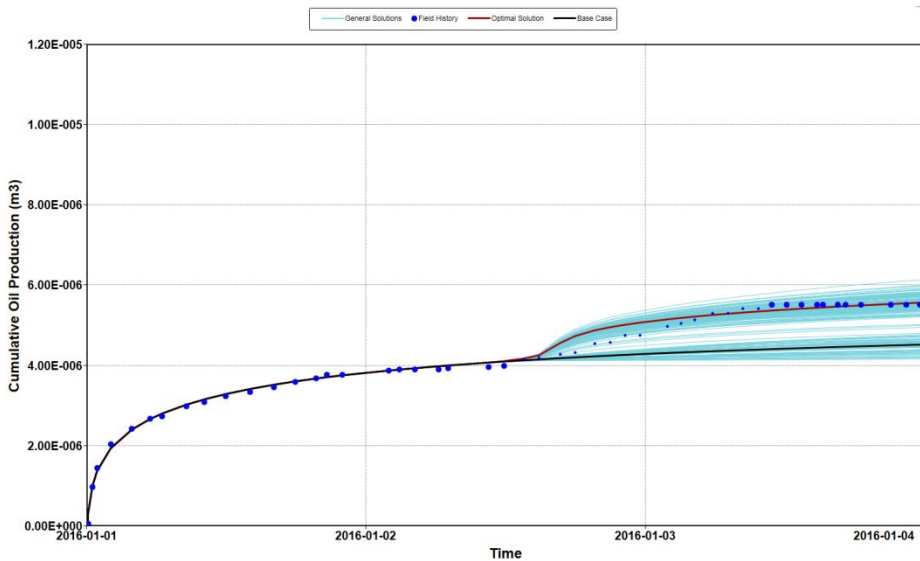


Figure 2. History matched oil production in coreflood.

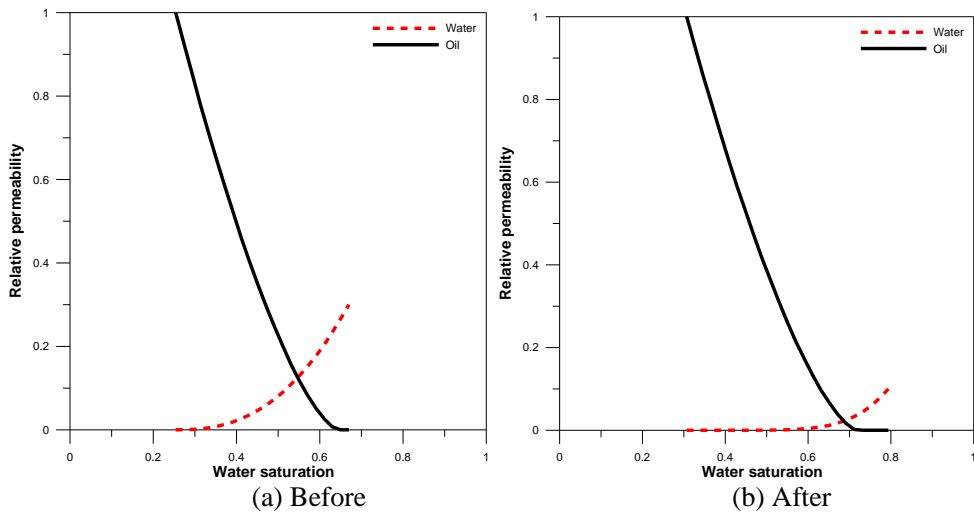


Figure 3. Estimated relative permeability curves before and after LSWF through history matching process.

Relative permeability curves before and after low salinity water injection is drawn and also shown in Figure 3.

LSWF (92 °C)

In this study, ion exchange of Ca^{2+} to carbonate rock surface is assumed to be responsible for wettability modification. The amount of adsorbed ion on carbonate rock surface is calculated with equivalent fraction of ion, which is equivalent to concentration. At the end of seawater and LSWF, equivalent fractions of Ca^{2+} are represented in Figure 4.

As low salinity water is injected, equivalent fraction increases and changes water-wetness of reservoir. The LSWF have caused the increase of equivalent fractions of Ca^{2+} , approximately by 300% and resulted in additional oil recovery as much as 15% due to wettability modification, as shown in Figure 5. The end point of oil has been estimated to be unity due to low oil mobility in not only seawater injection, but LSWF. However, end point of water becomes to a third and 8% of residual oil saturation gains mobility due to LSWF. To verify pronounced wettability alteration effects on mainly end point of water and residual oil saturation, sensitivity study has evaluated Corey parameters to distinguish sensitive factors in heavy oil core model. Reduced quadratic proxy model has been constructed and evaluated as shown in Figure 6. Experimental designs, which are subject to sensitivity study, have been chosen in history matching process accompanying acceptable error. It also has concluded residual oil saturation is primary sensitive factor and next one is end point of water.

Hot LSWF (115 °C)

As confirmed with Figure 3, 35% and 27% of oil barely mobile in seawater injection and LSWF.

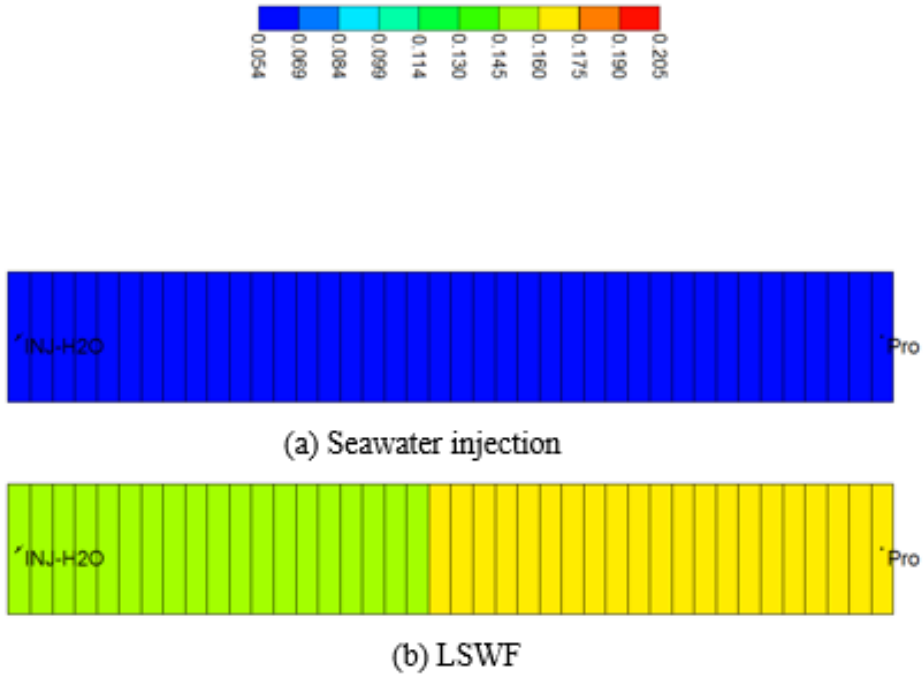


Figure 4. Profile of equivalent fraction of Ca^{2+} after seawater injection and LSWF.

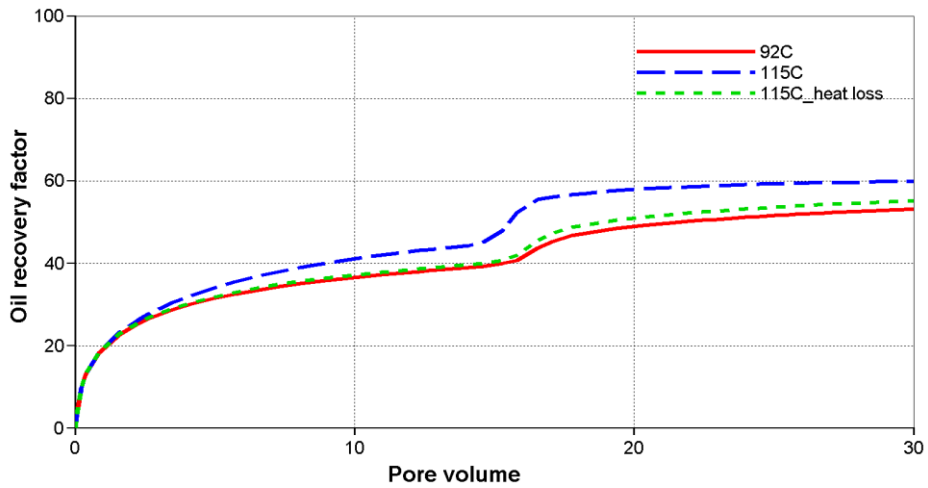


Figure 5. History of oil recovery factor of LSWF and hot LSWF with and without heat loss.

However, higher than the residual oil saturations, 62% and 47% of oil have remained due to unfavorable mobility of oil in seawater injection and LSWF. To overcome this problem arising in heavy oil production, hot waterflood supplements oil mobility to flow easily. Measured viscosity data up to 115°C is regressed in Figure 1 and reflected in this model. LSWF following seawater injections with temperature of 92°C and 115°C have been compared.

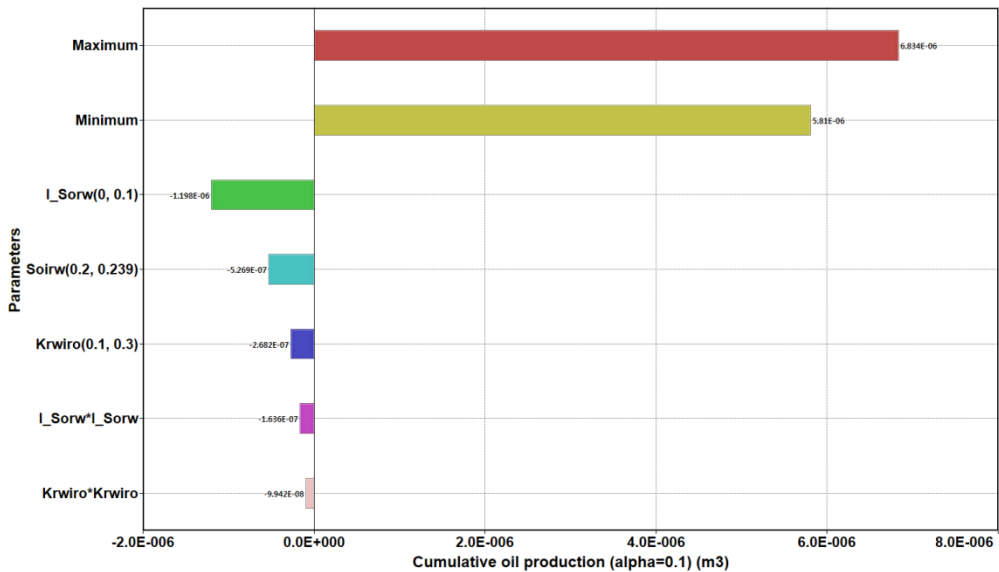


Figure 6. Results of sensitivity study for LSWF with respect to Corey parameters.

Hot LSWF has reduced oil viscosity up to approximately 45 cp, which is very low compared to 111.7 cp in LSWF with temperature of 92°C. In comparisons between seawater injections at 92°C and 115°C, hot seawater injection has contributed to 5.6% increase of oil recovery over seawater injection with temperature of 92°C. After hot seawater injection, successive hot LSWF has recovered additional oil up to 7.2% as well. As mentioned before, thermal energy influences not only oil viscosity reduction but also geochemical reaction to control wettability modification level. The improvement of oil production has come from both effects. In the seawater injection, increase of oil production due to thermal effect is mainly responsible for viscosity reduction. Negligible increase of the equivalent fraction of Ca^{2+} in hot seawater injection changes negligible wetness of reservoirs. However, in LSWF, thermal energy significantly increases the equivalent fraction, as shown in Figure 7, up to about 17% over LSWF with temperature of 92°C. This increase has attributed to significant temperature-induced mineral dissolution in LSWF. Overall 200% more dissolution of minerals considerably produces potential ion exchangeable Ca^{2+} due to high temperature in LSWF as shown Figure 8.

This approximately contributes to 1.6% increase of oil recovery while viscosity reduction effect involves 5.6% of additional oil recovery. The 1.6% increase is meaningful because generally conventional LSWF has been reported to enhance oil recovery up to about 10-20%. In this heavy oil simulation, this increase corresponds to 10% of improvement of original non-thermal LSWF, 15% increment of oil recovery. This highly potential hot LSWF has risk to overestimate oil production.

The conductive reservoir loses internal heat to overlying/underlying layers through mainly convection and conduction. This coreflood model considers only heat loss due to conduction and production with assumption of perfectly sealed by surrounding hypothetical shale. Thermal properties of reservoir and surrounding shale are listed in Table 3. Heat loss to underlying/overlying layers is calculated through analytical solution using method of Vinsome and Westerveld (1980).

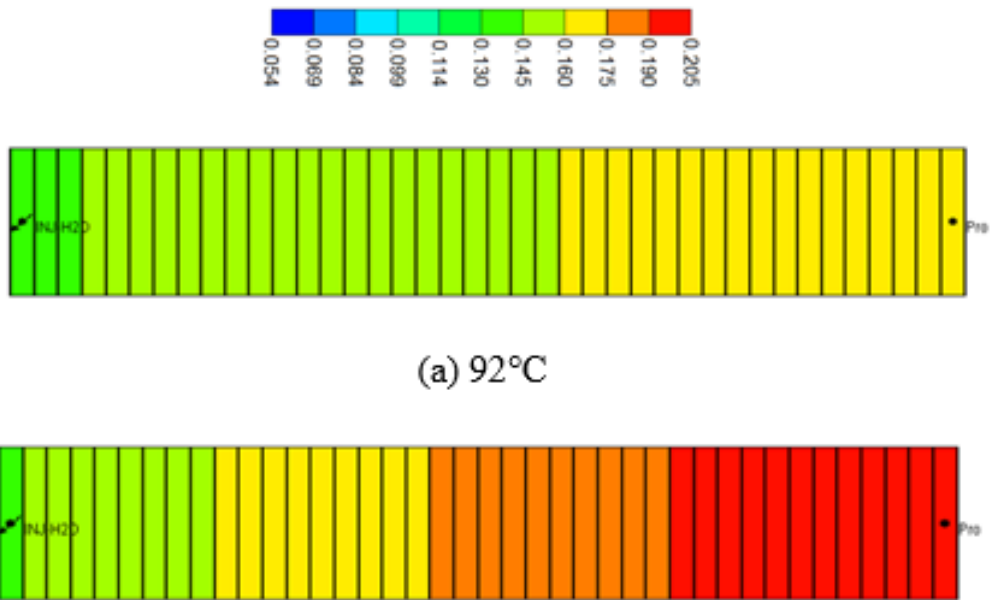


Figure 7. Profile of equivalent fraction of Ca^{2+} of LSWF and hot LSWF after 30 pore volume injection.

Table 3. Thermal properties of reservoir and shale

Reservoir	Density (kg/m^3)	2,450
	Heat capacity ($\text{J}/\text{kg}/^\circ\text{K}$)	968.7347
	Thermal conductivity ($\text{J}/\text{m}/\text{s}/^\circ\text{K}$)	2.3971
Shale	Density (kg/m^3)	1,995
	Heat capacity ($\text{J}/\text{kg}/^\circ\text{K}$)	1,214.2
	Thermal conductivity ($\text{J}/\text{m}/\text{s}/^\circ\text{K}$)	0.88

Figure 9 has shown temperature distribution after 30 PV injection in hot LSWF and corresponding oil viscosity and saturation. Heat loss mitigates thermal effects, lowering oil viscosity and promoting mineral dissolution. The overall mineral dissolution has been reduced as much as 58% compared to non-heat loss case as shown in Figure 8. Spatial variation of temperature in reservoir produces various levels of thermal effects spatially. In the vicinity of injector, reducing residual oil saturation, end point of water, and oil viscosity due to thermal energy are still effective. Still high viscosity and oil-wettability where is far from injector aggravates production. Because viscosity and wettability alteration level near producer is more important than injector to determine production, the final oil recovery is limited to only about 55%, compared to 60% in no heat loss case as shown in Figure 5. Regardless of heat loss, the hot LSWF is still more effective than LSWF with temperature of 92°C , 1.8% increase.

The productivity of hot LSWF substantially depends on thermal properties of reservoir and shale. Sensitivity study with respect to thermal properties is necessary to analyse an accurate production of hot LSWF. Variance-based Sobol's analysis has evaluated sensitive factors influencing heat loss represented in Figure 10.

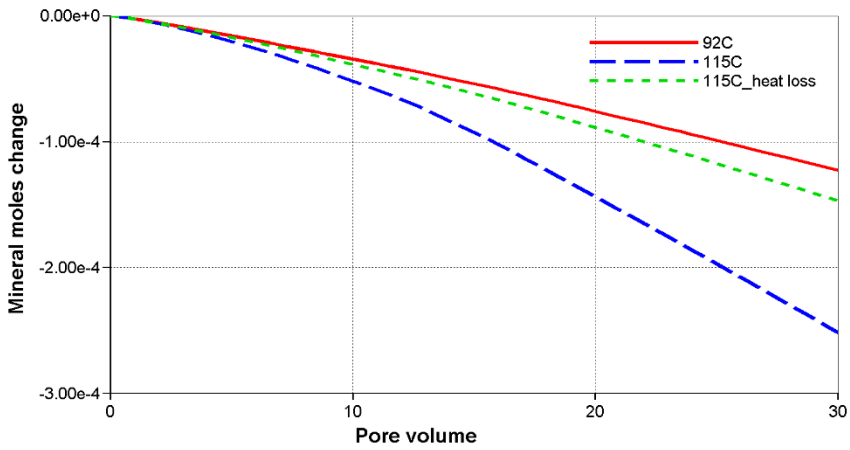


Figure 8. History of mineral dissolution of LSWF and hot LSWF with and without heat loss.

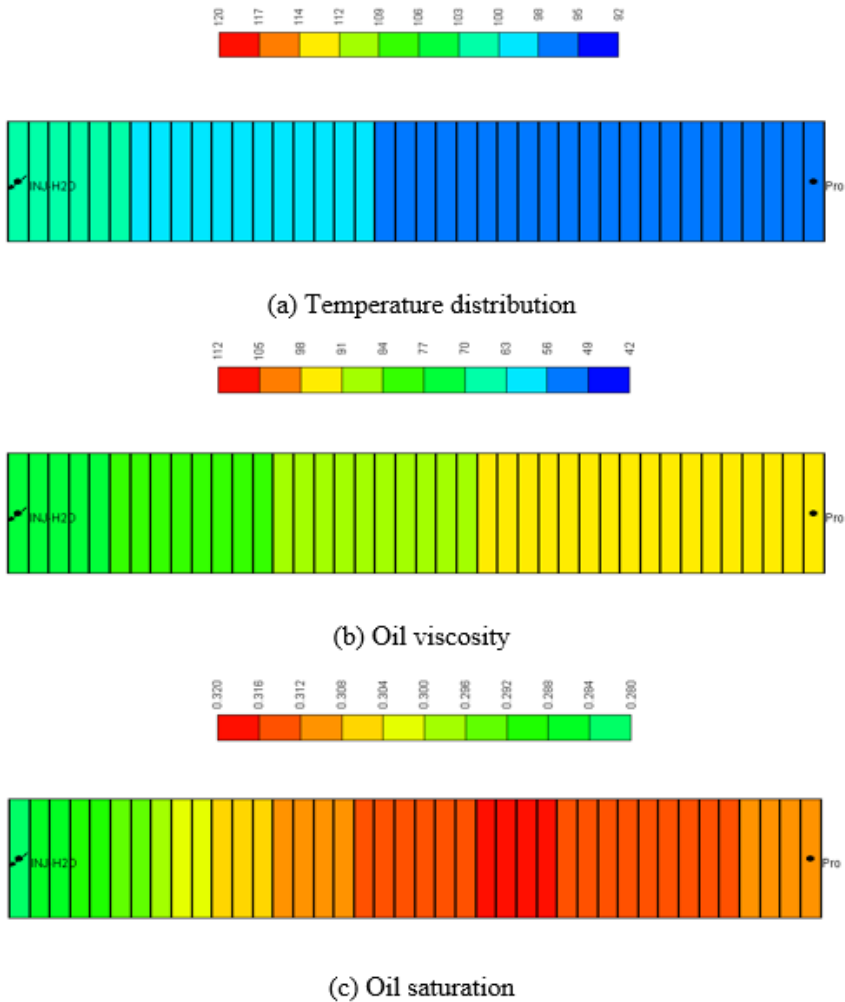


Figure 9. Results of hot LSWF considering heat loss after 30 pore volume injection.

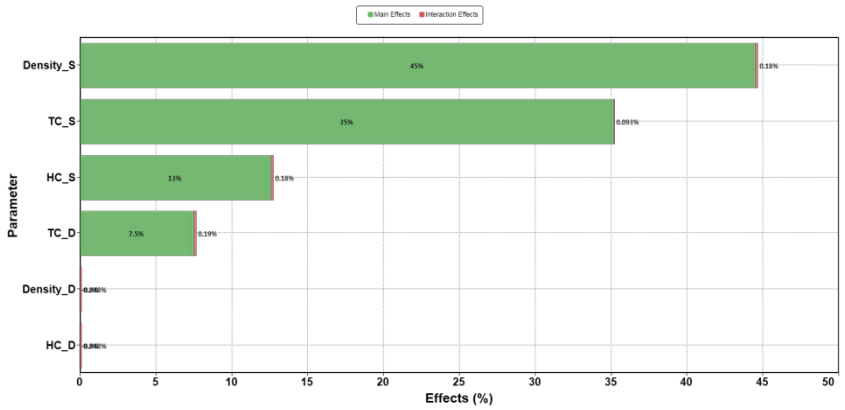


Figure 10. Results of variance-based Sobol's sensitivity study.

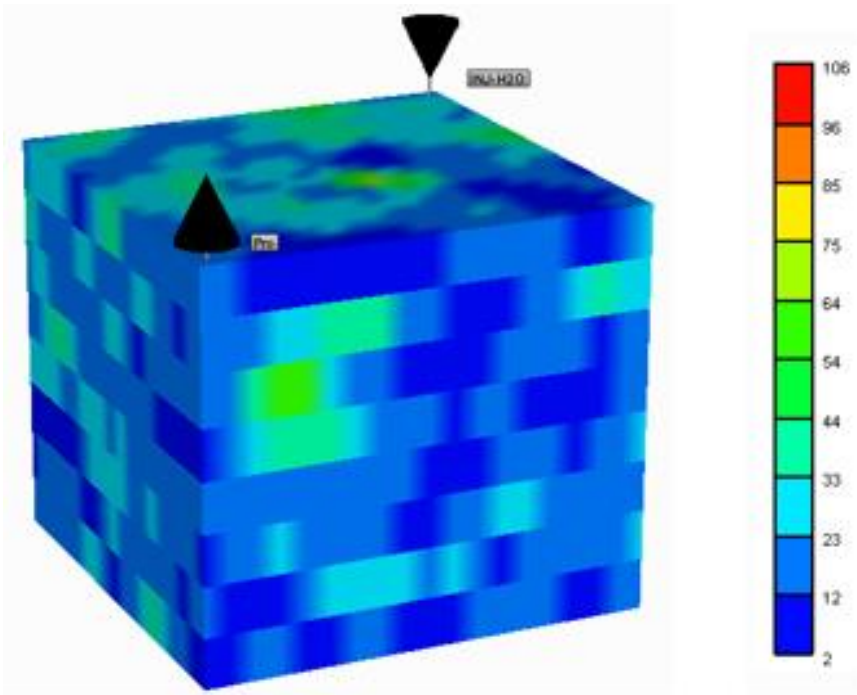


Figure 11. Heterogeneous permeability of pilot-scaled reservoir.

Following the results, shale properties are more important factor than reservoir properties to determine the oil production of hot LSWF. Density, thermal conductivity, and heat capacity of shale are factors to define thermal diffusivity of shale.

Application in Pilot-Scaled Reservoir

The performance of hot LSWF is evaluated in pilot-scaled reservoir. The target heterogeneous reservoir has pore volume as $1.80215 \times 10^5 \text{ m}^3$; porosity as 0.20065; oil volume

as 1.22312×10^5 m³; temperature as 92°C and is represented in Figure 11. Without seawater injection, LSWF with temperature of 92°C and 120°C has been deployed into heavy oil reservoirs. This simulation is set to be constant injection to compare oil production, quantitatively, under same condition.

Oil recovery for both processes is represented Figure 12. For 10 years, LSWF recovers approximately 31% of OOIP. Hot LSWF improves oil recovery up to 40% in spite of heat loss to overlying/underlying formations. The reasons of the remarkable improvement are viscosity reduction and dominant mineral dissolution controlling wettability modification levels. Figure 13 describes the profile of oil viscosity in LSWF and hot LSWF. In the LSWF, high pressurized zone near injector, oil viscosity arises up to 283 cp. In contrast, hot LSWF reduces viscosity significantly near injector corresponding to about 45 cp. This effect leads to favorable conditions for injectivity as well as oil production. Injectivity is another problem arising in heavy oil production. Figure 14 illustrates bottom-hole pressure at injector. Less required viscous force to displace oil reduces the bottom-hole pressure up to 20%. As well as advantages near injector, oil around producer becomes less viscous due to water breakthrough involving high thermal energy. As indicated in coreflood study, oil viscosity near producer significantly determines production.

With benefits of reduced oil viscosity, wettability of reservoir has become modified, significantly, in hot LSWF.

Ion exchange of Ca²⁺ has become accelerated, as shown in Figure 15, because of thermal energy. The mineral dissolution near injector is dominant. Overall dissolved minerals are more in hot LSWF than in LSWF up to about 19% as shown in Figure 16. Figure 17 describes history results of hot LSWF. With increase of mineral dissolution and decrease of Ca²⁺ production, decrease of Ca²⁺ in aqueous phase indicates increase of ion exchange of Ca²⁺.

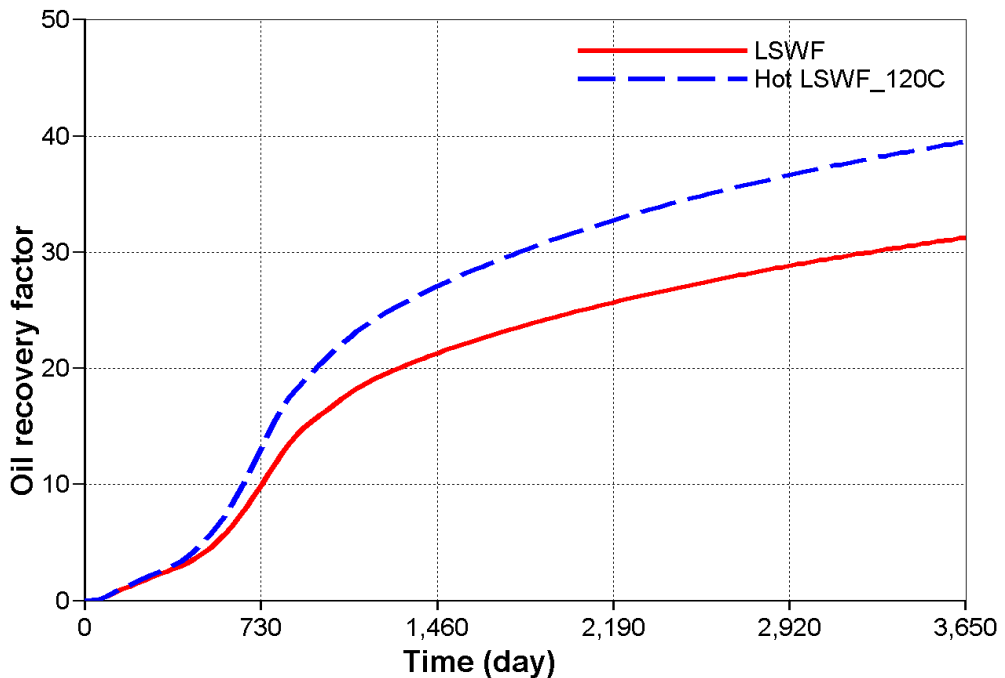


Figure 12. History of oil recovery for LSWF and hot LSWF in pilot-scaled reservoirs.

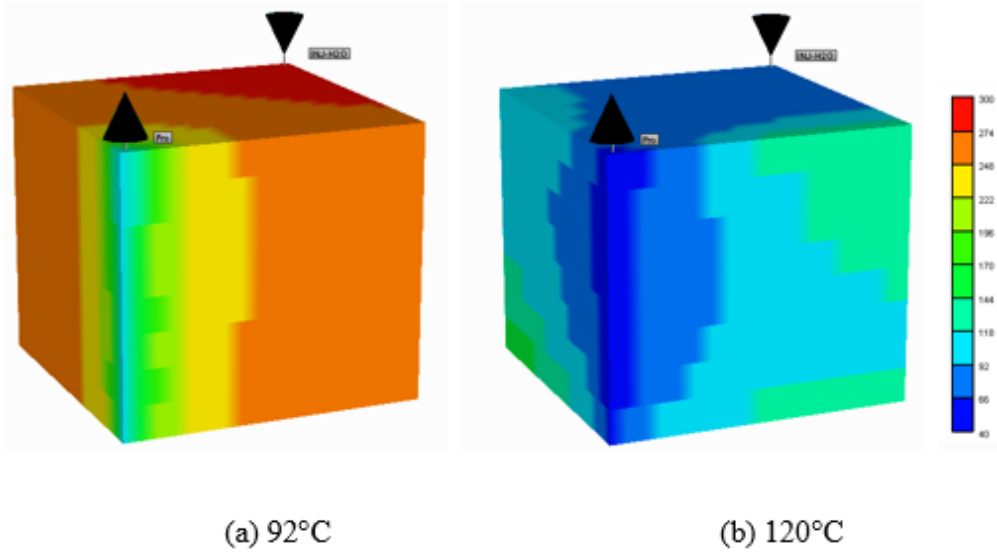


Figure 13. Profile of oil viscosity for LSWF and hot LSWF in pilot-scaled reservoirs after 10 years.

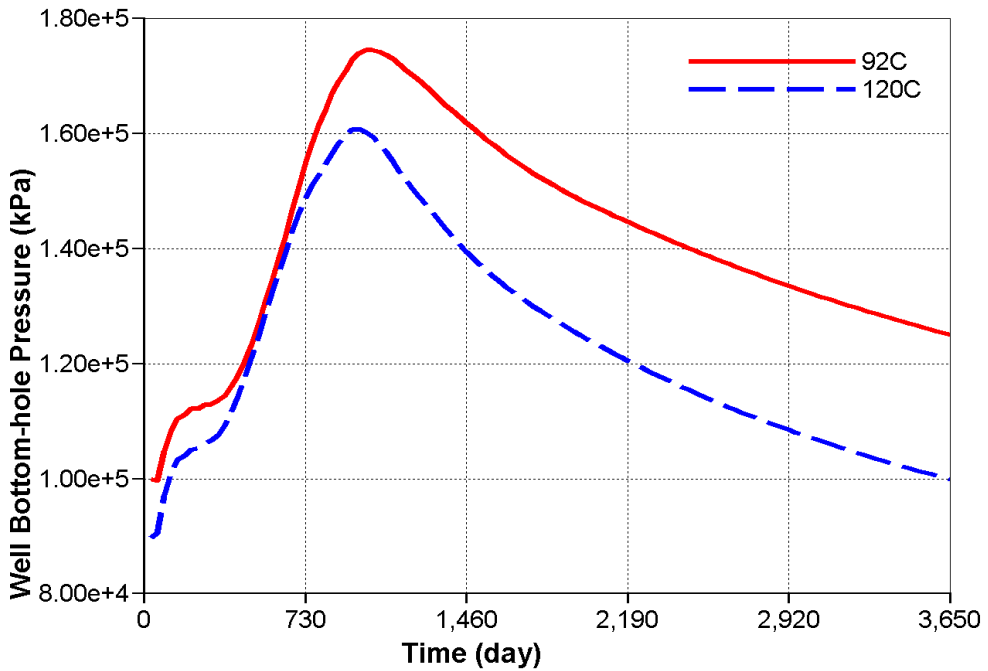


Figure 14. History of injector bottom-hole pressure for LSWF and hot LSWF in pilot-scaled reservoirs.

By 2 years, Ca^{2+} continuously adsorbs to carbonate surface. This leads to the increase of oil rate. After 2 years, Ca^{2+} in aqueous phase, which mainly comes from mineral dissolution, exceeds the capacity of ion exchangeable of Ca^{2+} in swept zone at reservoir condition and has started to be produced with significant increase of water production. Many studies have reported that LSWF induces reservoir conditions to be basic condition meaning pH increases.

In this simulation, LSWF increases pH of reservoir up to 10, while initial pH was 8.1. Thermal energy dissolves more minerals and produces carbonic acid. This has contributed to decrease of pH as shown in Figure 18. However, generally, LSWF combined process increases pH of reservoir.

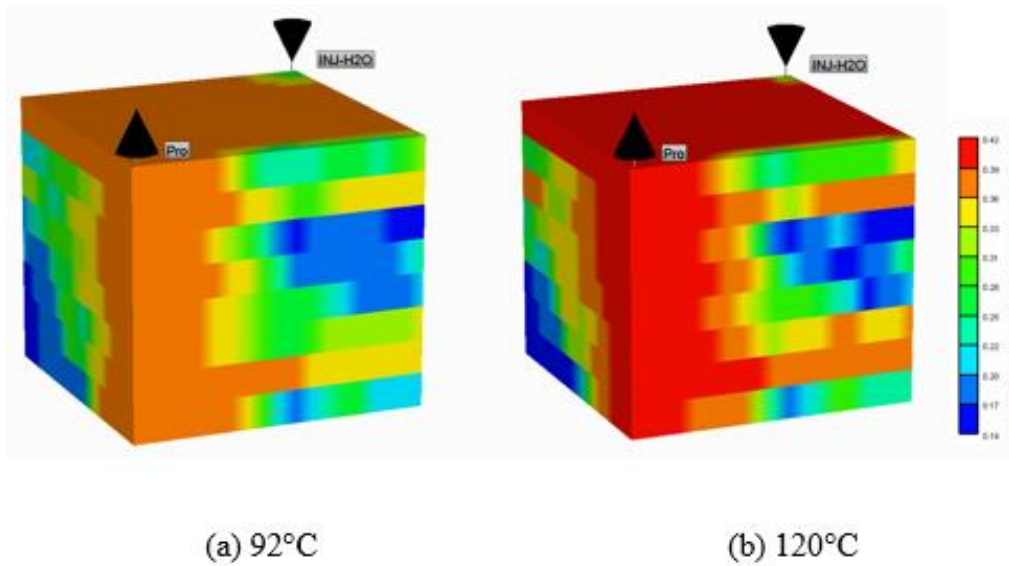


Figure 15. Profile of equivalent fraction of Ca^{2+} for LSWF and hot LSWF in pilot-scaled reservoirs after 10 years.

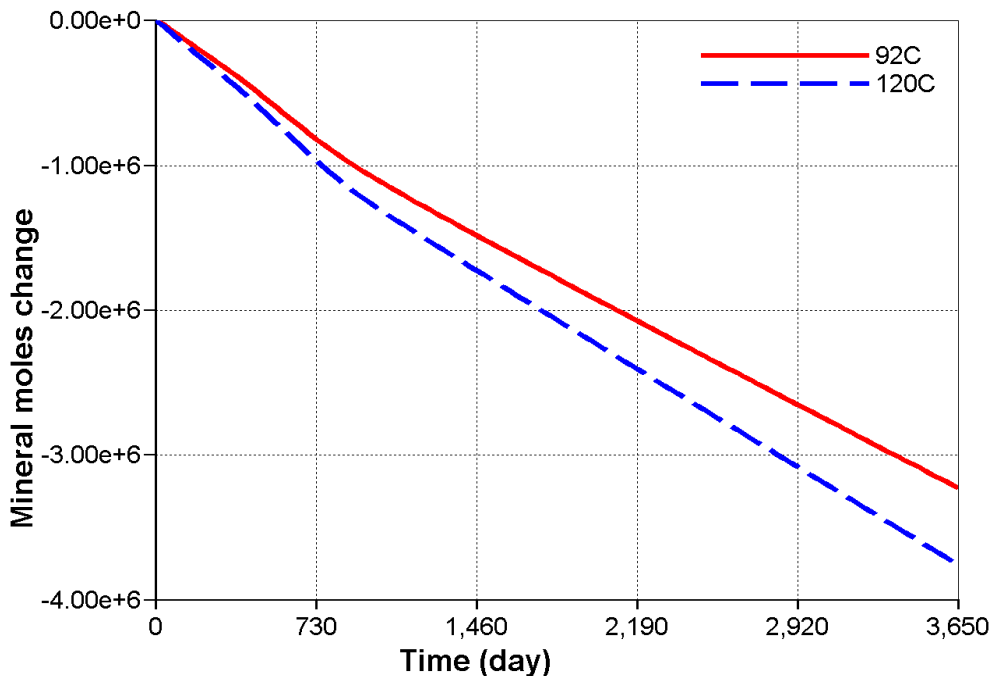


Figure 16. History of mineral dissolution of LSWF and hot LSWF in pilot-scaled reservoir.

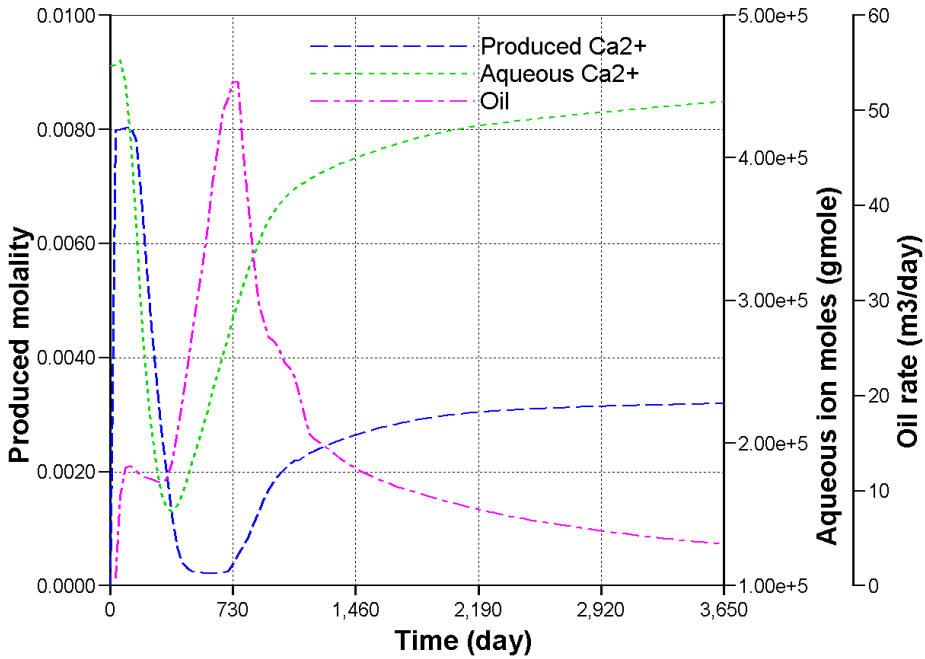


Figure 17. History of hot LSWF in pilot-scaled reservoir.

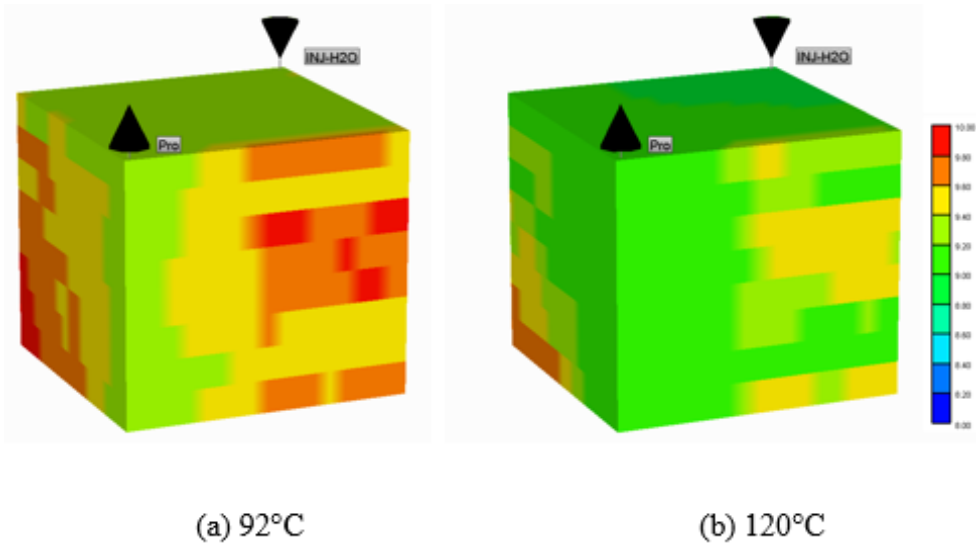


Figure 18. Profile of pH for LSWF and hot LSWF in pilot-scaled reservoirs after 10 years.

CONCLUSION

Hot LSWF definitely has mobility control effect through modification of viscosity and wettability as synergetic effect. This study evaluates the influence of thermal energy on LSWF effects in heavy oil carbonate reservoirs. Wettability modification is sensitive to

thermal energy, so that thermal energy influences on both viscosity of oil and wettability modification level. Thermal energy enhances mineral dissolution to provide ion exchangeable of Ca^{2+} and enhances supplementary wettability alteration except for non-thermal LSWF effect. These effects become dominant near injection. The synergetic effects have appeared to be enhanced oil production as well as improved injectivity. More dissolved minerals have produced carbonate acid and it slightly reduces pH in reservoirs. However, hot LSWF still elevates pH compared to initial pH condition. The characteristic of thermal dependent oil viscosity and wettability modification levels requires to consider heat loss to overlying/underlying layers. Thermal properties of shale control heat loss and determine degree of oil viscosity reduction and wettability modification. This study provides feasibility of hot LSWF process in heavy oil reservoirs and suggests careful evaluation of heat loss before deploying hot LSWF.

REFERENCES

- Austad, T.; Strand, S.; Madland, M. V.; Puntervold, T.; Korsnes, R. I. *SPE Reservoir Eval. and Eng.*, 2008, 11(4): 648-654.
- Austad, T.; Rezaei Doust, A.; Puntervold, T. Proc. SPE Improved Oil Recovery Symposium Tulsa, OK, USA, 24-28 April, 2010.
- Bethke, C. M. *Geochemical Reaction Modeling. Concepts and applications*, Oxford University Press, NY, USA, 1996, 397.
- Cuong, T. Q.; Nghiem, L. X.; Chen, Z.; Nguyen, Q. P. Proc. SPE Annual Technical Conference and Exhibition New Orleans, Louisiana, USA, 30 September-2 October, 2013.
- Farouq Ali, S. M. Proc. SPE Rocky Mountain Regional Meeting, Billings, Montana, USA, 15-16 May 1974.
- Gachuz-Muro, H.; Sohrabi, M. Proc. SPE Heavy and Extra Heavy Oil Conference Medellin, Colombia, 24-26 September, 2014.
- Gachuz-Muro, H.; Sohrabi, M. Proc. EAGE Annual Conference and Exhibition Incorporating SPE Europec London, UK, 10-13 June, 2013.
- Gupta, R.; Smith, P. G.; Hu, L.; Willingham, T. W.; Cascio, M. L.; Shyeh, J. J.; Harris, C. R. Proc. SPE Middle East Oil and Gas Show and Conference Manama, Bahrain, 25-28 September, 2011.
- Goodyear, S. G.; Reynolds, C. B.; Townsley, P. H.; Woods, C. L. Proc. SPE/DOE Improved Oil Recovery Symposium Tulsa, OK, USA, 21-24 April. 1996.
- Jadhunandan, P. P.; Morrow, N. R. *SPE Reservoir Eng.*, 1995, 40-46.
- Kwak, H. T.; Yousef, A. A.; Al-Saleh, S. Proc. SPE Improved Oil Recovery Symposium Tulsa, OK, USA, 12-16 April, 2014.
- Lager, A.; Webb, K. J.; Black, C. J. J.; Singleton, M.; Sorbie, K. S. *Petrophysics*, 2008, 49(1): 28-35.
- Messner, G. L.; Stelling, D. R. Proc. Annual Technical Meeting Calgary, AB, CA, 10-13 June, 1990.
- Oseterloh, W. T.; Jones, J. B. *SPE Reservoir Eval. and Eng.*, 2003, 6(2): 127-134.

- Ramlal, V. Proc. SPE/DOE Symposium on Improved Oil Recovery Tulsa, OK, USA, 17-21 April, 2004.
- Standnes, D. C.; Nogaret, L. A. D.; Chen, H. L.; Austad, T. *Energy and Fuels*, 2002, 16(6): 1,557-1,564.
- Strand, S.; Høgnesen, E. J.; Austad, T. *Colloids and Surfaces A: Physicochem. Eng. Aspects*, 2006, 275: 1-10.
- Tang, G. Q.; Morrow, N. R. *J. of Pet. Sci. and Eng.*, 1999, 24: 99-111.
- Vinsome, P. K. W.; Westervled, J. J. *Can. Petrol. Tech.*, 1980, 19(03): 87-90.
- Zhang, P.; Tweheyo, M. T.; Austad, T. *Energy and Fuels*, 2006, 20: 2,056-2,062.
- Zhang, P.; Tweheyo, M. T.; Austad, T. *Colloids and Surfaces A: Physicochem. Eng. Aspects*, 2007, 301: 199-208.
- Zhang, Y.; Morrow, N. R. Proc. SPE/DOE Symposium on Improved Oil Recovery Tulsa, OK, USA, 22-26 April, 2006.

Chapter 2

SAGD HISTORY FROM MODELING POINT OF VIEW

***Aria Rahimbakhsh¹, Morteza Sabeti², Amir H Mohammadi^{3,4,5,*}
and Khashayar Sharifi⁶***

¹Department of Petroleum Engineering,
AmirKabir University of Technology, Tehran, Iran

²Department of Chemical Engineering,
Isfahan University of Technology, Isfahan, Iran

³Institut de Recherche en Génie Chimique et Pétrolier (IRGCP),
Paris Cedex, France

⁴Discipline of Chemical Engineering, School of Engineering,
University of KwaZulu-Natal, Howard College Campus,
Durban, South Africa

⁵Département de Génie des Mines, de la Métallurgie et des Matériaux, Faculté des
Sciences et de Génie, Université Laval, Québec, Canada

⁶Iran Research Institute of Petroleum Industry (RIPI), Azadi Sport Complex,
P.O. Box 14665-1998, Tehran, Iran.

ABSTRACT

This chapter is aimed at delivering a terse review of the SAGD process history with the main focus on the modeling/mathematical aspect. Since when this reportedly beneficial technique was introduced, many modifications have been applied to its mathematical modeling, making it more accurate each time. Semi-analytical models seemed to ease and expedite the solution procedures as new assumptions were made to better formulate the problem. The revolutionary path from its inchoate state to the present closer-to-reality condition has been traced in this chapter, mentioning the more outstanding studies conducted. Geometry of the process has constantly been updated along their corresponding mathematical formulas. Accordingly, the better the simulation of steam-oil interface, the more accurate the predictive models become. At the end, the

* Corresponding Author: A.H. Mohammadi, E-mail: a.h.m@irgcp.fr and amir_h_mohammadi@yahoo.com.

application of a new technology has been stated in the SAGD process to both reduce the operational costs and improve the whole process's efficiency.

Keywords: SAGD process, oil-steam interface, steam chamber, semi-analytical models, thermal method, Enhanced Oil Recovery (EOR)

NOMENCLATURE

a	Coefficient of velocity
b	Coefficient of horizontal distance
C	Scale coefficient
C_R	Specific heat of formation
H	Height of reservoir
K	Permeability of reservoir bed
k_o	Relative permeability of oil
K_h	Thermal conductivity of formation
L	Interface length
L_s	Latent heat of steam
m	Viscosity coefficient
M_R	Formation heat capacity
N_{pe}	Peclet number
q_o	Dead oil drainage rate
q_r	Heat content of formation
\dot{Q}_{inj}	Rate of Latent heat injection
\dot{Q}_{loss}	Rate of energy loss through overburden
Q_R	Enthalpy required to heat oil ahead of the interface
\dot{Q}_R	Enthalpy rate required to heat oil ahead of the interface
\dot{Q}_s	Steam injection rate
\dot{Q}_{sz}	Enthalpy rate needed for expansion of steam chamber
r	Coordinate in cylindrical system
r^{\wedge}	Constant interface coordinate
R^{\wedge}	Dimensionless steam zone radius
R	Dimensionless radius
ΔS_o	Initial oil minus residual oil saturation of system
SOR	Steam-Oil ratio
t	Time
T^*	Dimensionless temperature
T_r	Temperature of reservoir
T_s	Temperature of steam
ΔT	Temperature difference between steam and virgin oil temperature
U	Interface velocity

U_m	Maximum horizontal velocity
U_v	Velocity perpendicular to the steam chamber edge
W_s	Half-width of steam chamber
x	Horizontal distance from wells
X	Steam quality

Greek Symbols

α	Thermal diffusivity of reservoir
η	Coordinate parallel to interface
ϕ	Porosity
θ	Angle of interface respect to horizontal
μ	Dynamic oil viscosity
ν	Kinematic oil viscosity
ν_{os}	Kinematic oil viscosity at steam temperature
ρ	Density
ρ_R	Density of formation
ρ_o	Density of oil
ρ_w	Density of water
γ	Heat penetration depth
ξ	Coordinate perpendicular to interface

INTRODUCTION

Heavy oil and Bitumen do have a naturally low tendency to move under pressure draw down brought about after pay zone completion and perforation. Already having received enough attention and research, Enhanced Oil Recovery (EOR) and Improved Oil Recovery (IOR) methods are thus well-known to raise the recovery to significant values. In-situ methods have proven reliable in practice.

Heavy oil reservoirs producing under gravity drainage reportedly can reach high recoveries [1, 2] which is mostly influenced by oil mobility [2]. One of the most effective ways to alter this parameter is employing thermal methods. According to the literature, thermally heated reservoirs act under gravity drainage which can contribute to significantly grow the recovery [3-6].

As one of the most important and popular methods to refer to is the steam injection method that tends to lower the heavy oil viscosity so as for it to move more readily toward the producing well. Obviously, the main problem facing petroleum engineers when dealing with heavy oil reservoirs by in-situ methods is that bitumen is immobile at reservoir conditions. To overcome this, either heating the bitumen or diluting it using a proper solvent might look vital. Then, the major challenge for applying either of them is clarifying the appropriate way of introducing the heat or the solvent to the bitumen in a practically acceptable manner. For instance, injecting hot steam into a reservoir to heat the hard-to-move heavy oil is useless in practice unless the supplied pressure exceeds that of formation resistance and a set of

fractures are created. Long ago, this method was exploited in Canadian reservoirs, for instance, and production from the same well hot steam with a pressure above formation fracture was injected through looked commercially promising [7]. Of course, cyclic steam injection used to be widely used in 1980s, but its efficiency proved not high enough as it could only contact a small fraction of the reservoir [8].

The steam assisted gravity drainage (SAGD) process lies among the most promising strategies for producing from extra-heavy oil and bitumen reservoirs. This common technique includes two horizontal wells completed in the pay zone, one above another. The one completed at the top of the reservoir is called the injector, through which hot steam is injected into the reservoir and the other, completed at the bottom of the pay zone, plays the role of a heated oil producer. Figure 1 gives a simple representative of a SAGD process.

However, there are a number of well configurations for such a process such as a vertical injection well and a horizontal producing well, or that including more than two wells. As mentioned, the most common arrangement is the one indicated in Figure 1.

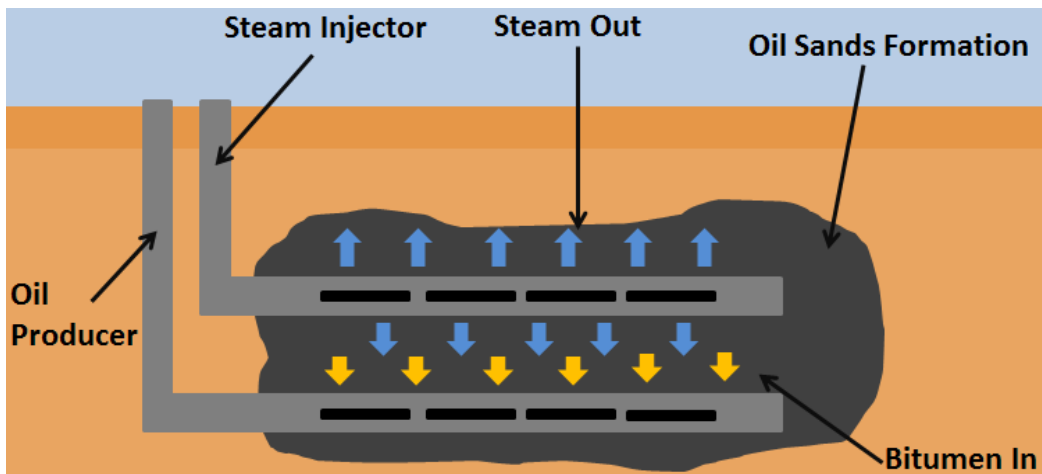


Figure 1. Schematic of a SAGD process.

The SAGD process usually begins with several months of steam circulation in either of the upper and lower horizontal wells so that a strong and clear communication between two boreholes is established. Thereafter, the upper well turns to steam injection and the lower well becomes a production well. As steam finds its way into the formation, it affects the region around the injector and the heat transfer mechanisms (mostly conduction) eases the downward flow of oil and results in the growth of the steam chamber.

Upon steam injection in the reservoir, a steam chamber is formed. As injection proceeds, this chamber enlarges and moves upwards and sidewise. After reaching the top of the reservoir in a relatively short span, the only direction will be toward reservoir boundaries and this sidewise expansion has been considered as responsible for heavy oil production. Figure 2 represents the indication of how the steam chamber is created in the reservoir once injection begins.

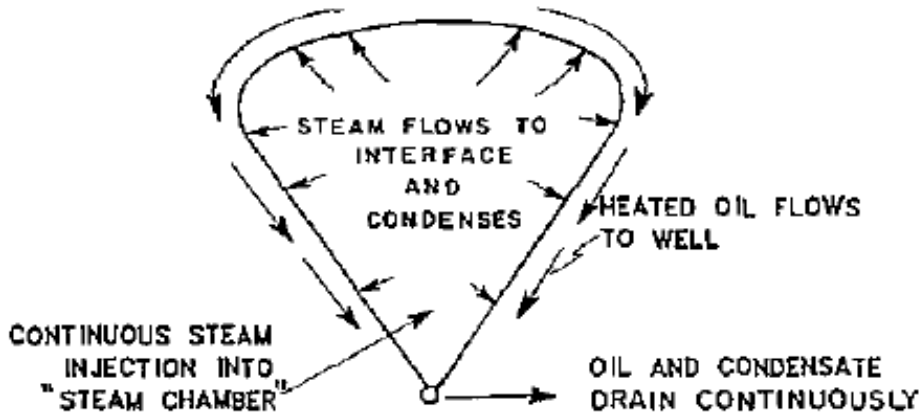


Figure 2. Steam chamber formation after Butler [7].

Mathematical modeling of the process in the beginning, when the steam chamber is enlarging upward and oil flows downward, looks very difficult due to great instability of the interface during this phase of the process. Its instability is attributed to severe viscous and gravity fingering that occurs within the counter current displacement of heavy oil by hot steam.

Several authors have proposed different models for the SAGD process since this method was first introduced, each considering a set of assumptions. Though, simulation of such a complicated process requires extensive studies taking into account many factors from steady or unsteady conditions, rate and amount of steam injection, reservoir height considerations and the shape of steam chamber to geomechanical effects [7, 9-17].

The base theory was focused on the rate at which the chamber moves sideways since this was expected to be the limiting factor [7]. It was firstly assumed by the researchers that the initial steam chamber acted as a vertical plane from the well, reaching the top of the steam chamber and that was intended to spread sideways. The initial chamber, as early researchers deemed, could be viewed as a fracture created above the horizontal well, filled with hot steam.

In practice, it is believed that the steam chamber moves along the reservoir giving off heat to the heavy oil surrounding it and causes a remarkable reduction in its viscosity. Heated oil then moves along the steam-oil interface toward the production well at the reservoir base. On the other hand, the hot steam in the chamber is condensed and like the heated oil slips downward to reach the perforations. Hence, condensed steam and heated oil are produced together in the SAGD process. The question might rise here that, why does the heated oil immediately ahead of the interface move along the interface and not vertically downward?

To answer, one should be aware that an oil element ahead of the interface has a much lower viscosity than that below it as the latter is yet to receive heat from the hot chamber. As a result, it cannot move as readily as the heated oil and with the same pace. Considering the common law that always the path with the lowest resistance is chosen, after being heated, the oil will move downward along the tilted interface to be produced. This has been assumed by many [7, 8, 18]. Figure 3 depicts this issue.

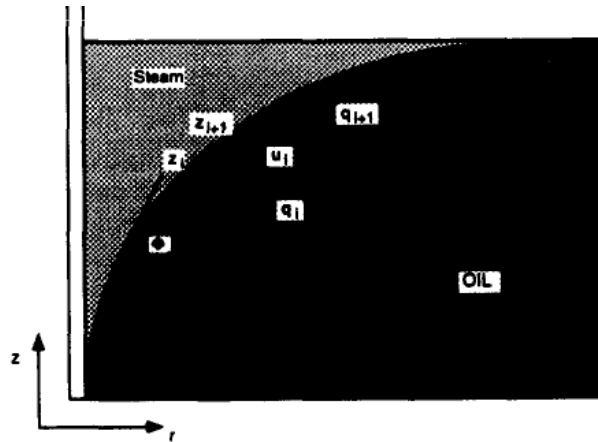


Figure 3. Steam-oil tilted interface after Pooladi-Darvish et al. [6].

Of great importance is employing the heat transfer mechanisms and their corresponding equations. However, experimental works have proven somehow that conduction is by far the dominant mechanism for heat transfer from the chamber to the virgin oil ahead of the interface [7]. Along with it, temperature distribution equation is a main factor showing the effect of steam chamber's temperature on viscosity, interface velocity and consequently the production rate.

As a stunning work by Butler proposed in 1985 [7], the case under study involved using an extended horizontal well at the bottom of the steam chamber. Horizontal wells, better than vertical ones, are considered to cause a more efficient contribution as the increased drainage rate corresponding to their extended length provides a major advantage. Having observed the geometry of steam chamber at his experimental work, he released the first mathematical model for estimating oil production rate in the SAGD process. Later on, many authors made several practical modifications to the initial model and published their works. This chapter provides a review on the progress of this process during recent decades and represents the current challenges as well as the latest inventions introduced to this useful industry.

HISTORY OF RESERVOIR MODELING APPLYING THE SAGD METHOD

Generally, simulation of a reservoir in a SAGD process culminates in two methods: The first method of simulating arises from some tedious numerical calculations, which a wide range of equations and conditions must be used so that researchers could find logical results [10]. Prevalently, commercial software in the petroleum engineering field takes the advantage of this method in its structures. It is believed that thanks to summing up all governing equations including all transform phenomena expressions and thermodynamic equations of state, numerical method would fulfill accurate results in various EOR manners [10, 19, 20]. However, the significant drawback which numerical methods almost have is its inability to converge on final results in a short time [19]. This weakness impelled researchers to find another way. Consequently, petroleum engineers have always been pursuing an alternative as a second method to tailor this issue. In the analytical method, the SAGD process has been tried to be adapted with main in-situ mechanisms and processes happening during the oil

recovery operation. As a result, several simplified assumptions have usually been considered by researchers to obtain an equation to estimate the oil production rate. Analytical methods lead to pretty accurate outcomes in a flash and to do so, they do not require a lot of raw data about reservoirs. Hence, the advantage of analytical methods largely outweighs the disadvantage of numerical method in the SAGD process [21].

Following this section, important semi-analytical models which had a significant impact on reservoir modeling during SAGD operation have been briefly delineated.

Original Model

An original theory presented equations that were written for a small part of the interface, as Figure 4 demonstrates [18]. The steam chamber was assumed to be at a constant temperature, T_s , just as the interface was considered so. Heat was assumed to be transferred into the oil that was at a lower temperature through this interface by conduction. Moreover, steady state condition was believed to exist for the temperature distribution beyond an interface expanding at a constant velocity, U .

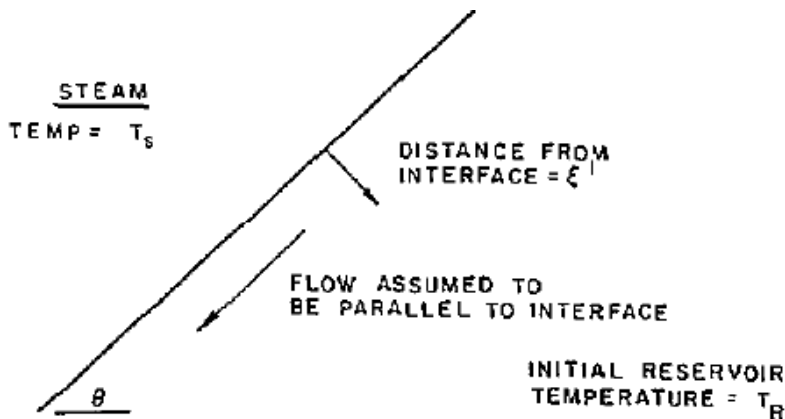


Figure 4. Interface segment [18].

The temperature distribution is given [7] by

$$T^* = \frac{T - T_r}{T_s - T_r} = \exp\left(-\frac{U\xi}{\alpha}\right) \quad (1)$$

Based on this, the viscosity is,

$$\frac{v_s}{v} = \left(\frac{T - T_r}{T_s - T_r}\right)^m \quad (2)$$

It has been shown that the value of m is dependent on viscosity-temperature characteristics of oil as well as steam and reservoir's temperature [22]. Hence,

$$m = \left[v_s \int_{T_r}^{T_s} \left(\frac{1}{v} - \frac{1}{v_r} \right) \frac{dT}{T - T_r} \right]^{-1} \quad (3)$$

Also, from Darcy's law, the flow within in element will be

$$dq_o = \frac{k_o g \sin \theta}{v} d\zeta \quad (4)$$

After integration, the oil drainage from at a point of interface can be presented as a function of velocity U and angle θ as

$$q_o = \frac{k_o g \sin \theta}{m v_s U} \quad (5)$$

Combining this relation with material balance equations would yield interface curves (Figure 5 shows interface curves.) and the relation below for oil production as below [18].

$$q_o = \sqrt{\frac{2\phi\Delta S_o k_o g \alpha (H - Y)}{m v_s}} \quad (6)$$

As it is well-known today, the steam chamber is almost fixed near the production well and what is presented in the above curve contradicts it. In a noble work in 1985 [7], Butler attempted to modify this theory to allow a fixed bottom of the chamber.

The main problem associated with the original theory was assuming a steady state condition for the temperature distribution. Of course, this assumption holds in the center of the chamber but fails at the ends.

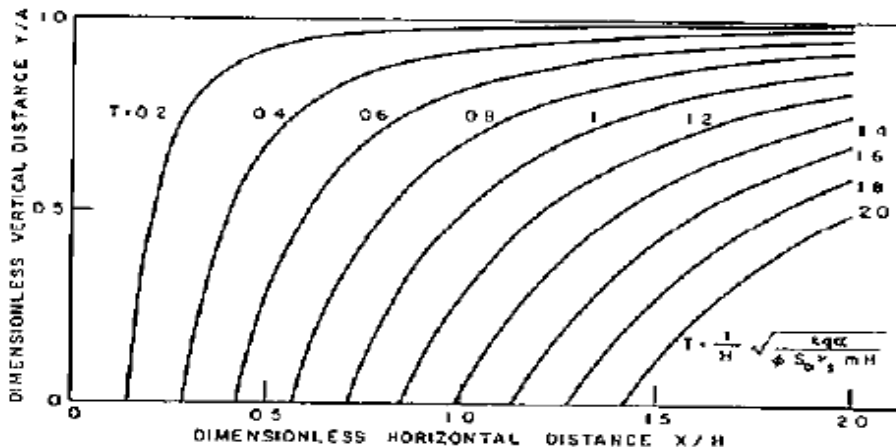


Figure 5. Interface curves [7].

Butler's Model- a Linear Interface

Butler in his study imagined the interface as a number of moving elements which could endure changes in their width as the process continued. Each was assumed a straight line behind which the depth of heat penetration would be calculated at every step.

Considering the relation below for the amount of heat behind a part of interface having an area of A [7],

$$\frac{\partial q_r}{\partial A} = \int_0^{\infty} \rho C_p (T - T_r) d\zeta \quad (7)$$

and introducing a new parameter, γ , to represent heat penetration, one might find

$$\frac{\partial q_r}{\partial A} = \gamma \rho C_p (T_s - T_r) \quad (8)$$

Considering all processes at steady state conditions, Butler [7] reached the below equation to express the flow:

$$q_o = \frac{\gamma k_o g \sin \theta}{m v_s} \quad (9)$$

As a net result of heat conduction to the oil ahead of the interface and the heat left in the reservoir, the differential heat equation was found to be as below

$$\frac{1}{A} \frac{dq_r}{dt} = -K_h \left(\frac{\partial T}{\partial \zeta} \right)_{\zeta=0} - U \rho C_p (T_s - T_r) \quad (10)$$

or,

$$\frac{d\gamma}{dt} = -\alpha \left(\frac{\partial T^*}{\partial \zeta} \right)_{\zeta=0} - U \quad (11)$$

The temperature gradient for both moving (constant U, $\frac{d\gamma}{dt} = 0$) and stationary ($T = T_r$ at $t=0$) interfaces were, respectively, represented as

$$\left(\frac{\partial T^*}{\partial \zeta} \right)_{\zeta=0} = -\frac{1}{\gamma} \quad (12)$$

and

$$\left(\frac{\partial T^*}{\partial \zeta}\right)_{\zeta=0} = -\frac{2}{\pi} \frac{1}{\gamma} \quad (13)$$

As can be seen, temperature gradient is inversely proportional to the heat penetration depth in either of the cases. Considering the temperature gradient to move between these two extreme cases, one might find

$$\left(\frac{\partial T^*}{\partial \zeta}\right)_{\zeta=0} = -\frac{2}{\pi\gamma} - \left(1 - \frac{2}{\pi}\right) \frac{U}{\phi\alpha} \quad (14)$$

Substituting in the differential heat equation will yield

$$\frac{d\gamma}{dt} = \frac{2}{\pi} \left(\frac{\alpha}{\gamma} - U \right) \quad (15)$$

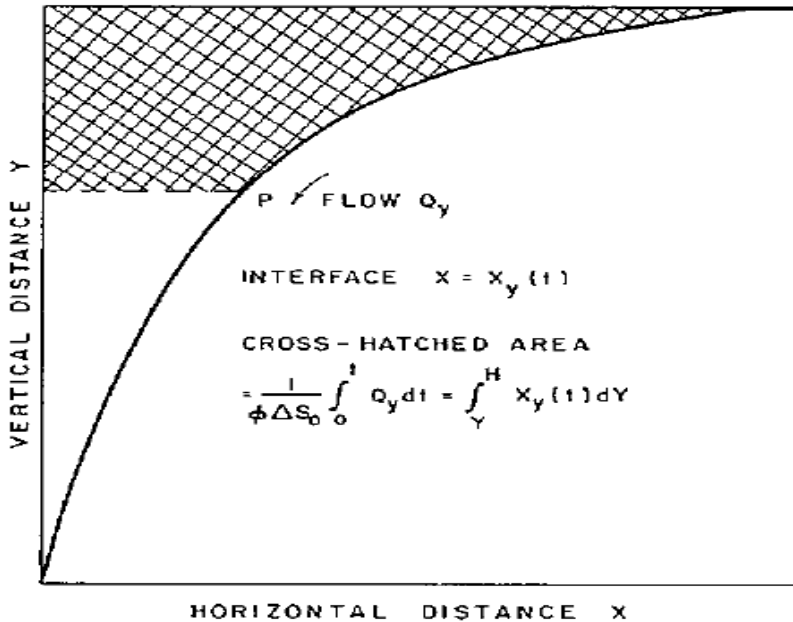


Figure 6. Relation between drainage rate and interface movement [7].

Introducing dimensionless parameters for oil drainage rate, temperature and frontal velocity, he obtained several useful results such as computing the relationship between drainage rate and the interface movement (Figures 6 and 7).

The amount of heat needed to provide can be known as the sum of three values. One to heat the steam chamber and oil drained with it, one to heat the reservoir and finally, one that

is lost by means of conduction to the overburden. These quantities are introduced in dimensionless forms for ease of mathematical manipulation. With regard to the steam-oil interface movement in dimensionless scales, Figure 8 represents the oil drainage rate in dimensionless coordinates as well as the three heat values. As can be seen, before a dimensionless time of about 0.2, the interface does not move greatly but as the rate of heat transfer is so high in the beginning of the process (dimensionless time of about 0.2), the oil production rate reaches its pinnacle and then slows down as heat transfer rate falls.

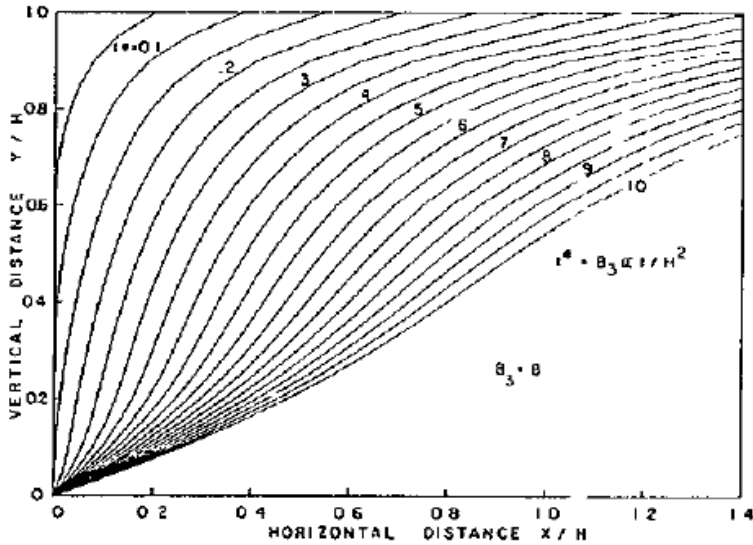


Figure 7. Position of interface [8].

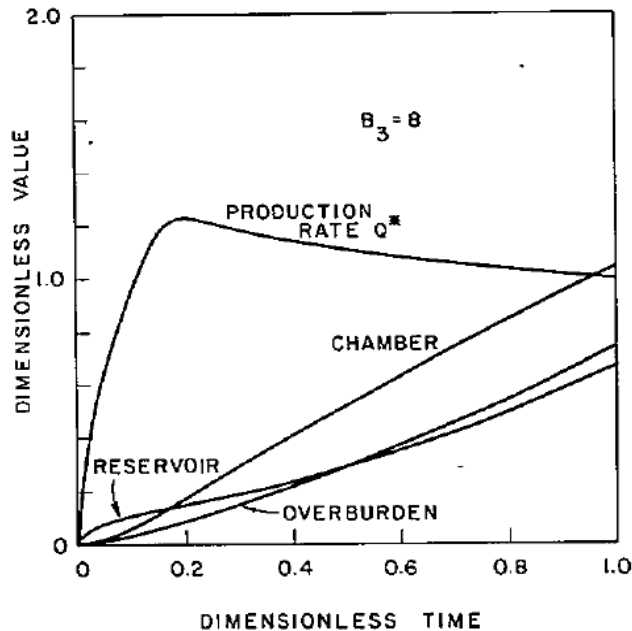


Figure 8. Production rate and cumulative heat distribution [8].

It must be noted that B_3 is a dimensionless parameter that depends on reservoir characteristics. In fact, petrophysical parameters are grouped together to form a dimensionless factor.

$$B_3 = \sqrt{\frac{k_o g H}{\alpha \phi \Delta S_o m v_{os}}} \quad (16)$$

However, he did research on a number of other matters including well confinement, which he claimed to increase the thermal efficiency through reducing the steam override. In fact, a closer well spacing will lead to higher thermal efficiency. Besides, three mass transfer mechanisms are known to impede the providing of steam to the advancing ends of the chamber; the counter-current condensate flow from the upper boundary layer, presence of considerable liquid saturations in the capillary layer just above the drainage surface and non-condensable gases that make a barrier against mass transfer.

Reis's Model- an Inverted Triangle

In two successive works in 1992 and 1993, Reis proposed two models for the SAGD process considering linear and radial geometries e.g., for horizontal and vertical wells, respectively. In his first work, considering the linear geometry for horizontal wells, he imagined the steam chamber to be so much an inverted triangle with its vortex being pivoted to the production well at the bottom of the pay zone. The grounds for his work was the same as Butler's i.e., the energy balance and total amount of heat required was the sum of three portions.

$$\sum Q' = Q'_{sz} + Q'_R + Q'_L \quad (17)$$

The first term on the right hand side of the above equation shows the heat required to be given to the steam zone, the second represents the amount needed to preheat the formation ahead of the interface under his study and the last is the amount of heat lost to the overburden. Figure 9 represents Reis's proposed interface shape.

Having proceeded on the same premise as Butler, he had in hand the same equation for oil production rate

$$q_o = \frac{k_o g \alpha \sin(\theta)}{\alpha v_{os} m U_m} \quad (18)$$

His work differed when he tried to relate this rate to the geometry of an inverted triangle through a material balance. According to him, the drainage rate along the oil-steam interface would be equal to a time derivative of steam zone cross-sectional area. Hence,

$$q_o = \frac{d}{dt} [\varphi \Delta S_o H W_s] \quad (19)$$

Considering the fact that the derivative of steam chamber's with respect to time is proportional to the maximum interface velocity as shown in below:

$$\frac{dW_s}{dt} = \frac{U_m}{\sin(\theta)} \quad (20)$$

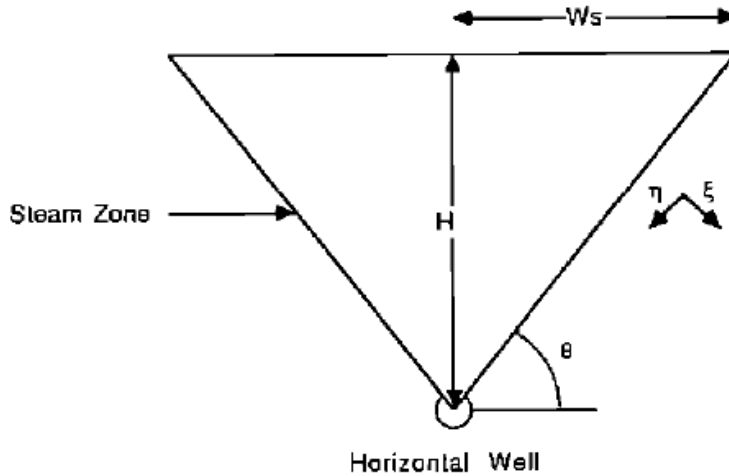


Figure 9. An inverted triangle shape for steam chamber after Reis (1992).

The drainage rate and the cumulative production will accordingly be computed by the following relations:

$$q_o = \sqrt{\frac{k \alpha \varphi \Delta S_o \cdot g \cdot H}{2 v_{os} \cdot a \cdot m}} \quad (21)$$

$$Q_o = \sqrt{\frac{k \alpha \varphi \Delta S_o \cdot g \cdot H}{2 v_{os} \cdot a \cdot m}} \cdot t \quad (22)$$

But the cumulative production from material balance is found to be

$$Q_o = \varphi \Delta S_o \frac{1}{2} H W_s \quad (23)$$

Combining the two latter formulas, the width of the steam chamber is determined as a function of time

$$W_s = \sqrt{\frac{2k_o g \alpha}{\phi \Delta S_o H v_{os} a m}} t \quad (24)$$

Also, the angle of the steam zone interface can readily be understood as

$$\theta = \arctan\left(\frac{H}{W_s}\right) \quad (25)$$

Reis assumed the temperature distribution to be

$$T^* = \exp\left(-\frac{U\xi}{\alpha}\right) \quad (26)$$

which shows it as a function of interface velocity. But this equation has some shortcomings as U tends to zero at the bottom. Another limitation for using the latter relation for the temperature profile of the oil-steam interface is that it is based on constant velocity while in practice U changes both in magnitude and direction. However, observations by Chung and Butler [12] revealed that temperature profile remains almost constant with time and is independent of position and hence velocity. Thus, temperature profiles can be measured through the same previous equation

$$T^* = \frac{T-T_r}{T_s-T_r} = \exp\left(-\frac{U\xi}{\alpha}\right) \quad (27)$$

After some mathematical procedures, they found the maximum interface velocity as

$$U_m = \sin(\theta) \frac{dW_s}{dt} = \sqrt{\frac{2k_o g \alpha}{\phi \Delta S_o H v_{os} a m}} \sin(\theta) \quad (28)$$

Also, each of the three heat measures contributing to the total heat required were found as

$$Q'_{sz} = M_R \Delta T \sqrt{\frac{k_o g H \alpha}{2\phi \Delta S_o a v_{os} m}} \quad (29)$$

$$Q'_R = M_R \Delta T H \sqrt{\frac{\phi \Delta S_o v_{os} m H \alpha}{2a k_o g}} \quad (30)$$

$$Q'_L = 2\alpha M_R \Delta T \sqrt{\frac{2k_o g}{\pi \phi \Delta S_o H a v_{os} m}} t^{1/2} \quad (31)$$

The first, second and third equation represent the amount of heat required to be injected into the steam zone, the amount stored ahead of the oil-steam interface in the formation and the amount given off to the overburden, respectively. Hence, total heat injection will be

$$Q'_{ing} = M_R \Delta T \sqrt{\frac{k_o g}{\phi \Delta S_o a v_{os} m}} \left[\sqrt{\frac{H \alpha}{2}} + \frac{4 \alpha t}{H a} \sqrt{\frac{\alpha}{2 H}} + 2 \alpha \sqrt{\frac{2 t}{\pi H}} \right] \quad (32)$$

Similar to the oil drainage rate formula, this injection applies merely to one side of the chamber and to get the total amount, they must be doubled both.

One noteworthy factor in a SAGD process assessment is the steam-oil ratio (SOR). It is found after dividing the total steam injection rate by the production rate. Thus,

$$SOR = \frac{M_R \Delta T}{\rho_w L_s X \phi \Delta S_o} \left[1 + \frac{4 \alpha t}{H^2 a} + \frac{4}{H} \sqrt{\frac{\alpha t}{\pi}} \right] \quad (33)$$

Figure 10 depicts SOR for the example under consideration in Reis's study. As obvious, SOR goes high almost linearly to above 8 in a period of 10 years. Reis did not validate this model for angles below 30 and using it, one must be on the alert.

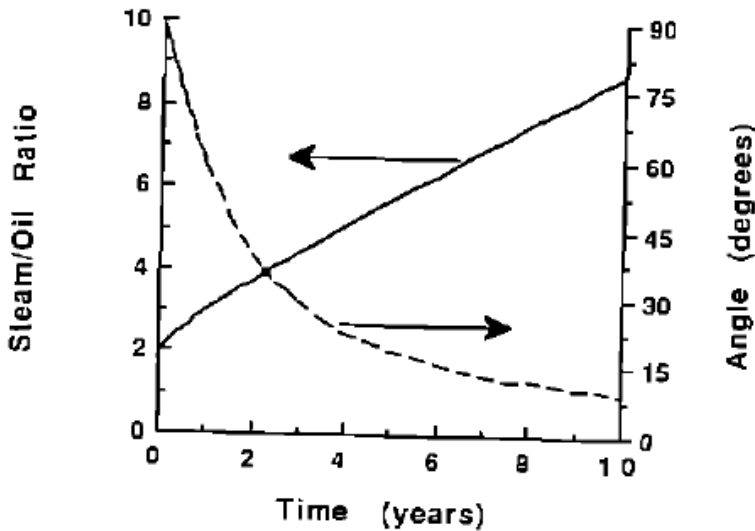


Figure 10. SOR for Reis's example [8].

Reis's Model- an Inverted Conical Interface

Nearly a year after, Reis conducted a similar study on radial geometry and obtained promising results after assuming a conical shape for the steam-oil chamber [11]. To solely

give a brief mention of his findings, below are presented some more demanding aspects of his research.

He used the so-called single well injection/production streamflow (SIPS) or the vertical HASDrive process [23, 24]. Neglecting his mathematical manipulations here, he found the below relationship for the oil drainage rate

$$q_o = \frac{\alpha B}{a} \left[\frac{A a \beta R_s^2}{m \alpha B} - \frac{1}{4 \beta^2} \right]^{\frac{1}{2}} \quad (34)$$

Where, geometrical parameters in the above equation have been presented in Figure 11 and R_s is the cone radius found by

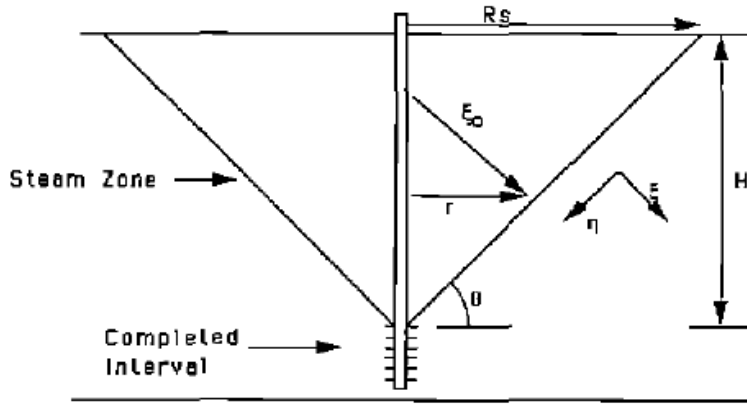


Figure 11. Schematic of a vertical injection/production well and the steam chamber [11].

$$R_s = \left(\frac{\phi \Delta S_o H m \alpha v_{os}}{3 a \beta k_o g} \right)^{\frac{1}{3}} \left[\left(\frac{3 k_o g \beta t}{\phi \Delta S_o H m v_{os}} \right)^2 + \left(\frac{1}{2 \beta} \right)^2 \right]^{\frac{1}{3}} \quad (35)$$

This equation can be reduced to the proceeding form for all times and locations but the early time and near the bottom of the steam chamber where conduction dominates.

$$R_s = \left(\frac{3 k_o g \beta \alpha}{\phi \Delta S_o H m \alpha v_{os}} \right)^{\frac{1}{2}} t \quad (36)$$

Also, the maximum interface velocity is

$$U_m = \frac{3 q_o \sin(\theta)}{2 \pi \phi \Delta S_o H R_s} \quad (37)$$

In an alert observation, Reis found this relation to connect the temperature to that calculated in his previous work.

$$T'_{rad} = \left(1 - \frac{\zeta \sin(\theta)}{2r} \right) T'_{lin} \quad (38)$$

For a SAGD process in a radial geometry the profile of temperature ahead of the steam zone, is reported to be expressed as

$$T'_{rad} = \exp \left[- \left(\frac{aU_m}{\alpha} + \frac{\sin(\theta)}{2r} \right) \zeta \right] \quad (39)$$

Finally, he offered the formula for the steam oil ratio as

$$SOR = \frac{M_R \Delta T}{\rho_w L_s X} \left[\frac{1}{\phi \Delta S} + \frac{v_{os} m H}{k_o g t \sin^2(\theta)} [1 + 2 \cos^2(\theta)] + \frac{4 \sqrt{c t}^{\frac{1}{2}}}{\sqrt{\pi} \phi \Delta S_o H} \right] \quad (40)$$

As can be seen from Figure 12, SOR is initially at a high value since the drainage area is small. It then falls to its minimum after about a year and rises almost linearly to figures as large as 9 within 10 years. It has to be pointed out that this SOR is just slightly greater than that in the linear geometry, hence proving promising.

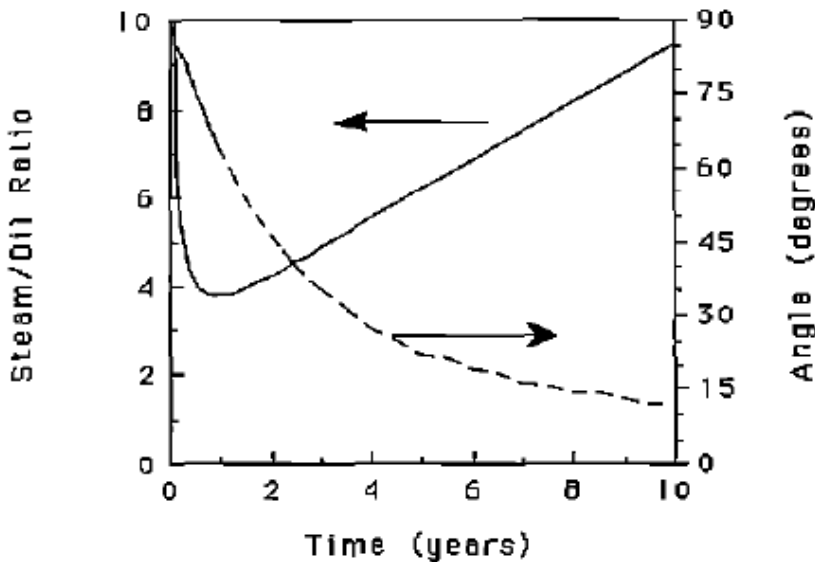


Figure 12. SOR and angle for a SAGD process vs. time [11].

After a long time, the interface angle drops to about 15 degrees and at angles this low, conductive heat losses will increase. Thus, immense care must be taken when this model at low angles.

Introduction of HIM

In 1995, Pooladi-Darvish et al. [6] suggested a new semi-analytical model using the Heat Integral Method (HIM) to approximate a 2D heat transfer in the formation. He conducted his studies employing the cylindrical coordinates and finally proved his work as predicting high production rates and a sweep efficiency [6]. In his work, he took account of both moving interface and the unsteady state condition. As was corroborated earlier in this chapter, they claimed that the two mechanisms responsible for the heat transfer are convection and conduction with the latter playing the major role. Most of the proposed models thus far either neglected the impact of the mobile interface or consider a steady state condition for the process, which refer to two extremes. The effect of moving interface can be neglected when it is moving very slowly while a steady state holds when it moves very fast. This work considers both effects.

As other investigators [7, 8], Pooladi-Darvish assumed flow of heated oil due to conduction parallel to the interface. In their paper, they developed a semi-analytical model that predicts gravity driven oil flow backed by heat conduction ahead of a steam-oil interface. They found the shape of the interface as a part of the solution, and thus, it was not known in priori. The non-linear partial differential equation (PDE), expressing the heat conduction beyond a moving interface, was transformed with the aid of the Heat Integral Method (HIM) to a first order ordinary differential equation (ODE). The latter was combined with Darcy's law and an equation of state (EOS) to forecast the oil rate. Having made a number of assumptions such as incompressible fluids, a constant pressure inside the chamber, considering only steam to be the only phase flowing behind the interface and describing the heat transfer in the oil zone by a 1D equation, they developed their model. They looked at the problem as a combination of heat and fluid flow problem and studied each one separately. The equation below shows the 1D heat transfer equation in the reservoir and ahead of the interface.

$$\frac{\partial^2 T}{\partial r^2} + \frac{1}{r} \frac{\partial T}{\partial r} = \frac{1}{\alpha} \frac{\partial T}{\partial t} \quad (41)$$

But,

$$r^{\wedge}(z, t) = \int_0^t U ds + r_w \quad (42)$$

which shows the radius as variable with time.

$$\zeta = r - r^{\wedge}(z, t) \quad (43)$$

And this helps to handle the moving steam-oil interface as stationary. Thus, the 1D heat transfer equation can be rewritten as

$$\frac{\partial^2 T}{\partial \zeta^2} + \left[\frac{1}{\zeta + r^{\wedge}(z, t)} + \frac{U}{\alpha} \right] \frac{\partial T}{\partial \zeta} = \frac{1}{\alpha} \frac{\partial T}{\partial t} \quad (44)$$

This non-linear PDE can be transformed to an ODE that can be readily solved by numerical methods such as that proposed by Runge Kutta. For mathematical simplifications the dimensionless variables are introduced as

$$\begin{aligned} \eta &= \frac{\xi}{H} \\ R_w &= \frac{r_w}{H} \\ \tau &= \frac{\alpha t}{H^2} \\ \theta &= \frac{T - T_R}{T - T_s} \end{aligned} \quad (45)$$

And the latter equation in the dimensionless form is

$$\frac{\partial^2 \theta}{\partial \eta^2} + \left[\frac{1}{\eta + R^{\wedge}(z, \tau)} + N_{pe} \right] \frac{\partial \theta}{\partial \eta} = \frac{\partial \theta}{\partial \tau} \quad (46)$$

Employing HIM to find solutions for processes of non-isothermal oil flow regarding conduction mechanism was embarked on by some authors in 1990s [25, 26]. They used a polynomial to express the unsteady-state temperature distribution beyond of the oil-steam interface as

$$\theta = a_1(\tau) + a_2(\tau)\eta + a_3(\tau)\eta^2 + \dots + a_{n+1}(\tau)\eta^n \quad (47)$$

Which then, considering no effect ahead of the heat transfer penetration depth and thus a value of zero for θ and all its derivatives with respect to η in those regions, can be written as

$$\theta = \left(1 - \frac{\eta}{\delta(\tau)}\right)^n \quad 0 \leq \eta \leq \delta(\tau) \quad (48)$$

Using the suitable boundary conditions, they obtained

$$\frac{d\delta^2}{d\tau} = 2(n+1) \left(n - \left[\frac{1}{R^\wedge(z, \tau)} + N_{pe} \right] \delta \right) \quad (49)$$

This formula is the 1D HIM solution to the heat transfer in the reservoir. The 2D heat transfer equation can be described as

$$\frac{\partial^2 \theta}{\partial z^2} + \frac{\partial^2 \theta}{\partial \eta^2} + \left[\frac{1}{\eta + R^\wedge(z, \tau)} + N_{pe} \right] \frac{\partial \theta}{\partial \eta} = \frac{\partial \theta}{\partial \tau} \quad (50)$$

where a variable interface velocity exists, as well as cases of small wellbore radius, the 1D representation showed poor accuracy. Considering the fluid flow problem, they found

$$q_o(\tau) = \frac{2\pi H^2 g k_o \sin(\theta)}{v_{os}} \frac{\delta \left[\delta + (nm+2)R^\wedge(z, \tau) \right]}{(nm+2)(nm+1)} \quad (51)$$

This determines the oil rate as a function of a number of dynamic variables and fixed rock and fluid properties. Experimental data backed their offered method.

Of course, it is compulsory to mention that the HIM solution usually underestimates the temperature distribution in cases of small steam zone radius. This is because the HIM solution suits better the situations in which conduction dominates the heat transfer while in occasions of small radius (at the bottom), a large and effective convective mechanism is existent. It must be mentioned that they studied more than what is briefly presented here.

During time, several authors focused on improving the simulating models and considered other important factors such as geomechanics, reservoir height and new steam chamber geometries [9, 14, 16, 27-31].

Geomechanics Effect on SAGD

A problem with many of the developed models was that they tended to solve the hydro-thermal equations, ignoring the important role of the geomechanics. In other words, the physics of this process was totally ignored and the reason why these simulations mostly failed to predict the real reservoir under SAGD process became more lucid as researchers began to note geomechanics effects. Several authors have thus far asserted the essence of taking into account the effect of geomechanics on the SAGD process [32-34].

However, computing the characteristics of geomechanical reservoir models is roughly time-consuming and thus, models that consider only the most important parameters would be of great value. In 2009, Azad et al. offered an introduced geomechanics to a Butler's SAGD model [35].

As the first modification to the old model proposed by Reis, they managed to incorporate the heterogeneity of permeability through assumption of an elliptical anisotropy, as depicted Figure 13.

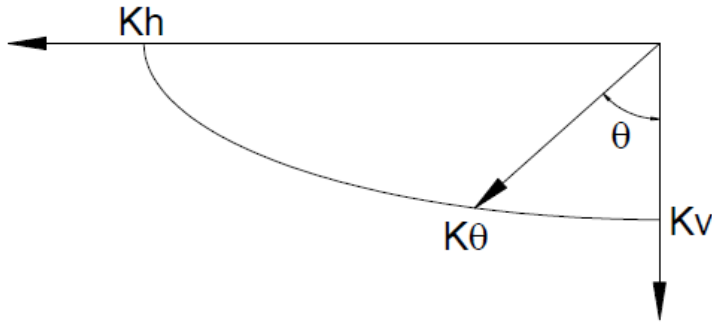


Figure 13. Elliptical permeability anisotropy, after Azad et al. [35].

Assuming $k_h = nk_v = k_o$ and based on Figure 13, the permeability value at any arbitrary angle θ will be

$$K_{\theta}^2 = \frac{K_o^2}{(\sin \theta)^2 + (n \cos \theta)^2} \quad (52)$$

In their work, Azad et al. proposed a new predictive model in derivation of which heterogeneity and corrected integral bounds were considered. They obtained

$$dq_o = \frac{K_{\theta} \rho_o g (\cos \theta)^2}{\mu_o} \exp\left(\frac{-\alpha m (U_{\max} \cos \theta) x}{\alpha}\right) dx \quad (53)$$

that when combined with the new permeability formula, yields

$$q_o = \frac{2K_o \rho_o g \alpha \cos \theta}{\mu_o \alpha m U_{\max} \left[(\sin \theta)^2 + (n \cos \theta)^2 \right]^{0.5}} \quad (54)$$

From material balance, the relation between velocity and oil rate is

$$q_o = 2 \frac{d}{dt} \left[\varphi \Delta S_o \frac{1}{2} H_i B \right] = (\varphi \Delta S_o) (H_i U_{\max}) \quad (55)$$

In formulas above, ρ_o represents oil density, μ_o shows oil viscosity at steam temperature, α is the reservoir thermal diffusivity, φ is the reservoir porosity and ΔS_o presents the difference between initial and residual oil saturation.

To introduce geomechanics to the flow simulation, a linearly moving shear zone is deemed to exist ahead of the steam chamber and the whole model is taken as in equilibrium. The linear movement of the layer mentioned above is exhibited in Figure 14.

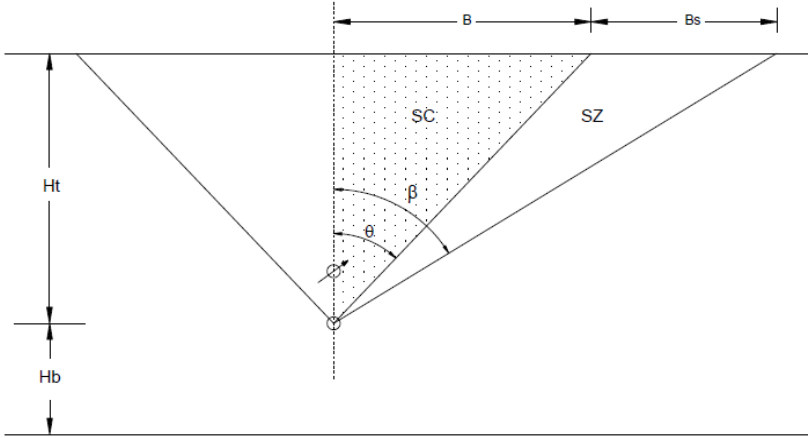


Figure 14. Moving shear zone in geomechanical model of SAGD [35].

Thermal stress comes into existence as a result of the difference between steam temperature and that lying behind the interface in the reservoir. ΔT , the maximum temperature difference, is depicted by L-bar on Figure 15.

With the help of thermo-static theory, the average thermal stress exerted on a specific wedge can be mathematically expressed as

$$P_{thermal} = \frac{1}{2} (\alpha \Delta T) E H_t / \cos \beta \quad (56)$$

Having calculated this, equations pertaining to x and y-direction force equilibriums as well as Mohr-Coulomb's failure criteria are exploited to reach the geomechanical solution.

$$\begin{aligned} \sum F_x &= \sum F_y = 0 \\ F_{s,1} &= N'_{s,1} \tan \theta' \\ F_{s,2} &= N'_{s,2} \tan \theta' \end{aligned} \quad (57)$$

$$N'_{s,1} = \frac{\left(\frac{P_{thermal}}{\cos \beta - \sin \beta \tan \theta'} \right) - \left(\frac{P_{thermal} - W_s - P_{surcharge}}{\sin \beta + \cos \beta \tan \theta'} \right)}{\left(\frac{\cos \theta - \sin \theta \tan \theta'}{\cos \beta - \sin \beta \tan \theta'} - \frac{\sin \theta + \cos \theta \tan \theta'}{\sin \beta + \cos \beta \tan \theta'} \right)}$$

The last equation may be used to calculate the force brought about by the SAGD thermal process on the wedge (its edge). At each time step, a unique shear zone exists where the total volumetric strain happens. Using this procedure allows for a deformation boundary condition to be determined, and having computed the total reservoir expansion, obtaining the average volumetric strain would thereafter be of no significant difficulty as the boundary of expansion is known.

To find reservoir's total expansion, occurring as a result of steam injection, they modified the primitive model suggested by Wong and Lau in 2006 [36].

$$\begin{aligned}
 V_s &= q_s \Delta t \\
 V_{LH} &= (q_s \Delta t) L_s \left[\frac{(1-\phi)\alpha_s + \phi S_w \alpha_w + \phi S_o \alpha_o}{(1-\phi)c_s + \phi S_w c_w + \phi S_o c_o} \right] = (q_s \rho_w \Delta t) L_s \\
 V_h &= (q_s \Delta t) \Delta T' \left[\frac{(1-\phi)\alpha_s + \phi S_w \alpha_w + \phi S_o \alpha_o}{(1-\phi)c_s + \phi S_w c_w + \phi S_o c_o} c_w - \alpha_w \right] \\
 V_p &= q_o \Delta t \\
 V_{total, \Delta t} &= (q_s \Delta t) \left[L_s \Gamma + \Delta T' (\Gamma c_w - \alpha_w) + 1 \right] - q_o \Delta t
 \end{aligned} \tag{58}$$

In these formulas, the total volume equals the volume of injected steam, V_s , thermal expansion corresponding to the latent heat, V_{LH} , volume change because of cooling of the injected fluid is V_h , and the drained oil from the reservoir is demonstrated by V_p . Also, q_s is the steam injection rate, Δt specifies time differential, $\Delta T'$ shows the temperature difference at the equilibrium condition, $\alpha_s / \alpha_o / \alpha_w$, respectively, represent thermal expansion coefficient pertaining sand, oil and water, and finally, $c_s / c_o / c_w$ are heat capacity values of solid grains, oil, and water.

The volumetric changes cause permeability and porosity to change. Below are new formulas to calculate them

$$\begin{aligned}
 k / k_o &= (1 + \varepsilon_v / \phi_o)^3 / (1 + \varepsilon_v) \\
 \phi &= \frac{(\phi_o + \varepsilon_v)}{(1 + \varepsilon_v)}
 \end{aligned} \tag{59}$$

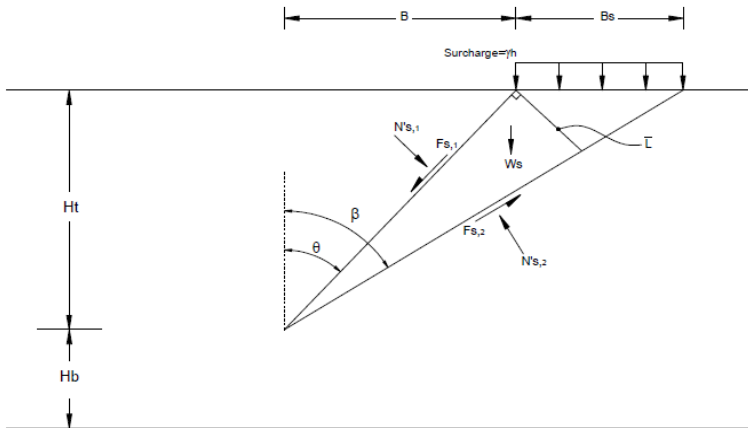


Figure 15. Effective forces exerted on a specific wedge [35].

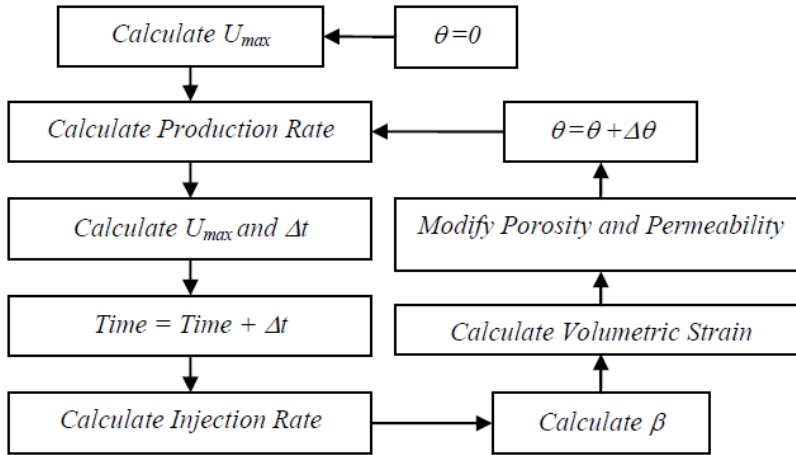


Figure 16. Azad et al. algorithm for involving geomechanics of reservoir formation in the Reis model [35].

To see how geomechanics influence the solution process, consider the flowchart by Azad et al. [35] in Figure 16 as, accordingly, the volumetric strain modifies porosity and permeability values for each critical shear zone. Comparing their results with available numerical data enunciated an excellent coincidence for cumulative production figures as well as an acceptable agreement for the steam injected.

Effect of Drainage Height on SAGD

Our knowledge of this commercially beneficiary technique is mostly founded on simplified assumptions and models that often lack acceptable assessment of all influential parameters and thus, constant modifications are being made to get better and more reliable predictive models. In 2009, Heidari et al. investigated the effect of drainage height and permeability as their multiplication (kH) appears in drainage formulas and some important dimensionless numbers (for instance, the Rayleigh number, B_3 etc.) and is hence, of interest [14]. The results of their work showed good agreement with experimental production data reported earlier by Chung et al. in 1988 [12]. Their predictive semi-analytical model suggested that increasing permeability and drainage height both have a similar effect on the production rate; they tend to increase it. But increasing permeability tends to raise the drainage rate immediately while the other needs some time to exert its influence, as depicted in Figure 17.

However, several simulator runs revealed that the initial rate will not be affected by changing the drainage height. An interesting point is that keeping the product kH constant while changing each k and H tends to alter the performance. If we imagine that model 1 has a permeability value twice as large as the base model and a drainage height half of that, and inversely, model 2 has a height twice as large and a permeability value half of the base model, Figure 18 then gives the comparison between their production rates.

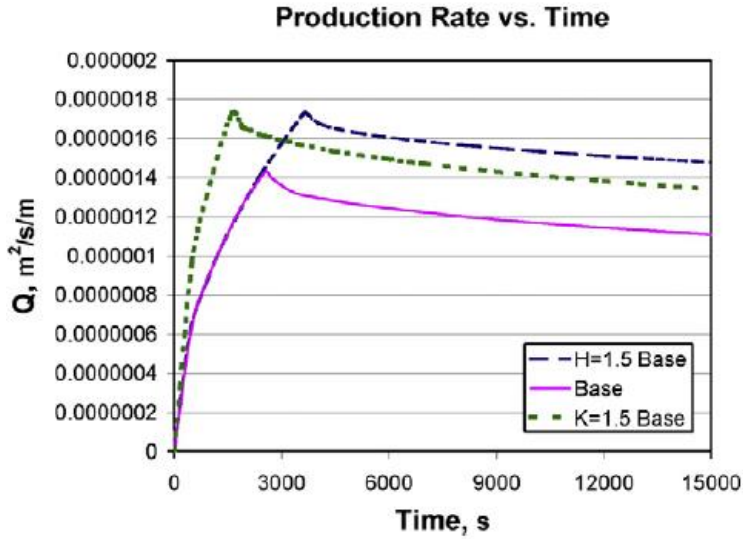


Figure 17. Effect of drainage height and permeability changes on production rate [14].

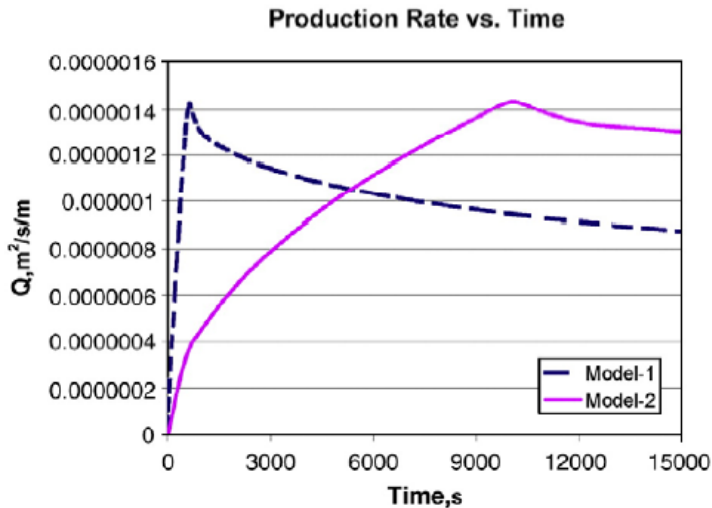


Figure 18. Effect of varying drainage height and permeability on production rate while keeping the product kH fixed [14].

Latest SAGD Simulation Modifications

This section focuses on more recent modifications made to SAGD simulation as well as a new technique to increase its efficiency. The geometry of the process has constantly been updated since Butler introduced a linear expansion of the steam chamber in 1985 [7] and several authors tended to propose geometries that would yield more accurate predictions as well as better coincidence with available field data. In 2012, Azad et al. proposed a circular geometry for sidewise expansion of the steam chamber [9], for instance. According to their

findings, there exists a close agreement between circular geometry model outcomes and the experimental laboratory data which reveals two important aspects of their model. First, their offered model refuses to predict constant oil rate unlike many other previous models and is capable of following the oil production variations and second, in contrast to one-directional models, it can predict the results of a real SAGD process. Also, other previous methods fail to give a good history match for the SOR while this model looks promising in this area. The great match of their outcomes' model with either experimental or numerical data has been presented in Figure 19 and Figure 20.

Wei et al., in 2014, considered a shape between an inverted triangle and a symmetric parabola and showed that the steam injection rate is the dominant factor determining the steam chamber shape [17]. In 2016, Sabeti et al. assumed an exponential geometry for the oil-steam sidewise growth and modeled the steam chamber as below.

$$f(x) = C[1 - e^{-bx}] \quad (60)$$

with C and b being coefficients that determine the curvature of the oil-steam interface at any moment. As part of the solution they found the interface length by

$$\begin{aligned} &= \int_0^x \sqrt{1 + (f'(x))^2} dx = \int_0^x \sqrt{1 + (Cbe^{-bx})^2} dx = \\ &= \frac{1}{2b} \left[2 \ln(1 + \sqrt{1 + C^2 b^2 e^{-2bx}}) - 2(1 + \sqrt{1 + C^2 b^2 e^{-2bx}}) - \ln(C^2 b^2 e^{-2bx}) \right]_0^x \quad (61) \end{aligned}$$

They reached the below-represented formula to express the oil drainage rate

$$q_o = \underbrace{\sqrt{\frac{k_o \alpha \phi \Delta S_o \cdot g \cdot H}{2v_{os} \cdot a \cdot m}}}_{\substack{\text{First Term} \\ \text{(Inverted Triangle} \\ \text{Model)}}} \cdot \underbrace{\sqrt{2 \left[(H - C) - \frac{H}{\ln\left(1 - \frac{H}{C}\right)} \right] \sqrt{1 + \left(\frac{1}{bC}\right)^2 e^{-2\ln\left(1 - \frac{H}{C}\right) \frac{1}{L}}}}}_{\substack{\text{Second Term} \\ \text{Modification} \\ \text{(to Inverted Triangle Model)}}} \quad (62)$$

which, as indicated, is a multiplication of two linear and curved assumptions for the interface. They also found the total energy to be injected as

$$Q'_{inj} = M_R \Delta T \left[U_m \left((H - C) - \frac{H}{\ln\left(1 - \frac{H}{C}\right)} \right) + \frac{\alpha}{a} \frac{d\left(\frac{L}{U_m \sin \theta}\right)}{dt} + 2 \sqrt{\frac{\alpha}{\pi}} U_m \cdot \sqrt{t} \right] \quad (63)$$

Figure 21 shows how steam injection and production rates predicted by their model excel that by previous models.

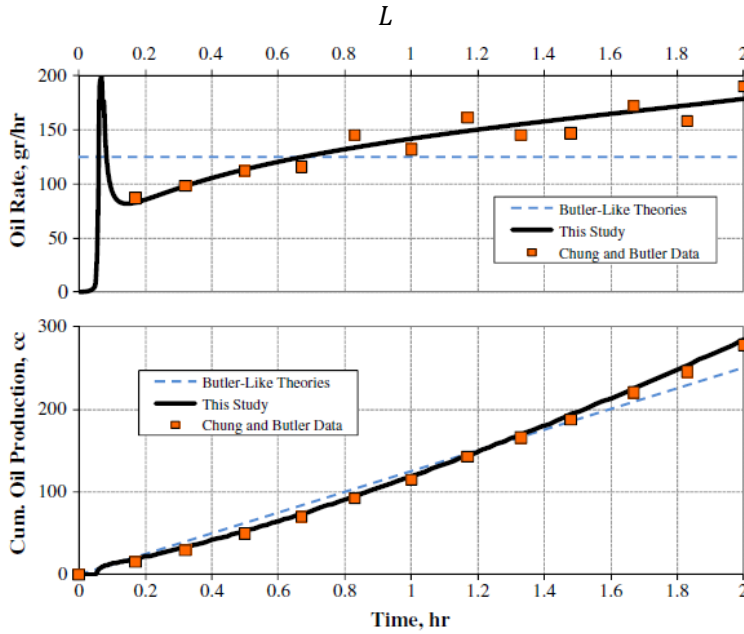


Figure 19. The results of circular geometry model vs. previous data [9].

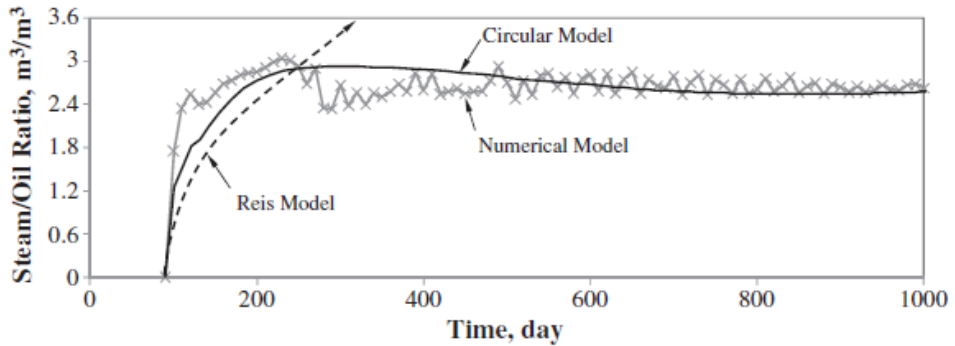


Figure 20. SOR history match by Reis and circular model vs. available data [9].

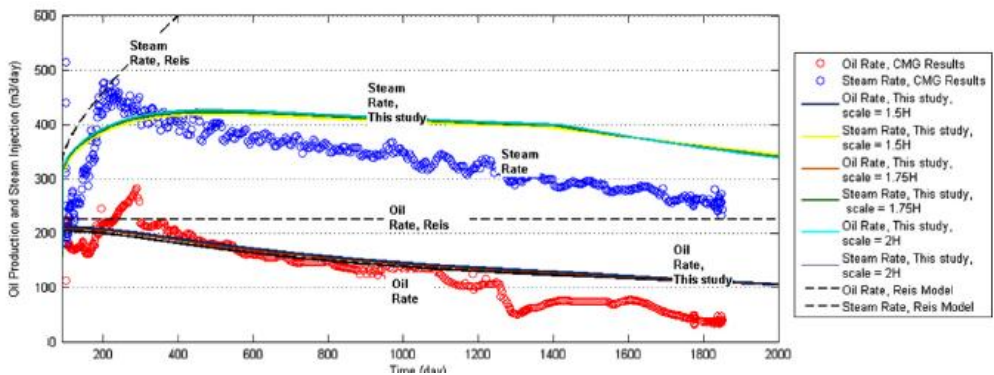


Figure 21. Comparison of steam injection and production rates between previous works and Sabeti et al. model [16].

ONGOING SAGD ISSUES

Among many contributions to further improve the SAGD process, one looks more demanding at the time. The application of Inflow Control Valves (ICVs) and Inflow Control Devices (ICDs) [37] has proved promising in horizontal wells during the past recent years. Implementing such devices in SAGD wells can be of magnificent usefulness especially in steam injection wells since the ability to inject the steam through desired zones prevents excessive heat losses and the process becomes further economical.

Reservoir heterogeneity around the horizontal wellbores brings several difficulty and losses to the process and inflow devices can help achieve better process efficiency. According to a number of authors, using ICDs can lower the SOR, result in more cumulative oil production, avoid steam breakthrough, reach effective steam distribution in the reservoir, improve recovery factors and so on [37-40]. By the way, this technology is still young and needs time to show all it has to offer.

CONCLUSION

A brief but lucid review of the SAGD process since its onset has been given in this chapter. Obviously, the keystone set by Butler was to endure modifications both from the geometrical point of view and the mathematical procedure. Fortunately, experimental and field data were available and this allowed for relatively satisfying model evaluations once one was proposed. During time, several authors tried to go deeper and scrutinize the process in order for more accurate simulations to be made and hence, year after year, model updates were promulgated. However, the trend has not ceased as semi-analytical models keep improving.

Of many factors affecting the process efficiency, the global preference has been to consider the most important ones that have immediate effects on the process. As a result, formation permeability, height, mathematical manipulations and geomechanics have been taken into account and studied as well as the geometry of the problem. The last considerable model is that presented in a work by Sabeti et al. in 2016 where an exponential geometry has been assumed for the steam chamber sidewise expansion.

Finally, among the new technologies introduced to the SAGD process, applying inflow control devices was named as it has shown a potential to remarkably enhance the efficiency through effective injection power and also to make it more economical as the amount of heat loss can be significantly lowered.

REFERENCES

- [1] Cardwell Jr, W. and R. Parsons, *Gravity drainage theory*. Transactions of the AIME, 1949. **179**(01): p. 199-215.
- [2] Dykstra, H., *The prediction of oil recovery by gravity drainage*. Journal of Petroleum Technology, 1978. **30**(05): p. 818-830.

-
- [3] Vogel, J., *Gravity drainage vital factor for understanding steam floods*. Oil and gas journal, 1992. **90**(48): p. 42-47.
- [4] Farouq Ali, S., *Steam injection theories: a unified approach*. 1982.
- [5] van Wunnik, J.N. and K. Wit, *Improvement of gravity drainage by steam injection into a fractured reservoir: An analytical evaluation*. SPE reservoir engineering, 1992. **7**(01): p. 59-66.
- [6] Pooladi-Darvish, M., W. Tortike, and S. Ali. *A new semi-analytical model for thermal recovery processes*. In *SPE Western Regional Meeting*. 1995. Society of Petroleum Engineers.
- [7] Butler, R., *A new approach to the modelling of steam-assisted gravity drainage*. Journal of Canadian Petroleum Technology, 1985. **24**(03): p. 42-51.
- [8] Reis, J.C., *A steam-assisted gravity drainage model for tar sands: linear geometry*. Journal of Canadian Petroleum Technology, 1992. **31**(10).
- [9] Azad, A. and R.J. Chalaturnyk, *An improved SAGD analytical simulator: Circular steam chamber geometry*. Journal of Petroleum Science and Engineering, 2012. **82**: p. 27-37.
- [10] Mozaffari, S., et al., *Numerical modeling of steam injection in heavy oil reservoirs*. Fuel, 2013. **112**: p. 185-192.
- [11] Reis, J.C., *A steam assisted gravity drainage model for tar sands: radial geometry*. Journal of Canadian Petroleum Technology, 1993. **32**(08).
- [12] Chung, K. and R. Butler, *Geometrical Effect Of Steam Injection On The Formation Of Emulsions Nn The Steam-Assisted Gravity Drainage Process*. Journal of Canadian Petroleum Technology, 1988. **27**(01).
- [13] Hashemi-Kiasari, H., et al., *Effect of operational parameters on SAGD performance in a dip heterogeneous fractured reservoir*. Fuel, 2014. **122**: p. 82-93.
- [14] Heidari, M., et al., *Effect of drainage height and permeability on SAGD performance*. Journal of Petroleum Science and Engineering, 2009. **68**(1): p. 99-106.
- [15] Sharma, J., *Advanced Analytical Modelling of Steam-Assisted Gravity Drainage and its Variants*. 2011, University of Calgary.
- [16] Sabeti, M., A. Rahimbakhsh, and A.H. Mohammadi, *Using exponential geometry for estimating oil production in the SAGD process*. Journal of Petroleum Science and Engineering, 2016. **138**: p. 113-121.
- [17] Wei, S., et al. *Steam chamber development and production performance prediction of steam assisted gravity drainage*. In *SPE Heavy Oil Conference-Canada*. 2014. Society of Petroleum Engineers.
- [18] Butler, R., G. McNab, and H. Lo, *Theoretical studies on the gravity drainage of heavy oil during in-situ steam heating*. The Canadian journal of chemical engineering, 1981. **59**(4): p. 455-460.
- [19] Sabeti, M., et al., *Estimation of effect of diffusion and dispersion parameters on VAPEX process*. Journal of Petroleum Science and Engineering, 2015. **132**: p. 53-64.
- [20] Keshtkar, S., M. Sabeti, and A.H. Mohammadi, *Numerical approach for enhanced oil recovery with surfactant flooding*. Petroleum, 2015.

-
- [21] Dianatnasab, F., et al., *Study of reservoir properties and operational parameters influencing in the steam assisted gravity drainage process in heavy oil reservoirs by numerical simulation*. Petroleum, 2016.
- [22] Butler, R., *New interpretation of the meaning of the exponent "m" in the gravity drainage theory for continuously steamed wells*. AOSTRA Journal of research, 1985. **2**(1): p. 67-71.
- [23] Duerksen, J. *Simulation of a Single-Well Injection/Production Steamflood (SWIPS) Process in an Athabasca Tar Sand*. In *SPE California Regional Meeting*. 1990. Society of Petroleum Engineers.
- [24] Reis, J., *The HASDrive process for oil recovery from tar sands. In Situ*,(United States), 1992. **16**(2).
- [25] Pooladi-Darvish, M. and S. Ali. *Steam heating of fractured formations containing heavy oil: basic premises and a single-block analytical model*. In *SPE Annual Technical Conference and Exhibition*. 1994. Society of Petroleum Engineers.
- [26] Pooladi-Darvish, M., W. Tortike, and S. Ali. *Non-isothermal gravity drainage under conduction heating*. In *Annual Technical Meeting*. 1994. Petroleum Society of Canada.
- [27] Alali, N., M.R. Pishvaie, and H. Jabbari, *A new semi-analytical modeling of steam-assisted gravity drainage in heavy oil reservoirs*. Journal of Petroleum Science and Engineering, 2009. **69**(3): p. 261-270.
- [28] Queipo, N.V., J.V. Goicochea, and S. Pintos, *Surrogate modeling-based optimization of SAGD processes*. Journal of Petroleum Science and Engineering, 2002. **35**(1): p. 83-93.
- [29] Akin, S., *Mathematical modeling of steam assisted gravity drainage*. SPE Reservoir Evaluation and Engineering, 2005. **8**(05): p. 372-376.
- [30] Akin, S., *Mathematical modeling of steam-assisted gravity drainage*. Computers and geosciences, 2006. **32**(2): p. 240-246.
- [31] Nukhaev, M.T., et al. *A new analytical model for the SAGD production phase*. In *SPE Annual Technical Conference and Exhibition*. 2006. Society of Petroleum Engineers.
- [32] Li, P., *Numerical simulation of the SAGD process coupled with geomechanical behavior*. 2006.
- [33] Collins, P.M. *Geomechanical effects on the SAGD process*. In *SPE International Thermal Operations and Heavy Oil Symposium*. 2005. Society of Petroleum Engineers.
- [34] Chalaturnyk, R.J., *Geomechanics of the steam-assisted gravity drainage process in heavy oil reservoirs*. 1996.
- [35] Azad, A. and R. Chalaturnyk. *Geomechanical coupling simulation in SAGD process; a linear geometry model*. In *Proceedings of the 3rd Canada-US (CANUS) Rock Mechanics Symposium and 20th Canadian Rock Mechanics Symposium, Rock Engineering in Difficult Conditions. Toronto, Canada*. 2009. Citeseer.
- [36] Wong, R. and J. Lau, *Surface heave induced by steam stimulation in oil sand reservoirs*. Journal of Canadian Petroleum Technology, 2008. **47**(01).
- [37] Shad, S. and M. Majdi Yazdi. *Wellbore modeling and design of nozzle-based inflow control device (ICD) for SAGD wells*. In *SPE Heavy Oil Conference-Canada*. 2014. Society of Petroleum Engineers.
- [38] Riel, A., et al. *An Innovative Modeling Approach to Unveil Flow Control Devices Potential in SAGD Application*. In *SPE Heavy Oil Conference-Canada*. 2014. Society of Petroleum Engineers.

- [39] Noroozi, M., et al. *Investigation of Orifice Type Flow-Control Device Properties on the SAGD Process Using Coupled Wellbore Reservoir Modeling*. In *SPE Heavy and Extra Heavy Oil Conference: Latin America*. 2014. Society of Petroleum Engineers.
- [40] Kyanpour, M. and Z. Chen. *A New Approach for Designing Steam Splitters and Inflow Control Devices in Steam Assisted Gravity Drainage*. In *SPE Heavy Oil Conference-Canada*. 2013. Society of Petroleum Engineers.

Chapter 3

OIL PRODUCTION OPTIMIZATION VIA OPTIMUM ARTIFICIAL LIFT DESIGN

*Abbas Khaksar Manshad,¹ Mehdi Jabbari,²
and Amir H Mohammadi^{3,4,5,*}*

¹Department of Petroleum Engineering, Abadan Faculty of Petroleum Engineering,
Petroleum University of Technology (PUT), Abadan, Iran

²Department of Petroleum Engineering, Omidiyeh Branch, Islamic Azad
University, Omidiyeh, Iran

³Discipline of Chemical Engineering, School of Engineering, University of KwaZulu-
Natal, Howard College Campus, Durban, South Africa

⁴Département de Génie des Mines, de la Métallurgie et des Matériaux, Faculté
des Sciences et de Génie, Université Laval, Québec, Canada

⁵Institut de Recherche en Génie Chimique et Pétrolier (IRGCP),
Paris Cedex, France

ABSTRACT

During the production of hydrocarbon under natural depletion, reservoir energy is recognized as the cause of fluid flowing into the well and producing in the surface. By producing from reservoir and decreasing pressure, natural production declines and eventually stops. Artificial Lift methods are needed when bottomhole pressure is not enough as to bring up the oil to the surface. This study presents optimization of the production conditions of a well by using artificial lift method. For this purpose, single well model is created to predict future production conditions in the well drainage area and the recommended optimum production conditions. In the next steps, we will try to present an optimal scenario for continuous production of intended well with evaluation of the parameters affecting artificial lift methods. Application of ESPs (Electric Submersible Pump) is also studied and compared with gas lift method. Finally, considering the technical and economic aspects of each method, different approaches are compared to determine the optimum production scenario via artificial lift designs. The results of this

* Corresponding author: Email: amir_h_mohammadi@yahoo.com AND a.h.m@irgcp.fr.

study show that both gas lift and ESP are able to achieve the desired well flow rate in the studied field. However, in terms of initial cost and net present value of the project, gas lift is more economical.

Keywords: optimum production, artificial lift, gas lift, electric submersible pump (ESP), cost

INTRODUCTION

Application of artificial lift techniques is a common practice of oil well production. The new main challenge for a field is optimal selection of lift technique for each well or for an entire field. Wrong decision can cause high production cost [1].

In this communication, the application of artificial lift techniques in an oil field in south west of Iran is investigated. Two practical techniques for this field are gas lift and electric submersible pump (ESP). For this purpose, 3 wells of the oil field A are studied. Based on the current understanding in this field, the reservoirs are relatively heterogeneous with medium to poor properties in the Bangeestan oil reservoirs. The support from the aquifer is expected to be very limited and the main reservoir energy is fluid expansion. Therefore, a rapid pressure decline will take place in the well drainage area as a result of oil production. The reservoir fluids in upper zones are heavy and together with high drawdown of the wells will result in a low flowing well head pressure. This will necessitate using artificial lift for maintaining the expected potential of the wells.

Many parameters are involved in a successful artificial lift operation. This study is an attempt to specify these parameters in such a way that the production and the operation's net present values are maximized. According to the recommended reservoir development plan, the initially allocated daily oil production rate for each well in field A is up to about 2000 B/d. The disadvantage of gas lift is the high investment on building up gas lift equipment on the surface. The advantage of gas lift is simple operation and management. For ESP, compared with gas lift, the initial investment is relative low and ESP can also be rented from ESP manufacturer. The workover and operating cost is more than gas lift. The results of this study will enable us to compare the gas lift with ESP and finally, the optimum and best option will be selected.

PVT Model

The well models in this work are prepared by PROSPER software. The first step in the simulation procedure of the well models is to construct a PVT model for the reservoir fluid [2].

The Black oil PVT model is used for well fluids in this study. When both basic fluid data and some PVT laboratory measurements are available, the program can modify the black oil model correlations to the measured lab data [2].

According to the correlation parameters, the best correlations fitted with measured data are identified for studied wells.

Table 1. Best overall fit correlation of PVT models

	A-02	A-03	A-04
P_b, R_s, B_o	Glaso	Standing	Standing
Oil viscosity	Beal et al	Beal et al	Beal et al

Table 2. Summary of well data

	Well-02	Well-03	Well-04
IPR model	PI entry	PI entry	PI entry
Reservoir pressure (psia)	4950	4200	4200
Reservoir temperature (°F)	214	208	208
Water cut, %	0	0	0
Total GOR, (scf/STB)	308	200	157
k, md	4.3	8.7	11.3
Oil gravity	20	22	22
Gas specific gravity	1.8	1.15	1.7
TVD, m	3250	2972	2800
Casing ID (in)	6.105	6.105	6.105
Tubing ID (in)	4.5	4.5	4.5
Productivity index (STB/day/psi)	0.68	0.71	0.85
Wellhead pressure, psi	214	208	208
Rate, STB/D	126	510	396

VLP Matching

PROSPER uses a non-linear regression to tune the VLP correlations to best match with the measured data [3]. Parameters of software found very much close to unity with Fancher Brown correlation for current well test data of well A-02.

Table 3. Best match correlations for VLP of wells

Well	Best match correlation
Well #02	Fancher Brown 1.24 1.00
Well #03	Beggs and Brill 1.04 1.00
Well #04	Duns and Ros Original 1.04 1.00

IPR Matching

This step ensures that PROSPER model can reproduce the well test. When the desired correlation is selected, in this step the IPR is tuned so that the intersection of VLP and IPR fits to the well test rate measurements [3].

Gas Lift Design

To design gas lift in studied wells, there are a number of parameters that must be selected optimally. For this purpose, a series of system analysis are performed to consider the effects of these parameters and select optimum values for them.

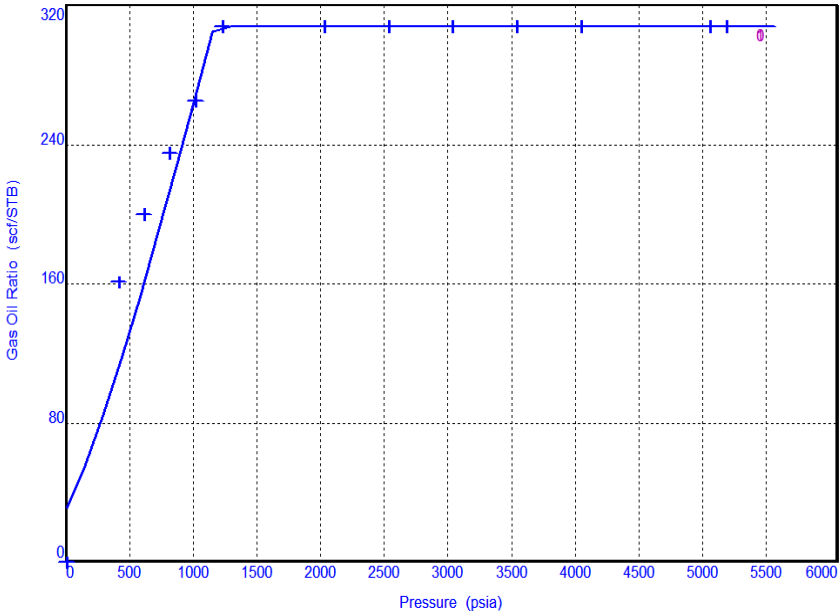


Figure 1. Plot of measured GOR data and best matched correlation for well A-02.

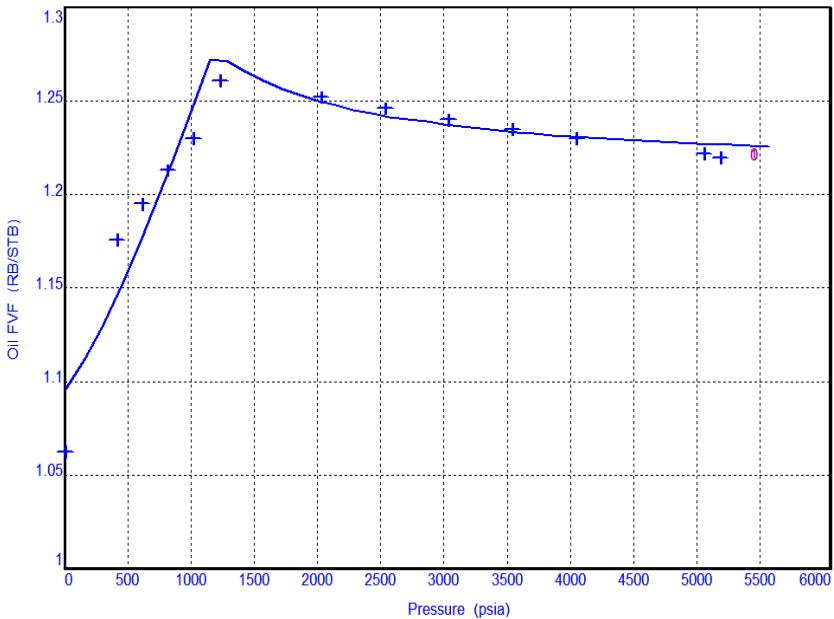


Figure 2. Plot of measured B_o data and best matched correlation for well A-02.

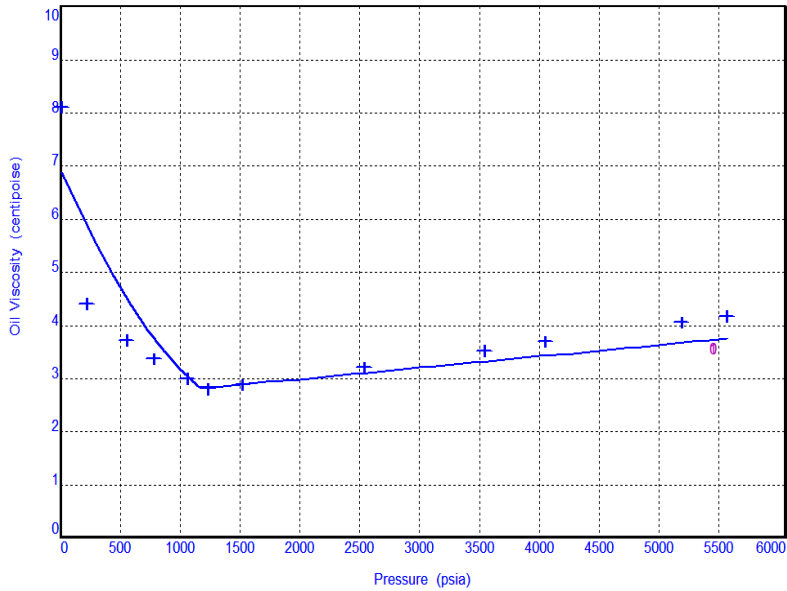


Figure 3. Plot of measured viscosity data and best matched correlation for well A-02.

Table 4. Data comparison for well A-02

	Well #02		Well #03		Well #04	
	Liquid rate (STB/D)	BHP (psia)	Liquid rate (STB/D)	BHP (psia)	Liquid rate (STB/D)	BHP (psia)
Well test Data	120.0	4779.41	183.0	4074.13	173.0	3996.89
Prosper Data	115.5	4780.15	185.6	4074.06	172.5	3997.01
Deviation (%)	-3.75	0.015587	1.4	-0.001815	-0.26491	0.0029857

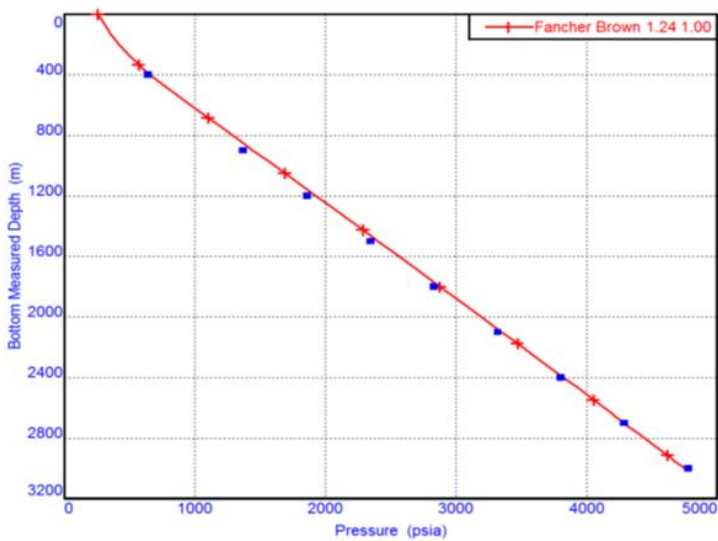


Figure 4. Best matched correlation and measured data of well A-02.

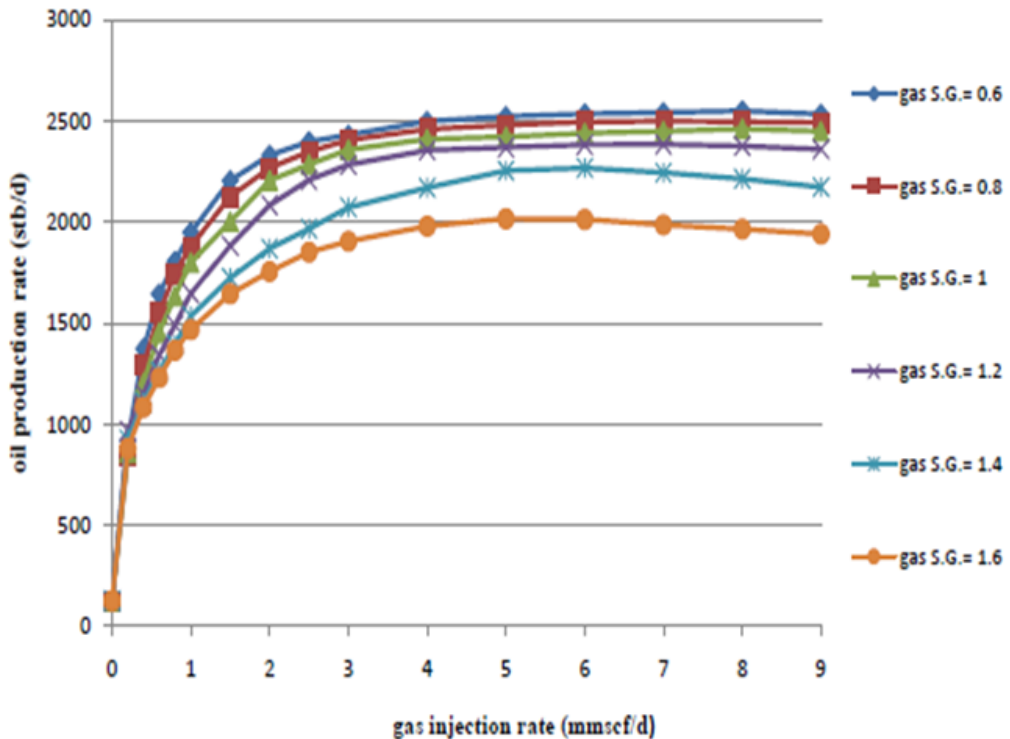


Figure 5. Effect of gas injection pressure on GLPC in well A-02.

Gas Injection Pressure

The surface gas injection pressure has a direct impact on gas-lift performance because of its effect on the injection depth. Increasing the surface injection pressure allows for deeper gas injection. However, once the gas is injected at the end of the tubing string, an increase in the injection pressure will not benefit for gas-lift operation. This effect is illustrated in Figure 5 where the results corresponding to injection pressures from 2000, 2200 and 2400 psig coincide. As a result, increasing the injection pressure beyond 2000 psig only increases the compression cost.

Injection Gas Characteristics

As shown in the Figure 6, at a constant gas injection rate, the higher the gas specific gravity, the lower the oil production rate. Although by the increase in gas specific gravity, the injection depth can be increased and consequently increased the oil production but on the other hand will cause an increase in the bottom hole pressure which decreases the production rate. According to this analysis, an injection gas with specific gravity of 0.8 is selected for gas lift design.

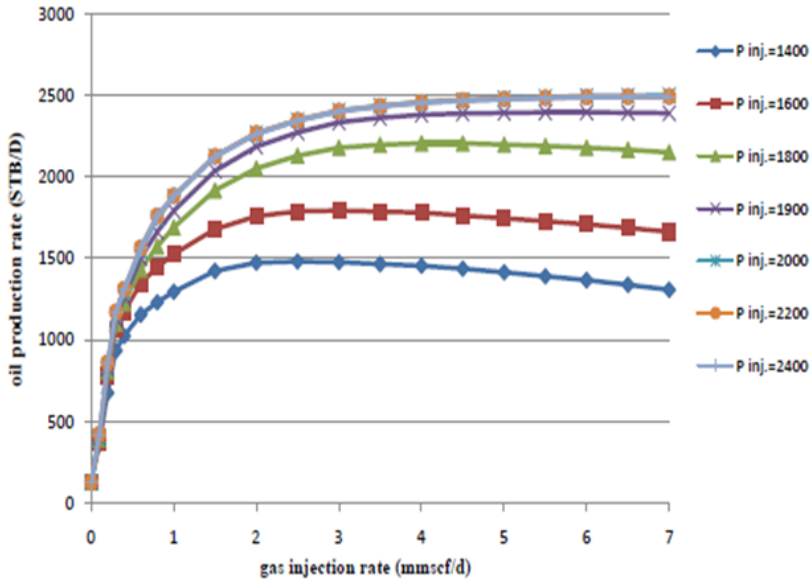


Figure 6. Effect of injected gas specific gravity on GLPC in well A-02.

Tubing Diameter

In determining the size of tubing installed in a gas lift well, it is important to consider the producing capabilities of the reservoir. Improperly sized tubing (either too large or too small) can result in a gas lift installation that will produce at less than maximum fluid rate. Referring to Figure 7, it can be seen that definite increases in fluid production rate can be obtained with larger tubing sizes. It can be concluded that the best selection for the size of tubing is 4.5 in.

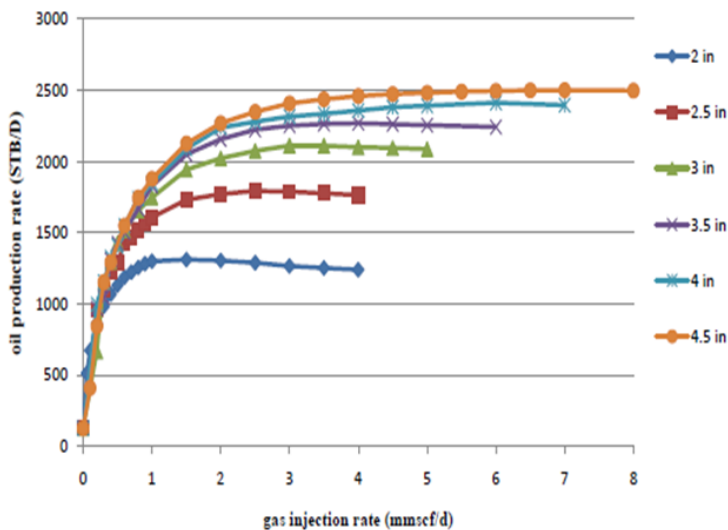


Figure 7. Effect of tubing inside diameter on GLPC in well A-02.

Design Input Data

According to the input parameters determined in previous sections and some other parameters, gas lift can be designed. Desired pressure drop across valves of 150 psi is entered to ensure the well and gas injection system stability. From well test data, a static gradient of 0.376 psi/ft is assumed as the load fluid before gas lift start. Minimum spacing between valves is set to 60 m and also maximum injection depth for each well is set.

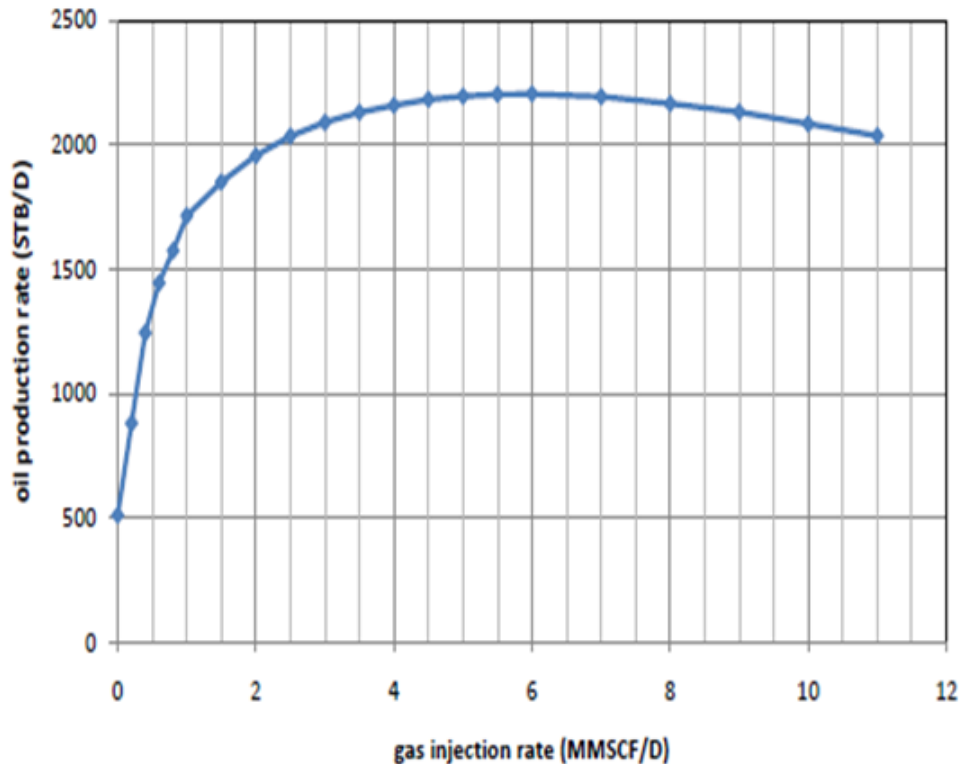


Figure 8. Gas lift performance curve for well A-02.

Table 5. Result of the gas lift design

	A-02	A-03	A-04
Optimum gas injection rate (MMSCF/D)	6	5.5	7.5
Maximum production rate (STB/D)/D)	2500	2204	2340
desired liquid rate (STB/D)	2000	2000	2000
Injected gas rate for desired liquid rate (MMSCF/D)	1.25	2.3	1.2

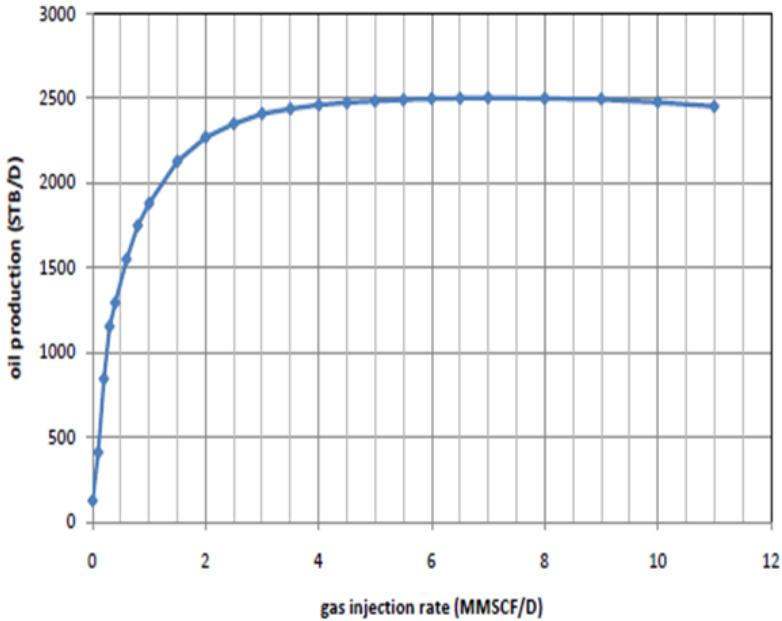


Figure 9. Gas lift performance curve for well A-03.

ELECTRICAL SUBMERSIBLE PUMP DESIGN

First step in design of ESP installation using PROSPER is entering some input data for studied wells. These are listed in the Table 6.

After selecting each pump from database of the software, it can be displayed the design operating point superimposed on the pump performance curve and check which pump has the operating point close to the best efficiency line.

Once a pump has been selected, the pump efficiency is known and the motor power requirement can be calculated. When the motor power and voltage have been determined, a suitable cable must be selected.

The operating point should lie between the minimum and maximum operating range of the pump performance curve to ensure an acceptable run life. As shown in the figure for well A-02 the operating points of future conditions falls in operating range of the pump and close to the best efficiency line. Selected pump needs 584 stages and will require 178 HP at the design rate.

Table 6. ESP design input data

	A-02	A-03	A-04
Pump Depth (Measured) (m)	2000	1200	2000
Operating Frequency (Hertz)	50	50	50
Maximum Pump OD (inches)	5.7	9	6.105
Length Of Cable (m)	2030	1230	2030
Gas Separator Efficiency (%)	80	0	0
Design Rate (STB/day)	2000	2000	2000
Top Node Pressure (psig)	200	200	200

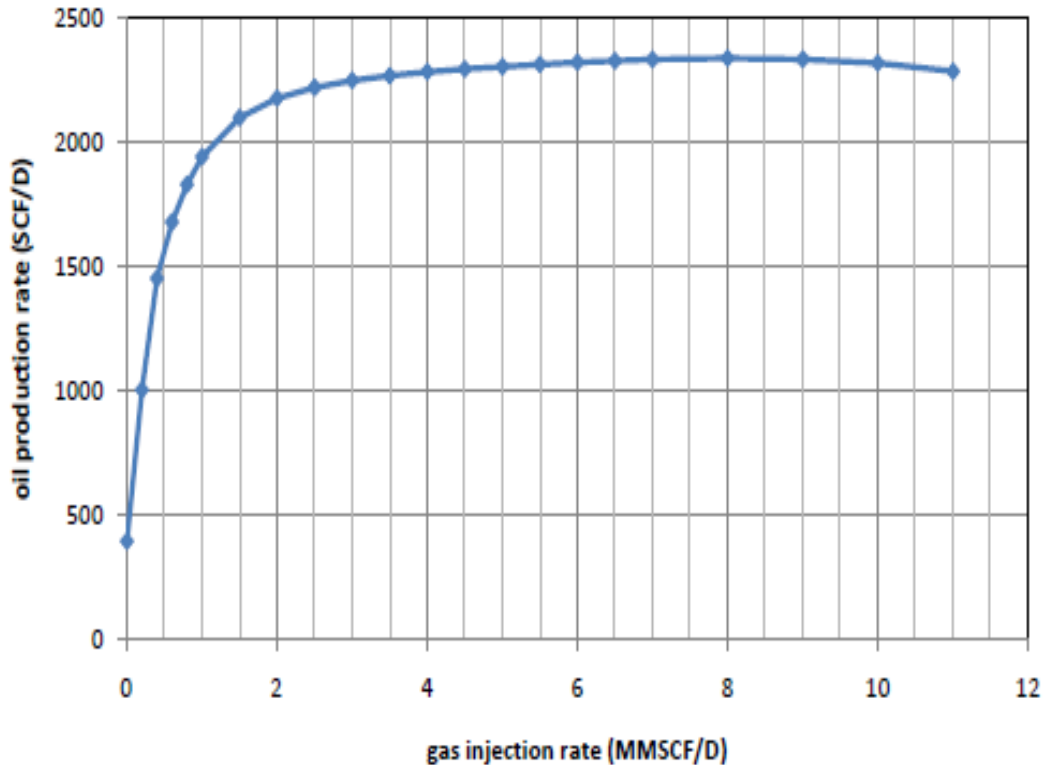


Figure 10. Gas lift performance curve for well A-04.

Table 7. Result of the ESP design

	A-02	A-03	A-04
Design Rate (STB/day)	2000	2000	2000
Number Of Stages	584	180	175
Power Required (hp)	179.19	60.0964	111.15

Table 8. Detailed gas lift installation costs

Item	Description	Unit	Unite price (1000\$)	No. of units	Total cost (million \$)	Total cost for one well (million \$)
1	Work over	Job	900	3	2.7000	0.9
2	Gas lift valve	No	2.5	5	0.0125	0.0041
3	Packer	No	100	3	0.3000	0.1000
4	Gas lift station	Hp	3.5	701	2.4535	0.8178
5	Gas lift ring	in-km	10	54	0.5400	0.18
6	Ten years overhaul	Job	66	10	2.0000	0.666
7	Power	kwh	0.0001	45814800	9.302	3.1
8	Power network	Kw	523	0.0182	0.006
Total cost					17.3262	5.774

ECONOMICAL EVALUATION

Before making a final decision a thorough economical analysis should be performed. As previously mentioned, it is the profitability of a project that has to be the final decision criteria. In this section, the value of each project through its entire lifetime taking capital and operating costs into account. These estimations can give a good indication of the project magnitude. The numbers vary depending on different parameters such as interest rate and operating company.

Table 9. Detailed ESP installation costs

Item	Description	Unit	Unit price (1000\$)	No. of units	Total cost (million \$)	Total cost for one well (million \$)
1	Work over	Job	900	9	8.10000	2.7000
2	Pump string	No	550	9	4.95000	1.6500
3	Power	Kwh	0.0001	29959200	6.08283	2.0276
4	Power network	Km	77.523887	9	0.69870	0.2329
		Kwh	342	0.01174	0.0039
5	Wellhead modification	No	150	3	0.4500	0.1500
Total cost					20.2932	6.7644

GAS LIFT INSTALLATION COST

The gas lift installation cost for wells which are studied in this project along 10 years duration is shown in Table 3.

ESP INSTALLATION COST

Costs of operating an ESP installation is shown in Table 4.

PROJECT PROFITABILITY

In this section, the previous economic results are used to consider the profitability evaluation of the projects. There are several methods to evaluate the profitability of projects. The Net present value (N.P.V.) method is used here. In this method, the valuation of all the project costs and revenues are based on the year 2016 and the interest rate of 15%. The total production rate that is obtained from implementation of gas lift and ESP methods in the studied wells is 6000 stb/d. It is required to forecast the production rate of each method in the coming years. For this purpose, according to the reservoir condition, an average reservoir pressure drop of 50 psi per year is assumed. Accordingly, the production of each method is anticipated for future years and income of projects is determined for next 10-year duration. These income is determined based on 50 percent of oil sale revenue and oil price of 70\$ per barrel.

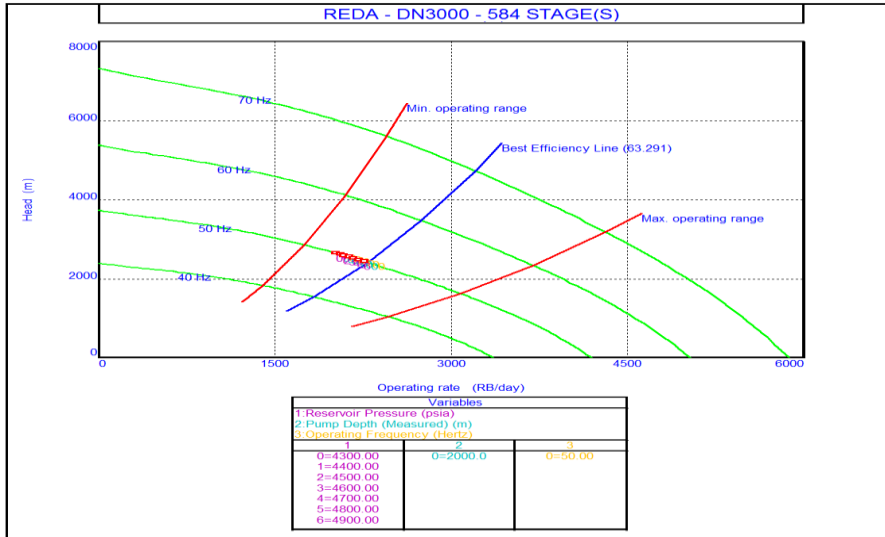


Figure 11. Pump performance curve of well A-02.

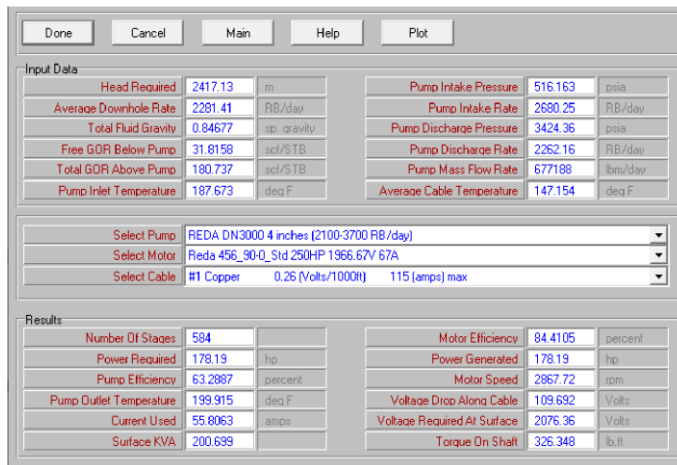


Figure 12. ESP design results of well A-02.

Table 10. Annual cost and revenue of ESP project from 2016 to 2026 (million \$)

YEAR	Total operating cost	Capital cost	Total cost (operating + capital)	cumulative cost	Oil sale revenue	50% Oil sale revenue	Net revenue
2016	0	8.810	8.810	8.810	0	0	-8.810
2017	0.300	0	0.300	9.110	124.480	62.240	61.940
2018	0.345	0	0.345	9.455	121.822	60.911	60.567
2019	0.396	0	0.396	9.851	119.165	59.583	59.186
2020	1.824	0	1.824	11.675	116.457	58.228	56.404
2021	0.524	0	0.524	12.199	113.749	56.874	56.350
2022	0.603	0	0.603	12.802	111.015	55.507	54.905
2023	0.693	0	0.693	13.495	108.255	54.128	53.435
2024	3.191	0	3.191	16.686	105.522	52.761	49.570
2025	0.916	0	0.916	17.602	102.711	51.356	50.439
2026	1.054	0	18.656	100.028	50.014	50.014	48.960

Table 11. Annual cost and revenue of gas lift project from 2016 to 2026 (million \$)

YEAR	Total operating cost	Capital cost	Total cost (operating + capital)	cumulative cost	Oil sale revenue	50% Oil sale revenue	Net revenue
2016	0	6.024	6.024	6.024	0	0	-6.024
2017	0.556	0	0.556	6.58	125.093	62.546	61.9904
2018	0.64	0	0.64	7.22	122.896	61.448	60.80775
2019	0.736	0	0.736	7.956	120.749	60.375	59.63865
2020	0.846	0	0.846	8.802	118.526	59.263	58.41723
2021	0.973	0	0.973	9.775	116.304	58.152	57.1788
2022	1.119	0	1.119	10.894	114.030	57.015	55.89583
2023	1.287	0	1.287	12.181	111.756	55.878	54.59085
2024	1.48	0	1.48	13.66	109.635	54.818	53.33753
2025	1.702	0	1.702	15.362	107.463	53.732	52.02965
2026	1.957	0	1.957	17.319	105.189	52.595	50.638

CONCLUSION

According to the results of this study, a total gas of 4.75 MMscf/day at the high pressure of 2000 psig can increase the total production of these three wells from 1032 to 6000 stb/day. Furthermore, the total power of 350 HP is required to run ESP for these wells to achieve the same oil production rate as that is considered in gas lift design. For this field, both gas lift and ESP are able to achieve the desired flow rate from these wells. But, both in terms of initial cost and net present value of the project, gas lift is more economical. The initial and operating costs shown are relative and may change with different cost of procurement, electricity price, number of wells or different operating company. Since the costs of each method are relatively close together, changing any of these parameters may alter the preferred method.

REFERENCES

- [1] Khasano, M. M., Khabibullin R. A., Pashali A. A., Semenov, A. A., "Approach to selection of the optimal lift technique in Vankor Field", paper SPE 134774 presented at the Annual Technical Conference and Exhibition held in Florence, Italy, September 2010.
- [2] Ibrahim, A. M.: "Optimization of Gas Lift System in Varg Field", MSc. Thesis, The department of Petroleum Engineering of Stavanger University, 2007.
- [3] Beggs, H. D., "Production Optimization Using Nodal Analysis", OGCI and Petro-skills Publications, Tulsa, Oklahoma, Second Edition, 2003.
- [4] Petroleum expert limited, "PROSPER user manual version 10", Integrated Production Modeling Toolkit (IPM), May 2008.

Chapter 4

**POLYVINYL ALCOHOL (PVA) AS AN EMULSIFYING
AGENT FOR VISCOSITY REDUCTION OF
HEAVY AND EXTRA-HEAVY OILS**

***Olalekan S. Alade^{1,2}, Kyuro Sasaki¹, Bayonile Ademodi²,
Adeniyi S. Ogunlaja³, Yuichi Sugai¹
and Ryo Ueda⁴***

¹Resources Production and Safety Engineering Laboratory, Department of Earth
Resources Engineering, Kyushu University, Fukuoka, Japan

²Petroleum and Petrochemical Engineering Laboratory, Department of Chemical
Engineering, Obafemi Awolowo University, Ile-Ife,
Osun State, Nigeria

³Department of Chemistry, Nelson Mandela Metropolitan University,
Port-Elizabeth, South Africa

⁴Research Center, Japan Petroleum Exploration, CO., Ltd., Chiba, Japan

ABSTRACT

Heavy and extra-heavy oils represent important energy resources and have contributed significantly to the world energy supply. Emulsification technology (specifically, formation of oil-in-water emulsion) has been considered an innovative approach to reduce the high viscosity of heavy oil and subsequently cut production and transportation costs. However, resolution of emulsion remains a costly task. A promising solution to this problem is the use of polyvinyl alcohol (PVA) in dispersing heavy oil particle in aqueous solution to form emulsion which is easy to resolve thereby nullifying the need for expensive demulsification process. Although PVA has been used in many industrial applications due to its excellent properties, applications in heavy oil recovery and transportation have not received adequate attentions. In this article, the basic technical aspects of emulsification technology in reducing viscosity and improving flow property of heavy oil are presented. Moreover, properties of PVA and few research efforts on its suitability as an emulsifying agent in heavy and extra-heavy oil

emulsification are reviewed. This is with the aim of creating further awareness on the use of the chemical to solve heavy oil flow problems.

1. INTRODUCTION

The need for continuous energy provisions is unavoidable due to increasing world energy consumption. As shown in Figure 1, continuous increase in the world energy consumption from 549 quadrillion Btu in 2012 to 815 quadrillion Btu in 2040 has been forecasted (U.S. EIA, 2016). Therefore, various energy resources including the unconventional hydrocarbons, and renewable biobased ones have been considered as suitable alternatives to the popular conventional hydrocarbons such as crude oil.

Crude oil as an energy source plays critical roles in the world energy supply and the global economy at large (Elraies and Tan, 2012). Presently, the unconventional source of crude oil including heavy oil, extra heavy oil (bitumen), and shale oil have become significantly important due to their relative abundance (see Figure 2). About six trillion barrels of these resources are deposited in different locations worldwide with more than 2 trillion barrels oil equivalent of natural bitumen available in Canada (Clark et al., 2007). The reserves of natural bitumen (extra-heavy oil) and heavy oil, deposited in the south-western region of Nigeria have been estimated as well over 38 billion barrel oil equivalent.

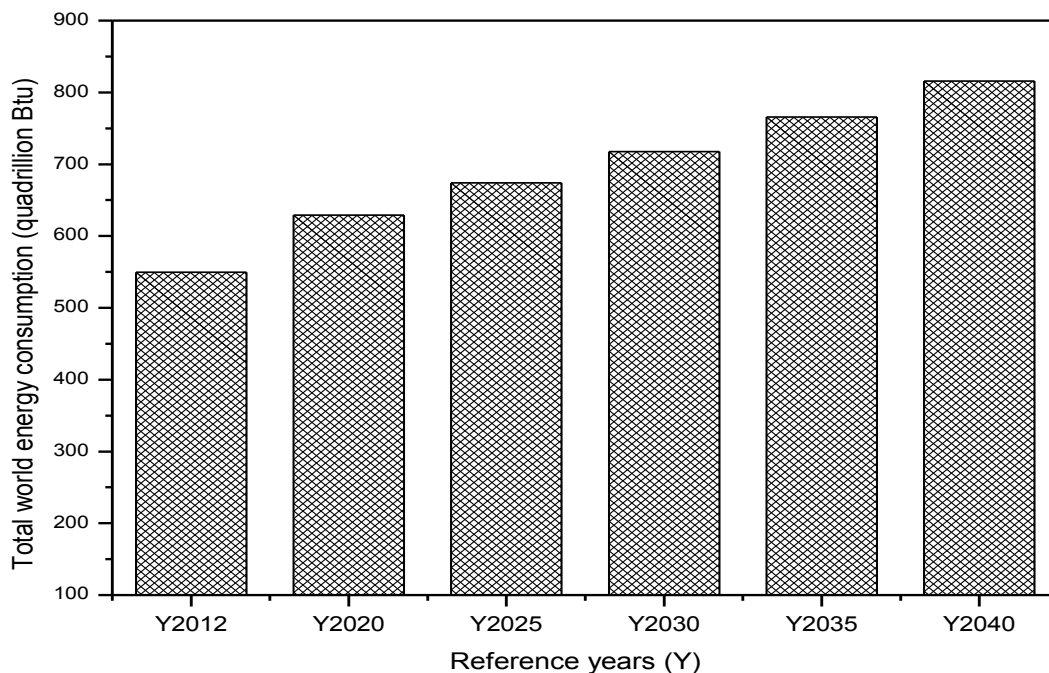


Figure 1. Projection of world total energy consumption, reference case 2012 – 2040 (Adapted from: US EIA, May, 2016).

However, the intrinsic high viscosity (and associated difficulties in recovery and production) compounded with the current regime of low price oil (Figure 3) has negatively

affected different stake holders in the heavy oil and bitumen production industries. Accordingly, concerns have recently been raised that the popular thermal fluid injection processes of bitumen recovery including the steam assisted gravity drainage (SAGD) may no more be economically sustainable considering the high cost of steam generation and continual fall in oil prices (WHOC, 2016). Therefore, a holistic approach to tackling these challenges is essentially to cut production cost.

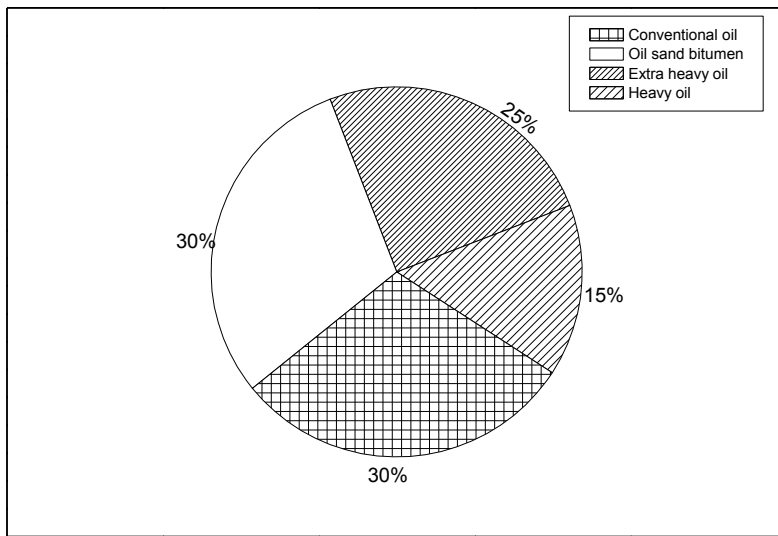


Figure 2. Total world oil reserves.

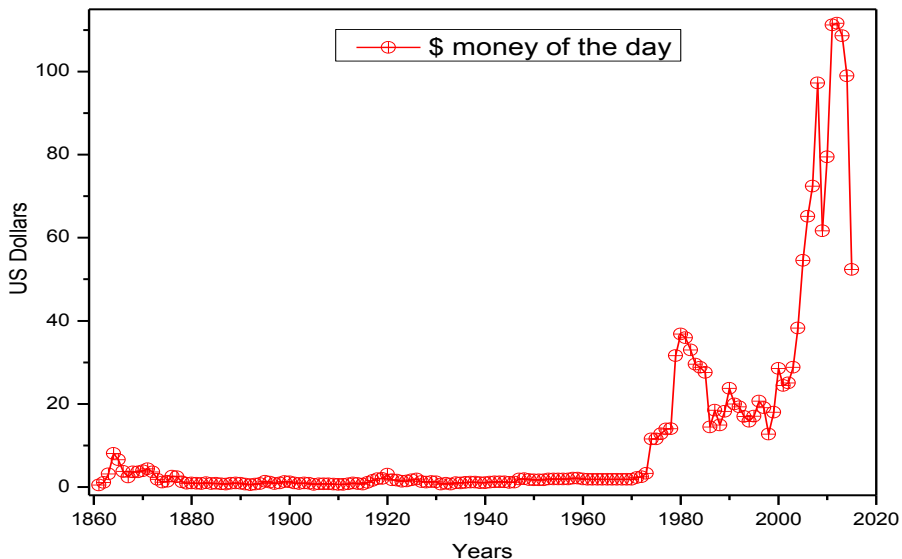


Figure 3. Crude oil prices 1861 – 2015 (BP statistical review of world energy, 2016).

An innovative means of solving viscosity problem and subsequently increasing production with relatively lower cost is the application of emulsification technology

(specifically, formation of oil-in-water emulsion) in enhanced recovery of heavy oil (Fletcher et al., 2012; Nguyen and Balsamo, 2013; Alade et al., 2016a; Alade et al., 2016b) and pipeline transportation (dos Santos et al., 2011; Martinez-Palou et al., 2011). Dispersion of heavy oil particle in water as oil-in-water emulsion assisted with surfactants has been viewed as an efficient technology for both in-situ and ex-situ viscosity reduction of heavy oil (Al-Roomi et al., 2004; Ashrafizadeh and Kamran, 2010; dos-Santos et al., 2011; Martinez-Palou et al., 2011; Fletcher et al., 2012; Nguyen and Balsamo, 2013; Martinez-Palou et al., 2015; Alade et al., 2016a). At lower processing cost, emulsification technology offers advantages such as viscosity reduction as low as 50 mPa.s (dos-Santos et al., 2011; Martinez-Palou et al., 2011) and reduction in the pipe corrosion (e.g., in the crudes with high sulfur content) since water is the continuous phase and crude oil has no contact with the pipe wall (Ashrafizadeh and Kamran, 2010).

2. DEFINITION AND ORIGIN OF HIGH VISCOSITY OF HEAVY OIL

2.1. Definition and Categorization

The generic term heavy oil has been arbitrarily used to describe both the heavy oils that require thermal stimulation of recovery from the reservoir and the bitumen (or extra-heavy oil) in bituminous sand formations (see Figure 4) from which the heavy bituminous material is recovered by mining operation (Speight, 2006). In addition, bitumen has generally been defined as an involatile, adhesive and waterproofing material derived from crude petroleum (as vacuum residue), or present in natural asphalt, which is completely or nearly completely soluble in toluene, and very viscous or nearly solid at ambient temperatures (Lesueur, 2009; Redelius, 2015).

Furthermore, petroleum and the equivalent term crude oils generally include various materials consisting of mixtures of hydrocarbons and other compounds containing variable amounts of sulfur, nitrogen, and oxygen, which may vary widely in volatility, specific gravity, and viscosity (Speight, 2006). This may exist as gas at normal temperatures and pressures (composed of small hydrocarbon molecules), or as liquids at normal temperatures and pressures, when it is composed of larger hydrocarbon molecules (McCain, 1990). The liquid petroleum is chemically classified based on the structure of the dominant molecules in the mixture. As an overall descriptor, the chemical nature of the crude oil is generally described as paraffinic, naphthenic or aromatic if a majority of saturate, cyclic or aromatic structures, respectively, are present (Speight, 2006). Consequently, the combinations of the terms paraffinic, naphthenic, aromatic, and asphaltic have been used in categorizing them (McCain, 1990). Moreover, various systems of classifications based on different standpoints including hydrocarbon resource, chemical composition, correlation index (CI – developed by the U.D. Bureau of Mines), viscosity, density, API gravity, carbon distribution, viscosity-gravity constant (VGC),

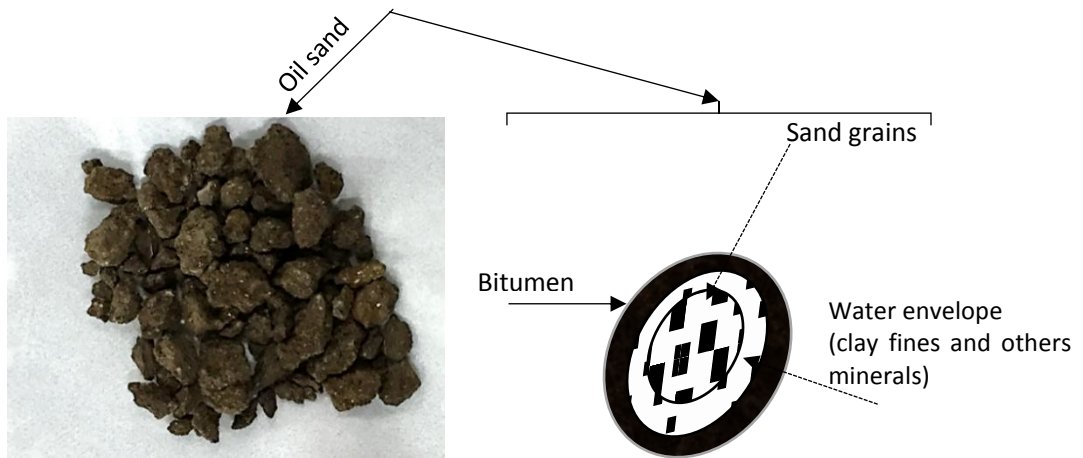


Figure 4. Sample of oil (tar) sand containing bitumen.

UOP Characterization Factor (K – calculated from API gravity and distillation or viscosity data), pour point etc. have been used in categorising crude oil. The viscosity can be related with temperature using viscosity-temperature models such as the Arrhenius equation defined as given in Eqn. 1.

$$\mu_{(T)} = \mu_{(o)} \exp\left(\frac{E_a}{RT}\right) \tag{1}$$

where $\mu_{(T)}$ is the viscosity (mPas) at temperature, T (K), $\mu_{(o)}$ is a coefficient which can be derived from the experimental data, E_a is the activation energy (kJ/mol), and R is the universal gas constant ($8.3144598 \text{ Jmol}^{-1}\text{K}^{-1}$).

The American Petroleum Institute (API) gravity is defined using Eqn. 2 as:

$$API \text{ gravity} = \frac{141.5}{S.G., \text{at } 60^\circ F} - 131.5 \tag{2}$$

Thus, as illustrated in Figure 5, the conventional light crude oil has viscosity of 10 – 100 mPas at the reservoir temperature and pressure, and greater than 20° API gravity. Crude oil is categorized as heavy oil if they have the viscosity between $10^3 - 10^5$ mPas, and lower than 20° API, and are referred to as extra heavy oil or bitumen if it has lower than 10° API with the viscosity of up to 10^6 mPas or greater at the reservoir conditions.

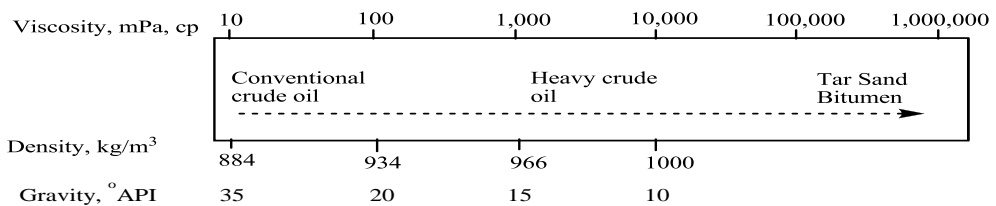


Figure 5. Classification of crude oil according to the API gravity and viscosity. Adapted from Speight (2006).

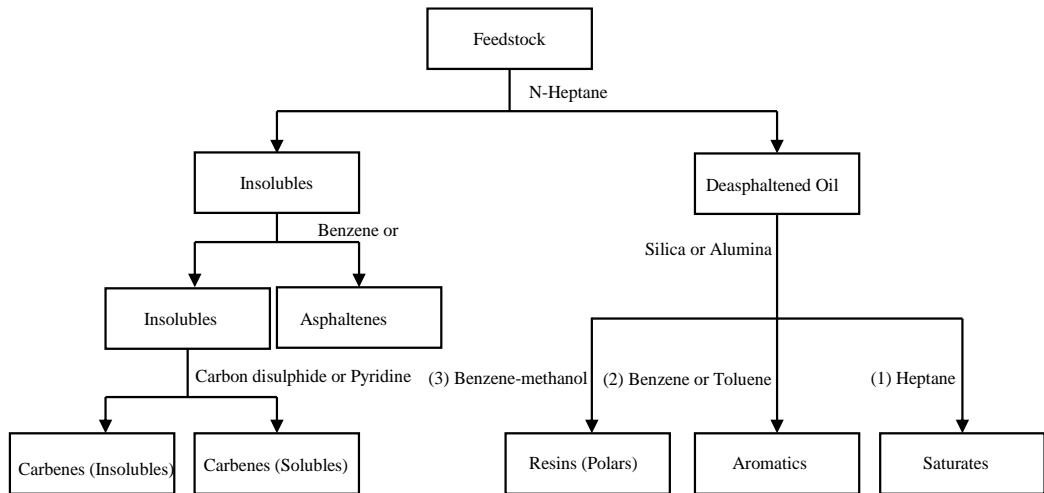


Figure 6. Simplified representation of the fraction of petroleum. Adapted from Lesueur (2009).

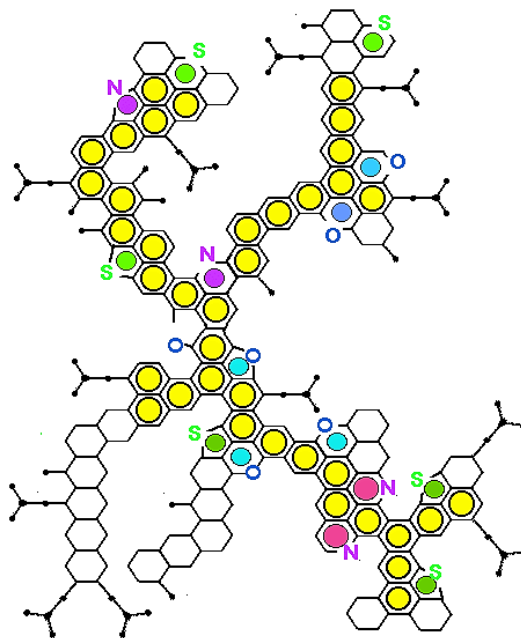


Figure 7. Possible structure of asphaltene showing sulphur and Nitrogen containing compounds (http://mansoori.people.uic.edu/Asphaltene.Molecule_html).

2.2. Origin of High Viscosity of Heavy Oil

The high viscosity and low API gravity of heavy oils (including bitumen) are due to the presence of high concentration of asphaltene as well as a relative low proportion of low molecular weight compounds which represent lack of light ends (Lesueur, 2009; Martinez-Palou et al., 2011). Generally, fractionation of crude oil using specific solvent leads to

identification of four main chemical families: saturates, aromatics, resins, asphaltenes (SARA) as shown in Figure 6.

Asphaltene molecules (Figure 7) are the heaviest and most aromatic, polar fraction of a crude oil and constitute a class of substances defined on the basis of their solubility in organic solvents i.e., they are soluble in toluene but insoluble in alkanes such as *n*-pentane (Saniere et al., 2004). In addition, the more viscous crude oils are characterized by the presence of metal-containing constituents, notably those compounds that contain vanadium and nickel, in significant amounts up to several thousand parts per million and can have serious consequences during their processing in the refinery and other uses (Speight, 2006; Clark et al., 2007).

3. EMULSION AND EMULSIFICATION PROCESS AS RELATED TO THE PETROLEUM INDUSTRIES

3.1. Basic Concept of Emulsification and Types of Emulsion

Emulsion is basically a liquid-liquid colloidal system in which particles of one liquid is dispersed in the other (Shaw, 2003). Colloid science concerns systems in which one or more of the components has at least one dimension within the nanometre (10^{-9} m) to micrometre (10^{-6} m) range, i.e., it concerns, in the main, systems containing large molecules and/or small particles. The major examples of colloidal system are listed in Table 1.

The technological and economic importance of emulsification process and/or emulsion in the food, chemical, pharmaceutical and petroleum industries cannot be underestimated (Pal, 1994b; Badolato et al., 2008; Abdel-Raouf, 2012; Wong et al., 2015). Emulsification is a collective process which involves formation, characterization, and application of emulsion. There is originally the presence of interfacial barrier (known as the interfacial tension – IFT) which prevents mixing of two immiscible liquids.

Table 1. Practical Examples of Colloidal Disperse Systems (Shaw, 2003)

Dispersed phase (particle)	Dispersed Medium	Name of system	Example
Liquid	Gas	Liquid aerosol	Fog, liquid sprays
Solid	Gas	Solid aerosol	Smoke, dust
Gas	Liquid	Foam	Foam on soap solutions
Liquid	Liquid	Emulsion Sol, colloidal	Milk, mayonnaise Au sol, AgI sol,
Solid	Liquid	solutions	toothpaste
Gas	Solid	Solid foam	Expanded polystyrene
Liquid	Solid	Solid emulsion	Opal, pearl
Solid	Solid	Solid suspension	Pigmented plastics

Essentially, the formation of emulsions needs an energy input, which is traditionally achieved through shaking, stirring or some other kind of intensive dynamic and/or static mixing processes (Bennion et al., 1993; Hasan et al., 2010) and is aided by surface active substance (i.e., surfactants) which assists in lowering the IFT and stabilizes particles of the dispersed medium (Clausse et al., 2005; Fradette et al. 2007).

Emulsification by mechanical agitation, illustrated in Figure 8a, can be defined, according to the volume specific energy input or the energy density E_v to form emulsion, as the ratio of energy input E per unit homogenized volume of the system – Eqn. 3 (Gingras, et al., 2005; Jochen, 2008).

$$E_v = \frac{\text{Energy input } E}{\text{homogenized volume } V} = \frac{P_w}{\dot{V}} \quad (3)$$

where E_v is the specific energy (Jm^{-3}), E is energy input (J), V is the volume (m^3), P_w is the power consumption (W) and \dot{V} is the volumetric flow rate (m^3s^{-1}).

The average particle diameter (x) is related to the specific energy as given in Eqn. 4.

$$x_{3,4} = \alpha(E_v)^\beta \quad (4)$$

where $x_{3,4}$ is the volume mean diameter of particle (μm), α , and β are the constants depending on the system.

Comprehensive reports on emulsion types, usefulness (Pal, 1994a and 1994b; Martínez-Palou et al., 2011; Abdel-Raouf, 2012) and the categories of desirable and undesirable ones in the petroleum industry are listed in Table 2. As illustrated in Figure 8b, the popularly reported types of emulsion encountered in the petroleum industry includes oil-in-water (O/W), water-in-oil (W/O), and complex ones (water-in-oil-in-water (W/O/W), water-in-oil-in-oil (W/O/O) etc.) (Pal, 1994a and 1994b; Martínez-Palou et al., 2011). Usually, during the production of crude oil, due to mixing force (shearing, turbulence or surface contact between the oil and liquid phases) and the presence of the natural surface active substances (such as asphaltene and resin in the crude oil), and clay, an undesirable water-in-oil emulsion is mostly formed in the reservoir or in the flow line (Antes et al., 2015; Martínez-Palou et al., 2015; Wong et al., 2015; Wen et al., 2016). An oil-in-water (O/W) emulsion is a liquid-liquid colloidal system in which the particles of oil are dispersed in continuous water phase. On the other hand, water-in-oil (W/O) emulsion contains water molecules dispersed in a continuous oil phase. While W/O (and complex forms of emulsion) is usually associated with crude oil production where mixing occurs or during the EOR method using thermal fluid (steam) which subsequently leads to increased viscosity (Bennion et al., 1993; Al-Bahlani and Babadagli, 2009), the O/W emulsion leads to reduction in apparent viscosity of the original oil (due to the presence of continuous water phase) and is desirable in both heavy oil production and long distance pipeline transportation of heavy oil including bitumen (Martínez-Palou et al., 2011; Alade et al., 2016a and 2016b).

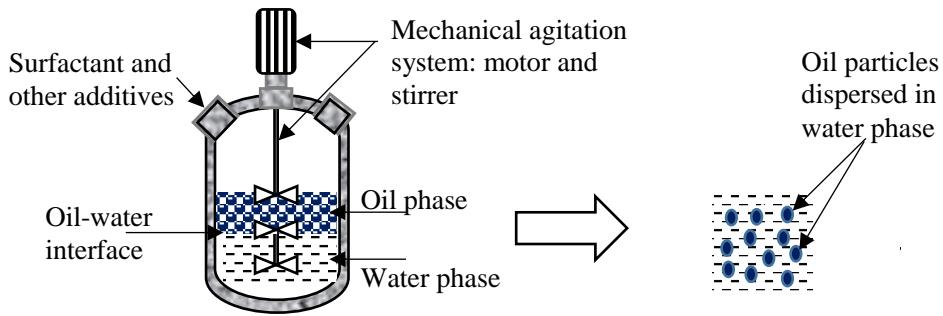


Figure 8a. Oil-water emulsification of process using mechanical agitation.

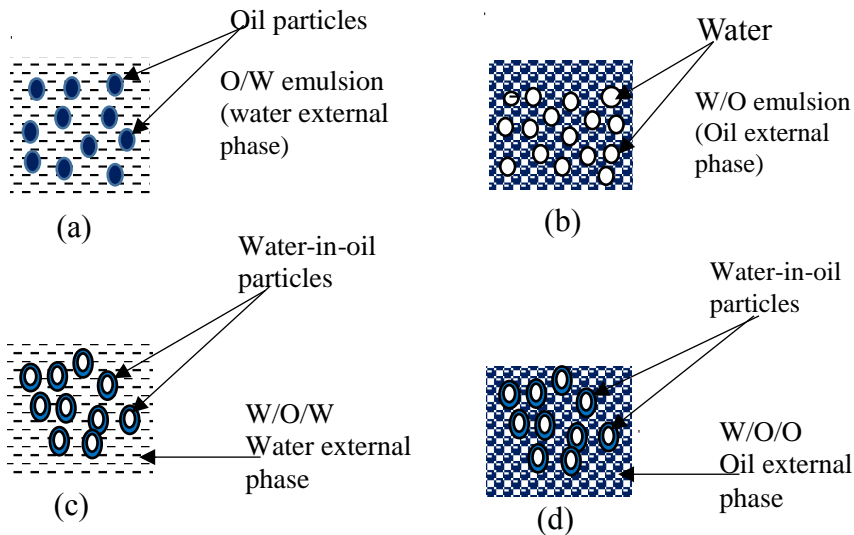


Figure 8b. Types of emulsion

It should however be noted that several factors including oil/water ratio, types and concentration surfactants, chemistry of the crude oil, homogenization system, chemistry of the aqueous phase etc. affect the types and behaviour of emulsion.

3.2. Emulsification in the Aspect of Heavy Oil Transportation

High viscosity, which leads to poor mobility and relatively low recovery efficiency, is by far the major hurdle facing production and transportation of heavy oil (Barrufet and Setiadarma, 2003; Nabipour et al., 2007; Abdurahman et al., 2012). Therefore, transportation of heavy oil has become a complex and highly technical operation (Hasan et al., 2010). This is due to the advancement in recovery methods which has subsequently increased heavy oil production and the need to transport the recovered oil refinery. Pipeline transportation is considered the cheapest and safest means of transporting heavy oil to the refinery or the point where it will be needed for other utilization. Three general approaches have been considered for pipeline transportation of heavy and extra heavy oil: (a) viscosity reduction which

includes dilution with other substances, formation of an oil-in-water emulsion, increasing and/or conserving oil's temperature by heating and depressing crude oil's pour point, (b) drag minimization and (c) in-situ oil upgrading (Martinez-Palou et al., 2011).

However, several factors including cost of energy, logistic and compatibility problems, are the challenges facing the thermal and diluents methods. In addition, for field production to be transported by pipeline using a diluent, two pipelines would be required (one for the oil and one for the diluent). Therefore, in the recent times, transport of viscous crudes as oil-in-water (O/W) emulsions is one of the newest alternatives in the pipeline transportation techniques (Al-Room et al., 2004; Ashrafizadeh and Kamran, 2010). Emulsification technology has received major attention in long distance transportation of heavy oil due to cheaper cost and operability. Through emulsification method, crude oil-in-water emulsions can reach a viscosity as low as 50mPas, and most pipeline operations of heavy oil are limited to viscosity values up to 400mPas (Rimmer et al., 1992; Nunez et al., 1996; Martinez-Palou et al., 2011; dos-Santos et al., 2011). Moreover, this method offers advantages such as effectiveness in the transportation of crude oils with viscosities higher than 1000 cP especially in cold regions and reduction in the pipe corrosion (e.g., in the crudes with high sulfur content) since water is the continuous phase and crude oil has no contact with the pipe wall (Ashrafizadeh and Kamran, 2010; dos-Santos et al., 2011). Also, restarting a pipeline after an emergency shutdown and re-emulsification of oil may not pose major problems (Simon and Poynter, 1970). Reported field application of this technology includes the Orimulsion® process developed by PDVSA (Petróleos de Venezuela) in the eighties and commercialized by its filial Bitumenes Orinoco S.A. (Salager et al., 2001). Similarly, technical viability of emulsion transportation of heavy oil has been demonstrated in an Indonesian pipeline in 1963 and in a 13 mile long, 8 inch diameter, pipeline in California (Ahmed et al., 1999; Ashrafizadeh and Kamran, 2010). Figure 9a is the schematic illustration of pipeline transportation of heavy oil as oil-in-water emulsion.

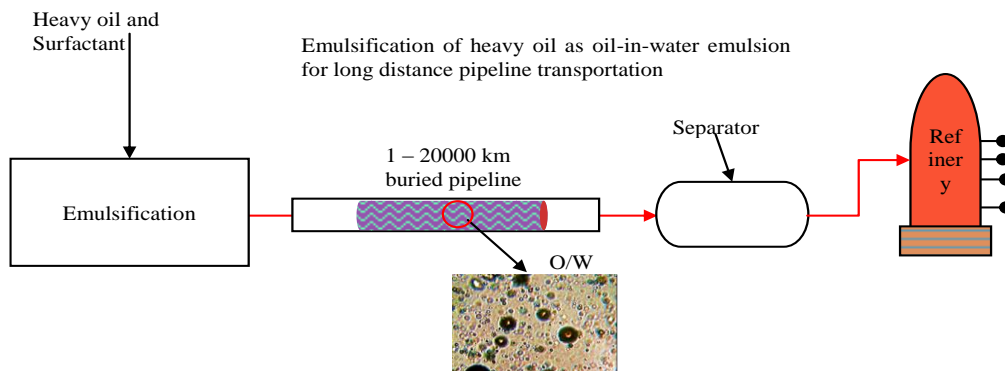


Figure 9a. Simplified flow diagram for heavy oil emulsification for long distance pipeline transportation.

3.3. Emulsification in the Aspect of Heavy Oil Recovery

The insitu Thermal EOR (TEOR) methods including steam assisted gravity drainage (SAGD), cyclic steam stimulation (CSS) or Huff and Puff method, steam flooding, and their

hybrids involve injection of steam, and chemical additives (including solvents and surfactants) into the heavy oil reservoir for the purpose of reducing the viscosity and increasing mobility (Bennion et al., 1993; Yamazaki et al., 1994; Al-Bahlani and Babadagli, 2009). During these processes, the thermal energy possessed by the liquid is transferred to the oil in situ. Thus, emulsification occurs through the reduction of interfacial barrier between the thermal liquid and oil; thereby causing dispersion of the liquid particles into the oil phase stabilized by the natural emulsion stabilizers (the asphaltene and resin) present in the oil. In addition, emulsification can be assisted by the shearing force essentially generated as result of movement of oil and the fluid through the pores space of the reservoir rock (Mohammadzadeh and Chatzis, 2010).

Usually, the steam injection methods lead to the formation of highly viscous water-in-oil emulsion which exhibit higher viscosity than the original oil. This however depends on other factors such as oil-water ratio, and other prevailing reservoir conditions (Bennion et al., 1993; Al-Bahlani and Babadagli, 2009; Alade et al., 2016c).

On the other hand, chemical flooding using alkaline solutions (sodium hydroxide and carbonates) and surfactants leads to in-situ emulsification (formation of oil-in-water emulsion) as a result of the chemical reactions accompanied by mass at the oil/water interface and low transient dynamic interfacial tension (Gholap et al., 2004; Liu et al., 2007; Dong et al., 2009; Chen et al., 2013; Sheng, 2015). And since the lower API gravity crude oils generally have a higher content of natural petroleum acids, spontaneous emulsification can be triggered by the interaction between the alkaline solution and the natural acids in heavy oils (Dong et al., 2009). Pore-scale emulsification process in heavy oil reservoir due to thermal fluid injection and/or surfactant is illustrated in Figure 9b.

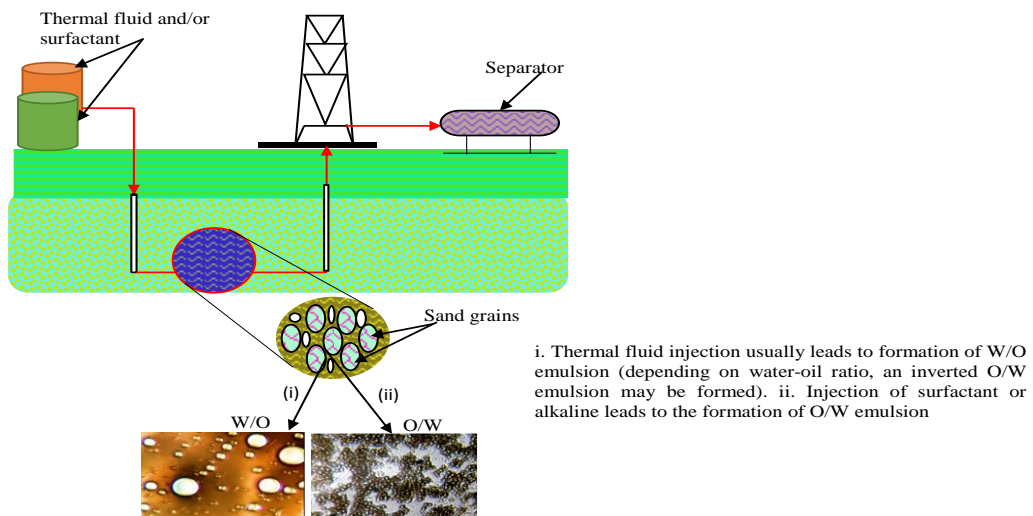


Figure 9b. Illustration of pore scale insitu emulsification in EOR.

3.4. Important Properties of Emulsion

Emulsion stability and viscosity are the most important properties of practical applications in EOR and pipeline transportation (Salager et al., 2001; Shaw, 2003; dos-Santos

et al., 2011; Fletcher et al., 2012; Abdurahman et al., 2012; Nguyen and Balsamo, 2013). These properties are however governed by many variables including temperature, composition of emulsion and particle morphology (Hasan et al., 2010). Notably, the particle morphology including particle size and distribution is a critical factor affecting the stability and rheological behaviour of complex fluid such as heavy oil or bitumen emulsions.

Furthermore, the particle morphology of an emulsion majorly affects emulsion destabilization process. As illustrated in Figure 10, the forces that contribute to destabilization of an emulsion include gravitational force, sedimentation or creaming, coalescence, flocculation, Ostwald ripening, and phase inversion (Taylor, 1998; Fingas, 2005; Badolato et al., 2008; Kang et al., 2012; Yang et al., 2013). These forces also depend on other factors such as the type and concentration of surfactants, chemistry of the crude oil and its physical properties, interfacial activities, temperature, phase ratio (Fingas, 2005; Badolato et al., 2008; Al-Sabagh et al., 2013). Moreover, the particle size of emulsion is affected by several emulsification variables including the energy input during mixing (mixing speed and time of mixing), type of mixer, oil composition, oil-water ratio, type and concentration of surfactant or surface active agent present, and formation temperature (Al-Roomi et al., 2004; Dong et al., 2009; Hasan et al., 2010; Fan et al., 2010; dos-Santos et al., 2011).

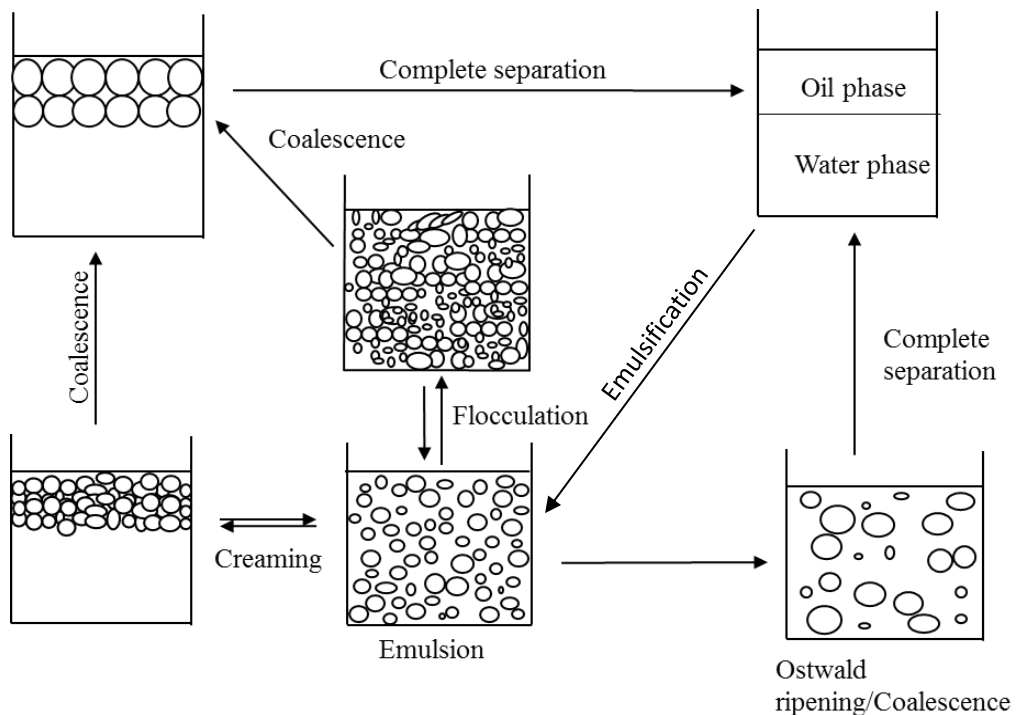


Figure 10. Emulsion destabilisation and separation processes. Adapted from Taylor (1998).

The two most popular moment means that have been used in calculating the size of particles including emulsions are given in Eqns. 5 and 6 (Holdich, 2002; Richardson et al., 2002; Rawle, 2016):

1. Surface Area Moment (D[3,2]): Sauter Mean Diameter

$$D[3,2] = \frac{\sum d^3}{\sum d^2} \quad (5)$$

2. Volume or Mass Moment Mean (D[4,3]): De Brouckere Mean Diameter

$$D[4,3] = \frac{\sum d^4}{\sum d^3} \quad (6)$$

In addition, based on method of emulsification, emulsion should contain drops of similar or very different sizes, with the associated variety in statistical distribution categorized as monodispersed or polydispersed, symmetrical or asymmetrical, unimodal or polymodal (Salager et al., 2001). The Lognormal probability density function (Eqn. 7) is one of the most widely used statistical expressions of size distribution of particles. A typical particle size distribution curve fitted to the lognormal probability density function (PDF) is shown in Figure 11.

$$f(x) = \frac{1}{x\sigma\sqrt{2\pi}} e^{-\frac{(\ln(x)-\omega)^2}{2\sigma^2}} \quad (7)$$

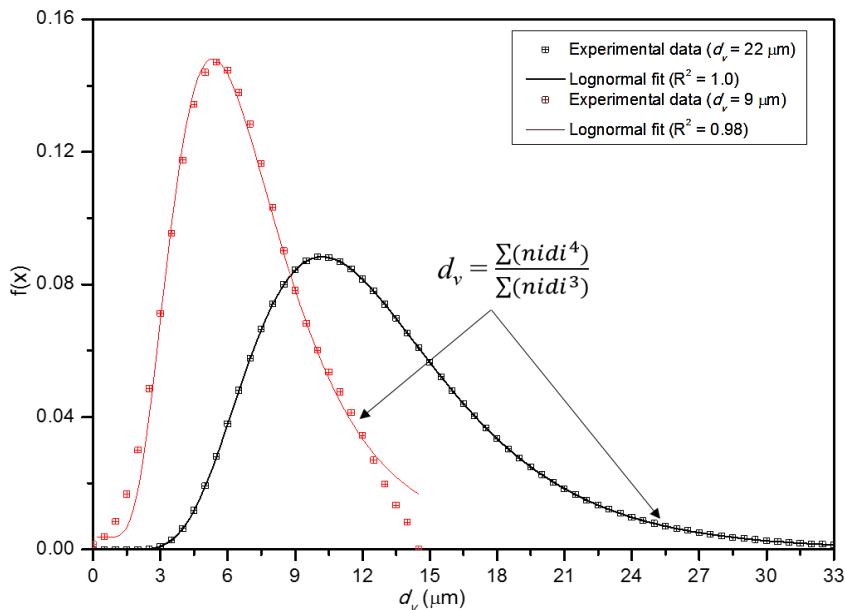


Figure 11. A typical particle size distribution curve fitted to the lognormal probability density function (PDF).

4. POLYVINYL ALCOHOL AS A SURFACTANT

4.1. Role of Surfactants or Emulsifying Agents

Ordinarily, homogenization of two immiscible liquids, without the inclusion of emulsifying agent or stabilizer, does not produce a stable emulsion due to particle

coalescence. Thus, stability is enhanced with the use of a stabilizer or emulsifier which can be either a surface-active materials (surfactants), naturally occurring materials (crude oil natural acids – naphthenic acids, asphaltene and resins) or finely divided solids such as clay (see Figure 12). Surfactant lowers the interfacial tension between the two phases and/or form an adsorbed film around the dispersed droplets (typical of asphaltene and resin stabilized water-heavy oil emulsion) thereby assists in preventing coagulation and coalescence (Shaw, 2003).

Surfactants form a unique class of chemical compound which acts as surface active agent and is characterized by the tendency to absorb at surfaces and interfaces between two immiscible phases (Salager, 2002; Holmberg et al., 2003; Schramm et al., 2003; Shaw, 2003). Through this action, it lowers the free energy at the phase boundary (the interfacial surface tension - IFT), thereby breaking the barrier between the immiscible fluids; allows mixing and stabilizes the dispersed particles.

A simple structural description has been used to define a surfactant. As shown in Figure 13a and 13b, surfactant molecules as an amphiphilic compound consist of a hydrophilic part (water soluble part) and a hydrophobic (water insoluble part). In the simplest terms, it contains at least one non-polar group and one polar (or ionic) group. The unique surface active properties of aqueous surfactant solutions can be ascribed to the presence of a hydrophilic head group and a hydrophobic chain (or tail) in the molecule. The polar or ionic head group usually interacts strongly with an aqueous environment, in which case it is solvated *via* dipole–dipole or ion–dipole interactions. Accordingly, surfactants are categorised into different groups depending on the nature of the polar head group (Schramm et al., 2003).

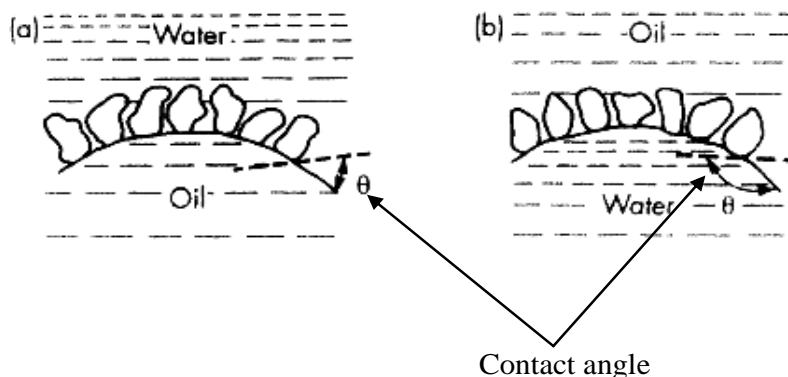


Figure 12. Stabilisation of emulsions by finely divided solids - clay (a) preferential wetting by water leading to an O/W emulsion; (b) preferential wetting by oil leading to a W/O emulsion. Adapted from Shaw (2003).

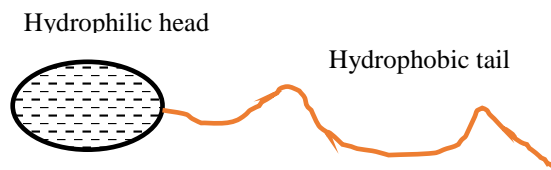


Figure 13a. Surfactant molecules as an amphiphilic compound.

The four major classes of surfactants based on their dissociation in water is shown in Figure 14. Anionic surfactants are the most commonly used surfactants and account for about 50% of the world production. They are dissociated in water in an amphiphilic anion, and a cation, which is in general an alkaline metal (Na^+ , K^+) or a quaternary ammonium. On the other hand, cationic surfactants are dissociated in water into an amphiphilic cation and an anion, most often of the halogen type. Thus, ionic surfactants (anionic and cationic) are affected by the solution chemistry including the salinity (and types of salt) and pH. The third type is the non-ionic surfactants whose hydrophilic group is of a non-dissociable type and thus do not ionize in aqueous solution. Therefore, they are not affected by the environment of the system in which they are applied. Other classes of surfactants include amphoteric or zwitterionic surfactants and the polymeric surfactants. The amphoteric or zwitterionic surfactants refers to a single surfactant molecule which exhibits both anionic and cationic dissociations while the polymeric surfactants are the group of surface active polymers including PVA, which result from the association of one or several macromolecular structures exhibiting hydrophilic and lipophilic characters, either as separated blocks or as grafts (Salager, 2002; Schramm et al., 2003).

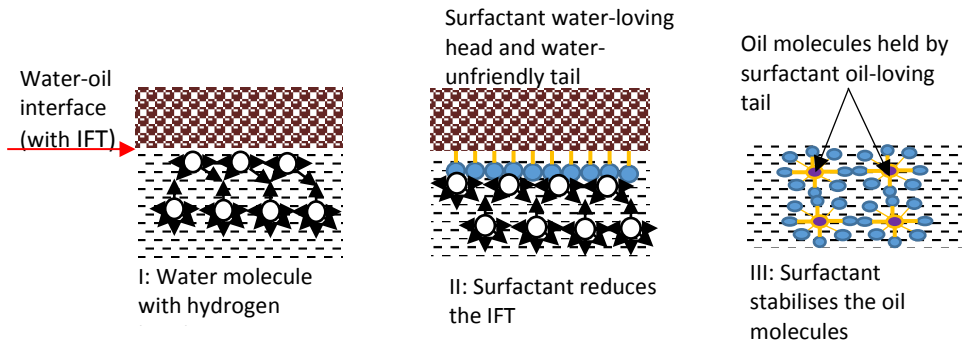


Figure 13b. Simplified action of surfactant.

4.2. Desirability of PVA in Forming Heavy Oil-in-Water Emulsion for Viscosity Reduction

Several ionic and non-ionic surfactants have been used to reduce the viscosity of heavy oil by forming oil-in-water emulsion (Brooks and Richmond, 1994; Al-Room et al., 2004; Hassan et al., 2010; dos Santos et al., 2011; Abdurahman et al., 2012; Schulz et al., 2016). However, emulsions formed with the low molecular weight surfactants have been difficult to break, and thus limiting their application in the field (Fletcher et al., 2012; Nguyen and Balsamo, 2013). Although, various technological advancements including development of chemical demulsifier, electrical demulsification system, gravitational system, thermal separation system and their combinations have been proposed and employed in breaking petroleum emulsions, these methods are known to be expensive.

Therefore, the application of certain hydrophilic polymeric surfactants such as Poly vinyl alcohol (PVA) in producing moderately stable oil-in-water emulsion which is easier to resolve compared to the low molecular weight surfactants is an attractive solution to this problem (Fletcher et al., 2012; Nguyen and Balsamo, 2013). PVA has been used in forming

oil-in-water emulsion with low stability and significant reduction in viscosity of original heavy oil (Fletcher et al., 2012; Nguyen and Balsamo, 2013; Alade et al., 2016a and 2016b). PVA and other polymeric surfactants have also been used in enhanced oil recovery as solution thickeners and/or emulsifier (Son et al., 2015; Raffa et al., 2016).

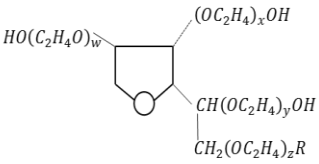
Class	Examples	Structures
Anionic	Sodium stearate	$CH_3(CH_2)_{16}COO^-Na^+$
	Sodium dodecyl benzene sulfonate	$CH_3(CH_2)_{11}SO_3^-Na^+$
	Sodium dodecyl benzene sulfonate	$CH_3(CH_2)_{11}C_6H_4SO_3^-Na^+$
Cationic	Laurylamine hydrochloride	$CH_3(CH_2)_{11}NH_3^+Cl^-$
	Trimethyl dodecylammonium chloride	$C_{12}H_{25}N^+(CH_3)_3Cl^-$
	Cetyl trimethylammonium bromide	$CH_3(CH_2)_{15}N^+(CH_3)_3Br^-$
Non-ionic	Polyoxyethylene alcohol	$C_nH_{2n+1}(OCH_2CH_2)_mOH$
	Alkylphenol ethoxylate	$C_9H_{19} - C_6H_4 - (OCH_2CH_2)_nOH$
	Polysorbate 80 $w + x + y + z = 20$ $R = (C_{17}H_{33})COO$	
	Propylene oxide-modified polymethylsiloxane (EO = ethyleneoxy. PO = propyleneoxy)	$(CH_3)_3SiO((CH_3)_2SiO)_x(CH_3SiO)_ySi(CH_3)_3$ $CH_2CH_2CH_2O(EO)_m(PO)_nH$
Zwitterionic	Dodecyl betaine	$C_{12}H_{25}N^+(CH_3)_2CH_2COO^-$
	Lauramidopropyl betane	$C_{11}H_{23}CONH(CH_2)_3N^+(CH_3)_2CH_2COO^-$
	Cocoamido-2-hydroxypropyl sulfobetaine	$C_nH_{2n+1}CONH(CH_2)_3N^+(CH_3)_2CH_2COO^-$

Figure 14. Types of surfactants. Adapted from Schramm et al., (2003).

4.3. Chemical Property of PVA

Polyvinyl alcohols are hydrophilic (water soluble) polymers manufactured by alcoholysis of polyvinyl acetate. PVA has a relatively simple structure with a pendant hydroxyl group (Figure 15a); and is produced by the polymerization of vinyl acetate to polyvinyl acetate (PVAc), followed by hydrolysis of PVAc which is subsequently polymerized to PVA. Figure 15b illustrates the chemical reaction for synthesis of PVA.

4.3.1. Computational Modeling of PVA

Motivation for the use of PVA was shown through the use of molecular modelling, the chemical properties of poly-vinyl alcohol, PVA was compared with that of poly-vinyl phenol, PVP. Geometry optimizations and vibrational analyses of polymer PVA was performed using the Gaussian09 software. B3LYP functional was employed with a 6-31G (d) basis set. Attractive and repulsive forces between interacting atoms and molecules, due to their electropositive and electronegative properties, were explained through electrostatic potential energies. The electrostatic potential for PVA was color-mapped based on the electron density

distribution (Figure 16a). The color map shows the electrostatic potential energy (in hartrees) for the various colors. The red end of the spectrum shows regions of highest stability for a positive test charge (more favorable to interactions), magenta/blue show the regions of least stability for a positive test charge (less favorable to interactions). The negative characteristic electrostatic potential, represented in red color, are reactive as they are rich in electrons ($-OH$ functionalities).

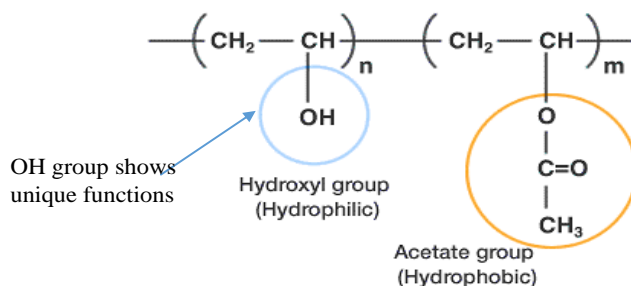


Figure 15a. Chemical structure of Polyvinyl Alcohol.

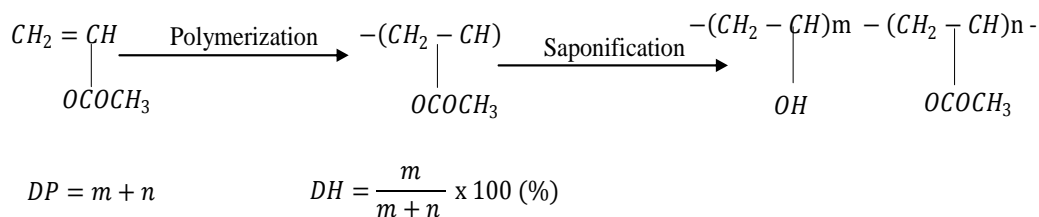


Figure 15b. Chemical structure of Polyvinyl Alcohol.

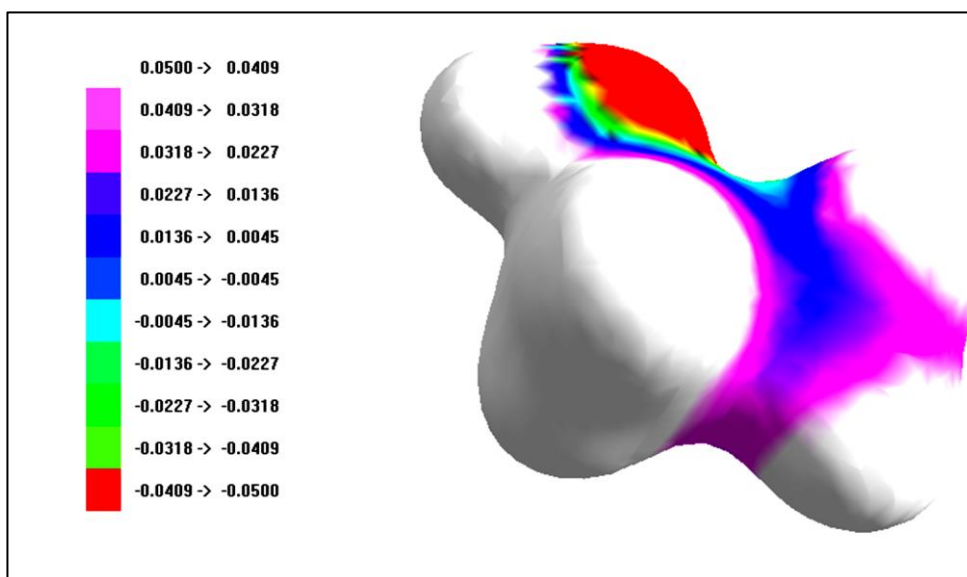


Figure 16a. Electrostatic potential on electron density of polyvinyl alcohol (PVA)-Inset structure of PVA. Red colour indicate regions which have the highest negative domain.

The strength of a dipole interaction depends on the size of each dipole, dipole energies and on their relative orientation. A molecule (polymer) with a permanent dipole moment will induce a dipole moment in a second molecule that is located nearby in space, and this phenomenon is known as polarization (Kim et al. 2006). Polar molecules (a functional polymer and heavy oil containing polar compounds), do interact through dipole-dipole intermolecular forces and hydrogen bonds. The extent of charge separation within the polymer, PVA, is characterized by its dipole moment which also explains their nature of polarity. Polarity prompted by dipole moment brings about a number of physical properties some of which are solubility (wettability), surface tension and boiling points (Kim et al. 2006). The dipole of poly-vinyl phenol and poly vinyl alcohol increases in the order of polyvinyl phenol (1.5630 Debye) < polyvinyl alcohol (1.5634 Debye). Polyvinyl alcohol presented a higher dipole moment when compared with polyvinyl phenol, and this confirms that the polymer shows better wettability properties from a neighbouring polar molecule.

4.3.2. Orbital Energies

Interaction between atoms or molecules happens most likely between the HOMO of one molecule and the LUMO of the other molecule. The amount of energy required to add or remove electrons in a molecule can be obtained from the HOMO and LUMO energy values. HOMO characterizes the nucleophilicity of a species, i.e., its tendency to donate an electron, while LUMO characterizes the electrophilicity of a species, i.e., its tendency to receive an electron (Hizaddin et al. 2013).

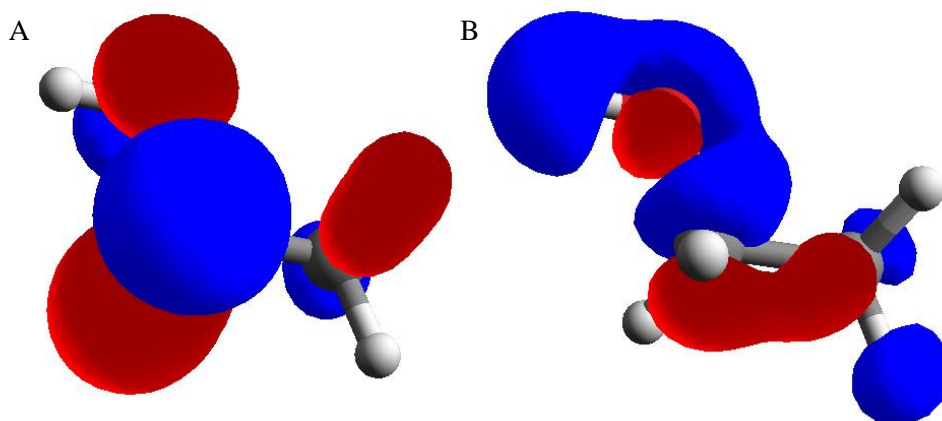


Figure 16b. HOMO and LUMO locations of polyvinyl alcohol (PVA) unit: (a) HOMO and (b) LUMO.

Optimized geometries of polyvinyl alcohol showing HOMO and LUMO positions are presented in Figures 16b. Polymers with low HOMO energy values indicate a molecule with better electron donor and high ionization potential, while polymers with higher LUMO energy shows a molecule with high electron affinity, i.e., better electron acceptor. The HOMO and LUMO properties of PVA is -0.26154 a.u. and 0.07656 a.u. respectively as compared to PVP which has HOMO and LUMO values of PVA is -0.21398 a.u. and -0.00041 a.u. respectively. The optimization energies of PVA and PVP -9.7×10^4 and -26.7×10^4 kcal/mol respectively and this confirms that PVA has a slightly higher energy which confirm higher compactness/firmness as compared to PVP (Isarankura et al. 2008).

4.4. Unique Properties of PVA and Applications

PVA is the world's largest volume synthetic polymer produced for its many excellent physical and chemical properties that has led to broad practical and industrial applications (Gholap et al., 2004; Jelinska et al., 2010). Different grades of PVA are synthesized according to different degrees of polymerization and hydrolysis, which are controlled in the polymerization and the saponification processes respectively. In an overview, the characteristics properties of PVA are affected by the degree of polymerization (DP) and the degree of hydrolysis (DH). It has been reported that the solubility decreases with increasing DP and DH, while PVA solution viscosity increases with increasing DP and DH. The strength of PVA film increases with increasing DP and DH, while the emulsifying capacity (including emulsion stability) increases with increasing DP and decreases with increasing DH (www.denka.co.jp; www.kuraray-poval.com).

Furthermore, PVA has numerous desirable properties including water solubility, adhesion strength, mechanical strength, gas barrier and aging resistance, biocompatibility and biodegradability, thermo-stability, chemical resistance and film forming ability, low fouling potential, pH stability, high polar character, good mechanical properties and easy processability (Biehn and Ernsberger, 1948; Coker, 1957; Gholap et al., 2004; Jelinska et al., 2010; Fletcher et al., 2012; Nguyen and Balsamo, 2013; Raffa et al., 2016), it has therefore been greatly applied in several such as pharmaceuticals, medicine and medical sciences, environmental engineering, and engineering materials in general. Moreover, PVA being a non-ionic hydrophilic polymer (with non-dissociable –OH group) functions as a surface active substance (an emulsifying agent) by lowering the interfacial tensions of solution. Besides, PVA is tolerant to substantial concentrations of electrolytes (particularly acids), compatibility with other emulsifying agents, salinity of water, and other chemicals such as wax crystal modifiers, pour point depressants, and corrosion inhibitors (Biehn and Ernsberger, 1948; Coker, 1957; Fletcher et al., 2012; Nguyen and Balsamo, 2013; Alade et al., 2016a and 2016b).

4.5. Reports from Recent Application of PVA in Heavy and Extra-Heavy Oil Emulsification for Viscosity Reduction

Hitherto, in the aspect of heavy oil emulsification, the most desirable advantage of PVA application is the formation of emulsion which is easier to resolve compared to the low molecular weight surfactants (Fletcher et al., 2012). Other benefits include cost (PVA is relatively cheap), tolerance to salinity and electrolytes, reusability, and biodegradability.

Apart from very few reports (Biehn and Ernsberger, 1948; Coker, 1957), on the use of PVA as an emulsifying agent, application of PVA as a surfactant in heavy oil emulsification is relatively new. Comparison of emulsification property of PVA with other emulsifying agents such as soaps, sulfated alcohols, and sulfonated compounds had been investigated by Biehn and Ernsberger (1948). PVA was used as a surfactant to aid the dispersion of mineral oils, vegetable oils, and other organic liquids. The ability of PVA to reduce the IFT of the mineral oil employed (Nujol) was fairly compared to other emulsifying compounds. The effect of PVA on the surface tension was found to be dependent of the degree of hydrolysis. The solution of partially hydrolysed PVA resulted into lower IFT compared to the completely

hydrolysed solution. Ability to emulsify was basically quantified in terms of droplet size of emulsion. It was reported that the effective concentration of PVA was found to be 0.5% or greater depending on the total formulation; and at 0.1% or less, PVA was less effective for emulsification. In addition, there was insignificant differences in the size of the droplets due to the degree of hydrolysis. The stability of emulsions was observed to be dependent of the type of the dispersed phase, concentration of PVA, and its combination with other emulsifying agents, degree of hydrolysis, and the pH of solutions. The effectiveness of PVA was confirmed, depending on the degree of hydrolysis, over a wide pH range. However, the stability of emulsion was adversely affected by the presence of salt. Similarly, PVA has also been reported to perform excellently as an emulsifying agent in vinyl polymerizations to prepare fine particle lattices of polystyrene, poly vinyl chloride, and butadiene-copolymer (Coker, 1957). Other attractive performance is the ease of operability of the system involving PVA in emulsification. This includes direct use of dry PVA powder (eliminating the need first stage preparation of the solution); and possibility of low mechanical agitation in forming oil-in-water emulsion using aqueous solution of PVA (Biehn and Ernsberger, 1948).

Recently, with the objective of reducing the viscosity, PVA has been used in preparing oil-in-water emulsion for heavy and extra-heavy oil emulsification (Tobin, 2005; Fletcher et al., 2012; Nguyen and Balsamo, 2013; Alade et al., 2016a and 2016d). Heavy and extra-heavy oils with original viscosities of 13400 mPa.s at 25°C (Nguyen and Balsamo, 2013), ≈ 100000 and ≈ 1000000 mPa.s at 35°C (Alade et al., 2016a and 2016b), $9700 - 1.4 \times 10^6$ mPa.s (at 20°C) and 1.4×10^6 at 25°C (Fletcher et al., 2012) have been dispersed as oil-in-water emulsions (50 - 75% oil contents) in the aqueous solution containing 1000 – 5000 ppm of PVA (with or without brine concentration as high as ≈ 70000 ppm TDS). The results reported from these investigations showed that less – moderately stable emulsions were formed (depending on the method of preparation, particle size, salinity and storage conditions); and viscosity reduction up to $\approx 99\%$ was reported. In addition, compatibility of PVA with caustic solution and thermal tolerance ($\approx 175^\circ\text{C}$) were confirmed.

CONCLUSION

An expository discussion has been presented on the potential application of PVA as an emulsifier in forming heavy oil-in-water emulsion. The current negative impact of low price oil on the production of the highly viscous crude oil can be mitigated through application of alternative cost-reduction technology such as emulsification in EOR and pipeline transportation. PVA is a cheap, highly water soluble and biodegradable polymeric surfactant which had attracted many industrial applications due to its excellent physical and chemical properties. Successful emulsification of heavy and extra-heavy oil as oil-in-water emulsion with significant viscosity reduction and flow properties assisted by PVA as an emulsifier (under favorable conditions of mixing) has been reported. Compared to typical emulsions formed using the low molecular weight surfactants, emulsions formed using PVA has been found to be less stable therefore eliminating the need for expensive separation process.

However, research effort on the applicability of the chemical (most especially for insitu emulsification of heavy and extra-heavy oils and pipeline transportation) has not attracted

adequate attentions. It is therefore suggested that further research efforts on PVA and heavy oil emulsification should look into practical applications such as development of process for insitu emulsification through injection of PVA into the reservoir, thermodynamic properties of PVA under typical reservoir conditions, and process optimization with the focus of expanding the range of applicability of PVA in both pipeline transportation and heavy oil recovery.

REFERENCES

- Abdel-Raouf, M.E. (2012). *Factors Affecting the Stability of Crude Oil Emulsions Composition Stability and Characterization*. Retrieved from www.intechopen.com/books/crude-oil, pp.183-204.
- Abdurahman, N.H., Rosli, Y.M., Azhari, N.H., Hayder, B.A. (2012). Pipeline Transportation of Viscous Crudes as Concentrated Oil-in-water Emulsions. *Journal of Petroleum Science and Engineering*, 90-91, 139–144.
- Ahmed, N. S., Nassar, A. M., Zaki, N. N., Gharieb, K. (1999) Stability and rheology of heavy crude oil-in-water emulsion stabilized by an anionic–nonionic surfactant mixture. *Petroleum Science and Technology*, 17, 553–576.
- Al-Bahlani, M., Babadagli, T. (2009). SAGD laboratory experimental and numerical simulation Studies: A Review of Current Status and Future Issues. *Journal of Petrol Science and Engineering*, 68, 135-150.
- Alade, O. S., Sasaki, K., Sugai, Y., Ademodi, B., Nakano, M. (2016a). Bitumen emulsification using a hydrophilic polymeric surfactant: Performance evaluation in the presence of salinity. *Journal of Petroleum Science and Engineering*, 138: 66-76.
- Alade, O. S., Sasaki, K., Ogunlaja, A. S., Sugai, Y., B. Ademodi, Junpei K., Ryo Ueda and Nakano, M. (2016b). Thermal tolerance and Compatibility of NaOH-Poly(vinyl alcohol) in Bitumen Emulsification for Improved Flow properties, *Energy Fuels*, DOI: 10.1021/acs.energyfuels.6b02060.
- Alade, O. S., Sasaki, K., Sugai, Y., Ademodi, B., Jumpei, K., Nakano, M. (2016c). An aspect of bitumen emulsification by steam condensation: effect of formation temperature and bitumen content. *Energy Source, Part A*, 38, 1790 – 1797.
- Al-Roomi, Y., George, R., Elgibaly, A. and Elkamel, A. (2004) Use of a novel surfactant for improving the transportability/transportation of heavy/viscous crude oils. *Journal of Petroleum Science and Engineering*, 42, 235–243.
- Al-Sabagh, A. M., Nasser, N.M., Abd El-Hamid, T.M. (2013). Investigation of kinetic and rheological properties for the demulsification process, *Egyptian Journal of Petroleum*, 22, 117-127.
- Antes, F.G., Diehl, L.O., Pereira, J.S.F., Guimarães, R.C.L., Guarnieri, R.A., Ferreira, B.M.S., Dressler, V.L., Flores, E.M.M. (2015). Feasibility of Low Frequency Ultrasound for Water Removal from Crude oil Emulsions. *Ultrasonics Sonochemistry*, 25, 70–75.
- Ashrafizadeh, S. N. and Kamran, M. (2010) Emulsification of heavy crude oil in water for pipeline transportation. *Journal of Petroleum Science and Engineering*, 71, 205–211.
- Badolato, G.G., Aguilar, F., Schuchmann, H.P., Sobisch, T., Lerche, D. (2008).

- Evaluation of Long Term Stability of Model Emulsions by Multisample Analytical Centrifugation. *Progress in Colloidal and Polymer Science*. 134, 66-73.
- Balsamo, V., Nguyen, D., Phan, J. (2014). Non-conventional techniques to characterize complex SAGD emulsions and dilution effects on emulsion stabilization. *Journal of Petrol Science and Engineering*, 122, 331–345.
- Barrufet, M. A. and Setiadarma, A. (2003). Experimental viscosities of heavy oil mixtures up to 450 K and high pressures using a mercury capillary viscometer. *Journal of Petroleum Science and Engineering*, 40, 17–26.
- Bennion, D. B., Chan, M., Sarioglu, G., Courtnage, D., Wansleeben, J., Hirata, T. (1993). The in-situ formation of bitumen-water stable emulsions in porous media during thermal stimulation. SPE International Thermal Operations Symposium (Bakersfield, California), SPE-25802-MS.
- Biehn, F.G.; Ernsberger, M.L. (1948). Polyvinyl Alcohol as an emulsifying agent. *Ind. Eng. Chem.* 40(8), 1449 -1453.
- BP statistical review of World energy June 2016 (www.bp.com). Retrieve October, 2016 from www.google.com.
- Brooks, B. W., Richmond, H. N. (1994). Phase inversion in non-ionic surfactant—oil—water systems—I. The effect of transitional inversion on emulsion drop sizes. *Chemical Engineering Science*, 49(7), 1053-1064.
- Chen, L.; Zhang, G.; Ge, J.; Jiang, P.; Tang, J.; Liu, Y. Research of the heavy oil displacement mechanism by using alkaline/surfactant flooding system. *Colloids Surf A Physicochem. Eng. Asp.* 2013, 434, 63– 71.
- Clausse, D., Gomez, F., Dalmazzone, C., Noik, C. (2005). A Method for the Characterization of Emulsions, Thermosgranulometry: Application to water-in-crude oil Emulsion. *Journal of Colloid and Interface Science*, 287, 694–703.
- Clark, B., de Cardenas, J. L., and Peats A. (2007). Working Document of the NPC Global Oil and Gas Study: Heavy Oil, Extra-Heavy Oil and Bitumen, Unconventional Oil. Retrieved (March 2011) from www.npc.org
- Coker, J. N. (1957). Poly(vinyl Alcohol) as an emulsifying agent in Vinyl Polymerizations. *Ind. Eng. Chem.* 49(3), 382-385.
- Denka poval catalog (www.denka.co.jp/eng/chemical/product/poval_catalog_e.pdf). Retrieved October 2016 from www.google.com.
- Dong, M., Ma, S. and Liu, Q. (2009). Enhanced heavy oil recovery through interfacial instability: A study of chemical flooding for Brintnell heavy oil. *Fuel*, 88, 1049–1056.
- dos Santos, R. G., Bannwart, A. C., Briceno, M. I. and Lohd, W. (2011). Physico-chemical properties of heavy crude oil-in-water emulsions stabilized by mixtures of ionic and non-ionic ethoxylated nonyl phenol surfactants and medium chain alcohols chemical engineering research and design.
- Elraies, K. A., Tan, I. M. (2012). The Application of a New Polymeric Surfactant for Chemical EOR, Introduction to Enhanced Oil Recovery (EOR) Processes and Bioremediation of Oil-Contaminated Sites, Dr. Laura Romero-Zerón (Ed.), ISBN: 978-953-51-0629-6, InTech, Available from: <http://www.intechopen.com/books/introduction-to-enhanced>.
- Energy Information Administration (EIA) (2016). International Energy Outlook 2016 with Projection to 2040. US Department of Energy, Washington, DC. <http://www.eia.gov/forecasts/ieo>.

- Fan, Y., Simon, S. and Sjöblom, J. (2010). Interfacial shear rheology of asphaltenes at oil–water interface and its relation to emulsion stability: Influence of concentration, solvent aromaticity and nonionic surfactant. *Colloids and Surfaces A: Physicochemical Engineering Aspects*, 366, 120–128.
- Fingas, M. (2005). *Stability and Resurfacing of Dispersed Oil*. <http://pwsrccac.org/docs/d0026200.pdf>. Retrieved August, 2015 from www.google.com.
- Fletcher, P., Bolton, G., Forsyth, J., Jaska, C., Cobos, S. (2012). The pipeline transportation of heavy oil using water based dispersions. World Heavy Oil Congress, Aberdeen Scotland, 2012. WHOC12-185.
- Foucault, S., Ascanio, G., Tanguy, A.P. (2005). Power Characteristics in Coaxial Mixing: Newtonian and Non-Newtonian Fluids. *Industrial Engineering and Chemical Research*, 44, 5036-5043.
- Fradette L., Brocart, B., Tanguy, P. A. (2007). Comparison of Mixing Technologies for the Production of Concentrated Emulsions. *Chemical Engineering Research and Design*. Trans IChemE, Part a, Institution of Chemical Engineers
- Gilman, J.W; Hart, D. L. V.; Kashiwagi, T. (1994). Thermal decomposition chemistry of poly(vinyl alcohol). Char characterization and reactions with bismaleimides. In *Fire and polymers II: Materials and test for hazard prevention*. Washington, DC: American Chemical Society (ACS Symposium Series 599, August 21–26, 1994).
- Gingras, J., Tanguy, P. A., Mariotti, S., Chaverot, P. (2005). Effect of process parameters on bitumen emulsions. *Chemical Engineering and Processing*, 44, 979-986.
- Gholap, S. G., Jog, J. P., Badiger, M. V. (2004). Synthesis and characterization of hydrophobically modified poly(vinyl alcohol) hydrogel membrane. *Polymer*, 45, 5863–5873.
- Hasan, S.W., Ghannam, T.M., Esmail, N. (2010). Heavy crude oil viscosity reduction and rheology or pipeline transportation. *Fuel*, 89, 1095–1100.
- Hizaddin, H.F., Hashim, M.A. and Anantharaj, R. (2013). Evaluation of molecular interaction in binary mixture of ionic liquids+ heterocyclic nitrogen compounds: Ab Initio method and COSMORS model. *Industrial and Engineering Chemistry Research*, 52, 18043-18058.
- Holdich, R. G. (2002). *Fundamentals of Particle Technology*. Midland Information Technology and Publishing, Leicestershire, LE12 9AD, U.K.
- Holmberg, K., Jonsson, B., Kronberg, B., Lindman, B. (2003). *Surfactants and Polymers in Aqueous Solution*. 2nd Edt, John Wiley and Sons Ltd., West Sussex, England.
- Isarankura-Na-Ayudhya, C., Nantasenamat, C., Buraparungsang, P., Piacham, T., Ye, L., Bülow, L. and Prachayasittikul, V. (2008). Computational insights on sulfonamide imprinted polymers. *Molecules* 13, 3077-3091.
- Jelinska, N., Kalnins, M., Tupureina, V., Dzene, A. (2010). Poly (Vinyl Alcohol)/Poly (Vinyl Acetate) blend films. *Scientific Journal of Riga Technical University Material Science and Applied Chemistry*. 21, 55-61.
- Jochen W. (2008). Emulsion Workshop. November 13-14th, 2008, Amherst, MA.
- Kang, W., Guo, L., Fan, H., Meng, L., Li, Y. (2012). Flocculation, coalescence and migration of dispersed phase droplets and oil-water separation in heavy oil emulsion. *Journal of Petroleum Science and Engineering*, 81, 177-181.

- Kim, J.H., Ma, X., Zhou, A. and Song, C. (2006). Ultra-deep desulfurization and denitrogenation of diesel fuel by selective adsorption over three different adsorbents: A study on adsorptive selectivity and mechanism. *Catalysis Today*, 111, 74-83.
- Kuraray poval (www.kuraray-poval.com/products/kuraray-povaltm/). Retrieved October 2016 from www.google.com.
- Langevin, D., Poteau, S., Henaut, I., Argillier, J. F. (2004). Crude oil emulsion properties and their application to heavy oil transportation. *Oil and Gas Science and Technology Review*, 59(5), 511–521.
- Lee, S. C.; Oh, J. T.; Jang, M. H.; Chung, S. I. (1999). Quantitative analysis of polyvinyl alcohol on the surface of poly(D, L-lactide-co-glycolide) microparticles prepared by solvent evaporation method: effect of particle size and PVA. *J. Control Release*, 59(2), 123-132.
- Lesueur, D. (2009). The colloidal structure of bitumen: Consequences on the rheology and on the mechanisms of bitumen modification. *Advances in Colloid and Interface Science*, 145(1- 2), 42 – 82.
- Lewandowska, K. (1999). Miscibility and thermal stability of poly(vinyl alcohol)/chitosan mixtures. *Thermochim. Acta.*, 42-48.
- Liu, Q.; Dong, M.; Ma, S.; Tu, Y. (2007). Surfactant enhanced alkaline flooding for Western Canadian heavy oil recovery. *Colloids Surf A Physicochem. Eng. Asp.*, 293, 63–71.
- Li, W.J.; Lu, S.Y.; Wang, R.P.; Lin, C.Q.; Li, X.D.; Yan, J.H. (2016). Combustion and Emission Characteristics of Coal Logs with Different Binders for Transportation in a Hydraulic Pipeline. *Energy Fuels*, 30, 1335–1340.
- Martínez-Palou, R., María de Lourdes, M., Zapata-Rendón B., Mar-Juárez, E., Bernal-Huicochea, C., Juan de la Cruz C. and Jorge, A. (2011). Transportation of heavy and extra-heavy crude oil by pipeline: A review. *Journal of Petroleum Science and Engineering*, 75 274– 282.
- Martínez-Palou, R., Reyes, J., Cerón-Camacho, R., Ramírez-de-Santiago, M., Villanueva, D., Vallejo, A.A., Aburto, J. (2015). Study of the formation and breaking of extra-heavy-crude- oil-in-water emulsions—A proposed strategy for transporting extra heavy crude oils. *Chemical Engineering and Processing*, 98, 112–122.
- Mccain, W. D. (1990). *The Properties of Petroleum Fluids*, 2 nd Ed. PennWell Books, Tulsa.
- Mohammadzadeh, O. and Chatzis, I. (2010): Pore-level investigation of heavy oil recovery using steam assisted gravity drainage (SAGD). *Oil and Gas Science and Technology – Rev IFP Energy's nouvelles*, 65(6), 839 – 857. DOI: 10.2516/ogst/2010010.
- Moradi, M.; Alvarado, V.; Huzurbazar, S. (2011). Effect of salinity on water-in-crude oil emulsions: evaluation through drop-size distribution proxy. *Energy Fuels*, 25, 260-268.
- Nabipour, M., Escrochi, M., Ayatollahi, S., Boukadi, F., Wadhahi, M., Maamari, R. and Bemani, A. (2007). Laboratory investigation of thermally-assisted gas–oil gravity drainage for secondary and tertiary oil recovery in fractured models. *Journal of Petroleum Science and Engineering*, 55, 74–82.
- Nguyen, D.; Balsamo, V. (2013). Emulsification of heavy oil in aqueous solutions of poly (vinyl alcohol): A method for reducing apparent viscosity of production fluids. *Energy Fuels* 27, 1736-1747.
- Nunez, G., Briceno, M., Mata, C., Rivas, H. and Joseph, D. (1996). Flow characteristics of concentrated emulsions of very viscous oil in water systems. *Journal of Rheology*, 40, 405– 423.

- Pal, R. (1994a). Metering of Two-Phase Liquid-Liquid Emulsions: A State of the Art Review. *Industrial and Engineering Chemistry Research*, 3(6): 1413 - 1435.
- Pal, R. (1994b). Techniques for measuring the composition (oil and water content) of emulsions — a state of the art review. *Colloids and Surfaces A: Physicochemical and Engineering Aspects*, 84(2-3), 141 - 193.
- Pei, H.; Zhang, G.; Ge, J.; Jin, L.; Ding, L. (2013). Study on the variation of dynamic interfacial tension in the process of alkaline flooding for heavy oil. *Fuel*, 104, 372–378.
- Pilehvari, A., Saadevandi, B., Halvaci, M., Clark, D. E. (1988). *Pipeline transportation of heavy crudes as emulsions*. In: Roco, M.C. (Ed.), Proc. 3rd Int. Symp. Liquid Solid Flows ASME, New York, p. 161.
- Plegue, T. H., Frank, S. G. and Zakin, J. L. (1989). Studies of water-continuous emulsions of heavy crude oils prepared by alkali treatment. *SPE Production Engineering*, 4(2), 181–183.
- Raffa, P., Broekhuis, A. A., Picchioni, F. (2016). Polymeric surfactants for enhanced oil recovery: A review. *Journal of Petroleum Science and Engineering*, 145, 723–733.
- Rawle, A. (2016). *Basic principles of particle size analysis*. Malvern Instruments Limited, Worcestershire, UK. Retrieve October, 2016 from www.google.com.
- Redelius, P.; Soenen, H. (2015). Relation between bitumen chemistry and performance. *Fuel*, 140, 34-43.
- Richardson, J. F., Harker, J. H., Backhurst, J. R. (2002). *Coulson and Richardson's Chemical Engineering Volume 2: Particle Technology and Separation Processes*. Chemical Engineering Science. Butterworth-Heinemann, Elsevier Science, Linacre House, Jordan Hill, Oxford, Woburn, MA.
- Rimmer, D. P., Gregoli, A. A., Hamshar, J. A. and Yildirim, E. I. (1992). *Pipeline emulsion transport for heavy oils*. In: Schramm, L.L. (Ed.), *Emulsions: Fundamentals and Applications in the Petroleum Industry*. American Chemical Society, Washington, DC.
- Salager, J., Briceno, M. I. and Bracho, C. L. (2001). Heavy Hydrocarbon Emulsions. Making use of the State of the Art in Formulation Engineering. In *Encyclopaedic Handbook of Emulsion Technology*. Johan Sjoblom Ed, Marcel Dekker New York 2001. pp 455-495.
- Salager, J. (2002). Surfactants types and uses. *FIRP Booklet: Teaching aid in surfactant science and engineering*. Retrieve October, 2016 from www.google.com.
- Saniere, A., Henaut, I. and Argillier, J. F. (2004). Pipeline transportation of heavy oils, a strategic, economic and technological challenge. *Oil and Gas Science and Technology Review*, IFP, 59(5), 455–466.
- Schulz, E. N., Ambrusi, R. E., Miraglia, D. B., Schulz, E. P., García, S. G., Rodriguez, J. L., Schulz, P. C. (2016). Evaluation of oil-in-water emulsions with cationic – anionic surfactants mixtures for potential use in the oil industry. *Colloids and Surfaces A: Physicochemical and Engineering Aspects*, 490, 145-154.
- Schramm, L. L., Stasiuk, E. N., Marangoni, D. G. (2003). Surfactants and their applications. *Annual Reports Section "C" (Physical Chemistry)*, 99, 3 – 48.
- Schumacher, M. M. (1980). *Enhanced recovery of residual and heavy oils*. 2nd ed. New Jersey: Noyes Data Corporation.
- Shaw, D. J. (2003). *Colloid and Surface Chemistry*. Butterworth-Heinemann, Elsevier Science Linacre House, Jordan Hill, Burlington.
- Sheng, J.J. (2015). Investigation of alkaline - crude oil reaction. *Petroleum*, 1, 31-39.
- Simon, R. and Poynter, W. G. (1970). Pipelining Oil/Water Mixtures. US Patent 3519006.

- Son, H. A.; Yoon, K. Y.; Lee, G. J.; Cho, J. W.; Choi, S.K.; Kim, J. W.; Im, K. C.; Kim, H. T.; Lee, K.S.; Sung, W.M. (2015). The potential applications in oil recovery with silica nanoparticle and polyvinyl alcohol stabilized emulsion. *J. Pet. Sci. Eng.* 126, 152-161.
- Speight, J. G. (2006). *The Chemistry and Technology of Petroleum*, Fifth Edition. CRC Press Taylor and Francis Group, Boca Raton, FL.
- Speight, J. G. (2009). *Enhanced Recovery Methods for Heavy Oil and Tar Sands*. Gulf Publishing Company, Houston, Texas.
- Strassner, J. E. (1968). Effect of pH on interfacial films and stability of crude oil–water emulsions. *Journal of Petroleum Technology*, 303–310.
- Suslick, S. B., Schiozer, D. J., Nepomuceno, F. and Furtado, R. (2003). Forecasting the development of heavy-oil reserves in ultra-deep waters using technological risk models. In: Proceedings of the SPE Hydrocarbon Economics and Evaluation Symposium, Dallas, TX, USA.
- Takahasi, A. and Ogino, K. (2005). Canada: a petroleum superpower with oil sands as conventional resources. *Journal of Japanese Association for Petroleum Technology*, 70(2), 157-163.
- Taylor, P. (1998). Ostwald ripening in emulsions. *Advances in Colloids and Interface Science*, 75, 107-163.
- Tobin, A.; Collins, P. (2005). Improved method and additive for the viscosity of crude oil. U.S. Patent WO2005100517A1.
- Wen, J., Zhang, J., Wang, Z., Zhang, Y. (2016). Correlations between emulsification behaviors of crude oil-water systems and crude oil compositions. *Journal of Petroleum Science and Engineering*, 146, 1-9.
- Wong, S.F., Lim, J.S., Dol, S.S. (2015). Crude oil emulsion: A review on formation, classification and stability of water-in-oil emulsions. *Journal of Petroleum Science and Engineering*, 135, 498-504.
- World Heavy Oil Congress (WHOC 2016), September 6 – 9, Stampede Park, Calgary, Alberta, Canada.
- Yang, Q., Ke, D., Yang, M., Hong, J., Ran, Q., Wang, X. (2013). Effect of salt concentration on the phase separation of bitumen emulsions. *Colloids and Surfaces A: Physicochemical and Engineering Aspects*. 425, 1-5.

Chapter 5

AN INTRODUCTION TO ASPHALTENES CHEMISTRY

*Jalil Bahman¹, Masoud Nasiri², Morteza Sabeti³
and Amir H. Mohammadi^{4,5,6,*}*

¹Faculty of New Sciences and Technologies, Semnan University, Semnan, Iran

² Faculty of chemical, gas and petroleum engineering,
Semnan University, Semnan 35195-363, Iran.

³Department of Chemical Engineering, Isfahan University of Technology, Isfahan, Iran

⁴Institut de Recherche en Génie Chimique et Pétrolier (IRGCP),
Paris Cedex, France

⁵Discipline of Chemical Engineering, School of Engineering,
University of KwaZulu-Natal, Howard College Campus, Durban, South Africa

⁶Département de Génie des Mines, de la Métallurgie et des Matériaux,
Faculté des Sciences et de Génie, Université Laval, Québec, Canada

ABSTRACT

Depleting conventional oil reservoirs, people of the world today are in need of exploiting other resources as a substitution to obviate their daily requirements for energy. One of the well-known resources being currently under exploitation is unconventional reservoir beds or so-called heavy oils. Unlike conventional ones, heavy oils unfortunately contain a wide range of problematic components such as asphaltenes. Asphaltenes are somehow unclear and undefined materials, which a large number of researchers have been scrutinized their entities day in, day out. This controversial subject has a lot of literatures, each of which has a different point of view about asphaltene. Therefore, it can be expected that naïve or even educated researchers get overwhelmed when they are on the point of asphaltene study. To mitigate its challenge, a big effort was made to sum up all facts and theories about asphaltene. In this communication, it was tried to delineate the contents of the chapter in a simple way so that no one encounters complicate and ambiguous concepts. In this work, asphaltene is introduced initially; then, other significant information about asphaltene's molecular weight, proposed chemical structures and chemical components are eluded, respectively. Afterwards, the difference

* Corresponding Author E-mail: a.h.m@irgcp.fr and amir_h_mohammadi@ yahoo.com.

between various heavy compounds such as asphaltene, resin and wax is clarified in detail. In the end, five-cases-model's classification is illustrated. Such models are typically utilized for predicting the asphaltene phase behavior as well as the amount of asphaltene precipitation when crude oils are exposed to external changes.

Keywords: asphaltene precipitation, molecular weight, chemical structure, resin, asphaltene phase behavior, thermodynamic model

1. INTRODUCTION

A lot of people consider petroleum as a hydrocarbon that consists of hydrogen and carbon, but it has been proven that the effective components in the physical and chemical properties of petroleum contain heteroatoms. Most heteroatoms including nonmetals, e.g., nitrogen, oxygen and sulfur; and problematic metals, e.g., nickel and vanadium, have been concentrated in asphaltene fraction of oil [1] although their concentration in various aromatic and heavy fractions is quite small.

In terms of geological maturation and petroleum generation, asphaltenes are partially matured kerogens, as shown in Figure 1. Kerogens originates from biomolecules, such as amino-acids, sugars, lipids and phenols in diagenesis stage of transformation of organic matter to hydrocarbon [2]. Asphaltene fraction found in bitumen, coal and lightest to heaviest oils but gas and retrograde gas reservoirs are free of that.

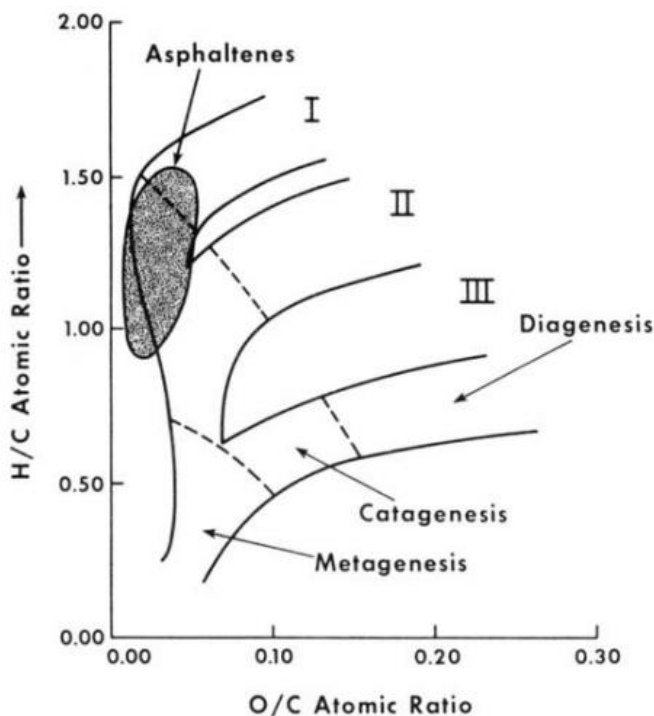


Figure 1. Asphaltene position in kerogen maturation diagram. H/C vs. O/C atomic ratios [12].

Asphaltenes are complex and poorly understood fraction; and have a high polarity and coking tendency. They are no-distillable fraction of crude oils. Their tendency toward clogging pipes in petroleum refineries has caused asphaltenes to be known as “the cholesterol of petroleum”. In fact, asphaltenes naturally do not make any troubles as long as they are stable. Any changes in temperature, pressure and oil compositions during enhanced oil recovery (EOR) processes; or mixing the oil with diluents or other oils; and during stimulation treatments with acid may disturb their chemical stabilities, and then result in their precipitation and deposition [3-5]. Generally, pressure and composition have major effects while temperature’s effect is minor.

As seen the earlier paragraphs, it is obvious that the subject of asphaltene is too hard to be explained concisely in just one chapter. However, a tremendously big effort was made to sum up all important asphaltene aspects as a review in following headings. Needless to say that, for more information about a specific subject about asphaltene, you should refer to other papers as well.

2. ASPHALTENE DEFINITION

Asphaltenes in residues are dark brown to black friable solids that have no definite melting point, and when they are heated, usually intumesce, then decompose leaving their carbonaceous residues. Asphaltenes are a fraction (or a part) of heavy oils and bitumens that are soluble in light aromatics and cyclic solvents (e.g., toluene, benzene); and carbon disulfide and chloroform (or other chlorinated hydrogen solvents) but insoluble in light normal alkanes (e.g., nC5, nC6, nC7); and carbon dioxide [6-7]. In ASTM D-3279/90 (IP 143/90) approach, asphaltene is also defined on the base of solubility.

3. FACTORS INFLUENCING AMOUNT AND COMPOSITION OF PRECIPITATED ASPHALTENE

There are several important parameters that influence amount and composition of asphaltene precipitation, some of which are presented in the following paragraphs:

3.1. Solvent Type

Adding solvents with different contents to a crude oil having an asphaltene fraction can cause various amounts of asphaltene precipitation. As a rule of thumb, the more carbon numbers a solvent has, the lower value of precipitation asphaltene it makes. However, the amount of precipitated asphaltene decreases till n-C7 solvent, and then for a higher carbon number than n-C7 its decrease is negligible (Figure 2). To meticulously consider the types of used precipitant culminating in an asphaltene precipitation in a mixture, Speight et al. proposed to name asphaltene precipitation by its precipitant, for instance, nC5-asphaltenes, nC6-asphaltenes, nC7-asphaltenes and so on. These reserchers indicated the direct relation between the aromaticity degree of asphaltene precipitation with the carbon number of their

applied solvents. They showed that by increasing the carbon number of used solvents, the aromaticity degree of precipitated asphaltene increases, or in other words, the H/C ratio of asphaltene decreases. On the other hand, its molecular weight increases by increasing carbon number of precipitants (Figure 3) [7]. Titration with n-C7 usually results in higher N/C, O/C and S/C ratios in precipitated asphaltene. That means crude oil initially has been had a lot of N, O and S elements [3].

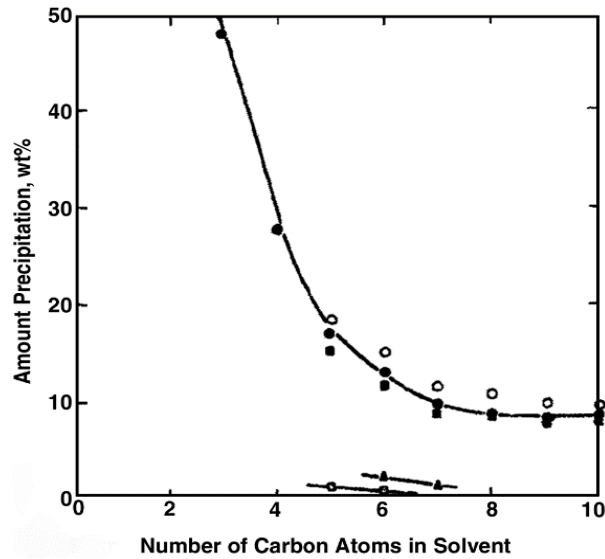


Figure 2. Amount of precipitated asphaltene for different paraffin precipitant [6].

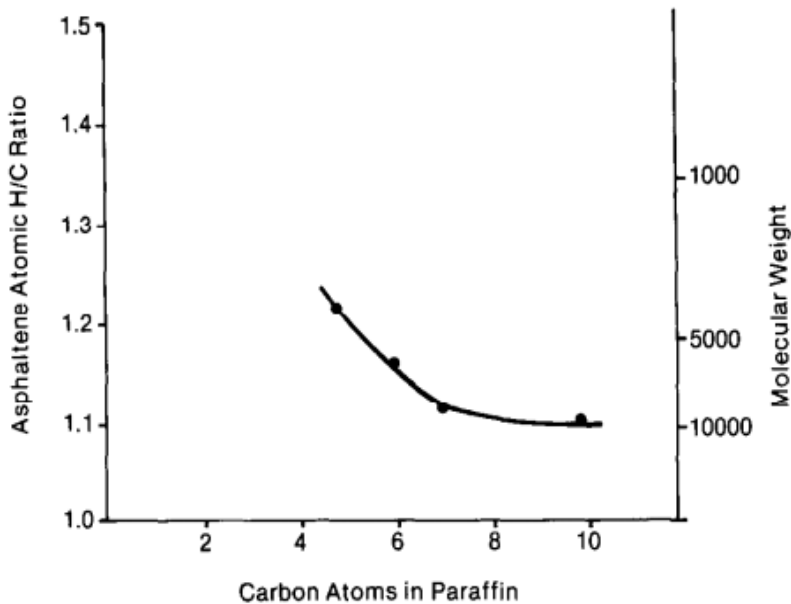


Figure 3. Aromaticity degree (H/C) and molecular weight of asphaltenes vs. carbon number of precipitant [7].

Table 1. Solvent-Oil ratio of standard methods for asphaltene precipitation [8]

Method	Precipitant	Volume precipitant per g of sample (ml)
ASTM D-893	<i>n</i> -pentane	10
ASTM D-2006	<i>n</i> -pentane	50
ASTM D-2007	<i>n</i> -pentane	10
ASTM D-3279	<i>n</i> -heptane	100
ASTM D-4124	<i>n</i> -heptane	100
IP 143	<i>n</i> -heptane	30
Syncrude method	<i>n</i> -pentane	20

3.2. Solvent-Crude Oil Volume Ratio

At different references for each of solvents, an optimum solvent-oil ratio has been proposed for precipitating asphaltene from oil. This means that any ratios less than the optimum values lead to losing some asphaltene content of oil, which results in an incorrect chemical analyzing of asphaltene molecules. On the other hand, adding an extra solvent is useless as well. Therefore, for practical usage of solvents in order for researchers could advance their investigations, Speight [8] has tabulated the optimum value of solvent-oil ratios taking advantage of some literatures [4-5, 9-12]. This classification has been presented in Table 1.

3.3. Temperature

At high temperatures, about from 200 to 600°C (typically at $T > 350^\circ\text{C}$), asphaltenes are degraded and yield carbon and volatile products. At temperatures higher than 350 °C, CS₂ (carbon disulfide) is an important compound as gaseous by-products of asphaltenes [11]. Asphaltene solubility and temperature are in an inverse relationship [6]. It should be mentioned that analysis of samples that have been endured such high temperatures are somehow misleading, for example, samples prepared from a reservoir after in-situ combustion is hard to scrutinize.

3.4. Solvent (Precipitant) – Oil (Sample) Contact Time

Speight et al. did experiments to survey the role of this factor, and their results are shown in Figure 4 [7]. According to their studies, required time for precipitated asphaltene to be stabilized is about 8 hours. In order to ensure the reproducibility of asphaltene content of samples, contact times should be counted till 12-16 hours. On the other hand, for contact times longer than 16 hours, resins will be adsorbed on isolated asphaltenes' surface; consequently, it introduces a severe condition for instructors to remove the adsorbed resins from the asphaltene surface; and eventually, the adsorption diminishes the accuracy of measurements.

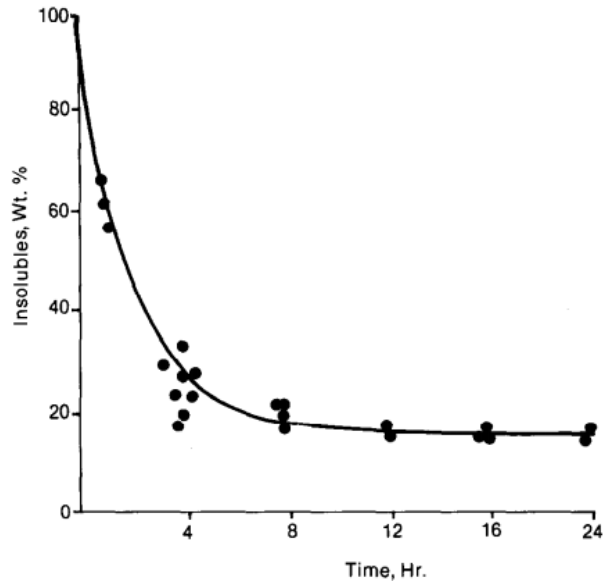


Figure 4. Amount of asphaltene precipitation vs. solvent-sample contact time [7].

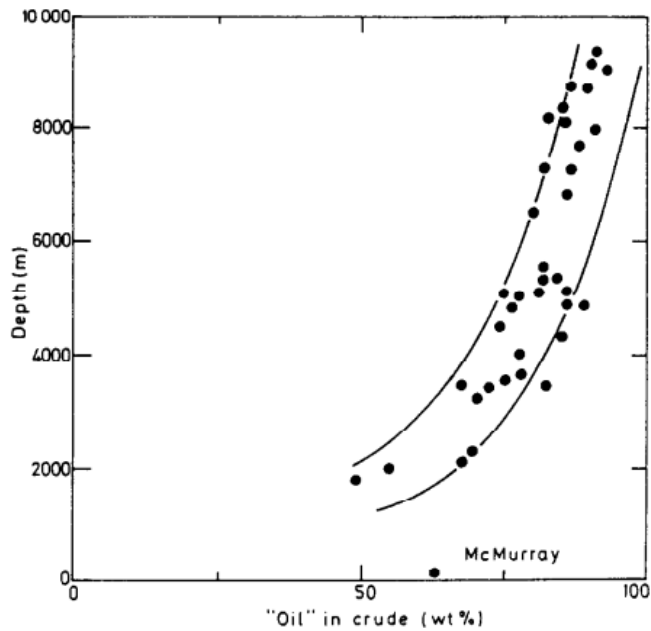


Figure 5. Burial depth of oil vs. oil percent of crude oil [13].

3.5. Origin of Crude Oil or Bitumen

Initial composition and molecular weight of carbonaceous source; and sedimentation's and oxidation's environment have a major effect on nature of asphaltenes. Koots and Speight surveyed the effects of burial depth and API gravity of oil on asphaltics (i.e., asphaltenes plus reins) content of oil (Figure 5 and 6) [13]. It was cited by Ancheyta et al. [14] that Speight

and coworkers [15] also studied the effect of geographic region and depth of oil zone on the API and quality of produced oil. These two factors affect the content and properties of separated asphaltene from the crude oil. As shown in Figure 7, Ancheyta et al. have presented schematically the effect of API gravity on asphaltene content of crude oil samples from difference references [14].

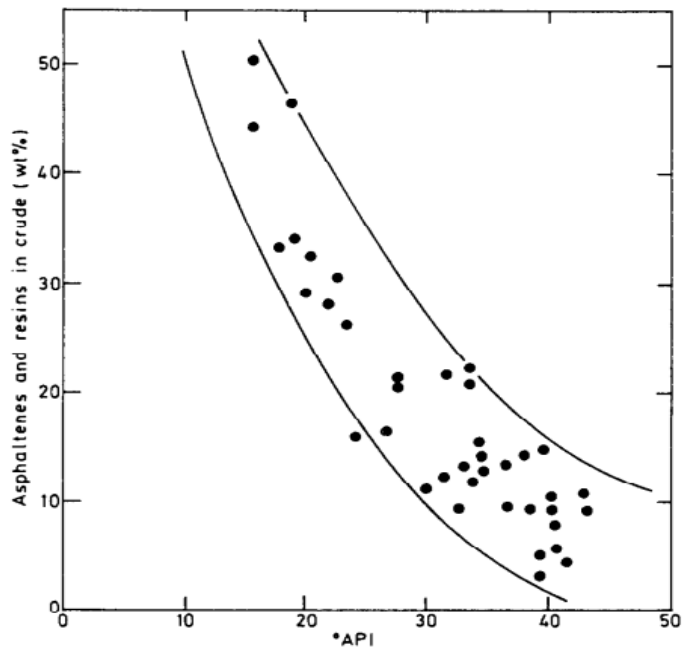


Figure 6. API gravity effect on asphaltic content of crude oil [13].

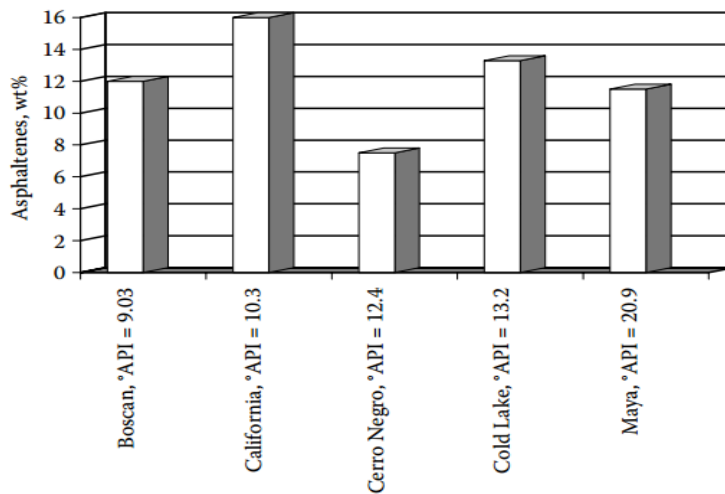


Figure 7. Asphaltene content of different crude oil [14].

To ensure the stability of separated asphaltene drawn from oil phase using the titration approach, Speight suggested to employ the following parameters [8]:

Use either n-pentane or n-heptane (preferentially n-heptane)

Solvent-oil ratios should be greater than 30ml:1g

8-10 hours is suitable for contact time of solvent-oil

To reach better results, try to conduct the precipitation sequence in three times to remove any adsorbed low molecular resins from asphaltene fraction. The precipitation sequence involves dissolution of asphaltene constituents in benzene or toluene (10 ml per gm asphaltene) followed by addition of hydrocarbon (50 ml precipitant per ml toluene or benzene) to solution.

4. SARA ANALYSIS

Economically, the effectiveness of an EOR process depends on the crude oil composition of a reservoir bed. Crude oil mixture usually contains from the lightest to heaviest components. Many analytical methods using chromatography have been applied for better knowing of its compounds. It should be noted that the amount of derived information from every chromatographic separation depends on the detectors used in experiments [16].

4.1. Analytical Group Analysis Methods [17]

- PONA (Paraffins, Olefins, Naphthalene and Aromatics).
- PIONA (Paraffins, Iso-Paraffins, Olefins, Naphthalene and Aromatics).
- PNA (Paraffins, Naphthalene, and Aromatics).
- PINA (Paraffins, Iso-Paraffins, Naphthalene and Aromatics).
- SARA (Saturates, Aromatics, Resins, and Asphaltenes).
- PIN (n-Paraffins, Iso-Paraffins and Naphthalene). Further fractionation of Saturate fraction of SARA analysis into PIN [18].
- USBM-API (U.S. Bureau of Mines- American Petroleum Institute): Acids, Bases, Neutral Nitrogen compounds, Saturates, and (mono-, di-, and poly-) Aromatic compounds.
- Multi-dimensional (Hybrid) techniques: These types are a combination of two or more chromatograph techniques mentioned above for gaining further information about individual components of each chemical fractions.

Due to huge global demands of fuel energies, requests for more oil production either by new sources' exploitation such as oil shale or applying enhanced oil recovery process are raising every year. More oil production has been associated with reducing oil quality and oil API gravity [19]. Thus, characterization of heavy end of the crude oil is an important issue today. One of the group type analysis methods that has been presented for separating heavy crudes is SARA analysis [20-21]. According to this method, crude oil is classified into four main chemical classes based on solubility, polarizability and polarity.

4.2. Fractions Separated During SARA Analysis

- The letters in SARA stands for Saturates, Aromatics, Resins and Asphaltenes.
- Saturates: This fraction includes the straight or branched saturated hydrocarbon chains (paraffins and iso-paraffins respectively) and also cyclic saturated hydrocarbons (cyclo-paraffins), e.g., cyclo-pentane.
- Aromatics: Hydrocarbons with one or more unsaturated ring structures; i.e., one or more benzene's structures or its derivatives.
- Resins and Asphaltenes: These groups primarily are a subclass of aromatics although some resin molecules may contain only naphthalene's structures. Resins and asphaltenes are the most polar components of petroleum. Additionally, they are large molecules with 3 to 10 or more ring structures per molecule.

SARA analysis is being used for heavy oils, including vacuum distillates, atmospheric and vacuum residues, bitumens and asphalts that their light end losses are minimal. Conventional crude oils can be topped to $T > 270^{\circ}\text{C}$ prior to SARA analysis so as to reduce light end losses at subsequent separations and let $T < 270^{\circ}\text{C}$ distillates to be analyzed by other methods, usually GC-MS method [22]. Heavy or bio graded crude oils with few light ends can be analyzed directly without losing considerable light end components.

4.3. Techniques for SARA Separation and Analysis

These approaches can be subdivided into three types:

4.3.1. Gravimetric Adsorption Chromatography

It was first presented by Jewell et al. [21] as the founders of SARA fractions separation. This technique is also known as ASTM D2007 method or open column (glass column) clay-gel adsorption chromatography method. In ordinary column chromatography, the gravity force is an agent of passing mobile phase (solvent and liquid) through column, and there is no any pressurizing of mobile phase in this technique. In addition, stationary phase usually is activated silica gel or aluminum oxide. ASTM D2007 usually combines with ASTM D1319 and ASTM D6560 [23]. ASTM D1319 uses a fluorescent indicator for quantification of saturates, olefins, and aromatics in lighter fraction of crude oil. ASTM D6560 is used for precipitating and quantify heavier fraction of crude oil (n-heptane insoluble). The deasphalted remained oil is further fractionated by ASTM D2007. This combination presented here is a very preparative useful method for a large volume of a sample and solvent. It should be noted that the mentioned technique needs intrinsically a large amount of time and sample (and solvent) for its operation, which it can be named as two important disadvantages of this technique. Besides, it does not usually yield pure fractions of each group, and the cross contamination causes considerable inaccuracies in the results [24].

4.3.2. High Pressure (or Performace) Liquid Chromatography (HPLC)

Suatoni and Swab [25] proposed using of automated high pressure liquid chromatography column in oil industry, as it is a rapid analytical analysis of feedstock. This method requires small amount of sample compared with open column chromatography.

Its instruments typically include: I) a sampler for injection sample to column, II) a pump to pass pressurized (50-350 bar) mobile phase -solvent containing the sample mixture-through column and III) a detector.

HPLC is faster, more producible and more readily automated than open column technique; and also, it is applicable for all boiling ranges. Both techniques, open (normal) column and HPLC column techniques have been utilized for analyzing of deasphalted samples or maltenes (Figure 8). Additionally, only saturates and aromatic fractions are eluted and quantified with both methods and resin fraction is back-flushed and quantified gravimetrically. Therefore, both preparative techniques face a difficult procedure for sample preparing.

4.3.2.1. Evaluation of Different Detectors for HPLC Technique [26]

4.3.2.1.1. Refractive Index Detector (RID)

This detector measures the refractive index of an analyte relative to the solvent. Suatoni and Swab [25] claimed that HPLC column is applicable for all boiling ranges and for different samples, but at first, its refractive index detector must be calibrated. Needless to say that, calibration of refractive index detector (RID) is really a tedious work to do.

4.3.2.1.2. Flame Ionization Detector (FID)

Although flame ionization detector (FID) is the best in gas chromatography particularly for organic volatile species in gases, in the presence of "heteroatoms", such as oxygen and sulfur, the detector performance is reduced. Also, it is associated with noise problems and reproducibility of analysis for heavy end of oil. Because an interface must be used to remove the mobile phase first. Afterwards, solvent must be removed and solute must be transported to FID. Doing this procedure makes errors in the SARA analysis.

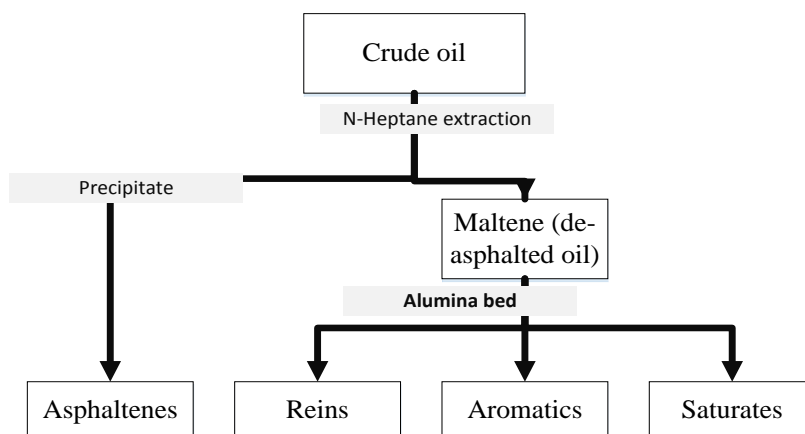


Figure 8. Two step SARA fractionation analysis [31].

4.3.2.1.3. *Tracor 945 LC-FID*

Pearson and Gharfeh [26] evaluated the Tracor 945 LC-FID [27] as a detector in HPLC for quantification. They concluded Tracor 945 LC-FID is having better performance than the former. The newest study about SARA analysis with HPLC method returns to the work of Bissada et al. [28]. They proposed a novel automated multidimensional high performance (or pressure) liquid chromatography (AMD-HPLC).

4.3.3. *Thin Layer Chromatography (TLC) with FID [29]*

Although HPLC technique is faster and more reproducible than normal column, both normal and high pressure liquid column are applicable for de-asphalted samples. In addition, because of general characteristics of these preparative methods, they have rather low accuracy and precision for analyzing a small volume of sample [30]. A severe shortcoming of most HPLC approaches is the difficulty in obtaining accurate response factors applicable to different distillate products. Unfortunately, accuracy can be compromised when these response factors are used to analyze hydro treated and hydrocracked materials having the same boiling range [16].

TLC method is a rapid and inexpensive analysis method for various mixtures. In TLC method, adsorbent material such as silica gel, aluminum oxide is packed on a sheet instead of a column and has been activated. For quantification in TCL method, a flame ionization detector (FID) is used. Combination of TLC with FID is known as Iatroscan technology that has a pretty high accuracy.

4.3.3.1. *TLC-FID Advantages [23, 31]*

1. It can be applied to whole crude oils without de-asphalting and an extensive sample preparation. SARA fractions can also be obtained simultaneously by means of this method.
2. It is the fastest and lowest cost; plus, can be conducted in a straightforward manner.
3. It has a high precise and needs very small amounts of sample and solvent.
4. Multiple samples can be analyzed simultaneously.

4.3.3.2. *TLC-FID Disadvantage*

Bisht et al. [23] have mentioned two main problems of TLC-FID method from various references:

1. Calibration and standardization for each fraction must be performed using the most representative pure. This work is required because the FID response is not uniform for all components even within individual fractions [32-35].
2. This technique is just useful for high boiling fractions' temperature. Because lighter and volatile materials get lost during spotting the layer, elution, drying and analysis [9, 34].

TLC-FID is utilized widely in different fields, such as biology, medicine, pharmacy and oil industry. A comprehensive study related to TLC-FID was published by Ranny [36].

5. DIFFERENCES BETWEEN ASPHALTENE AND OTHER HEAVY FRACTIONS OF A CRUDE OIL

There is a close relationship between asphaltenes, resins and higher molecular weight aromatic hydrocarbons in crude oils. Heavy aromatics are gradually oxidized and transformed to resins. By continuing oxidizing, resins will be transformed to asphaltenes [13].

5.1. Resins

- Resins are the most polar end of SAR series (Maltenes) even though they are less polar than asphaltenes. They usually contain heteroatoms similar to asphaltenes.
- Resins have lower molecular weight than asphaltenes, and also variation of resins' molecular weight's range is narrower with respect to asphaltenes' range.
- Resins have chemical structures similar to asphaltenes' but in much smaller size.
- Ring systems in asphaltenes are more complex than resins' ones.
- Resins have surrounded asphaltene molecules either through electron-pair donor-acceptor forces or through hydrogen bonding forces and bring about asphaltene's stability [12]. Therefore, adding more resin results in somewhat more asphaltene stability (Figure 9).
- Resins are a portion of maltenes that are absorbed by activated surface of materials, such as silica or alumina (aluminum oxide).
- In contrast to asphaltenes, resins are soluble in n-pentane and n-heptane.
- Liquefied petroleum gases, such as methane, ethane, propane diluents will precipitate more materials, because they precipitate both resins and asphaltenes. Commercially, propane is used in processing petroleum residues for asphaltene constituents and resin constituents [8]. Precipitated solid with liquid propane is called propane asphalt.
- Resins cannot associate and peptize asphaltenes from another crude oil source and disperse them as a colloid. It returns to the assumption of association of resins with asphaltenes in the manner of an electron-pair donor-acceptor system [13].
- Based on an experimental evidence, Wu et al. postulated that asphaltene molecules can associate with either themselves or resin chains whereas resin chains cannot associate with themselves [37]. It is related to the different number of association sites on each of them.
- Asphaltenes consist primarily of propagators (molecules with multiple active sites for association). Resins, which are well-known to affect asphaltene association, consist primarily of terminators (molecules with only one active site) [38].

5.2. Petroleum Wax (So-Called Wax)

- Petroleum Wax is composed entirely of paraffins with a carbon number typically greater than 18. In other words, they are made of saturate (PIN) fraction of oil [39].

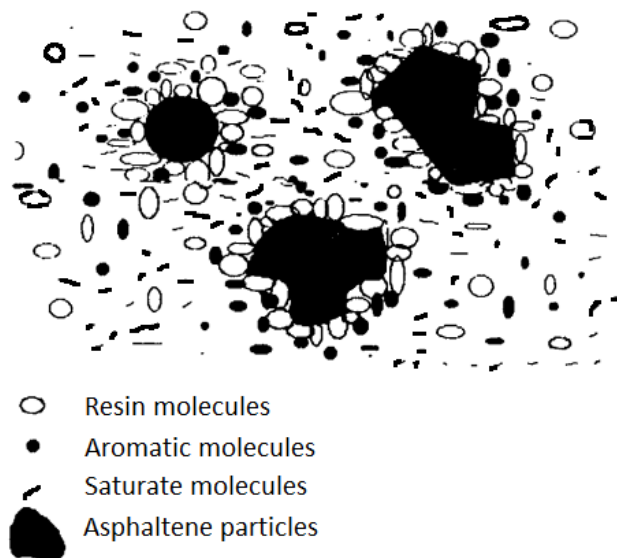


Figure 9. Asphaltene peptized by resins [63].

- Wax is solid at ambient temperature and it melts by heating.
- Asphaltene and wax precipitation and deposition are two independent processes. Actually, temperature, pressure and composition changes have different effects on these two processes. For example, pressure increase causes CPT (Cloud Point Temperature) in crude oil to be raised, and eventually culminates in more wax precipitation while pressure increase may cause or prevent of asphaltene precipitation [40].
- Wax deposition phenomenon is severely a temperature-dependent material. Temperature increase reduces wax precipitation (Figure 10) while temperature has a minor effect on asphaltene stability, and its change may cause or prevent of asphaltene precipitation.
- Asphaltene precipitation occurs typically at high pressures and temperatures. It means that asphaltene precipitation occurs earlier than wax deposition (Figure 10).
- Adding a light hydrocarbon to a crude oil reduces wax creation while excess light hydrocarbon makes an impact on asphaltene precipitation. Besides, adding a little amount of polar solvent can strongly affect asphaltene stability while such addition has a negligible effect on wax deposition.
- Precipitated asphaltene and wax are different in composition. Precipitated asphaltene is mainly composed of asphaltenes, resins and other aromatics while created wax is free of them.

Furthermore, it should be pointed out, cloud point and pour point of petroleum are two important parameters for controlling of wax deposition phenomena. When temperature is reduced during transportation through pipelines, waxes freeze out of crude oil and form crystals. Formed crystals have two structures, depending on their compositions. a) Macrocrystalline: composed of (n-i-) paraffins, (usually < C40), b) Microcrystalline:

composed of naphthalenes (usually $>C_{40}$). Unlike their apparent names, the Microcrystalline groups include more material varieties having more carbon numbers.

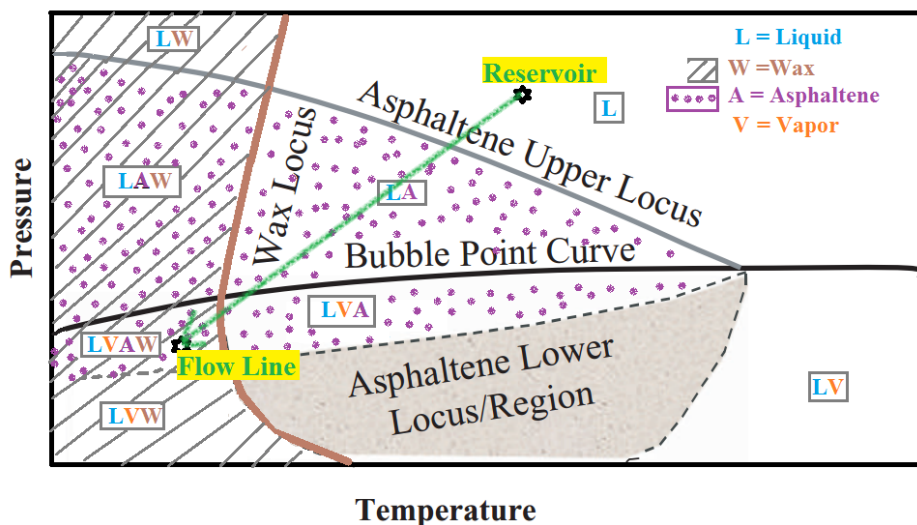


Figure 10. Pressure-temperature phase diagram for asphaltene and wax [22].

Usually separated asphaltene fraction with SARA separation methods consists of a high concentration of microcrystalline waxes ($>C_{40}$) that bring about a misinterpretation of geochemical characteristics of asphaltene fraction as well as total wax composition. Additionally, for phase behavior modeling of waxes and asphaltenes; we need to know an accurate indication of the wax and asphaltene content of oil. Misleading and ambiguous results will be obtained if fractions are cross-contaminated [41].

6. ASPHALTENE PRECIPITATION PROBLEMS

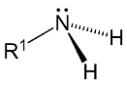
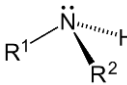
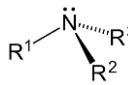
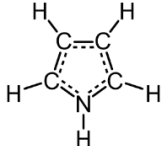

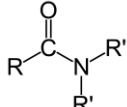
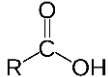
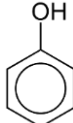
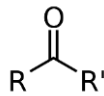
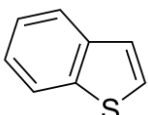
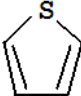
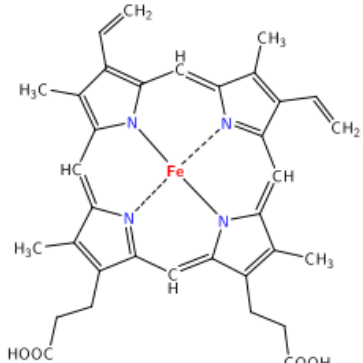
Asphaltenes molecules and precipitated solid particles of asphaltenes are not problematic by themselves, they need to be aggregated to be a troublemaker [42]. Asphaltene deposition problem may occur in porous media (formation), tubing's wall, transportation lines, end of deadlines that are closed, separation and transportation facilities. As soon as asphaltenes precipitate in separators; they may deposit on the bottom of the separators or they may act as a stabilizer of oil-water emulsions. If the latter occurs, oil water separation will be severely cumbersome.

Asphaltene existence makes catalysts inactive in refinement processes by depositing on their surfaces [43]. Asphaltene deposition on minerals' surfaces inside reservoir, specially near wells, will block pores, throats or even may change wettability of reservoirs to oil wet inevitably. Happening so, it decreases oil mobility. Asphaltene deposition during production or EOR processes reduces production rate and oil recovery significantly. Sometimes, asphaltene deposition's damage to production well or reservoir is irrecoverable. This may cause to lose completely the well. Inside pipelines, they gradually block the paths, so it is why asphaltene is known as "cholesterol of petroleum".

7. CHEMICAL COMPOSITION OF ASPHALTENES

Asphaltenes are a complex oil fraction that primarily consist of carbon, hydrogen, oxygen, nitrogen and sulfur, as well as trace amounts of iron, vanadium and nickel. Heteroatoms in asphaltenes can be found in the following forms (Table 2) [44]:

Table 2. Typical functional groups present in asphaltene molecules

			
Primary Amin (Nitrogen)	Secondary Amin (Nitrogen)	Tertiary Amin (Nitrogen)	Pyridine (Nitrogen)
			
Pyrrole (Nitrogen)	Amide (Nitrogen and Oxygen)	Carboxyl (Oxygen)	Phenol (Oxygen)
			
Ketone (Oxygen)	Benzothio-phenene (Sulfur)	Thiophene	Porphyrin (Nitrogen, Oxygen and Iron)

- Hetero-aromatic compounds whose sulfur presents in benzothiophene rings, and nitrogen presents in pyrrole and pyridine rings.
- Bi or polyfunctional molecules whose nitrogen presents in amines and amides, and oxygen presents in such groups as ketones, phenols and carboxylic acids.
- Metals, for example, nickel and vanadium are placed alongside pyrrole nitrogen atoms in porphyrin ring structures.

Briefly, the N, S and O atoms are placed in associated functional groups such as acids, ketones, thiophenes, pyridines, and porphyrins [38]. Moreover, it was reported that the concentration of nickel and vanadium in asphaltenes increases linearly as API gravity of crudes increases [45].

Depending upon Speight's studies [17], Kokal and Sayegh [3] summarized variation ranges of heteroatoms and their proportions from 57 different asphaltenes from 8 countries as follows.

O: 0.3-4.9%
S: 0.3-10.3%
N: 0.6-3.3%
O/C: 0.003-0.045
S/C: 0.001-0.045
N/C: 0.007-0.023

Using studies of Speight and Moschopedis [46], Kokal and Sayegh [3] also reported the carbon and hydrogen content of different isolated asphaltenes with n-heptane as follows:

C: $82 \pm 2\%$
H: $8.1 \pm 0.7\%$

Isolated asphaltenes using n-pentane have more hydrogen percents (higher H/C ratio) because lighter solvents bring about more precipitation of lighter compounds with higher paraffinic degrees.

8. CHEMICAL STRUCTURE OF ASPHALTENES

Asphaltenes have not been defined exactly like to methane, ethane or any other known species. Asphaltenes are defined on the basis of their solubility class as a fraction of oil. In fact, they are polydisperse in nature. Thereby, we cannot attribute an exact expression or define a clear chemical structure for this fraction. There are a few physical and chemical based methods to find out the structures of asphaltene, resin and other heavy species in crude oil. These methods are as follows:

- Physical based methods: X-ray diffraction, mass spectroscopy, ESR spectroscopy¹, NMR spectroscopy², GPC³, IR Spectroscopy⁴, ultra-centrifugation, vapor pressure osmometry
- Chemical based methods: Oxidation, Hydrogenation.

Some researchers have proposed structural models in order to account for the structural elements of asphaltenes.

¹ Electron Spin Resonance Spectroscopy.

² Nuclear Magnetic Resonance Spectroscopy.

³ Gel Permeation Chromatography.

⁴ Infrared spectroscopy.

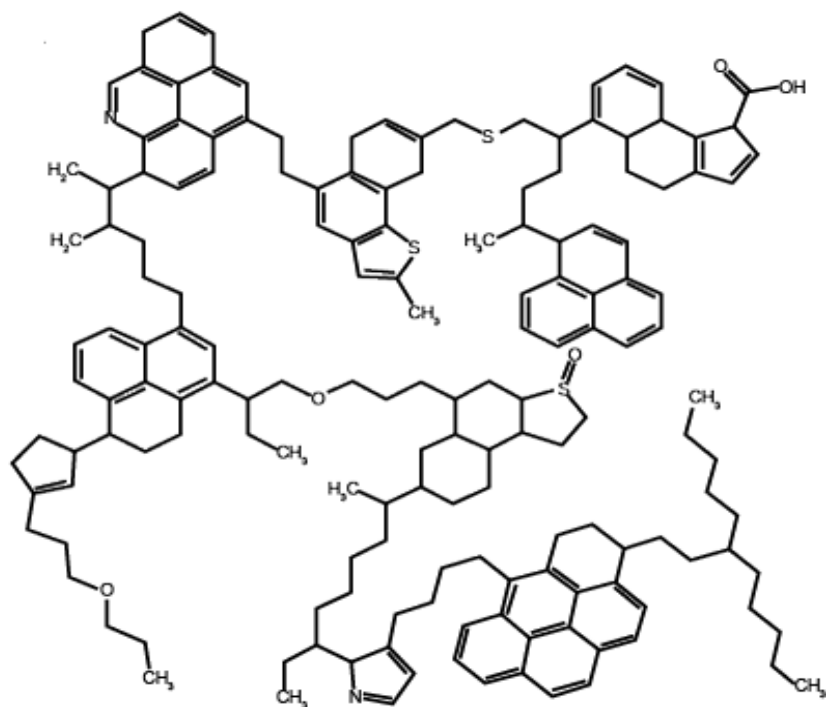


Figure 11. Archipelago structural model for asphaltenes [47].

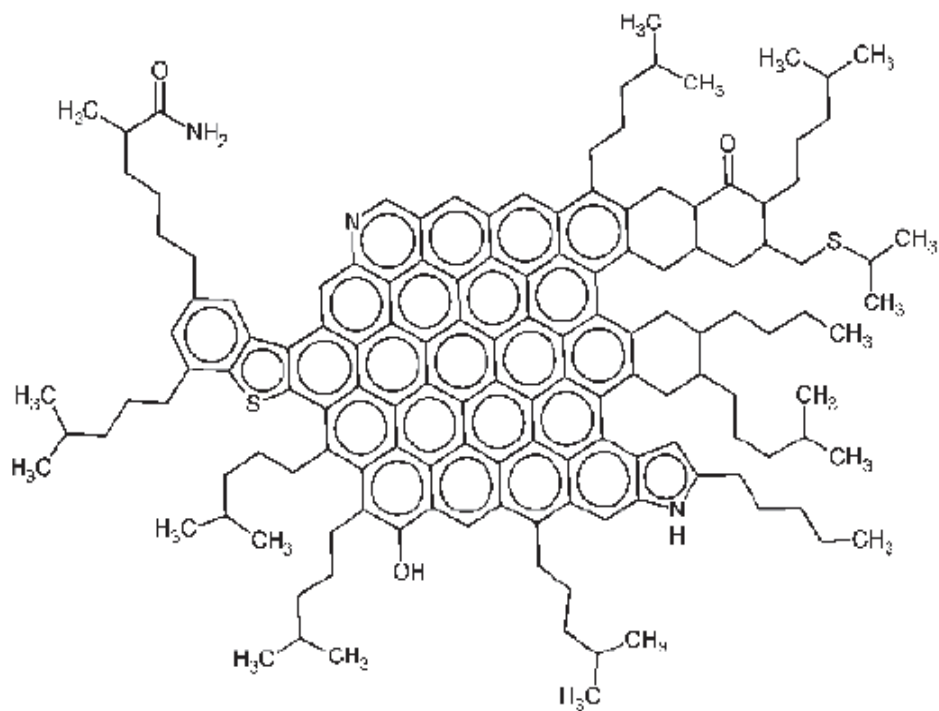


Figure 12. Continental (hand like) structural model for asphaltenes [48-49].

8.1. Archipelago Model

This structural model for asphaltenes has been proposed by Murgich et al. [47]. According to this model, each molecule is made from maximum 10 small poly aromatic hydrocarbons (PAH) that have been linked through aliphatic or sulfids bridge (Figure 11). This model is also called multi-aromatic core or multi-island model.

8.2. Continental Model

As sketched in Figure 12, to illustrate this model, Groenzin, Mullins and coworkers proposed a very large aromatic hydrocarbon that is surrounded with alkyl (aliphatic) branches [48-49]. In this model, that is also known as condensed aromatic cluster model, lower molecular weights for asphaltenes are estimated.

8.3. Modified Yen (Mullins-Yen) Model

It is the newest and most popular structural model. As it has been shown in Figure 13, the advantage of the modified Yen model [50] is its high ability to describe the hierarchical of cluster formation clearly. For light oils, this model considers asphaltene molecule as a single, moderately large poly-aromatic hydrocarbon (PAH) with peripheral alkyls. Some observations indicate in stable black oils, asphaltenes as nano-aggregates are dispersed throughout of their oil phase. This model also assumes that in stable black oils nano-aggregates are formed by cumulating of six numbers of asphaltene molecules comprised by a single disordered stack and peripheral alkyls interiorly and exteriorly, respectively. Furthermore, in unstable heavy oils which have higher asphaltene content, clusters can be formed by about eight piece of nano-aggregates [51]. This model has provided a framework for a tremendous number of studies to be conducted for asphaltene's entity.

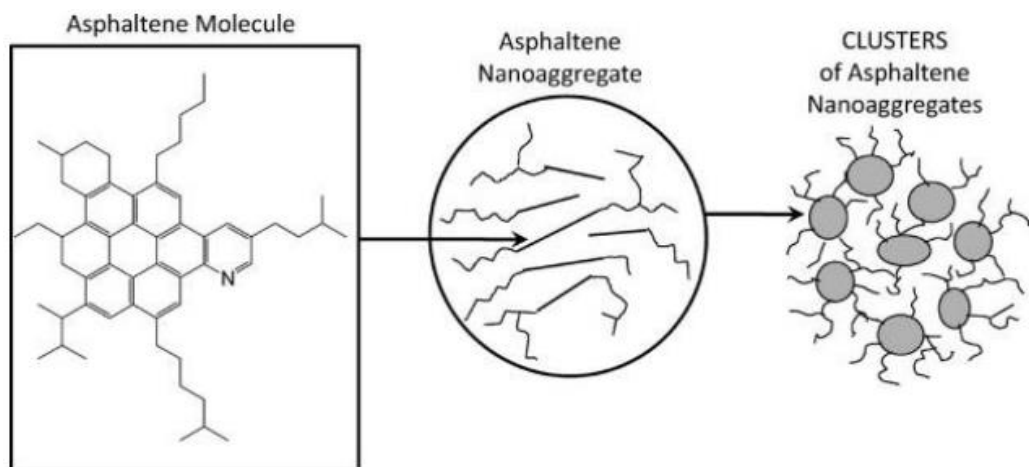


Figure 13. Modified Yen model [50].

9. MOLECULAR WEIGHT

Generally, asphaltenes have a high apparent molecular weight. Asphaltene's molecular weight depends on solvent's polarity and asphaltene's concentration, temperature, measurement technique and conditions. The absolute value of the asphaltene molecular weight is not important. What is essential in chemical engineering is the average and distribution of asphaltene's molecular weight [52].

Different ranges for molecular weight of asphaltene have been reported since asphaltenes tend to associate in the presence of non-polar (poorer) solvents and at low temperature. Due to polydispersity and self-association behavior of asphaltenes, their molecular weight depends on both temperature and concentration [53]. Asphaltene association may be due to hydrogen bonding and/or formation of charge-transfer complexes [54]. By using an additive to prevent asphaltenes from association or using high polar solvent such as pyridine their molecular weight falls into the range of 2000 ± 500 [8, 55-56].

Different techniques used to estimate the molecular weight of asphaltene include vapor pressure osmometry (VPO), viscometry, boiling point elevation, freezing point depression, light scattering, gel permeation chromatography (GPC), fluorescence depolarization, ultracentrifuge, and electron microscope studies. Amongst these methods, GPC and VPO are the most widely employed ones. Molecular weight range of asphaltenes with different methods has been tabulated by Dickie and Yen [57] and also summarized by Groenzin and Mullins [48].

Vazquez and Mansoori [58] obtained molecular weight distribution for n-C5, n-C6 and n-C7-separated asphaltene fraction with gel permeable chromatography. They observed that molecular weight distribution function for all the three types asphaltenes are bimodal (Figure 14).

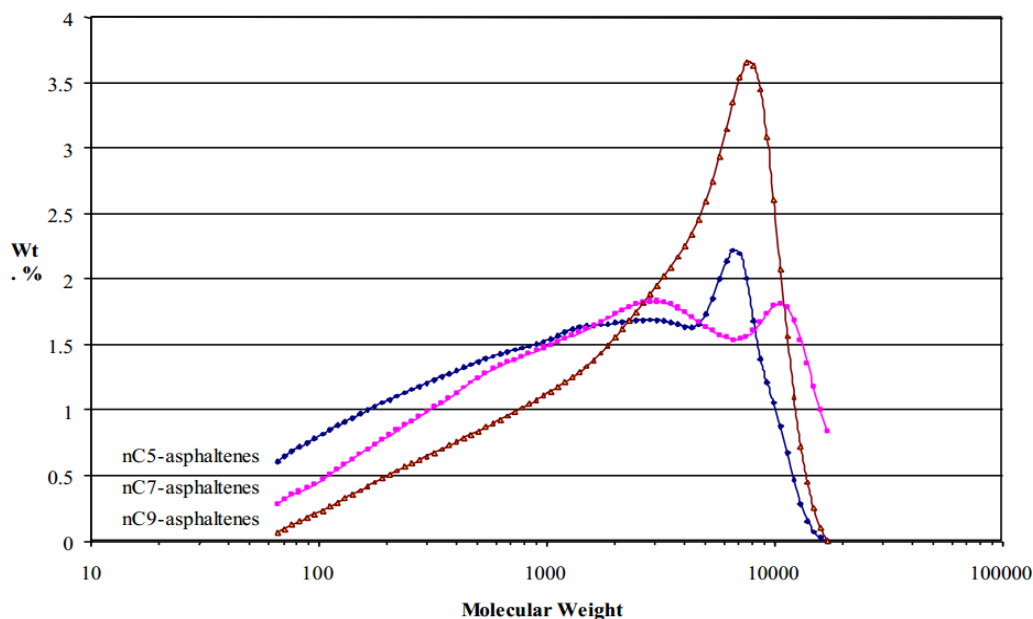


Figure 14. Molecular distribution function for all three n-(C5, C6 and C7) asphaltene [58].

10. STABILITY OF ASPHALTENE

Stability of asphaltene content of crude oil is independent of the amount and properties of asphaltene in the oil. Unexpectedly, asphaltene content of light crude oil is more apt to instability because light crude oils contain more light normal alkane (precipitant) and have lower asphaltene solubility. Therefore, light crude oils have a greater likelihood of asphaltene destabilization [59] whereas heavy crude oil's asphaltenes are less likely to cause problems because they contain plenty of intermediate components that cause asphaltenes to be stable.

Asphaltene's stability entirely depends on temperature, pressure, composition and shear rate. Change of these factors may be induced by a variety of processes, including primary depletion during primary oil recovery, injection of natural gas or carbon dioxide, thermal recovery, acidizing treatments and commingled production of incompatible fluids [60].

11. THERMODYNAMIC MODELS FOR PREDICTION OF ASPHALTENE STABILITY AND INSTABILITY

In the phase diagram, the region that asphaltene precipitates is called Asphaltene Precipitation Envelop (APE). Out of the APE region, asphaltene is stable in the crude oil. This region is limited to the upper and the lower onset pressure. The asphaltene precipitation phenomena can be controlled by analyzing and modeling asphaltene phase behavior in crude oil.

Traditionally, there are two points of view for behavior of asphaltene content in crude oil [61], known as solubility or lyophilic model [62] and colloidal or lyophobic model [63]. In the first point of view, asphaltenes are considered to be dissolved in oil and form a real solution and its precipitation is fully reversible. According to this view, asphaltene precipitation is due to reduction of solvent power. In the second point of view, asphaltene's molecules are assumed as suspended solid particles, which are peptized by resins. Existence of balance between adsorbed resins on the surface of asphaltene colloids and resins in the surrounding medium controls asphaltene stability. By adding any solvents that lead to lower resin concentration in oil phase, according to the Fick's law, resins are separated from asphaltene's surface and diffuse to oil phase. Afterwards, de-resined asphaltenes stick together and agglomerated asphaltenes are deposited. Apart above simple classification, Mohammadi and coworkers classified thermodynamic models for asphaltene behavior in oil to 5 classes as follows [64-65]:

1. Activity coefficient-based models
2. Equation of State (EOS) based models
3. Colloidal/Micellization models
4. Scaling laws, mathematical correlations and intelligent models
5. Association models

11.1. Activity Coefficient-Based Models

These models are based on regular solution or polymer solution theories [65]. Subramanian et al. [66] reviewed the most popular solution theories in their study. Simplest solution theory is regular solution theory. This solution has a moderately divergence from ideal solution. This theory attempts to explain solution non-ideality in terms of physical intermolecular interactions. A regular solution has the same ideal entropy of formation which is shown in Eq. (1). It is worth mentioning that for establishment of this equality (left-hand side of Eq. (1)), solution has to contain a random distribution of constituents. On the other hand, enthalpy of formation of the regular solution is non-zero unlike ideal solution (it means enthalpy has a value similar Eq. (2)).

Volume of regular solution is also equal to the sum of the volume of each constituent similar to the ideal solution.

$$\Delta S_{m_{ideal}} = \Delta S_{m_{regular\ solution}} = -nR(x_1 \ln(x_1) + x_2 \ln(x_2)) \quad (1)$$

$$\Delta H_{m_{regular\ solution}} = \beta x_1 x_2 \quad (2)$$

$$\Delta G_{m_{regular\ solution}} = \Delta H_{m_{regular\ solution}} - T\Delta S_{m_{ideal}} \quad (3)$$

1 and 2 subscripts denote mixture's constituents

x: mole fraction

n: mole number of all constituents of mixture

β : interaction parameter

Flory and Huggins were the first to calculate the entropy of mixing of long-chain molecules with the assumption that each segment of long-chain molecule occupies one site of the lattice similar to a molecule of the solvent. Namely, each segment of polymer chain has the same size of solvent molecule. They proposed the polymer-solvent interaction parameter, χ , as a dimensionless quantity that characterizes the difference between the solvent-polymer interaction energy and solvent-solvent interaction energy. Thus, a good solvent has a low Flory-Huggins interaction parameter's value, χ . This model was first developed for polymer solutions only, but was modified later by researchers such as Mohammadi, Nikookar and others [62, 65, 67-72] so as to determine the effects of pressure and composition on the onset conditions and the amounts of the precipitations, and was thus applied to materials other than polymer solutions. The expression for the Gibbs energy of the Flory-Huggins's solution is given by:

$$\Delta G_{m_{Flory\ Huggins}} = nRT(x_1 \ln(\phi_1) + x_2 \ln(\phi_2)) + nx_1\phi_2\chi \quad (4)$$

1 and 2 subscripts denote solvent and polymer, respectively

x: mole fraction

ϕ : volume fraction

V: volume

χ : Flory interaction parameter for solvent – polymer pair

If the polymer's segment number is equal to one, then the volume fraction will be equal to the mole fraction. Interaction parameter used in regular solution and Flory-Huggins theory can be calculated from solubility parameter via the Scatchard and Hildebrand's correlations [73-74].

One of the most prevalent models in this category is the Flory-Huggins model proposed by Hirschberg [62].

Models based on Flory-Huggins polymer solution theory assume either the precipitated phase consists of pure asphaltene or the precipitated phase consists of asphaltene and non-asphaltene components and the oil phase is free of asphaltene. This model may not be helpful for the conditions where the interaction parameter χ is near 0.5 and may require some modifications. Following that, Mohammadi and Richon [67] proposed a developed version of Flory-Huggins theory based model in which asphaltene is composed of a pseudo-component, whereby the precipitated and the oil phases could be comprised of asphaltene and nonasphaltene components. They showed that the existing traditional Flory-Huggins based models are specific cases of the developed model.

Another drawback of the Flory Huggins theory is that it has been derived for homogeneous polymer chain of uniform molecular weight (constant segment number) in a single uniform solvent. Unfortunately, this theory also ignores the free volume in lattice theory.

For heterogeneous polymer solution, Scott and Magat [75] extended Flory-Huggins theory to apply that for a polymer mixture of varying segment numbers. Their versatile theory is known as statistical mechanical Scott and Magat theory.

11.2. Equation of State (EOS) Models

This category includes models that use an equation of state for prediction of asphaltene stability in crude oils. Based on what equation of state is used, this class is divided into three subclasses:

11.2.1. Cubic Equation of State

This type of equation of state has physical parameters, such as critical temperature, critical pressure and acentric factor. As a result, they just consider the physical or van der Waals interactions of materials. A famous model for estimating asphaltene phase behavior that uses a cubic EOS was proposed by Nghiem and Coombe [76]. Nghiem and Coombe divided the heaviest pseudo component of crude oil, typically C32+, into two parts; non-precipitated component, C32A+, and precipitated component, C32B+ (as seen from Eq. 5). When asphaltene is stable, the amount of C32A+ is equal to C32+. By decreasing asphaltene stability, some amounts of C32A+ are converted to C32B+. Nghiem's model is known as solid model. This model considers asphaltene as a single-component solid phase that is in equilibrium with liquid phase. The prevalent EOSs used in oil industries and commercial simulators like CMG are cubic type, such as Peng-Robinson and Soave-Redlich-Kwong cubic equation of state. The major drawback of these cubic EOSs is their inaccuracy in prediction of fluid phase behaviors of materials containing complex and vastly different size molecules [77].

$$C32^+ \text{ mole fraction} = C32A^+ \text{ mole fraction} + C32B^+ \text{ mole fraction} \quad (5)$$

11.2.2. Cubic Plus Association Equation of State (CPA-EOS) Based Model

These equations of state consist of two terms, one term for considering physical interactions, which is intrinsically a cubic equation of state (normally PR or SRK cubic EOS), and another for considering association interactions [78]. The distribution of two mentioned terms as molecular interactions has been shown in Eq. 6.

$$Z = Z_{ph} + Z_{ch} \quad (6)$$

Firoozabadi and Li [61] applied the CPA equation of state for studying asphaltene precipitation of live oils involving pure components, pseudo-hydrocarbon components and hydrocarbon residues. They used liquid-liquid phase equilibrium for upper part of APE (between upper onset pressure and bubble point curve) and implemented a vapor-liquid-liquid phase equilibrium for lower part of APE (between lower onset pressure and bubble point curve) in their defined pressure-temperature phase diagram. Shirani et al. [79] modeled asphaltene precipitation for three different live oils. They also utilized CPA equation of state due to association nature of asphaltenes. For more information about CPA equation of state please refer to the book written by Kontogeorgis et al. [80].

11.2.3. SAFT Equation of State Based Model

SAFT equation of state is a statistical thermodynamic based EOS. This equation is derived using first order perturbation theory of Wertheim (TPT1) by Chapman et al. [81]. SAFT EOS is expressed by Helmholtz free energy. In original SAFT EOS, a hard sphere system was used as a reference system in order to add any physical or chemical perturbations. Eq. 7 demonstrates the three main components of residual Helmholtz free energy in SAFT equation of state.

$$a^{res} = a^{seg} + a^{ch} + a^{ass} \quad (7)$$

In the above equation, a and res represent the reduced and residual Helmholtz free energy, respectively. The seg , ch , ass superscripts denote segment, chain and association contribution of residual Helmholtz free energy, respectively.

Normally, a SAFT-type equation of state has three parameters for non-associating compounds and two more parameters for associating compounds. These parameters can be found by fitting the model with saturated liquid density and vapor pressure data, and the exactness of the predicted parameters is normally expressed in AAD percent (Average Absolute Deviation).

David et al. modeled asphaltene phase behavior in a model live oil (mixture of nC7-asphaltene, toluene and methane) and in a recombined oil (stack tank oil with its separator gas) utilizing SAFT EOS [82]. They determined SAFT parameters for asphaltene by means of precipitation data prepared from oil titration with n-alkanes at the ambient temperature. David et al. assumed that in the asphaltic crude oil, polar-polar interactions are negligible and molecular size and van der Waals interactions dominate asphaltene phase behavior. Although they ignored association term in their SAFT equation of state, they finally observed there is a

good agreement between predicted bubble points and asphaltene instability of their SAFT model against experimental data.

Tabatabaei-Nejad and Khodapanah [83] developed other SAFT model to predict the lower and upper onset pressure during asphaltene precipitation, and compared their results against CMG simulator to show accuracy of the presented model with respect to the solid model.

Gross and Sadowski [84] considered hard chain as a reference system and applied perturbation to this system and derived PC-SAFT version. This model works better than original SAFT model for modeling of asphaltene phase behavior [77, 85-87].

Gonzalez et al. [86] used PC-SAFT equation of state to predict the onset of asphaltene precipitation with a simple and recombined live oil during pressure depletion as well as light gas injection (CO₂, N₂, CH₄ and C₂H₆) in an oil reservoir. They determined PC-SAFT parameters for pure components by fitting the model with saturated liquid density and vapor pressure data, and parameters of pseudo-components were estimated from molecular weight based on correlations.

Sabeti et al. [85] set up a model based on PC-SAFT to estimate the amount of asphaltene precipitation in a fluid under various temperatures, pressures and in presence of different solvents. In so doing, they chose a fairly new approach in order to use a minimum number of physically relevant parameters for estimating asphaltene precipitation during solvent injection in vapor-liquid-quasi liquid state. The only inputs were pseudo-components and PC-SAFT parameters in their asphaltene model. It should be mentioned that the method of estimating asphaltene precipitation was similar to that employed by the solid model with the main difference that PC-SAFT equations were used instead of cubic EOSs; as a result, the need to find the adjustable volume shift when using the cubic EOSs was obviated.

11.3. Colloidal/Micellization Models

Colloidal and micellization models consider asphaltene as a lyophobic constituent. In this category, for evaluating asphaltene precipitation, oil constituents are divided into polar and non-polar groups. Polar group consists of polar polyaromatic components that may also contain heteroatoms. In fact, this group is the end of heavy and nonvolatile fraction of crude oil and can be subdivided to resins and asphaltenes' subdivisions. Nonpolar group includes (iso/normal) paraffins, naphthalenes or cyclo paraffins and intermediate molecular weight aromatics [40].

11.3.1. Colloidal Model

Leontaritis and Mansoori [63] on the base of this premise that asphaltene's molecules are dispersed in crude oil as suspended particles, proposed colloidal model for asphaltene phase behavior. In this way, resins could be adsorbed on the asphaltene surface, and make them be stable. Thus, resins must exist in the crude oil in order for asphaltenes remain stable. Basically, this model supposes a thermodynamic equilibrium exists between the resins in oil phase and the resins adsorbed on the colloidal asphaltene surfaces.

In the colloidal model, with adding poorer solvents in the crude oil the asphaltene instability grows. To put it in another way, by injecting diluents into the oil, resin's concentration in the oil is reduced, and according to the first Fick's law defined in Eq. 8, as

the concentration gradient of resin's molecules in the oil phase and on the asphaltene's surface is changed, resin's molecules will be desorbed from asphaltene's surface and will diffuse into the oil phase. On the other hand, adding any toluene solvents into the crude oil ahead of asphaltene agglomeration and flocculation, will reverse asphaltenes and resins toward their stable conditions in colloidal form. Reversibility of the asphaltene's precipitation is a controversial issue which was discussed in detail by Ashoori et al. [88].

$$J = -D\left(\frac{\delta C}{\delta x} + \frac{\delta C}{\delta y} + \frac{\delta C}{\delta z}\right) \quad (8)$$

J : Diffusion Flux (mol/(Length²Time¹))

D : Diffusivity or Diffusion Coefficient

$\frac{\delta C}{\delta x}$, $\frac{\delta C}{\delta y}$ and $\frac{\delta C}{\delta z}$: concentration gradient in x, y and z direction, respectively.

11.3.2. Micellization Model

Although colloidal model is pretty famous, Firoozabadi and coworkers perused differences between asphaltene and wax properties; therefore, they deduced that colloidal model initially presented for wax precipitation is not appropriate for asphaltene, and proposed another model for asphaltene precipitation namely micellization model. In this model, asphaltene precipitation is evaluated for liquid-liquid system. The first liquid phase was supposed to be the heavier phase -precipitated phase in liquid state- that is composed of resin's and asphaltene's molecules. The second liquid phase was considered as the lighter one that contains all constituents of crude oil and resin's and molecule's monomers as well. Assuming so, asphaltenes and resins can exist in both liquid phases in micellization model [40, 89]. This model is based on the stabilization of asphaltene micelles beside resin molecules, and takes into account the aggregation and micellization natures of asphaltene and resin components [37, 40, 90-91].

In the micellization model, the amount of and also the composition of each phase are calculated based on the fact that the Gibbs free energy of the system must be minimal. In contrast to colloidal model, micelle's size can be changed depending upon the temperature of media. A micelle is composed of a core or kernel containing n_1 molecules of asphaltene and a shell consisting of n_2 resins' molecules. Sometimes, for the Gibbs free energy of the system to be its minimal amount, solvents molecules need to coat micelles shell and to create a solvation shell.

The standard Gibbs free energy of the system that is being shown with G_m^{00} represents the discrepancy between standard Gibbs free energy (standard refers to infinite dilution of the solvent) among n_1 molecules of asphaltene in the micelle's core and among n_2 resin's molecules in the micelle's shell.

$$\Delta G_m^{00} = \mu_m^* - n_1 \mu_{1a}^* - n_2 \mu_{1r}^* \quad (9)$$

ΔG_m^{00} : standard Gibbs free energy of the system

μ_m^* : Standard chemical potential of the solvent

μ_{1a}^* : Standard chemical potential of asphaltene's monomers

μ_{1r}^* : Standard chemical potential of resin's monomers

n_1 : number of asphaltene's molecules in micelle's core

n_2 : number of resin's molecules in micelle's shell.

11.4. Scaling Equation, Mathematical Correlations and Intelligent Models

Rassamdana and coworkers [92-93] developed a polynomial equation of third order as a scaling equation with two adjustable parameters to determine amounts of asphaltene precipitations against titration with n-alkanes. Years later, Mohammadi et al. [94] applied a mathematical method based on the Leverage approach in order to improve precipitation prediction in comparison with Rassamdana works. Ashoori et al. [95] used an artificial neural network (ANN) to compare output results of ANN in comparison with the scaling equation method. Although the study showed promising results, it should be considered that their ANN method requires numerous data sets so that it is robust enough to lead into reliable outcomes. Zendehboudi and coworkers [96-97] promoted the ANN model by optimizing that by ICA method and designed a model which was capable of estimating the amount of asphaltene precipitation and bubble point pressure for a crude oil at conditions of enhanced oil recovery. For this purpose, they used their experimental results in a wide range of pressure, temperature and amount of injected solvent for training of ANN. They finally proved that the ICA-ANN model brings more convincing outcomes compared to other mathematical models with an average error percentage less than 5% for estimating the amount of asphaltene precipitation and the bubble point pressure.

Mohammadi and coworkers [64, 98] could predict asphaltene contents, the upper and lower asphaltene onset pressures using the LSSVM method. Generally, the LSSVM and ANN strategy are similar in which they both require experimental data for training set and testing set. However, the LSSVM needs two adjustable parameters for producing an equivalent function. Therefore, the authors used experimental data of oils from the Middle East region in order to obtain the two adjoining constants and estimate asphaltene precipitation accurately. Apart from that, Chamkalani et al. [99-100] developed a program code using the LSSVM strategy to create relationships between the SARA fractions and refractive index (RI) values so that they could improve the accuracy of previous results presented by themselves. Here, RI represents the speed of light in a studied substance. In their developed simulator, the SARA fractions data and reservoir conditions were the input variables and RI was the output result. Eventually, they applied the stability criteria introduced by Fan et al. [101] in the simulator in order to monitor the asphaltene stability region in crude oil samples. These mathematical models, similar to ANN, also require numerous data sets in order to be reliable and efficient and not to be limited over a specified range of performance.

11.5. Association Models

Agrawala and Yarranton proposed an asphaltene self-association model in a manner analogous to polymerization process. They considered linear polymerization type for simplicity, and then, eluded that polymerization in three-dimensional manner will give better results [38].

This model's category considers association interaction of asphaltenes in its mathematical calculations, so all equations of state, such as SAFT and CPA, containing association interaction terms can take the advantage of Agrawala's and Yarranton's theory.

CONCLUSION

As mentioned earlier, asphaltene deposition is one of the big challenges in today's oil industries. The aim of this essay was to show wide ranges of viewpoints indicated by many researchers. Asphaltene definition, factors affecting asphaltene precipitation, methods for SARA analysis, proposed compositions and structures of asphaltenes and finally thermodynamic models for prediction asphaltene stability are cases in point that were briefly introduced throughout of this manuscript. The enormous subjects presented here show loads of people are scrutinizing asphaltene from modeling and experimental views. As it was pointed out, some numerical models are on the basis of polymers and some investigators made an attempt to adapt the models to asphaltene conditions. It means, overcoming asphaltene challenges requires versatile information about different branches of science.

Not only is the accuracy of methods important, but other parameters such as the required volume of samples and amount of time are also vital in heavy components analyses. For example, although open column chromatography method is an accurate manner for SARA analysis, the vast amounts of crude oil and solvent expose researchers to many difficulties. As another example, PC-SAFT models for predicting the amount of asphaltene precipitation are too time consuming for a wide reservoir even though they are promising tools in asphaltene phase behavior estimations. In brief, what was demonstrated here is a superficial claim from a deep ocean of asphaltene, so it was suggested for apprehending more detail knowledge study of other papers.

REFERENCES

- [1] Kurian, V. and R. Gupta, Distribution of Vanadium, Nickel, and Other Trace Metals in Soot and Char from Asphaltene Pyrolysis and Gasification. *Energy and Fuels*, 2016. 30(3): p. 1605-1615.
- [2] Tissot, B.P. and D.H. Welte, *Petroleum formation and occurrence*. 2013: Springer Science and Business Media.
- [3] Kokal, S.L. and S.G. Sayegh. *Asphaltenes: The cholesterol of petroleum*. in *Middle East Oil Show*. 1995: Society of Petroleum Engineers.
- [4] Arnaud, C.H., Digging into asphaltenes. *Chem. Eng. News*, 2009. 87(38): p. 12-17.
- [5] Lichaa, P.M. and L. Herrera. Electrical and other effects related to the formation and prevention of asphaltene deposition problem in Venezuelan crudes. in *SPE oilfield chemistry symposium*. 1975: Society of Petroleum Engineers.
- [6] Mitchell, D.L. and J.G. Speight, The solubility of asphaltenes in hydrocarbon solvents. *Fuel*, 1973. 52(2): p. 149-152.
- [7] Speight, J.G., R.B. Long, and T.D. Trowbridge, Factors influencing the separation of asphaltenes from heavy petroleum feedstocks. *Fuel*, 1984. 63(5): p. 616-620.

-
- [8] Speight, J., Petroleum Asphaltenes-Part 1: Asphaltenes, resins and the structure of petroleum. *Oil and gas science and technology*, 2004. 59(5): p. 467-477.
- [9] Fan, T., J. Wang, and J.S. Buckley. Evaluating crude oils by SARA analysis. in SPE/DOE Improved Oil Recovery Symposium. 2002: Society of Petroleum Engineers.
- [10] Hotier, G. and M. Robin, Effects of different diluents on heavy oil products: measurement, interpretation, and a forecast of asphaltene flocculation. *Revue de l'IFP*, 1983. 38: p. 101.
- [11] Moschopedis, S.E., S. Parkash, and J.G. Speight, Thermal decomposition of asphaltenes. *Fuel*, 1978. 57(7): p. 431-434.
- [12] Speight, J.G., Chemical and physical studies of petroleum asphaltenes. *Developments in petroleum science*, 1994. 40: p. 7-65.
- [13] Koots, J.A. and J.G. Speight, Relation of petroleum resins to asphaltenes. *Fuel*, 1975. 54(3): p. 179-184.
- [14] Ancheyta, J., F. Trejo, and M.S. Rana, Asphaltenes: chemical transformation during hydroprocessing of heavy oils. 2010: CRC press.
- [15] Speight, J., et al., Chemistry of asphaltenes. Advances in Chemistry series. MJ Comstock series editor. Washington DC, 1981. 1: p. 195.
- [16] Hayes, P.C. and S.D. Anderson, Rapid determination of naphthenes in hydrocarbon distillates using on-line column switching high-performance liquid chromatography with dielectric constant detection. *Journal of Chromatography A*, 1987. 387: p. 333-346.
- [17] Speight, J.G., *The chemistry and technology of petroleum*. 2014: CRC press.
- [18] Bissada, K.A., et al., Group-type characterization of crude oil and bitumen. Part II: Efficient separation and quantification of normal-paraffins iso-paraffins and naphthenes (PIN). *Fuel*, 2016. 173: p. 217-221.
- [19] Swain, E.J., Sulfur, coke, and crude quality--Conclusion: US crude slate continues to get heavier, higher in sulfur. *Oil and Gas Journal*;(United States), 1995. 93(2).
- [20] Corbett, L.W., Composition of asphalt based on generic fractionation, using solvent deasphalting, elution-adsorption chromatography, and densimetric characterization. *Analytical Chemistry*, 1969. 41(4): p. 576-579.
- [21] Jewell, D., et al., Ion-exchange, coordination, and adsorption chromatographic separation of heavy-end petroleum distillates. *Analytical Chemistry*, 1972. 44(8): p. 1391-1395.
- [22] Hammami, A. and J. Ratulowski, Precipitation and deposition of asphaltenes in production systems: a flow assurance overview, in *Asphaltenes, Heavy Oils, and Petroleomics*. 2007, Springer. p. 617-660.
- [23] Bisht, H., et al., Efficient and quick method for saturates, aromatics, resins, and asphaltenes analysis of whole crude oil by thin-layer chromatography–flame ionization detector. *Energy and Fuels*, 2013. 27(6): p. 3006-3013.
- [24] Barman, B.N., Hydrocarbon-Type Analysis of Base Oils and Other Heavy Distillates by Thin-Layer Chromatography with Flame-Ionization Detection and by the Clay—Gel Method. *Journal of chromatographic science*, 1996. 34(5): p. 219-225.
- [25] Suatoni, J. and R. Swab, Rapid hydrocarbon group-type analysis by high performance liquid chromatography. *Journal of Chromatographic Science*, 1975. 13(8): p. 361-366.

-
- [26] Pearson, C.D. and S.G. Gharfeh, Automated high-performance liquid chromatography determination of hydrocarbon types in crude oil residues using a flame ionization detector. *Analytical Chemistry*, 1986. 58(2): p. 307-311.
- [27] Dixon, J., A new flame ionization detector (FID) for liquid-chromatography. *Chimia*, 1984. 38(3): p. 82-86.
- [28] Bissada, K.A., et al., Group-type characterization of crude oil and bitumen. Part I: Enhanced separation and quantification of saturates, aromatics, resins and asphaltenes (SARA). *Organic Geochemistry*, 2016. 95: p. 21-28.
- [29] Karlsten, D.A. and S.R. Larter, Analysis of petroleum fractions by TLC-FID: applications to petroleum reservoir description. *Organic Geochemistry*, 1991. 17(5): p. 603-617.
- [30] Collinson, J., Correlation in Hydrocarbon Exploration: Proceedings of the Conference Correlation in Hydrocarbon Exploration Organized by the Norwegian Petroleum Society and Held in Bergen, Norway, 3-5 October 1988. 2012: Springer Science and Business Media.
- [31] Keshmirizadeh, E., S. Shobeirian, and M. Memariani, Determination of saturates, aromatics, resins and asphaltenes (SARA) fractions in Iran crude oil sample with chromatography methods: study of the geochemical parameters. *Journal of Applied Chemical Research*, 2013. 7(4): p. 15-24.
- [32] Bharati, S., et al., A new North Sea oil-based standard for Iatroscan analysis. *Organic geochemistry*, 1997. 26(1): p. 49-57.
- [33] Bharati, S., G.A. Røstum, and R. Løberg, Calibration and standardization of Iatroscan (TLC-FID) using standards derived from crude oils. *Organic geochemistry*, 1994. 22(3): p. 835-862.
- [34] Masson, J., T. Price, and P. Collins, Dynamics of bitumen fractions by thin-layer chromatography/flame ionization detection. *Energy and fuels*, 2001. 15(4): p. 955-960.
- [35] Orea, M., et al. Alternative calibration and standardization procedure of iatroscan TLC-FID for SARA hydrocarbon class quantification: Application to Tar-Mat zone identification. in *Abstracts of Papers of the American Chemical Society*. 2002: Amer Chemical Soc 1155 16TH ST, NW, Washington, DC 20036 USA.
- [36] Ranny, M., *Thin-layer chromatography with flame ionization detection*. 1987: Springer Science and Business Media.
- [37] Wu, J., J.M. Prausnitz, and A. Firoozabadi, Molecular thermodynamics of asphaltene precipitation in reservoir fluids. *AIChE journal*, 2000. 46(1): p. 197-209.
- [38] Agrawala, M. and H.W. Yarranton, An asphaltene association model analogous to linear polymerization. *Industrial and engineering chemistry research*, 2001. 40(21): p. 4664-4672.
- [39] Srivastava, S., et al., Phase-transition studies in n-alkanes and petroleum-related waxes—A review. *Journal of Physics and Chemistry of Solids*, 1993. 54(6): p. 639-670.
- [40] Firoozabadi, A., *Thermodynamics of hydrocarbon reservoirs*. 1999: McGraw-Hill.
- [41] Thanh, N.X., M. Hsieh, and R. Philp, Waxes and asphaltenes in crude oils. *Organic Geochemistry*, 1999. 30(2): p. 119-132.
- [42] Leontaritis, K. Asphaltene deposition: A comprehensive description of problem manifestations and modeling approaches. in SPE production operations symposium. 1989: Society of Petroleum Engineers.

-
- [43] Martinez, M.T., A.M. Benito, and M.A. Callejas, Thermal cracking of coal residues: kinetics of asphaltene decomposition. *Fuel*, 1997. 76(9): p. 871-877.
- [44] Demirbaş, A., Asphaltene yields from five types of fuels via different methods. *Energy conversion and management*, 2002. 43(8): p. 1091-1097.
- [45] Nahid Siddiqui, M., Infrared study of hydrogen bond types in asphaltenes. *Petroleum science and technology*, 2003. 21(9-10): p. 1601-1615.
- [46] Speight, J.G. and S.E. Moschopedis, Some observations on the molecular nature of petroleum asphaltenes. *Am. Chem. Soc., Div. Pet. Chem., Prepr.;*(United States), 1979. 24(CONF-790917-(Vol. 24)(No. 4)).
- [47] Murgich, J., J. Rodríguez, and Y. Aray, Molecular recognition and molecular mechanics of micelles of some model asphaltenes and resins. *Energy and Fuels*, 1996. 10(1): p. 68-76.
- [48] Groenzin, H. and O.C. Mullins, Molecular size and structure of asphaltenes from various sources. *Energy and Fuels*, 2000. 14(3): p. 677-684.
- [49] Murgich, J., J.A. Abanero, and O.P. Strausz, Molecular recognition in aggregates formed by asphaltene and resin molecules from the Athabasca oil sand. *Energy and Fuels*, 1999. 13(2): p. 278-286.
- [50] Mullins, O.C., The modified yen model†. *Energy and Fuels*, 2010. 24(4): p. 2179-2207.
- [51] Mullins, O.C., The asphaltenes. *Annual Review of Analytical Chemistry*, 2011. 4: p. 393-418.
- [52] Wiehe, I.A., In defense of vapor pressure osmometry for measuring molecular weight. *Journal of dispersion science and technology*, 2007. 28(3): p. 431-435.
- [53] Yarranton, H.W., H. Alboudwarej, and R. Jakher, Investigation of asphaltene association with vapor pressure osmometry and interfacial tension measurements. *Industrial and engineering chemistry research*, 2000. 39(8): p. 2916-2924.
- [54] Wu, J., J.M. Prausnitz, and A. Firoozabadi, Molecular-thermodynamic framework for asphaltene-oil equilibria. *AIChE Journal*, 1998. 44(5): p. 1188-1199.
- [55] Acevedo, S., et al., Isolation and characterization of natural surfactants from extra heavy crude oils, asphaltenes and maltenes. Interpretation of their interfacial tension-pH behaviour in terms of ion pair formation. *Fuel*, 1992. 71(6): p. 619-623.
- [56] Mushrush, G., *Petroleum products: instability and incompatibility*. 1995: CRC Press.
- [57] Dickie, J.P. and T.F. Yen, Macrostructures of the asphaltic fractions by various instrumental methods. *Analytical chemistry*, 1967. 39(14): p. 1847-1852.
- [58] Vazquez, D. and G. Mansoori, Analysis of heavy organic deposits. *Sci. and Engineering*, 2000. 26(1-4): p. 49-56.
- [59] De Boer, R., et al., Screening of crude oils for asphalt precipitation: theory, practice, and the selection of inhibitors. *SPE Production and Facilities*, 1995. 10(01): p. 55-61.
- [60] Akbarzadeh, K., et al., Asphaltenes—problematic but rich in potential. *Oilfield Review*, 2007. 19(2): p. 22-43.
- [61] Li, Z. and A. Firoozabadi, Modeling asphaltene precipitation by n-alkanes from heavy oils and bitumens using cubic-plus-association equation of state. *Energy and Fuels*, 2010. 24(2): p. 1106-1113.
- [62] Hirschberg, A., et al., Influence of temperature and pressure on asphaltene flocculation. *Society of Petroleum Engineers Journal*, 1984. 24(03): p. 283-293.

-
- [63] Leontaritis, K. and G.A. Mansoori. Asphaltene flocculation during oil production and processing: A thermodynamic colloidal model. in SPE International Symposium on Oilfield Chemistry. 1987: Society of Petroleum Engineers.
- [64] Hemmati-Sarapardeh, A., et al., Asphaltene precipitation due to natural depletion of reservoir: Determination using a SARA fraction based intelligent model. *Fluid Phase Equilibria*, 2013. 354: p. 177-184.
- [65] Mohammadi, A.H., A. Eslamimanesh, and D. Richon, Monodisperse Thermodynamic Model Based on Chemical+ Flory–Huggins Polymer Solution Theories for Predicting Asphaltene Precipitation. *Industrial and Engineering Chemistry Research*, 2012. 51(10): p. 4041-4055.
- [66] Subramanian, S., S. Simon, and J. Sjöblom, Asphaltene Precipitation Models: A Review. *Journal of Dispersion Science and Technology*, 2016. 37(7): p. 1027-1049.
- [67] Mohammadi, A.H. and D. Richon, A monodisperse thermodynamic model for estimating asphaltene precipitation. *AIChE journal*, 2007. 53(11): p. 2940-2947.
- [68] Nikookar, M., M. Omidkhah, and G. Pazuki, Prediction of density and solubility parameter of heavy oils and SARA fractions using cubic equations of state. *Petroleum science and Technology*, 2008. 26(16): p. 1904-1912.
- [69] Nikookar, M., et al., Modification of a thermodynamic model and an equation of state for accurate calculation of asphaltene precipitation phase behavior. *Fuel*, 2008. 87(1): p. 85-91.
- [70] Pazuki, G. and M. Nikookar, A modified Flory-Huggins model for prediction of asphaltenes precipitation in crude oil. *Fuel*, 2006. 85(7): p. 1083-1086.
- [71] Pazuki, G.R., M. Nikookar, and M.R. Omidkhah, Application of a new cubic equation of state to computation of phase behavior of fluids and asphaltene precipitation in crude oil. *Fluid Phase Equilibria*, 2007. 254(1): p. 42-48.
- [72] Cimino, R., et al. Thermodynamic modelling for prediction of asphaltene deposition in live oils. in SPE International Symposium on Oilfield Chemistry. 1995: Society of Petroleum Engineers.
- [73] Scatchard, G., Equilibria in Non-electrolyte Solutions in Relation to the Vapor Pressures and Densities of the Components. *Chemical Reviews*, 1931. 8(2): p. 321-333.
- [74] Hildebrand, J., RL Scott, *Regular Solutions*. 1962, Englewood Cliffs, Prentice-Hall, New Jersey.
- [75] Scott, R.L. and M. Magat, The Thermodynamics of High-Polymer Solutions: I. The Free Energy of Mixing of Solvents and Polymers of Heterogeneous Distribution. *The Journal of Chemical Physics*, 1945. 13(5): p. 172-177.
- [76] Nghiem, L.X. and D.A. Coombe, Modelling asphaltene precipitation during primary depletion. *SPE Journal*, 1997. 2(02): p. 170-176.
- [77] Mohebbinia, S., et al. Simulation of Asphaltene Precipitation during Gas Injection Using PC-SAFT EOS. in SPE Annual Technical Conference and Exhibition. 2014: Society of Petroleum Engineers.
- [78] Kontogeorgis, G.M., et al., An equation of state for associating fluids. *Industrial and engineering chemistry research*, 1996. 35(11): p. 4310-4318.
- [79] Shirani, B., M. Nikazar, and S.A. Mousavi-Dehghani, Prediction of asphaltene phase behavior in live oil with CPA equation of state. *Fuel*, 2012. 97: p. 89-96.
- [80] Kontogeorgis, G.M. and G.K. Folas, *Front Matter*. 2009: Wiley Online Library.

-
- [81] Chapman, W.G., et al., New reference equation of state for associating liquids. *Industrial and Engineering Chemistry Research*, 1990. 29(8): p. 1709-1721.
- [82] David Ting, P., G.J. Hirasaki, and W.G. Chapman, Modeling of asphaltene phase behavior with the SAFT equation of state. *Petroleum Science and Technology*, 2003. 21(3-4): p. 647-661.
- [83] Tabatabaei-Nejad, S.A. and E. Khodapanah, Application of Chebyshev polynomials to predict phase behavior of fluids containing asphaltene and associating components using SAFT equation of state. *Fuel*, 2010. 89(9): p. 2511-2521.
- [84] Gross, J. and G. Sadowski, Perturbed-chain SAFT: An equation of state based on a perturbation theory for chain molecules. *Industrial and engineering chemistry research*, 2001. 40(4): p. 1244-1260.
- [85] Sabeti, M., et al., Estimation of asphaltene precipitation and equilibrium properties of hydrocarbon fluid phases using the PC-SAFT equation of state. *Journal of Molecular Liquids*, 2015. 209: p. 447-460.
- [86] Gonzalez, D.L., et al., Prediction of asphaltene instability under gas injection with the PC-SAFT equation of state. *Energy and fuels*, 2005. 19(4): p. 1230-1234.
- [87] Vargas, F.M., et al., Modeling asphaltene phase behavior in crude oil systems using the perturbed chain form of the statistical associating fluid theory (PC-SAFT) equation of state†. *Energy and Fuels*, 2009. 23(3): p. 1140-1146.
- [88] Ashoori, S., et al., Investigation of reversibility of asphaltene precipitation and deposition for an Iranian crude oil. *Iranian Journal of Chemistry and Chemical Engineering (IJCCE)*, 2006. 25(3): p. 41-47.
- [89] Pan, H. and A. Firoozabadi, Thermodynamic micellization model for asphaltene precipitation inhibition. *AIChE journal*, 2000. 46(2): p. 416-426.
- [90] Pan, H. and A. Firoozabadi. Thermodynamic micellization model for asphaltene precipitation from reservoir crudes at high pressures and temperatures. in SPE Annual Technical Conference and Exhibition. 1997: Society of Petroleum Engineers.
- [91] Victorov, A.I. and A. firoozabadi, Thermodynamic micellization model of asphaltene precipitation from petroleum fluids. *AIChE journal*, 1996. 42: p. 1753-1764.
- [92] Rassamdana, H., et al., Asphalt flocculation and deposition: I. The onset of precipitation. *AIChE Journal*, 1996. 42(1): p. 10-22.
- [93] Rassamdana, H. and M. Sahimi, Asphalt flocculation and deposition: II. Formation and growth of fractal aggregates. *AIChE journal*, 1996. 42(12): p. 3318-3332.
- [94] Mohammadi, A.H., et al., A novel method for evaluation of asphaltene precipitation titration data. *Chemical Engineering Science*, 2012. 78: p. 181-185.
- [95] Ashoori, S., et al., Comparison of scaling equation with neural network model for prediction of asphaltene precipitation. *Journal of Petroleum Science and Engineering*, 2010. 72(1): p. 186-194.
- [96] Zendejboudi, S., et al., Thermodynamic investigation of asphaltene precipitation during primary oil production: laboratory and smart technique. *Industrial and Engineering Chemistry Research*, 2013. 52(17): p. 6009-6031.
- [97] Zendejboudi, S., et al., Asphaltene precipitation and deposition in oil reservoirs– Technical aspects, experimental and hybrid neural network predictive tools. *Chemical Engineering Research and Design*, 2014. 92(5): p. 857-875.

-
- [98] Kamari, A., A. Safiri, and A.H. Mohammadi, A Compositional Model for Estimating Asphaltene Precipitation Conditions in Live Reservoir Oil Systems. *Journal of Dispersion Science and Technology*, 2014(just-accepted).
- [99] Chamkalani, A., et al., Diagnosis of asphaltene stability in crude oil through “two parameters” SVM model. *Chemical Engineering Science*, 2012. 81: p. 202-208.
- [100] Chamkalani, A., R. Chamkalani, and A.H. Mohammadi, Hybrid of Two Heuristic Optimizations with LSSVM to Predict Refractive Index as Asphaltene Stability Identifier. *Journal of Dispersion Science and Technology*, 2013(just-accepted).
- [101] Fan, T., J. Wang, and J.S. Buckley, Evaluating Crude Oils by SARA Analysis, in *Society of Petroleum Engineering*. 2002, SPE/DOE Improved Oil Recovery Symposium, Tulsa, Oklahoma.

Chapter 6

SCALING EQUATIONS FOR ASPHALTENE PRECIPITATION MODELING

Forough Ameli^{1,}, Abdolhossein Hemmati-Sarapardeh^{2,*},
Sassan Hajirezaie³, Amir H Mohammadi^{4,5,6,†} and Bahram Dabir^{2,7}*

Department of Chemical Engineering, Oil and Gas,
Iran University of Science and Technology, Tehran, Iran

²Department of Petroleum Engineering,
Amirkabir University of Technology, Tehran, Iran

³Department of Civil and Environmental Engineering,
Princeton University, Princeton, US

⁴Discipline of Chemical Engineering, School of Engineering,

University of KwaZulu-Natal, Howard College Campus, Durban, South Africa

⁵Institut de Recherche en Génie Chimique et Pétrolier (IRGCP), Paris Cedex, France

⁶Département de Génie des Mines, de la Métallurgie et des Matériaux,
Faculté des Sciences et de Génie, Université Laval, Québec, Canada

⁷Department of Chemical Engineering,
Amirkabir University of Technology, Tehran, Iran

ABSTRACT

Over the last decades, modeling asphaltene precipitation has been extensively conducted by many researchers. Among different models proposed for the prediction of asphaltene precipitation, scaling equation models have received much attention. The advantages of these models over the other models include no requirement to asphaltene properties and simple mathematical formulations. In these models, by fitting a limited set of experimental data, it is possible to predict asphaltene precipitation behavior at other conditions. Rassamdana et al. developed the first scaling equations based on an Iranian

* ameli@iust.ac.ir.

* aut.hemmati@gmail.com, aut.hemmati@aut.ac.ir.

† a.h.m@irgcp.fr&amir_h_mohammadi@yahoo.com.

crude oil sample. Afterward, several scaling equations have been proposed for predicting the amount of asphaltene precipitations at different conditions. In this study, all of the available scaling equations are reviewed. These equations are categorized into two groups as: the models developed for asphaltene precipitation titration data; the models developed for asphaltene precipitation during natural depletion of reservoir. Moreover, experimental measurements of asphaltene precipitation data are associated with many uncertainties; therefore, the quality of asphaltene precipitation data is discussed based on statistical models such as leverage approach. In this method, both quantitative and qualitative analyses are performed to check the reliability of the models and to find the suspected data points. This study provides a new insight into asphaltene precipitation modeling through scaling equations.

Keywords: asphaltene precipitation, scaling equation, modeling, prediction, assessment

1. INTRODUCTION

Asphaltene is one of the most important ingredients of crude oil and is known as an association of various colloidal particles and macromolecules [1]. Asphaltene would precipitate by changing the pressure, temperature and composition of crude oil [2]. There is no need to point out that precipitation of crude oil may result in many problems in reservoirs, and in facilities and equipment during production [1, 3-8]. Asphaltene precipitation models, based on study of Mohammadi et al. [9], are classified into five main groups, including 'association' models, 'equation of state (EoS)' based models, 'scaling laws,' 'activity coefficient' based models and 'colloidal/micellization' models [10-12]. The advanced equation of state models have been developed based on the models of Ting et al. [13], Wu et al. [14, 15], Christensen et al. [16], Buenrostro-Gonzalez et al. [17], Tabatabaei-Nejad and Khodapanah [18] Gonzalez et al. [19] and Vafaie-Sefti and Mousavi-Dehghani [20], Nikoogar et al. [21] and the developed PR and SRK EoS's. A more applicable form of Flory-Huggins equation was developed later by Mohammadi and Richon [22]. A new thermodynamic model for asphaltene deposition was recently developed in which the Flory-Huggins solution theory is combined with the chemical theory of association solution. In this modeling approach, precipitation process is known to be reversible. Hirschberg model [1] is based on the assumption that asphaltene is the only precipitating phase, while Cimino et al. [23] model is based on the assumption that non-asphaltene components are also present in the precipitating phase. Scaling equations based models have been much attended during the last two decades. The simplicity of scaling models is that asphaltene properties are not required for the modeling [24]. The first scaling equation was developed by Rassamdana et al. [24] at constant temperature with exponents Z and Z' . The effect of composition and temperature was studied by Hu and Guo [25] to predict the onset and amount of the precipitated asphaltene. This method was applied for core flooding experiments and the amount of precipitated asphaltene was measured. Rassamdana et al. [24] equation was modified and a new scaling equation was developed by Soulgani et al. [26] for live oil at various temperatures and pressures. Moreover, the model was optimized by adding some physical properties including onset pressure, critical temperature and bubble point pressure. Manshad et al. [27] model was developed by including temperature, pressure, dilution ratio and

molecular weight to determine the onset of asphaltene precipitation and total amount of it by using various solvents.

Over the last decades, artificial neural networks have been developed, which require large sets of data to develop a model with many adjustable parameters [28]. Deficiencies of these models include uncertainties and over fitting and under fitting of data. Least square support vector machine (LSSVM) is another technique for solving complex and nonlinear problems with more accurate results in comparison to other existing intelligent methods. Hemmati-Sarapardeh et al. [29] recently applied this method to predict the amount of asphaltene precipitation during natural depletion. Some other models based on scaling laws can be found in the literature [30-32]. This chapter is divided into three parts: models based on asphaltene precipitation titration data; models based on asphaltene precipitation during natural depletion of reservoir; and quality of the experimental data.

2. SCALING EQUATIONS FOR ASPHALTENE PRECIPITATION TITRATION DATA

Scaling equations are effective methods for correctly predicting asphaltene precipitation data. Rassamdana et al. [24] developed the first scaling equation using the following parameters, including solvent to crude oil ratio (R), solvent molecular (M) and weight percent of the precipitated asphaltene (W):

$$X = \frac{R}{M^Z} \quad (1)$$

$$Y = \frac{W}{R^{Z'}} \quad (2)$$

Z and Z' are the fitting parameters. The scaling equation would be of the following form:

$$Y = A_0 + A_1 X + A_2 X^2 + A_3 X^3; (X \geq X_C) \quad (3)$$

Hu, Y-F. et al. [33] studied the application of scaling equations for asphaltene precipitation. Their samples were from Suffield, Ventura [1] and Lindbergh [34] oil fields. The universality of the exponents was studied using this data. The variables applied in this method include asphaltene weight percent (W), dilution ratio (R) and solvent molecular weight (M). These variables were combined with Rassamdana [24, 35] model to reach to the following forms:

$$X = R/M^z \quad (Z = \text{const.}) \quad (4)$$

$$Y = W/M^{z'} \quad (Z' = \text{const.}) \quad (5)$$

The scaling equation was introduced by using the following polynomial:

$$Y = A_1 + A_2X + A_3X^2 + A_4X^3 \quad (X \geq X_c) \quad (6)$$

X_c is the amount of X at asphaltene onset pressure. The exponents of this equation should be tuned carefully. The universality of the exponents and their ranges were first examined. The results showed that the best predicted values were obtained at a constant value of -2 for Z' , and by adjusting the Z value to map the precipitation values of different n-alkanes into a single curve. The optimum values for Z were then obtained. For n-alkanes larger than C_5 , the results were promising as shown in Figures 1-3. These curves are presented by the following polynomials:

$$Y = 68.01 - 293.68X + 581.25X^2 - 30.18X^3; \quad (Z = 0.50)$$

$$Y = 8.12 - 77.72X + 255.64X^2 - 5.50X^3; \quad (Z = 0.30)$$

$$Y = 3.45 - 9.27X + 20.48X^2 - 0.077X^3; \quad (Z = 0.25) \quad (7)$$

This model was compared with Hirschberg [1] model in which the asphaltene molar volume is a function of molecular weight and oil composition, and solubility parameter is only a function of oil composition.

The results were in good agreement with the experimental data set for n-alkanes. The dilution ratio effect was predicted accurately. The best results were obtained for C_6 , C_8 , and C_{10} as reported in Figure 4.

The effect of temperature and molecular weight of n-alkane precipitants on asphaltene precipitation was studied by Hu and Guo [25] using Caoqiao crude oil sample. The amount of asphaltene for this oil sample was determined at different temperatures. Using scaling equations, the exponent Z' led to a constant value of -2 and the value of Z was reported as a function of oil composition in the range of $0.1 < Z < 0.5$ [24, 33, 35-38].

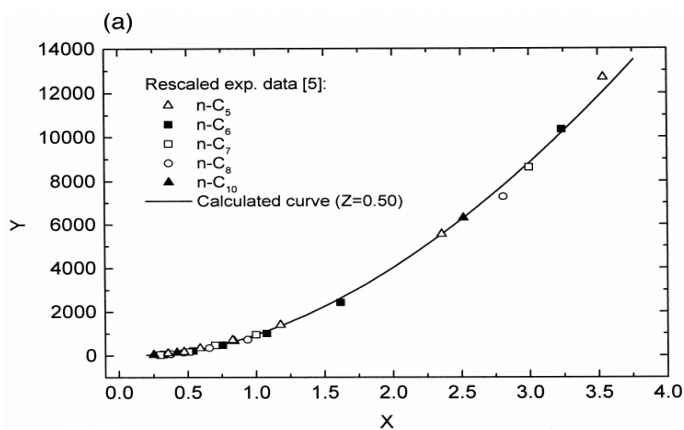


Figure 1. (Continued)

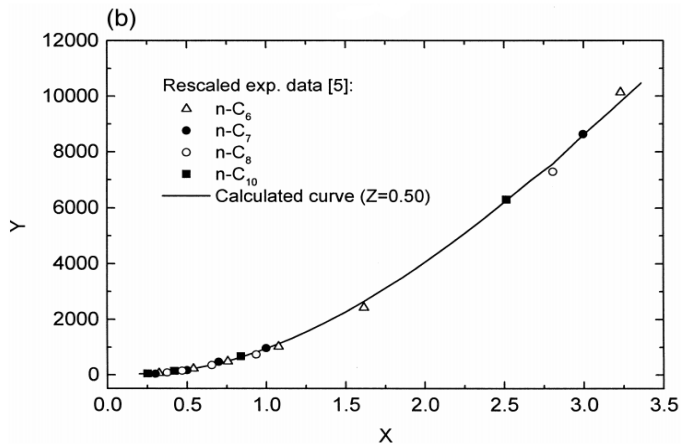


Figure 1.a. Comparison of the calculated and experimental asphaltene precipitation data for n-alkane-Suffield crude oil system. b Similar to Figure 1.a, excluding n-C₅ precipitation data from the regression [33].

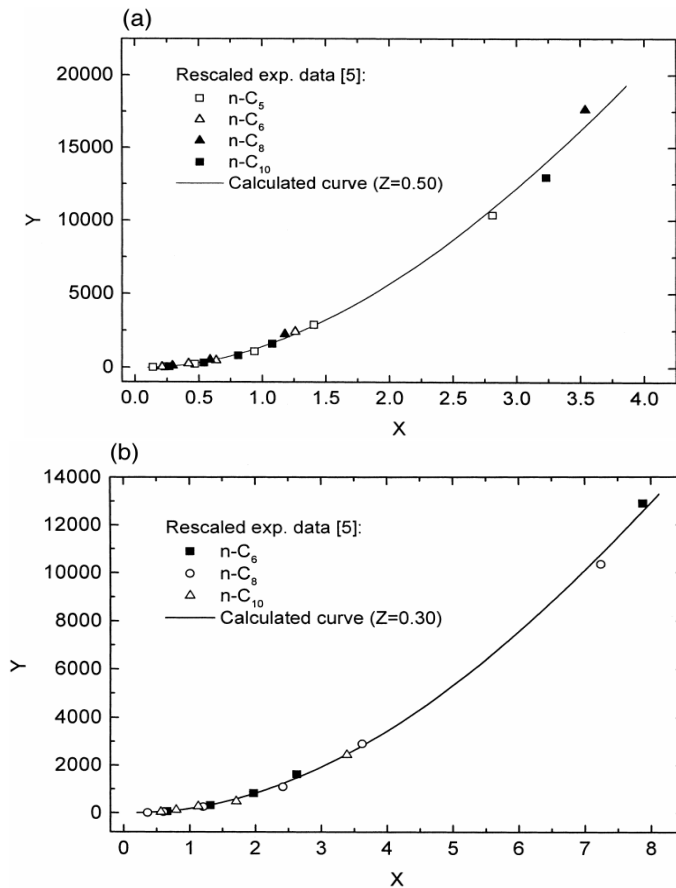


Figure 2.a. Comparison of calculated asphaltene precipitation with experimental data for n-alkane-Lindbergh crude oil system. b Similar plotting with (a) with n-C precipitation data excluded from the regression [33]

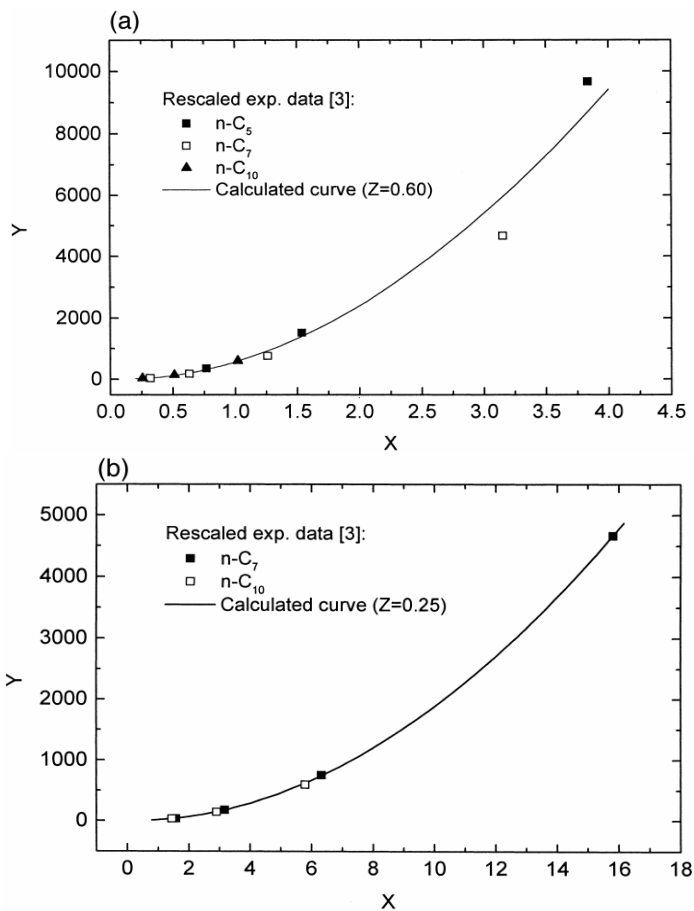


Figure 3.a. Comparison of calculated asphaltene precipitation with experimental data for the n-alkane-Ventura crude oil system. b Similar plotting with (a) excluded n-C precipitation data from regression [33]

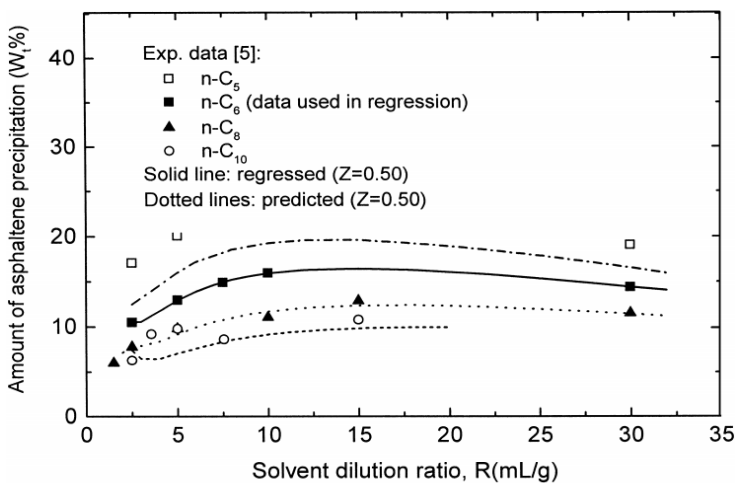


Figure 4. Comparison of calculated asphaltene precipitation with experimental data for w x n-alkane-Lindbergh crude oil system [33].

2.1. Application of Genetic Algorithm in Scaling Equations

Application of the new techniques for developing scaling equations would result in robust outcomes for predicting asphaltene precipitation. Asoodeh M., et al. [39] developed a new scaling equation using hybrid genetic algorithm-pattern search tool for asphaltene precipitation. Genetic algorithm (GA) is an optimization tool, which has been applied in various fields of science and engineering. This method has been optimized by integration with the pattern search tool method. In this technique, one needs to search for a set of points around the chromosomes and the mesh is set up by adding these points to a pattern, which is a set of vectors. A point with a better fitness score is substituted with the current point and the operators are employed for the new chromosome.

To develop a new scaling equation, the values of constant parameters should be modified. To do this, a hybrid GA-pattern model was developed to obtain the best values. To define the eight constants based on the divide-and-counter principle, the problem was broken into smaller parts and each part was solved separately. Using the first fitness function, the values of Z , C_1 , C_2 and Z' were obtained using the following equations:

$$R = \frac{\sum_{i=1}^N (x_i - \bar{x})(y_i - \bar{y})}{(N-1)S_x S_y} \quad (8)$$

$$FF1 = \frac{1}{1 + |R|} \quad (9)$$

R denotes the correction coefficient. $FF1$ is the first fitness function. N represents the number of data points and S denotes the standard deviation. The correlation coefficient between the experimental and predicted values of precipitated asphaltene using this technique is presented in Figure 5. The following equations are obtained by using the GA-PS tool.

$$x = \frac{R_v}{T^{2.76775449} M_w^{0.49401052}}$$

$$y = \frac{w_t}{x^{-0.00687377} R_v^{-0.85051076}} \quad (10)$$

The second fitness function is introduced for the next step to minimize the coefficients B_0 to B_3 as follows:

$$FF2 = MSE = \frac{1}{N} \sum_{j=1}^N (y_j - B_0 + B_1 x_j + B_2 x_j^2 + B_3 x_j^3)^2 \quad (11)$$

This would result in the following polynomial function:

$$y = -7.0030360 + 207741013x + 2008260917x^2 - 3.17e + 20x^3 \quad (12)$$

The obtained values are reported in Table 1.

Table 1. Extracted parameters by the hybrid GA-PS technique for scaling equation [39]

C1	C2	Z	Z'
2.767754	-0.006873	0.494010	-0.850510
B0	B1	B2	B3
-7.003036	207741012.923998	20082609170	-3.167861e+20

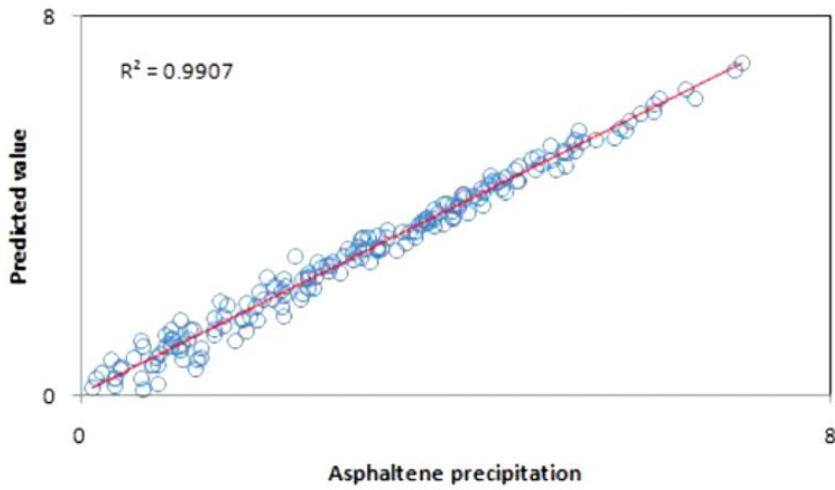


Figure 5. Crossplot showing correlation coefficient between the measured asphaltene amounts and predictions of GA-PS-based scaling equation[39].

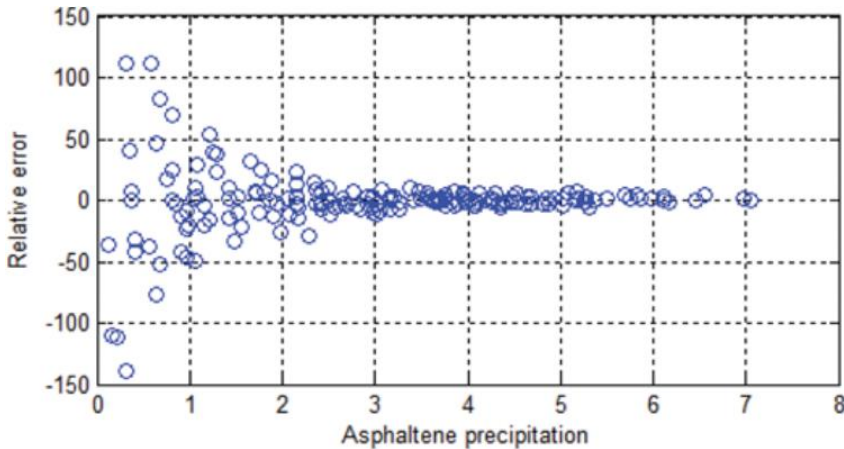


Figure 6. Relative error of the GA-PS-based scaling equation's predictions versus precipitated asphaltene amounts [39].

The comparison between the experimental and predicted values of precipitated asphaltene using this technique is presented in Figure 6.

The relative errors for precipitated asphaltene values are depicted in Figure 7. The results show that the model is highly reliable for the values of asphaltene precipitation more than 2.

Ashoori et al. [40] studied an asphaltenic crude oil from the Southwest Iran reservoir. The experiments were conducted at atmospheric pressure and were compared with different scaling equations by Rassamdana and Sahimi [35] and the one by Hu and Guo [25]. The results are depicted in Figures 8 and 9. As it is obvious, for the samples with large values of R_v (Solvent to oil dilution ratio), the results are in good agreement but for the values less than 4, this method leads to inappropriate results.

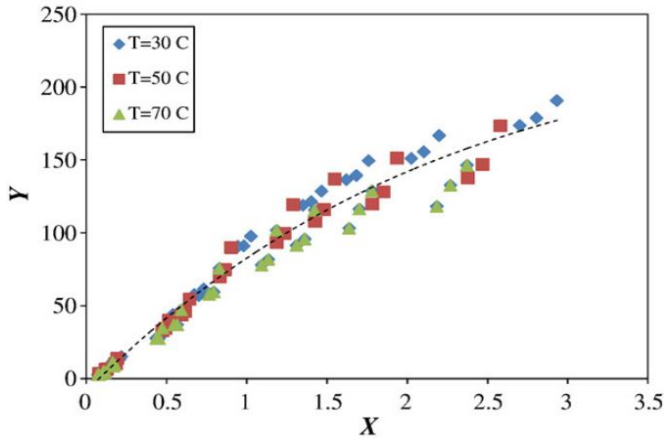


Figure 7. Collapse of the experimental data into a single curve using Rassamdana et al.[24] scaling equation.[40]

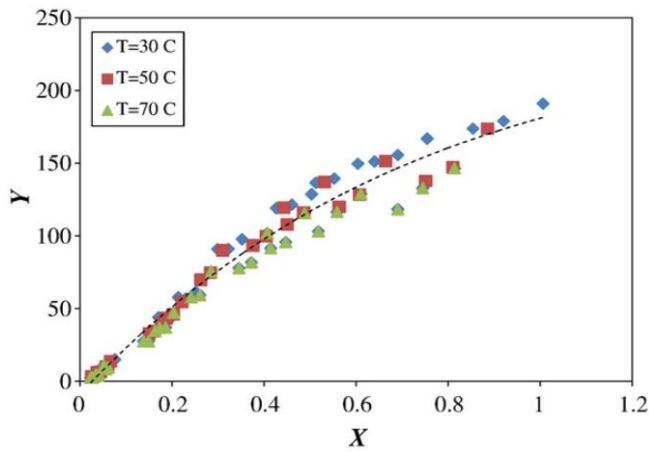


Figure 8. Collapse of the experimental data into a single curve using Hu and Guo [25] scaling equation.[40]

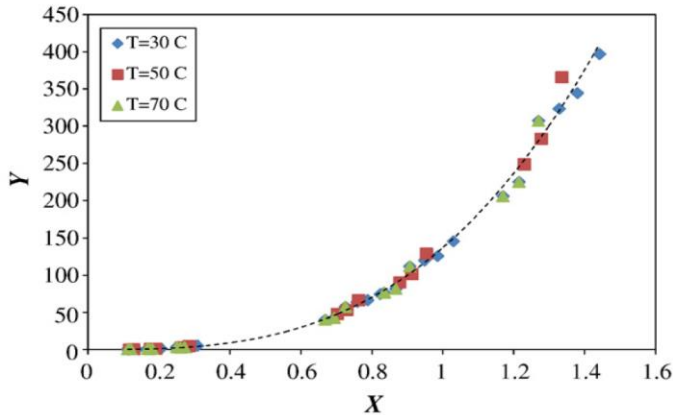


Figure 9. Collapse of our experimental data onto a single curve using our scaling equation at low values of dilution ratios, R_v , up to 7 and also greater than 7 [40]

Table 2. Comparison of standard deviation, R^2 and MSE between the GA-PS based scaling equation and the previous works [39]

Model	Standard Deviation	R2	RMSE
Rassamdana et al. [24]	0.3327	0.9570	0.11080
Hu and Guo [25]	0.3102	0.9630	0.09321
Ashoori et al. [40]	0.2743	0.9830	0.08562
GA-PS based scaling equation [39]	0.2294	0.9907	0.05235

As a result, the scaling equations were represented as follows:

$$\begin{aligned}
 X &= R_v / (T^n \cdot M_w^z) \\
 Y &= W_t / R_v^{z'}
 \end{aligned}
 \tag{13}$$

The exponent n would change between 0.1 and 0.25, and the values of Z and Z' exponents were 0.25 and -2, respectively. This leads to the collapse of all experimental data into a single curve for all R_v ranges up to 20. The results are depicted in Figure 9. The scaling function is of the following form:

$$Y = 9.768 - 122.5x + 267.5x^2 + 0.049x^3 \quad (X \geq X_c)
 \tag{14}$$

Moreover, the results of genetic algorithm pattern search (GA-PS) based scaling equation are compared with the studies of Ashoori et al. [40], Hu and Guo [25] and Rassamdana et al. [24]. The results show the superiority of the GA-PS based method over the existing algorithms as reported in Table 2. RMSE denotes the root mean square error using the following formula, which was used as optimization objective function in this study:

$$RMSE = \sqrt{\frac{1}{n} \sum_{i=1}^n (O_{iexp} - O_{iexp/pred})^2}
 \tag{15}$$

2.2. Support Vector Machine [32]

Support vector machine (SVM) is a method for mapping the input data from a specified space into a higher m -dimensional space for determining the best regression function. This function has the following form [41, 42]:

$$f(x, \omega) = \sum_{j=1}^m \omega_j g_j(x) + b \quad (16)$$

The results of this method are evaluated for asphaltene precipitation data for the training and validation data. The optimized parameters are reported in Table 3. To assess SVM efficiency, its correlation coefficient and error distribution were analyzed. Figure 10 represents the cross plot of the measured and predicted values for asphaltene precipitation

The value of prediction coefficient for SVM is 0.997 that verifies the reliable performance of this method. The SVM performance is compared to the other existing models using the statistical parameters. The results are reported in Table 4. As it is obvious, the results of SVM technique are more accurate in comparison to the other existing models.

Table 3. Results of statistical analysis of measured and predicted asphaltene amounts for the training and validation data sets [32]

Data set	Mean of target set (measured asphaltene amount)	Mean of predicted set (predicted asphaltene amount)	Variance in measured asphaltene amount set	Residual variance after SVR model
Training set	4.785666	4.742195	1.560983	0.004589
Validation set	4.785666	4.777019	0.3893282	0.008737

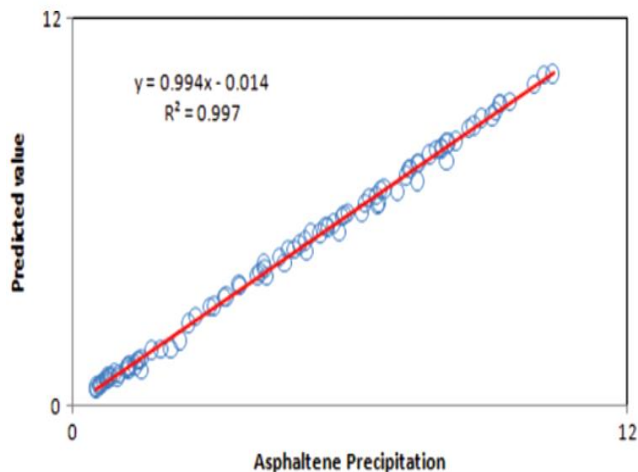


Figure 10. Cross plot showing the correlation coefficient between the measured and SVM predicted asphaltene amount [32].

Table 4. Comparison of standard deviation, R² and MSE of the constructed SVM model with the previous works [32]

Model	Error Standard Deviation	R2	MSE
Rassamdana et al. [24]	0.3327	0.957	0.1108
Hu and Guo [25]	0.3102	0.963	.09321
Ashoori et al. [40]	0.2743	0.983	.08562
SVM [32]	0.1554	0.997	0.258

2.3. Artificial Neural Network Model

A neural network could be trained to perform a certain action by adjusting the weight and bias elements. These elements work in parallel. The network is adjusted by comparing the target and the output until the outputs are matched [43]. There are different configurations of artificial neural networks (ANNs). Some networks are classified as feed forward neural network while others are named recurrent networks. A feed-forward neural network is depicted in Figure 11 with a single hidden layer for a multiple input single output (MISO) system. Moreover, on the basis of model learning, they are classified into supervised and self-organized training systems [44, 45]. On the other hand, multilayer perceptron (MLP) network is trained by adapting the synaptic weights using a back propagation technique. The input neuron to MLP model is multiplied by a weight factor, and the results are added to the bias term. Finally, a non-linear mathematical operation is performed by an activation function. The network output is compared to the desired network value [46]. Some additional linear weights may also be added to facilitate the network convergence. The training steps of the MLP network are represented in Figure 12. This is applied for training different single hidden layers which all are a part of MLP network.

Radial basis function (RBF) and Adaptive Linear Neuron (ADALINE) are the others. Wang et al. [47] represented that feed-forward neural network using two hidden layers is capable of approximating non-linear basis functions.

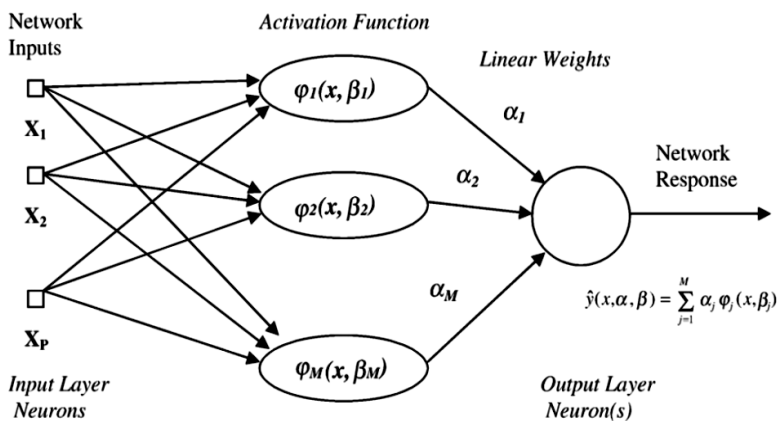


Figure 11. Architecture of the three-layered feed-forward neural network with a single hidden layer for a MISO system [40].

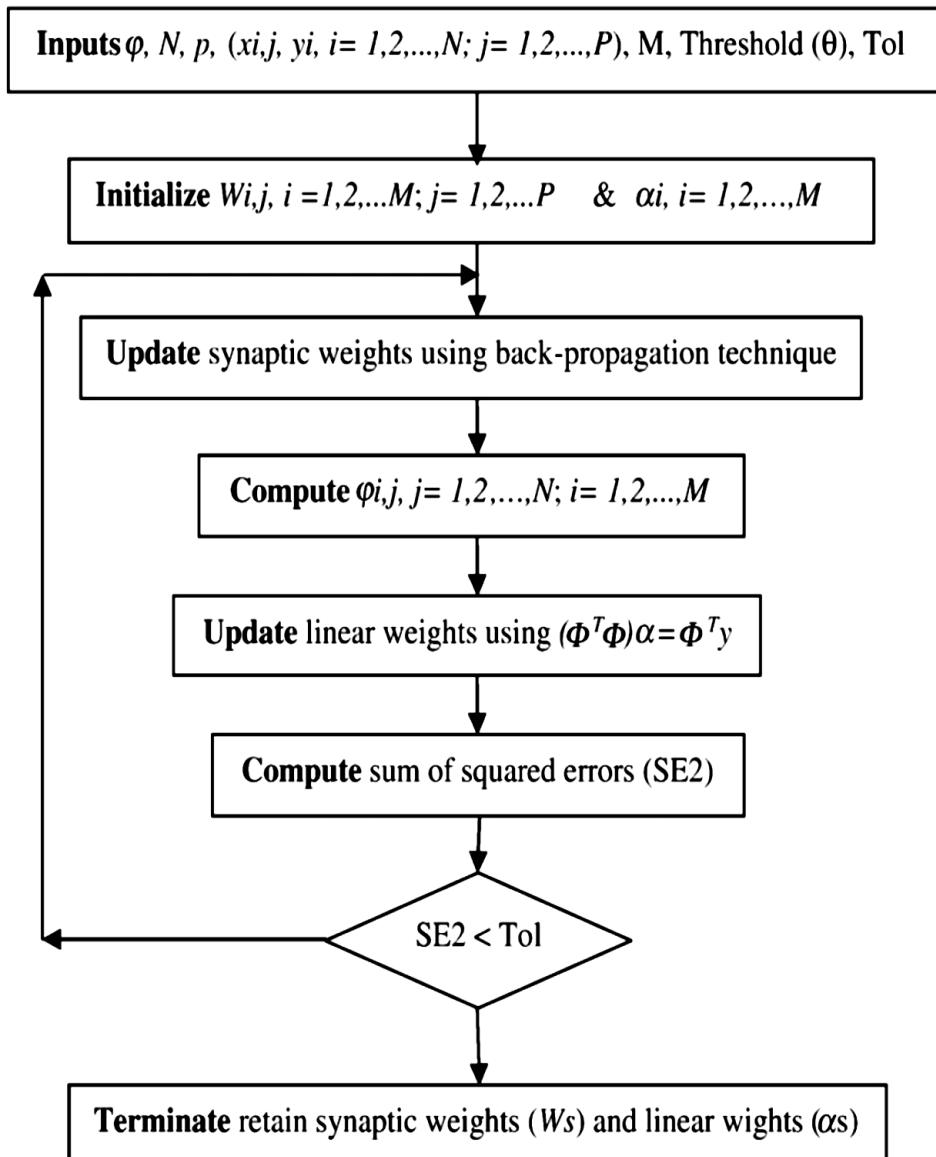


Figure 12. Training steps of MLP network [40].

For the case of asphaltene precipitation studies, experimental data were applied for training a single hidden layer with the learning algorithm represented in Figure 13. The values of dilution ratio, temperature and molecular weight were the input variables and the target data was the precipitated amount of asphaltene. 35% of the data were kept as the testing set to evaluate the capability of this technique. The comparative results between the model predictions and experimental data in the training and testing sets are illustrated in Figures 14 and 15.

The deviation of the ANN model predictions from the experimental data is less than that of the other scaling methods for asphaltene precipitation. This information is reported in Table 5.

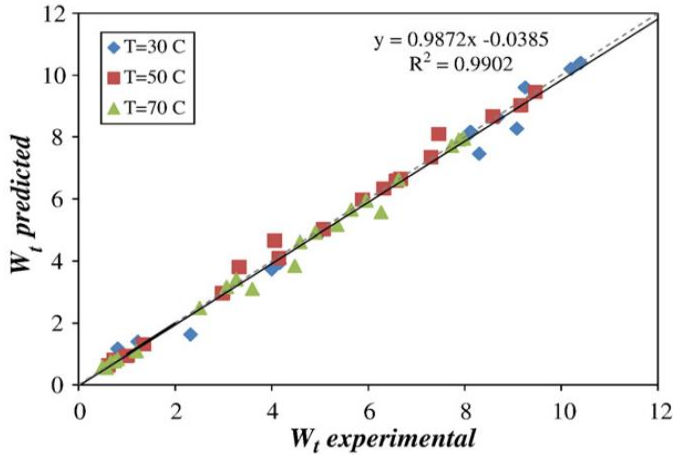


Figure 13. Comparison of predicted values of asphaltene precipitation by the proposed ANN model and experimental data for the training set [40].

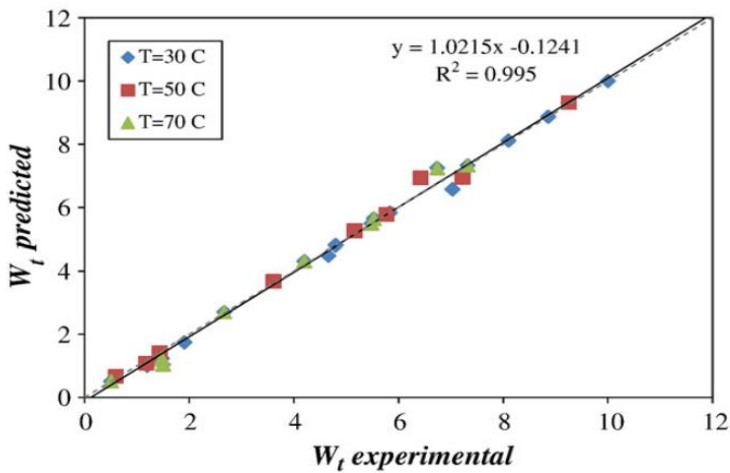


Figure 14. Comparison of predicted values of asphaltene precipitation by the proposed ANN model and experimental data for the testing set [40].

Table 5. Comparison of the deviation of predicted values obtained by ANN and the deviation of results obtained by the scaling equations [40]

Model	Rassamdana et al. [24]	Hu and Guo [25]	Ashoori et al. [40]	ANN model [40]
σ	16.94	16.51	9.78	5.03
∂	0.188	0.183	0.109	0.056

where σ is the relative absolute deviation and ∂ denotes the average relative absolute deviation.

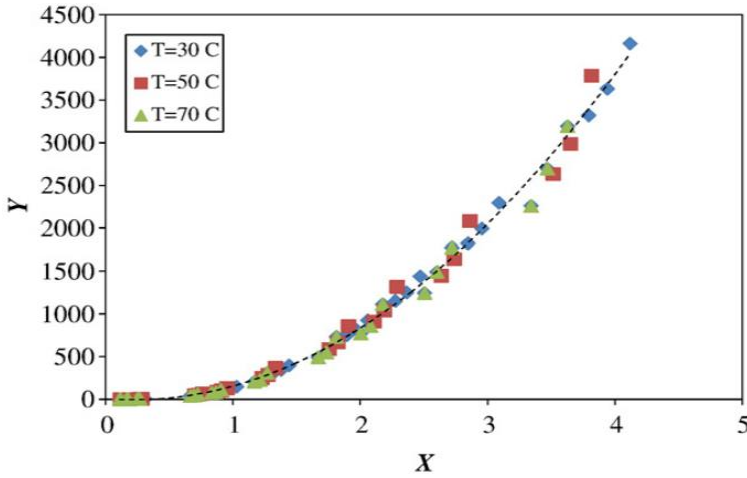


Figure 15. Collapse of our experimental data into a single curve using our scaling equation at different values of dilution ratios, R_v [40]

2.4. Fuzzy Logic Model

Asoodeh et al. [48] applied the fuzzy tuning approach for the scaling equations, which is called fuzzy tuning of scaling equations (FTSE). This approach compensates the effect of underestimation and overestimation of fuzzy rules. This approach breaks the whole model into small spaces and solves each of them separately. The results are obtained by aggregation of all of the outputs. The input functions are introduced as follows:

$$\mu_i(R) = \exp(-(R - m_{R_i})^2 / 2\sigma_{R_i}^2)$$

$$\mu_i(H) = \exp(-(H - m_{H_i})^2 / 2\sigma_{H_i}^2)$$

$$\mu_i(A) = \exp(-(A - m_{A_i})^2 / 2\sigma_{A_i}^2) \quad (17)$$

where μ denotes the membership degree. m and σ denote the mean and standard deviations and i expresses the rule number. Each rule is represented as follows:

$$\mu_i = \mu_i(R) \times \mu_i(H) \times \mu_i(A) \quad (18)$$

As a result, the output membership function (OMF) would be represented as follows:

$$OMF_i = \beta_{1i}R + \beta_{2i}H + \beta_{3i}A + \beta_{4i} \quad (19)$$

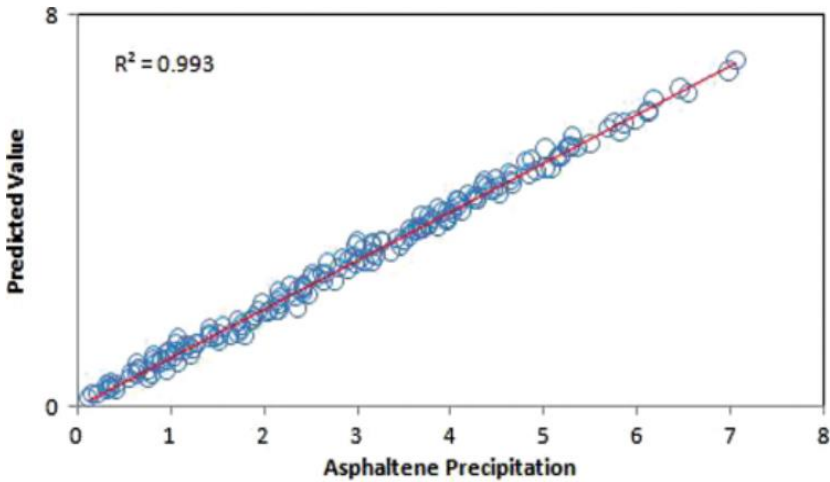


Figure 16. Cross plot showing the correlation coefficient between the measured and FTSE predicted asphaltene amounts [48].

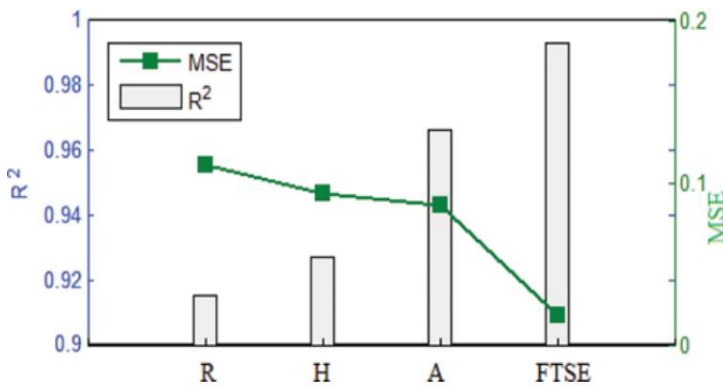


Figure 17. Comparison between the predicted values by different intelligent methods, and MSE and correlation coefficient. R, H, and A refer to Rassamdana et al. [24] Hu and Guo [25], and Ashoori et al. [40] models, and FTSE modeling [48] respectively.

Finally, the precipitated amount of asphaltene has the following form:

$$Asphaltene\ Precipitation = \frac{\sum_{i=1} \mu_i \times OMF_i}{\mu_i} \tag{20}$$

The cross plot of the measured and predicted amount of asphaltene precipitation is depicted in Figure 16 and the value of R² is equal to 0.993. This indicates that the developed method leads to promising results.

The values of correlation coefficient are also compared with the other existing scaling models in Figure 17, which denotes that the developed technique leads to more satisfying results in comparison to the individual scaling equations.

2.5. Least Square Support Vector Machine

Hemmati-Sarapardeh et al. [49] developed a new method for estimation of asphaltene precipitation using a large data bank of asphaltene precipitation under a wide range of thermodynamic conditions and various crude oil types. In their study, least square support vector machine (LSSVM) was optimized with a stochastic algorithm named coupled simulated annealing (CSA) to model asphaltene precipitation.

The data sets were divided into four groups as follows:

Model 1: Systems with nC₅ to nC₇ as solvent and $R_v \leq 5$

Model 2: Systems with nC₈ to nC₁₂ as solvent and $R_v \leq 5$

Model 3: Systems with nC₅ to nC₇ as solvent and $R_v > 5$

Model 4: Systems with nC₈ to nC₁₂ as solvent and $R_v > 5$

The optimized parameters of the model are reported in Table 6. The accuracy of the models is a function of solvent type and solvent to oil ratio with the following order:

Model 4 > Model 3 > Model 2 > Model 1

The statistical parameters of the model in different solvents are reported in Table 7 denoting the satisfactory predictions of the model.

Table 6. The solvent to oil ratio and type of n-alkane precipitants for each model as well as the optimum values of the models' parameters [49]

Model Name	Solvent to oil ratio(R_v)	n-alkane precipitant	Model parameters	
			σ^2	γ
Model 1	$R_v \leq 5$	nC5-nC6-nC7	0.0945	15.5057
Model 2	$R_v \leq 5$	nC8 to nC12	0.7584	4908.5657
Model 3	$R_v > 5$	nC5-nC6-nC7	0.1051	199.4735
Model 4	$R_v > 5$	nC8 to nC12	1.5008	5517.3495

Table 7. Statistical parameters of the proposed models in different n-alkane precipitants [49]

n-alkane precipitant	Point Numbers	APRE, %	AAPRE, %	SD
nC5	61	-1.20	11.74	0.19
nC6	70	-3.60	12.07	0.18
nC7	70	-3.25	13.50	0.21
nC8	38	2.27	10.57	0.14
nC9	25	0.62	3.33	0.04
nC10	38	-0.56	3.80	0.05
nC12	23	-1.16	8.50	0.13

Table 8. Statistical parameters of the proposed models in this study and previously published models for determination of asphaltene precipitation [49]

Model	APRE, %	AAPRE, %	SD
Rassamdana et al. [24]	14.89	43.42	0.76
Hu and Guo [25]	-1.52	27.13	0.54
Ashoori et al. [40]	-9.80	21.88	0.55
This study [49]	-1.53	9.46	0.17

The proposed technique is compared with the other existing models in Table 8. The average absolute relative error (AAPRE) in this study is 9.45%, which is the smallest in comparison to the other existing models. The AAPRE is calculated as follows:

$$E_a = \frac{1}{n} \sum_{i=1}^n |E_i| \quad (21)$$

E_i represents the relative deviation of the predicted values of the model from the experimental data:

$$E_i = \left[\frac{O_{i\text{exp}} - O_{i\text{exp}/i\text{pred}}}{O_{i\text{exp}}} \right] \times 100 \quad (22)$$

3. SCALING EQUATIONS FOR ASPHALTENE PRECIPITATION DUE TO NATURAL DEPLETION AND GAS INJECTION

Roshanaei Zadeh et al. [50] studied asphaltene precipitation due to gas injection and investigated the different effects of gas type, temperature, pressure and concentration on asphaltene instability. A new scaling equation was developed for reservoirs with and without gas injection. The inputs in this modeling approach were reservoir temperature, pressure, sample bubble point pressure, molecular weight and mole percent of the injected gas. The equations are in the following forms:

$$X = \frac{R_m}{M^z T^n} \quad (23)$$

$$Y = \frac{w}{R_m^z}$$

where,

$$R_m = e^{-h\left(\frac{P_b}{P}-1\right)^2} \times R \quad (24)$$

M represents the injected gas molecular weight, W denotes the asphaltene weight percent, and P and P_b express the pressure and the bubble point pressure, respectively. T and R indicate the temperature and ratio of the injected gas to weight of the crude oil. Various data sets were collected for gas injection [50]. The polynomial that locates all of the data into a single line has the following form for methane injection data.

$$Y = 3.3877X^3 + 0.4831X^2 - 0.0099X + 8 \times 10^{-6} \quad (25)$$

Figure 18 shows the results for the case of methane injection. This new scaling equation predicts asphaltene instability independent of asphaltene properties. The optimum value of Z was reported 0.11 in this work. Since h has a considerable influence on precipitation, tuning this parameter is very important, which is 7 for the case of CO_2 and methane, and 1 for nitrogen injection. According to the previous studies, the effect of temperature is negligible in comparison to other variables at different reservoir pressures. This scaling equation is applicable for dynamic conditions of the reservoir as well. The results for the case of nitrogen injection are depicted in Figure 19.

Kord and Ayatollahi [51] studied precipitation of asphaltene in live oil during natural depletion. As the developed scaling model of Rassamdana et al. [24, 35] and its generalized form presented by Hu et al. [33] are applicable only for dead oil systems, this method was extended to live oils.

For live oil systems, asphaltene deposition mechanism is different. Precipitation mechanism and asphaltene state change from soluble to colloidal state at a specific point. Considering the effect of pressure, five different variables were combined and the scaling parameters were introduced as follows:

$$X = \frac{\left(\frac{P - P_b}{P_b}\right) \times GOR^Z}{T^{Z''}}$$

$$Y = \frac{W}{W_c} \times \left(\frac{P - P_b}{P_b}\right)^{-z} \quad (26)$$

Where P and P_b are pressure and bubble point pressure, respectively. GOR represents the gas oil ratio. W denotes the value of deposited asphaltene, T expresses the temperature, and W_c is the total amount of asphaltene in the crude oil system. The exponents of Z , Z' and Z'' are correlated using the experimental data. The results depicted in Figure 20 show that the phase stability and the regions for asphaltene precipitation are well predicted.

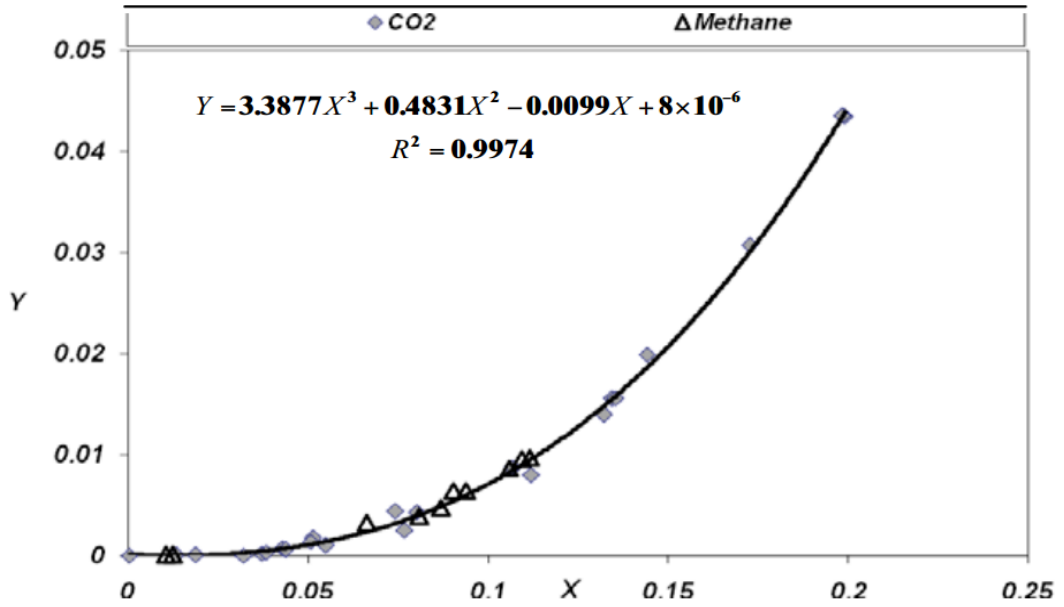


Figure 18. Collapse of methane injection data into a 3rd order polynomial [50]

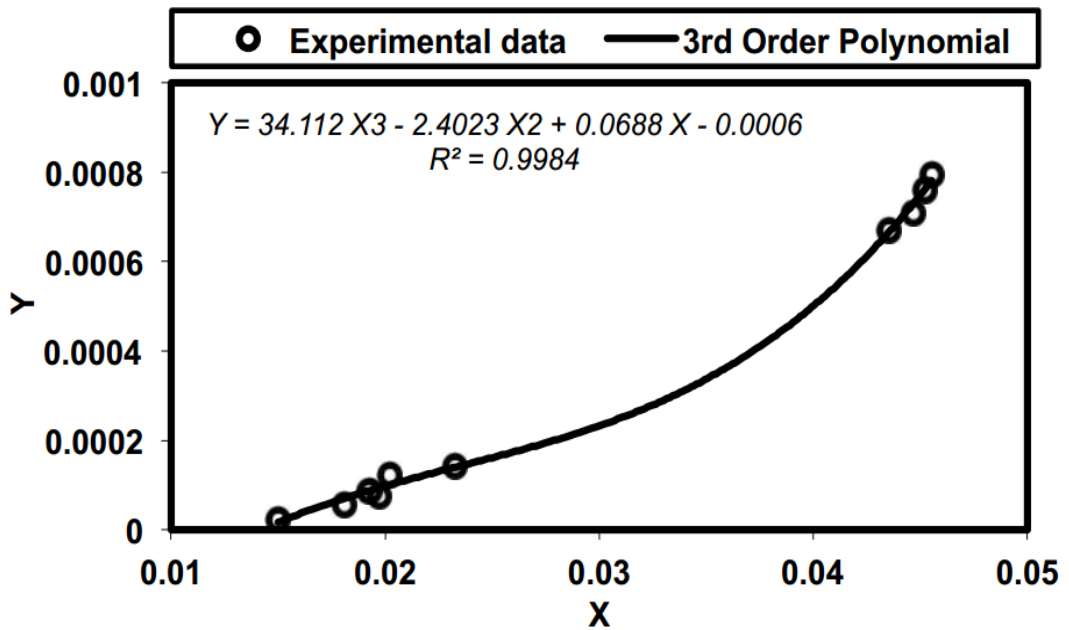


Figure 19. Collapse of nitrogen injection data into a 3rd order polynomial [50]

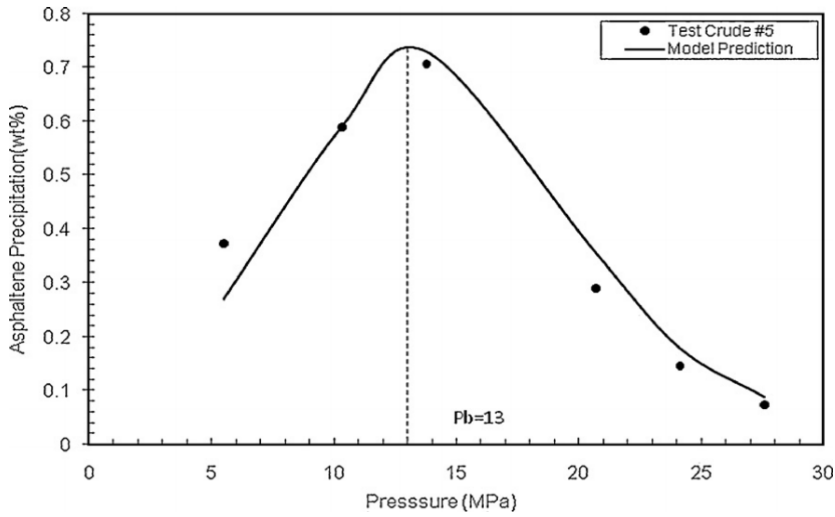


Figure 20. Prediction of asphaltene precipitation envelope by scaling equation in comparison with the experimental data of test crude No. 5[51]

Table 9. Relative error (%) of different models for prediction of test crude No. 5 precipitation [51]

Pressure (MPa)	FH model	MFH model	Solid model	Scaling model
31.03	43.39	58.39	3.02	0.08
24.13	16.12	40.86	2.61	0.45
17.24	8.35	24.14	2.53	0.67
10.34	22.79	14.97	2.19	0.28
6.89	12.57	25.93	1.76	0.10
5.52	8.39	29.89	2.19	0.82

As the thermodynamic models have deficiencies in predicting the amount of asphaltene precipitation, the scaling equations are introduced and applied. For the case of live oil at constant pressure, the values of Z and Z' are 0.2 and 2, respectively. The average error values are presented in Table 9 in which a good agreement is observed between the results of the model and experimental values.

$$RE(\%) = \frac{|W_{Exp} - W_{cal}|}{W_{Exp}} \times 100 \quad (27)$$

Behbahani et al. [52] developed a modified scaling equation for pressure depletion and gas injection cases for live oil. The bottom hole live oil characteristics were analyzed to find the best model configuration based on the following equations:

$$X = \frac{(GOR)^Z}{(T)^{1/3}(R_{RA})^{Z''}} \left[\frac{(P - P_{onset})}{P - P_b} \right] \tag{28}$$

$$Y = \left[\frac{(P - P_b)}{P - P_{onset}} \right]^{Z'} \frac{W_{AP}(R_{RA})^{Z''}}{W_A}$$

where GOR is the gas to oil ratio, R_{RA} denotes the ratio of resin to asphaltene, P_b and P_{onset} are the bubble and onset pressures respectively, and W_A represents the amount of asphaltene in the live oil. The experimental data of literature indicate a good performance for the new equations as depicted in Figures 21 and 22 for above and below the saturation pressures, respectively [52].

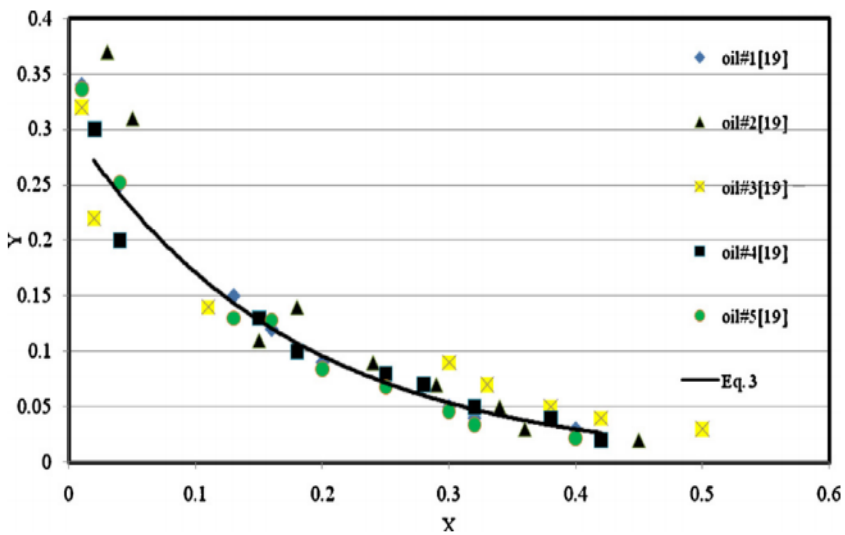


Figure 21. Collapse of experimental data into a single scaling curve for below saturation pressure [51]

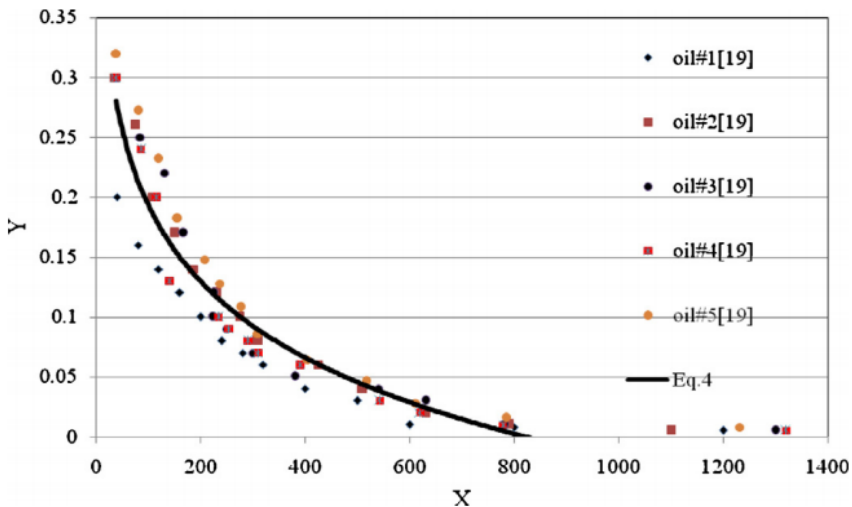


Figure 22. Collapse of experimental data into a single scaling curve for above saturation pressure [51]

Table 10. Correlation parameters for the proposed scaling model [52]

Adjusted parameter	$P \leq P_b$	$P \geq P_b$
Z	0.78	2.50
Z'	0.34	0.34
Z''	0.92	0.81
A	0.35	-0.09
B	-6.91	0.62

Table 11. Correlation parameters for PC-SAFT and Flory-Huggins models [52]

Adjusted parameter	Saturates	Aromatics \pm resins	Asphaltenes
m	6.213	6.0174	29.8
σ (A)	3.625	3.5950	4.215
ε / k /k (K)	257.400	289.7000	391.3
δ (MPa) ^{0.5}			19.20
Molar Volume (m ³ /kg mol)			0.60

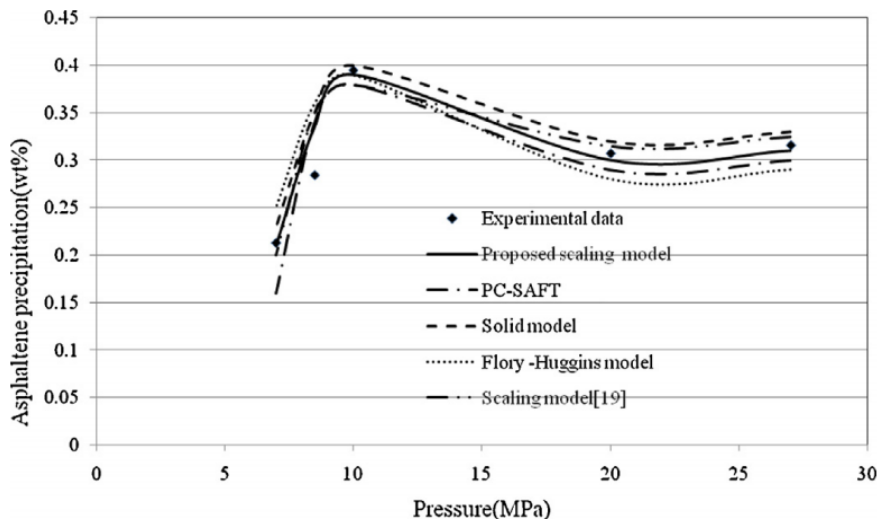


Figure 23. Comparison between the performance of the proposed scaling model and other studies in correlating the asphaltene precipitation weight percent, and the experimental data of the bottom hole live oil [52]

The values of Z, Z' and Z'' were optimized for pressure depletion and gas injection tests. The values of asphaltene precipitation parameters are reported in Table 10. In addition, these values are stated in Table 11 for the PC-SAFT and Flory-Huggins models.

The comparison of the results for the correlated precipitation weight percent during pressure depletion tests are reported in Figure 23 for the current study.

Table 12 reports the relative deviation of the asphaltene precipitation weight percent from experimental data and the proposed scaling equation. The results reveal that the present scaling equation offers better results in comparison to the previously published scaling

models [52]. The values for R^2 in the present model and previous scaling equation are 0.986 and 0.962, respectively. The promising point of this model was its independency from molecular weight and density. The same results are also achievable for the case of gas injection. The sensitivity analysis indicated that the developed scaling equation is a strong function of gas-oil ratio and resin to asphaltene ratio.

Khaksar et al. [53] also applied fuzzy logic, neural networks and genetic algorithms in live and tank crude oil systems. The results indicated that neural network could optimize the fuzzy systems and lead to better results in terms of fuzzy logic asphaltene modeling. The average error in this case was reported 1.6953%. The most sensible parameters were introduced as asphaltene content, pressure and molar percent of C_1 through C_3 . The correlation coefficient value was reported 0.99271 as shown in Table 13.

The fuzzy logic and the neural network models were then optimized by hybrid genetic algorithm-pattern search engine to improve the model efficiency. The results were compared to the open literature sources as shown in Figure 24.

Table 12. Deviation of the correlated asphaltene precipitation weight percent from their experimental results by the modified scaling model and studied thermodynamic models [52]

Pressure (MPa)	Deviation of asphaltene precipitation weight percent (%)				
	Proposed scaling model	PC-SAFT	Solid model	Flory-Huggins model	Scaling model
36	.06	0.54	2.86	38.12	0.12
30	.09	0.42	3.21	25.48	0.11
25	0.32	0.34	3.06	28.92	0.41
22	0.28	0.37	2.28	18.56	0.51
18	0.38	0.21	1.95	22.38	0.85
12	0.18	0.35	1.65	15.29	0.32
8	0.23	0.13	2.08	10.87	0.76
5	0.51	0.12	1.75	7.25	0.91

Table 13. Fitness and R^2 values for the training, validation and testing sets of genetic algorithm [53]

Statistical parameter	Best program	Best team
Training fitness	0.335040	0.005489
Validation fitness	0.228420	0.013637
T. V. fitness	0.015645	0.009563
Testing fitness	0.814538	0.401313
Training R^2	0.99979	0.9998
Validation R^2	0.9995	0.99965
T&V R^2	0.99965	0.99973
Testing R^2	0.98034	0.99271

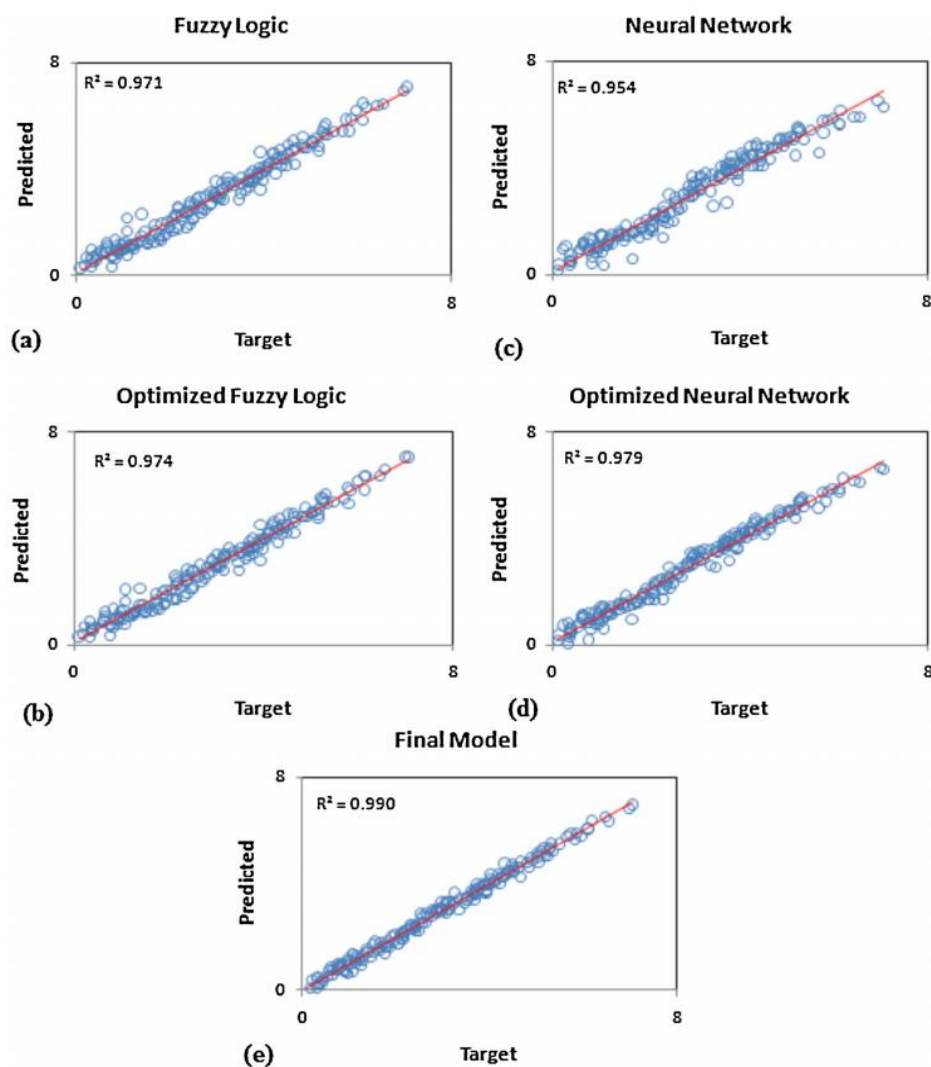


Figure 24. Cross-plots showing the correlation coefficient between measured and predicted asphaltene amounts by (a) fuzzy logic, (b) optimized fuzzy logic, (c) neural network (d) optimized neural network, and (e) committee machine (final model). This figure shows optimized models (b and d) perform better than non-optimized models (a and c). Eventually, committee machine (e) performs better than all other individual models (a–d) [31].

Table 14. Comparison between different models developed in this study and one of the best scaling equation models proposed by Hu and Guo [25] using the concepts of correlation coefficient and mean square error. [31]

Model	Correlation coefficient	Mean square error
Hu and Guo [25]	0.964	0.693960
Committee machine	0.990	0.027180
Fuzzy logic	0.971	0.081950
Optimized fuzzy logic	0.974	0.042112
Neural network	0.954	0.044460
Optimized neural network	0.979	0.031857

Various models are compared in terms of correlation coefficient and mean square error in Table 14. It is obvious that committee machine method results in more accurate outputs in comparison to the other stated methods.

Khaksar et al. [53] developed a new scaling equation considering reservoir pressure using genetic algorithm. This method is mostly applicable in predicting the onset and amount of asphaltene precipitation during gas injection for EOR processes. The results showed that they are in good agreement with experimental data. The variables are introduced as follows:

$$X = \frac{x}{P^{c1}} = \frac{R}{M_w^z \times P^{c1}} \tag{29}$$

$$Y = \frac{y}{x^{c2}} = \frac{w \times M_w^{(z \times c2 - z')}}{R^{c2}}$$

and,

$$X' = \frac{X}{T^{c3}} = \frac{R}{M_w^z \times P^{c1} \times T^{c3}}$$

$$Y' = \frac{Y}{X^{c4}} = \frac{w \times M_w^{(z \times c2 + z \times c4 - z')}}{R^{(c2+c4)}} \times P^{c1 \times c4}$$

$$Y' = a_0 + a_1 X' + a_2 X'^2 + a_3 X'^3 \tag{30}$$

Table 15. Constant parameters of the new scaling equation [27]

Z	C ₁	C ₂	C ₃	C ₄
0.1	3.9409	1.0642	-0.0376	0.0773

Table 16. Adjusted parameters of the new scaling equation [27]

	a ₀	a ₁	a ₂	a ₃
Oil 1	984.7977	960.9863	961.4814	793.3274
Oil 2	959.3549	976.8057	960.2316	911.0102
Oil 3	987.3159	938.7081	959.9271	991.6694
Oil 4	415.4045	847.8503	975.5652	959.9207
Ashoori et al. [40] experimental data	995.7975	434.9802	31.8433	-3.6041
Hu et al. [33] experimental data	933.7990	-111.0590	63.0079	-3.0380
Our experimental data	233.7105	256.5287	0.2193	-0.9219

Table 17. Static precipitation, test results of oil 1 experimental data [27]

R, mL/g	Pressure, Bar	Temperature, °C	Molecular weight of solvent	W _{exp} , %	W _{exp} %, scaling equation
0.053361	206.4422	100	42.5	0.738	0.0025
0.160082	206.4422	100	42.5	0.578	0.0087
0.053361	1	15.55556	42.5	14.97	4.0130
0.106721	1	15.55556	42.5	15.61	5.0300
0.213442	1	15.55556	42.5	15.14	5.0724
0.145274	206.4422	100	24.8	0.656	0.0242
0.290548	206.4422	100	24.8	0.807	0.0534
0.145274	1	15.55556	24.8	16.36	7.1385
0.290548	1	15.55556	24.8	15.69	7.3497
0.213442	206.4422	100	42.5	0.697	0.0120
0.072637	1	15.55556	24.8	15.71	11.0590
0.160082	1	15.55556	42.5	14.52	10.0498
0.072637	206.4422	100	24.8	0.699	0.0110
0.217911	206.4422	100	24.8	0.797	0.384
0.106721	1	15.55556	42.5	15.61	11.0300
0.106721	206.4422	100	42.5	0.726	0.0054

Constant parameters of the scaling equations resulted from the experimental data are reported in Tables 15 and 16. The unknowns are obtained by using the experimental data and genetic algorithm.

The static precipitation test results for one of the oil samples are reported in Table 17 showing a good agreement between the experimental data and the scaling model.

4. QUALITY OF ASPHALTENE PRECIPITATION TITRATION DATA

In order to detect the applicability domain of the proposed CSA-LSSVM models, Hemmati-Sarapardeh et al. [49] employed the Leverage approach in which the data residuals, Hat matrix and William plot are applied for detection of suspected data. More details about this approach can be found in the original paper[49]. As indicated in Figure 25 to 28, most of the data points are located within the applicability domain of the proposed models. Four outlier data points used from Ashoori et al. [40] were detected for model 1. For model 2, one data point was found to be a good high leverage data point, which was used from Hu and Guo [25] and one data point was found to be an outlier from the data sets of Rassamdana et al. [24]. Three data points were found to be outliers in model 3, two of which were used from the data banks of Ashoori et al. [40] and one from Hu and Guo [25]. Two data outliers were detected for model 4, which were collected from the data banks of Rassamdana et al. [24] and Hu and Guo [25]. All of these suspected data points are reported in Table 18. The results of leverage approach indicate that all the four proposed models are statistically valid and only a few data points are outside of the applicability domain of these models.

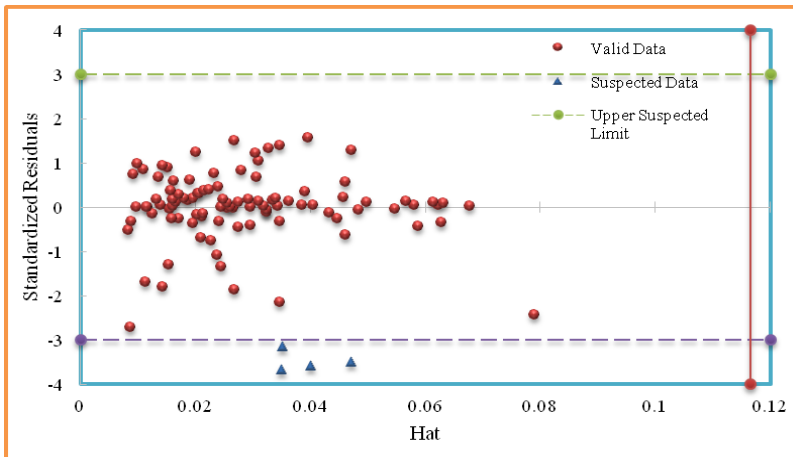


Figure 25. Williams plot of model 1 identifying the applicability domain and suspected data points [49]

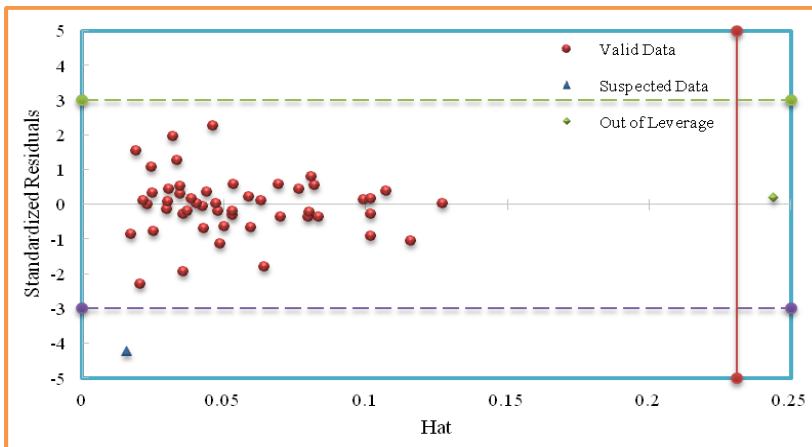


Figure 26. Williams plot of model 2 identifying the applicability domain and suspected data points [49]

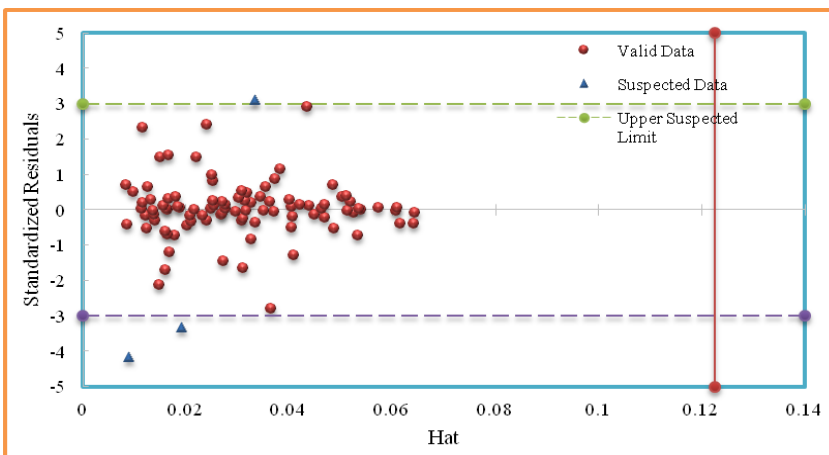


Figure 27. Williams plot of model 3 identifying the applicability domain and suspected data points [49]

Table 18. The doubtful experimental data based on the Leverage approach [49]

Ref.	n-alkane precipitant	T, °C	Rv(mL/g)	asphaltene (wt%)- Exp.	asphaltene (wt%)-model	hat	Standardized residuals
[40]	n-C5	30	5.00	5.83	3.50	0.040	-3.58
[40]	n-C5	50	5.00	5.16	2.90	0.047	-3.49
[40]	n-C5	30	10.00	9.25	6.50	0.009	-4.17
[40]	n-C6	30	5.00	5.03	2.98	0.035	-3.14
[40]	n-C6	30	10.00	8.13	5.94	0.019	-3.34
[25]	n-C6	65	20.00	4.02	6.03	0.033	3.10
[40]	n-C7	30	5.00	4.80	2.42	0.034	-3.65
[24]	n-C8	25	2.94	2.48	1.95	0.015	-4.22
[25]	n-C8	65	3.60	0.12	0.14	0.244	0.18
[24]	n-C10	25	10.00	2.99	3.50	0.025	3.43
[25]	n-C12	50	10.60	2.85	2.26	0.041	-3.94

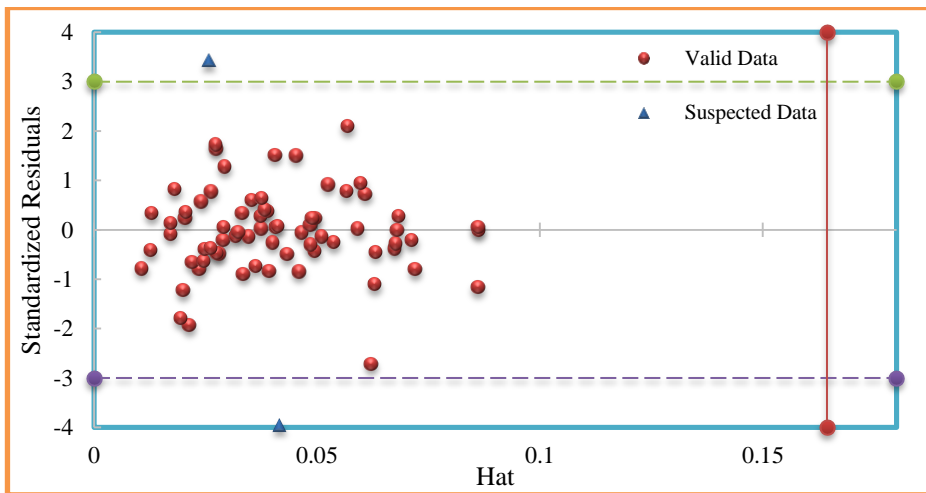


Figure 28. Williams plot of model 4 identifying the applicability domain and suspected data points [49]

CONCLUSIONS

In this chapter, asphaltene precipitation models for live and dead oil were reviewed using different scaling equations. These equations have no requirement to the properties of asphaltene and have simple mathematical formulations. All of the proposed scaling equations have been reviewed and the priority of them has been discussed over each other. In the category of asphaltene titration data, before developing the support vector machines, genetic algorithm based scaling equations resulted in the best results in terms of R². After developing the support vector machine, better results were obtained in comparison to the previously developed techniques.

For the case of natural depletion or gas injection, some scaling equations have been developed in which Roshanaei Zadeh et al. [50] developed a scaling equation for the case of gas injection independent of asphaltene properties. The results were in good agreement with experimental data. Kord and Ayatollahi [51] developed a scaling equation in the case of

natural depletion and its standard deviation was compared to the other existing thermodynamic models. This method resulted in more accurate results in comparison to the other models. Khaksar et al. [53] also applied fuzzy logic, neural networks and genetic algorithms in live and tank crude oil systems and reported the correlation coefficient of 0.99271. The model efficiency was then improved by hybrid genetic algorithm-pattern search engine.

The applicability domain of the proposed LSSVM models was studied by Hemmati-Sarapardeh et al. [49]. In this method, data residuals, Hat matrix and William plot were applied for detection of suspected data. The data bank of all previously studies were selected to compare the asphaltene precipitation data. They also showed that LSSVM method outperforms all of the existing models in terms of validity and accuracy at various temperatures, solvent types and dilution ratios. The applicability domain of the models was determined using the Leverage approach. All of the studied data were valid and only 3.3% of the data points were outliers.

This study provides a new insight toward asphaltene precipitation modeling through the scaling equations.

REFERENCES

- [1] Hirschberg, A., et al. Influence of temperature and pressure on asphaltene flocculation. *Society of Petroleum Engineers Journal*, 1984. 24(03): p. 283-293.
- [2] Ali, L. H. and K. A. Al-Ghannam, Investigations into asphaltenes in heavy crude oils. I. Effect of temperature on precipitation by alkane solvents. *Fuel*, 1981. 60(11): p. 1043-1046.
- [3] Chung, F., P. Sarathi, and R. Jones, Modeling of asphaltene and wax precipitation. 1991, *National Inst. for Petroleum and Energy Research*, Bartlesville, OK (USA).
- [4] Cimino, R., et al. Solubility and phase behavior of asphaltenes in hydrocarbon media, in *Asphaltenes*. 1995, Springer. p. 97-130.
- [5] Montel, V., et al. Asphaltene cake properties. *Energy and Fuels*, 2008. 22(6): p. 3970-3975.
- [6] Porte, G., H. Zhou, and V. Lazzeri, Reversible description of asphaltene colloidal association and precipitation. *Langmuir*, 2003. 19(1): p. 40-47.
- [7] Kord, S., et al. Asphaltene Deposition in Carbonate Rocks: Experimental Investigation and Numerical Simulation. *Energy and Fuels*, 2012. 26(10): p. 6186-6199.
- [8] Zanganeh, P., et al. Asphaltene Deposition during CO₂ Injection and Pressure Depletion: A Visual Study. *Energy and Fuels*, 2012. 26(2): p. 1412-1419.
- [9] Mohammadi, A. H., A. Eslamimanesh, and D. Richon, Monodisperse Thermodynamic Model Based on Chemical+ Flory–Huggins Polymer Solution Theories for Predicting Asphaltene Precipitation. *Industrial & Engineering Chemistry Research*, 2012. 51(10): p. 4041-4055.
- [10] Ramos, A., et al. Reversibility and inhibition of asphaltene precipitation in Brazilian crude oils. in *Latin American and Caribbean Petroleum Engineering Conference*. 1997: Society of Petroleum Engineers.

-
- [11] Kawanaka, S., S. Park, and G. Mansoori, Organic deposition from reservoir fluids: a thermodynamic predictive technique. *SPE ReservoirEngineering*, 1991. 6(02): p. 185-192.
- [12] Hammami, A. and J. Ratulowski, Precipitation and deposition of asphaltenes in production systems: A flow assurance overview, in *Asphaltenes, Heavy Oils, and Petroleomics*. 2007, Springer. p. 617-660.
- [13] David Ting, P., G. J. Hirasaki, and W. G. Chapman, Modeling of asphaltene phase behavior with the SAFT equation of state. *Petroleum Science and Technology*, 2003. 21(3-4): p. 647-661.
- [14] Wu, J., J. M. Prausnitz, and A. Firoozabadi, Molecular-thermodynamic framework for asphaltene-oil equilibria. *AIChE journal*, 1998. 44(5): p. 1188-1199.
- [15] Wu, J., J. M. Prausnitz, and A. Firoozabadi, Molecular thermodynamics of asphaltene precipitation in reservoir fluids. *AIChE journal*, 2000. 46(1): p. 197-209.
- [16] Christensen, A., C. Hadsbjerg, and P. V. Tybjerg, A study of the perturbed chain statistical associating fluid theory. Midterm Project, Technical University of Denmark, *Department of Chemical Engineering*, 2005.
- [17] Buenrostro-Gonzalez, E., et al. Asphaltene precipitation in crude oils: Theory and experiments. *AIChE Journal*, 2004. 50(10): p. 2552-2570.
- [18] Tabatabaei-Nejad, S. A. and E. Khodapanah, Application of Chebyshev polynomials to predict phase behavior of fluids containing asphaltene and associating components using SAFT equation of state. *Fuel*, 2010. 89(9): p. 2511-2521.
- [19] Gonzalez, D. L., et al. Prediction of asphaltene instability under gas injection with the PC-SAFT equation of state. *Energy and fuels*, 2005. 19(4): p. 1230-1234.
- [20] Vafaie-Sefti, M. and S. Mousavi-Dehghani, Application of association theory to the prediction of asphaltene deposition: Deposition due to natural depletion and miscible gas injection processes in petroleum reservoirs. *fluid phase equilibria*, 2006. 247(1): p. 182-189.
- [21] Nikookar, M., G. Pazuki, and R. Masoudi, A new approach in modeling asphaltene precipitation in heavy oil. SPE97939-MS-P, 2005.
- [22] Mohammadi, A. H. and D. Richon, A monodisperse thermodynamic model for estimating asphaltene precipitation. *AIChE Journal*, 2007. 53(11): p. 2940-2947.
- [23] Cimino, R., et al. Thermodynamic modelling for prediction of asphaltene deposition in live oils. in *SPE International Symposium on Oilfield Chemistry*. 1995: Society of Petroleum Engineers.
- [24] Rassamdana, H., et al. Asphalt flocculation and deposition: I. The onset of precipitation. *AIChE Journal*, 1996. 42(1): p. 10-22.
- [25] Hu, Y.-F. and T.-M. Guo, Effect of temperature and molecular weight of n-alkane precipitants on asphaltene precipitation. *Fluid Phase Equilibria*, 2001. 192(1): p. 13-25.
- [26] Soulgani, B. S., et al. A new thermodynamic scale equation for modelling of asphaltene precipitation form live oil. in *Canadian International Petroleum Conference*. 2009: Petroleum Society of Canada.
- [27] Manshad, A. K., et al. Developing a scaling equation as a function of pressure and temperature to determine the amount of asphaltene precipitation. *Petroleum Science and Technology*, 2013. 31(21): p. 2169-2177.

- [28] Salahshoor, K., et al. Asphaltene deposition prediction using adaptive neuro-fuzzy models based on laboratory measurements. *Fluid Phase Equilibria*, 2013. 337: p. 89-99.
- [29] Hemmati-Sarapardeh, A., et al. Asphaltene precipitation due to natural depletion of reservoir: Determination using a SARA fraction based intelligent model. *Fluid Phase Equilibria*, 2013. 354: p. 177-184.
- [30] Fattahi, H., et al. Estimation of asphaltene precipitation from titration data: a hybrid support vector regression with harmony search. *Neural Computing and Applications*, 2015. 26(4): p. 789-798.
- [31] Asoodeh, M., A. Gholami, and P. Bagheripour, Asphaltene precipitation of titration data modeling through committee machine with stochastically optimized fuzzy logic and optimized neural network. *Fluid Phase Equilibria*, 2014. 364: p. 67-74.
- [32] Na'imi, S. R., A. Gholami, and M. Asoodeh, Prediction of crude oil asphaltene precipitation using support vector regression. *Journal of Dispersion Science and Technology*, 2014. 35(4): p. 518-523.
- [33] Hu, Y.-F., et al. A study on the application of scaling equation for asphaltene precipitation. *Fluid Phase Equilibria*, 2000. 171(1): p. 181-195.
- [34] Kokal, S. L., et al. Measurement and correlation of asphaltene precipitation from heavy oils by gas injection. *Journal of Canadian Petroleum Technology*, 1992. 31(04).
- [35] Rassamdana, H. and M. Sahimi, Asphalt flocculation and deposition: II. Formation and growth of fractal aggregates. *AIChE journal*, 1996. 42(12): p. 3318-3332.
- [36] Mozaffarian, M., et al. Asphalt flocculation and deposition IV. Dynamic evolution of the heavy organic compounds. *Fuel*, 1997. 76(14): p. 1479-1490.
- [37] Rassamdana, H., et al. Asphalt flocculation and deposition. V. Phase behavior in miscible and immiscible injections. *Energy and Fuels*, 1999. 13(1): p. 176-187.
- [38] Dabir, B., et al. Asphalt flocculation and deposition. III. The molecular weight distribution. *Fuel*, 1996. 75(14): p. 1633-1645.
- [39] Asoodeh, M., A. Gholami, and P. Bagheripour, Renovating scaling equation through hybrid genetic algorithm-pattern search tool for asphaltene precipitation modeling. *Journal of Dispersion Science and Technology*, 2014. 35(4): p. 607-611.
- [40] Ashoori, S., et al. Comparison of scaling equation with neural network model for prediction of asphaltene precipitation. *Journal of Petroleum Science and Engineering*, 2010. 72(1): p. 186-194.
- [41] Suykens, J. A. and J. Vandewalle, Least squares support vector machine classifiers. *Neural processing letters*, 1999. 9(3): p. 293-300.
- [42] Pelckmans, K., et al. LS-SVMLab: a matlab/c toolbox for least squares support vector machines. Tutorial. KULeuven-ESAT. Leuven, Belgium, 2002.
- [43] Ripley, B. D., Pattern recognition and neural networks. 2007: Cambridge university press.
- [44] Poggio, T. and F. Girosi, Regularization algorithms for learning that are equivalent to multilayer networks,(1990), 978-982. *Science*. 247.
- [45] Poggio, T. and F. Girosi, Networks for approximation and learning. *Proceedings of the IEEE*, 1990. 78(9): p. 1481-1497.
- [46] Haykin, S., Neuronal Networks-A comprehension Foundation. 1999, New York, Prentice Hall, 842p.

-
- [47] Wang, X., R. Luo, and H. Shao. Designing a soft sensor for a distillation column with the fuzzy distributed radial basis function neural network. in Decision and Control, 1996., *Proceedings of the 35th IEEE Conference on. 1996: IEEE.*
 - [48] Asoodeh, M. and P. Bagheripour, Asphaltene precipitation modeling using fuzzy tuning of scaling equations. *Journal of Dispersion Science and Technology*, 2014. 35(4): p. 577-580.
 - [49] Hemmati-Sarapardeh, A., et al. On the evaluation of asphaltene precipitation titration data: Modeling and data assessment. *Fluid Phase Equilibria*, 2016. 415: p. 88-100.
 - [50] Roshanaei Zadeh, G. A., et al. Comprehensive study of asphaltene precipitation due to gas injection: experimental investigation and modeling. in SPE Enhanced Oil Recovery Conference. 2011: Society of Petroleum Engineers.
 - [51] Kord, S. and S. Ayatollahi, Asphaltene precipitation in live crude oil during natural depletion: Experimental investigation and modeling. *Fluid Phase Equilibria*, 2012. 336: p. 63-70.
 - [52] Behbahani, T. J., et al. A modified scaling equation based on properties of bottom hole live oil for asphaltene precipitation estimation under pressure depletion and gas injection conditions. *Fluid Phase Equilibria*, 2013. 358: p. 212-219.
 - [53] Khaksar Manshad, A., M. Khaksar Manshad, and S. Ashoori, Intelligent modeling of asphaltene precipitation in live and tank crude oil systems. *Petroleum Science and Technology*, 2012. 30(13): p. 1392-1403.

Chapter 7

ON THE ESTIMATION OF WAX DEPOSITION IN CRUDE OIL SYSTEMS

*Abbas Khaksar Manshad,¹ Habib Rostami,²
Hojjat Rezaei,³ Seyed Moein Hosseini,³ Hasan Niknafs⁴
and Amir H Mohammadi^{5,6,7,*}*

¹Department of Petroleum Engineering, Abadan Faculty of Petroleum Engineering,
Petroleum University of Technology (PUT), Abadan, Iran

²Department of Computer Engineering, School of Engineering,
Persian Gulf University, Bushehr, Iran

³Department of Petroleum Engineering, Ahwaz Faculty of Petroleum Engineering,
Petroleum University of Technology (PUT), Ahwaz, Iran

⁴Department of Petroleum Engineering, Engineering and Basic Science Faculty,
Khazar University, Baku, Azerbaijan

⁵Discipline of Chemical Engineering, School of Engineering, University of KwaZulu-
Natal, Howard College Campus, King George V Avenue, Durban 4041, South Africa

⁶Département de Génie des Mines, de la Métallurgie et des Matériaux, Faculté des
Sciences et de Génie, Université Laval, Québec, QC G1V 0A6, Canada

⁷Institut de Recherche en Génie Chimique et Pétrolier (IRGCP), Paris Cedex, France

ABSTRACT

Deposition of wax as a crude oil component is one of the major problems in the crude oil production and transportation. Changes in crude oil thermodynamics conditions such as pressure, temperature and composition cause this problem. Accurate prediction of wax deposition is therefore important. There are several methods such as experimental approach, thermodynamics models and correlations for determination of wax deposition. In this communication, we have developed a feed forward artificial neural network optimized by particle swarm optimization method to estimate the amount of wax deposition in crude oil system. In this model, oil composition, pressure, temperature and

* Corresponding Author E-mail: amir_h_mohammadi@yahoo.com and a.h.m@irgcp.fr.

oil specific gravity are considered as input parameters to neural network and the amount of wax deposition is regarded as output parameter. 94 experimental data sets of 8 different crude oil samples were used to develop the model. Comparing the performance and results of the algorithm developed in this work with multi solid thermodynamic model and the Genetic Programming Neural Network algorithm proves the performance and accuracy of the model developed in this study.

Keywords: wax deposition; paraffin; crude oil; artificial neural network; particle swarm optimization; Genetic Programming Neural Network; multi solid thermodynamic model

INTRODUCTION

Petroleum waxes are typically heavy paraffinic contents of crude oil and consist of C₂₀-C₆₀ (even heavier) hydrocarbon ranges [1, 2]. Wax deposition as one of major problems in petroleum industry causes the plugging of production facilities, well bores and transportation pipelines and decreases the efficiency of oil production [3-5]. Temperature reduction is regarded as one of main reasons for wax formation and deposition, because wax solubility in crude oil decreases as the temperature decreases [6-8]. Temperature, pressure, oil composition, laminar and turbulent flow regime [9-12], pipe roughness [13-15] and gas-oil ratio [16, 17] affect wax deposition.

Accurate prediction of wax deposition amount is therefore important [4]. There are several methods like experimental approach, thermodynamics models and correlations for estimating wax deposition.

Different thermodynamic models have been developed for this purpose [18, 19]. However, the results of the latter models are not very accurate in comparison with experimental results. Multi-solid phase model as a thermodynamics method is commonly used in the literature [5]. Lira-Galeana et al. [20] proposed a multi-solid (MS) wax model, in which each solid phase is not mixed with other solid phases and is considered as a pure component. Won [21] developed a thermodynamic model on the basis of vapor-liquid-solid phase equilibria for prediction of wax deposition. He considered wax phase as a non-ideal solution similar to liquid phase. Burger et al. [22] developed a widely accepted thermodynamic model in which crude oil is dissolved in a mixture of ether and acetone. Valinejad and Solaimany Nazar [23] worked experimentally on three waxy crude oils to determine wax deposition potential during laminar flow in a pipeline. An empirical model was developed by Kelechukwu et al. [24] for prediction wax deposition in oil production systems and the performance of this model was acceptable in comparison with the laboratory measurement. Akbarzadeh and Zougari [25] proposed a novel approach for modeling wax deposition in fluid flows. The mechanism of particle diffusion/deposition was introduced as the most important mechanism in wax deposition at the realistic transport conditions. One of the most recent approaches for prediction of wax deposition is neural network algorithm. Khaksar and Ashoori [26] proposed a model based on Genetic Programming Neural Network (GPNN) for prediction of wax deposition and their model performance and accuracy was better than a thermodynamic model studied in their work.

In the present work, PSO (particle swarm optimization) was used as an optimizing algorithm to train feed-forward artificial neural network (ANN) for estimating amount of wax

deposition as a function of pressure, temperature, oil composition and oil specific gravity. Comparison of performance and accuracy of the model with multi-solid thermodynamic model and Genetic Programming Neural Network algorithm indicates that the current developed model is more accurate and acceptable for prediction of Wax deposition amount.

ARTIFICIAL NEURAL NETWORK

Neural networks have been used in various fields of science and engineering for approximation of complex systems [27]. These computational algorithms provide a reliable model of nonlinear and complex systems by data gathering, learning, recognizing, organizing and generalizing, using inputs and outputs data sets [28]. There are different approaches for designing a neural network, multilayered feed forward is one of the best methods for this design. In this work, three layered feed forward neural networks with back propagation algorithm were used for nonlinear functions approximation with high accuracy. Data preprocessing, network training and style choosing steps must be followed for achieving a perfect network for the model construction [29, 30]. Training process as a step in achieving accurate network is done by changing the weight of node connections for achieving the network output that is closer to actual values. At the first, data sets are preprocessed, and then data bank is divided into three types; training, validating and testing. Training data is used for network training, validating set is for checking model accuracy and the testing data is for determination of model strength [31]. Figure 1 shows structural design of three layer feed-forward ANNs.

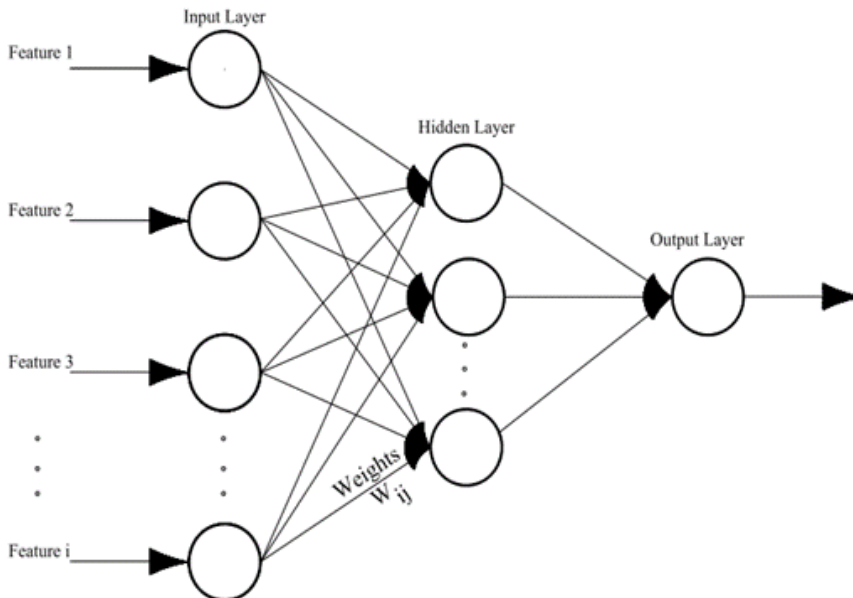


Figure 1. Structural design of a typical feed-forward ANN.

PARTICLE SWARM OPTIMIZATION

In 1995, the Particle Swarm Optimization approach as an optimization procedure was proposed by Eberhart and Kennedy [32]. This algorithm like the simulated annealing (SA) [33] and the genetic algorithm (GA) [34] tries to achieve the global optimum for nonlinear systems. In this algorithm, particles are accidentally distributed over the space for getting the goal of converging to the global optimum and each particles group have the chance of being a solution for optimization objective. Particles examine the space and continue paths of their position to reach global optimum solution. Personal best value and global best value were called by Kennedy and Eberhart [35] pBest and gBest, respectively. A best solution achieved by a particle is the pBest and and the best solution obtained by global optimization in PSO algorithm is the gBest.

In PSO algorithm, with the 'm' number of particles, the position of m_{th} particle is labeled by $X_m = \{X_{m1}, X_{m2}, \dots, X_{mN}\}$, where X_{mj} is the value of j_{th} coordinate in the N dimensional space. $P_m = \{P_{m1}, P_{m2}, \dots, P_{mN}\}$ is the best visited position of the m_{th} particles and $G = \{G_1, G_2, \dots, G_N\}$ is the best experience of all the particles in this algorithm. $V_p = \{V_{p1}, V_{p2}, \dots, V_{pN}\}$ is the set of the particles velocity as the change rate in particle position. At any iteration step, particle position changes according to its velocity. According to N-coordinate velocity and on the basis of Equation 1, particle 'm' changes its position. In Equation 1, effect of previous velocities on the present velocity is controlled by the ω called inertia weight factor.

$$v_{Nm}^{i+1} = \omega v_{Nm}^i + A_1 \text{rand}(0,1)(P_{Nm} - X_{Nm}) + A_2 \text{rand}(0,1)(G_N - X_{Nm}) \quad (1)$$

Positive constants b_1 and b_2 are responsible for acceleration of particles towards best position of the solution space called learning factors. In Equation 1, $\text{rand}(0, 1)$ is a function that is used for generation of a random number between 0 and 1 [36].

Maximum number of iterations is defined by the user and the PSO algorithm stops when reaches the maximum steps. At any iteration steps, the inertia weight is updated by using the equation:

$$\omega_i = \omega_{max} - \frac{\omega_{max} - \omega_{min}}{i_{max}} \times i \quad (2)$$

where i_{max} is the maximum steps of iterations, ω_i is called the inertia weight in each iteration step and ω_{min} and ω_{max} are the minimum and maximum inertia weights. The values of $\omega_{min} = 0.4$ and $\omega_{max} = 0.9$ are the suitable amounts in researches [37].

RESULTS AND DISCUSSION

In this study, PSO algorithm was used for weight training of multilayer feed forward network and for achieving the best network training procedure and fast convergence. The number of network weights is the same as the particles dimension number and series of

weights is determined based on the position of a particular particle, the range of $[-1,1]$ is the network initial weights range [32, 37].

We have developed the PSO-based ANN model for estimation of wax deposition amount (weight), using 9 input parameters (mole percentage of (C1- C3), mole percentage of (C4-C7), mole percentage of (C8- C15), mole percentage of (C16- C22), mole percentage of (C23- C29), mole percentage of (C30+), oil specific gravity, temperature, pressure) and amount of wax deposition as desired output as indicated in Figure 2. In this work, we have used 94 experimental data sets from 8 different crude oil samples and after data preprocessing, 87 data sets were chosen for network training. Maximum and minimum values of temperature, pressure, oil composition and properties are shown in Table 1.

Figure 3 indicates the ANN-PSO algorithm flowchart. As mentioned earlier, PSO is used in this model to examine and find the best solutions among solution space and after construction of the neural network, randomly particles initialize with an appropriate population size. Particle position and velocity are updated at any iteration step so weights of neural networks are updated, then by determination of fitness function of ANN corresponding to each weight of the particle pBest and gBest are updated.

In each step, this procedure will continue until final iteration where stopping condition will be achieved and the best global solution is obtained then predicted values of the network are reported as an output results.

By running the neural network by using different neuron numbers and layers, the best performance was achieved by 4-8-4-1 as the best structure (4 input units, 8 hidden neurons in first layer, 4 hidden neurons in second layer, 1 output neuron).

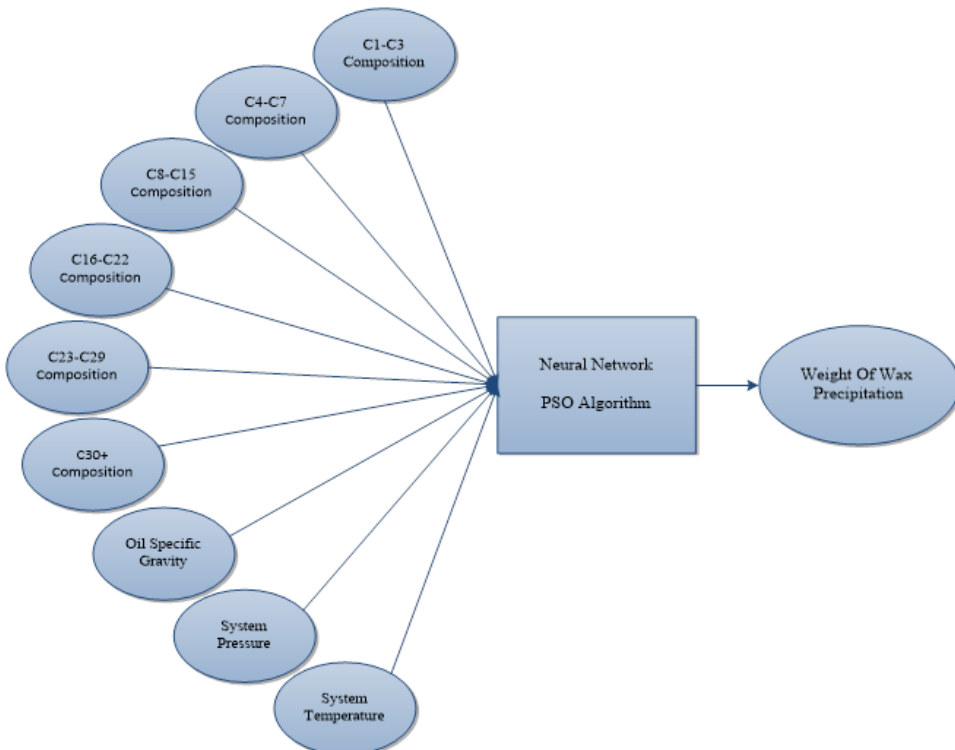


Figure 2. ANN inputs for estimating of wax deposition amount.

Table 1. Crude oil samples characterization information

Information	Minimum	Maximum
Wax deposition (Wt%)	0	13
Temperature (K)	230	313.15
Pressure (bar)	1	1
Specific gravity	0.872	0.963
Composition (mole%)		
C ₁ -C ₃	0.218	2.127
C ₄ -C ₇	3.057	30.952
C ₈ -C ₁₅	33.468	49.791
C ₁₆ -C ₂₂	16.029	57.335
C ₂₃ -C ₂₉	6.974	10
C ₃₀₊	8.177	13.23

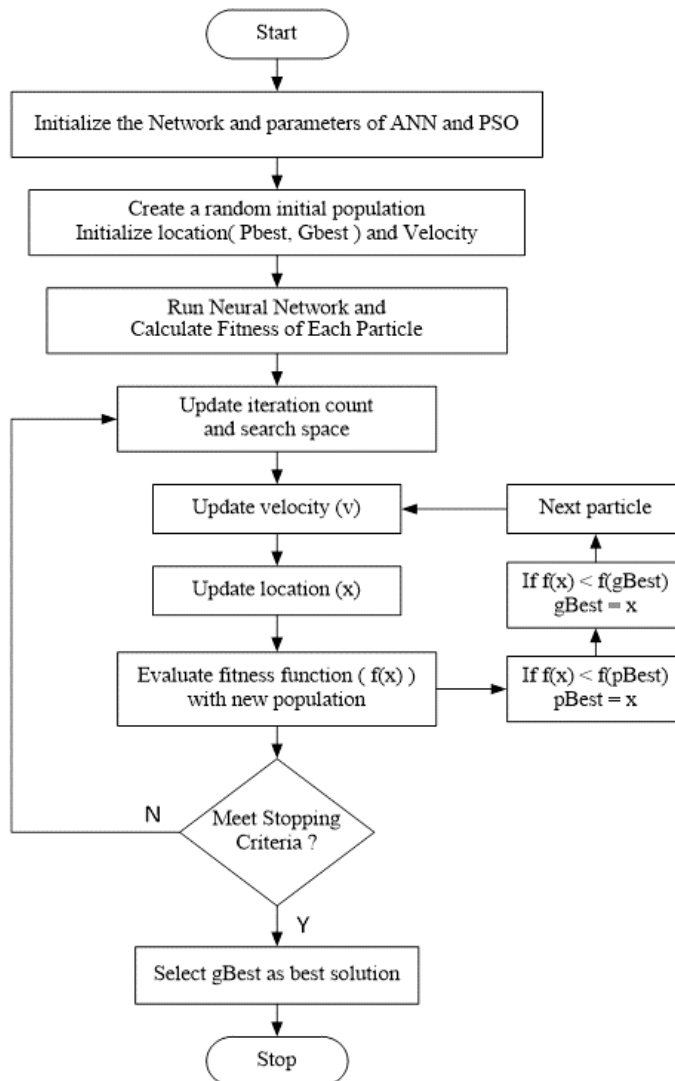


Figure 3. Flow chart for PSO-based ANN model.

Performance of data sets in various steps of network construction is shown in Figures 4-6. Figures 7 and 8 show the scatter plot of model prediction results with experimental values. Sensitivity analysis of the model and inputs, as independent variables dependency to output variable was checked using @Risk (2011) software and correlation coefficient determines the sensitivity analysis. As the correlations between any output and input parameters are higher, that input has more influence on the prediction of the output value. In Figure 9, it is shown that temperature has the most influence on the wax deposition amount.

The performance of the developed model was further checked by the parameter of Average Absolute Relative Errors (AARE).

$$AARE = \sum(abs(Y - X)/X)/N \quad (3)$$

where Y is the predicted amount of wax deposition and X is the experimental amount. The model accuracy will increase as $AARE$ approaches to zero and the network error will decrease. Table 2 indicates that the present model is more accurate than multi-solid thermodynamic model and Genetic Programming Neural Network algorithm.

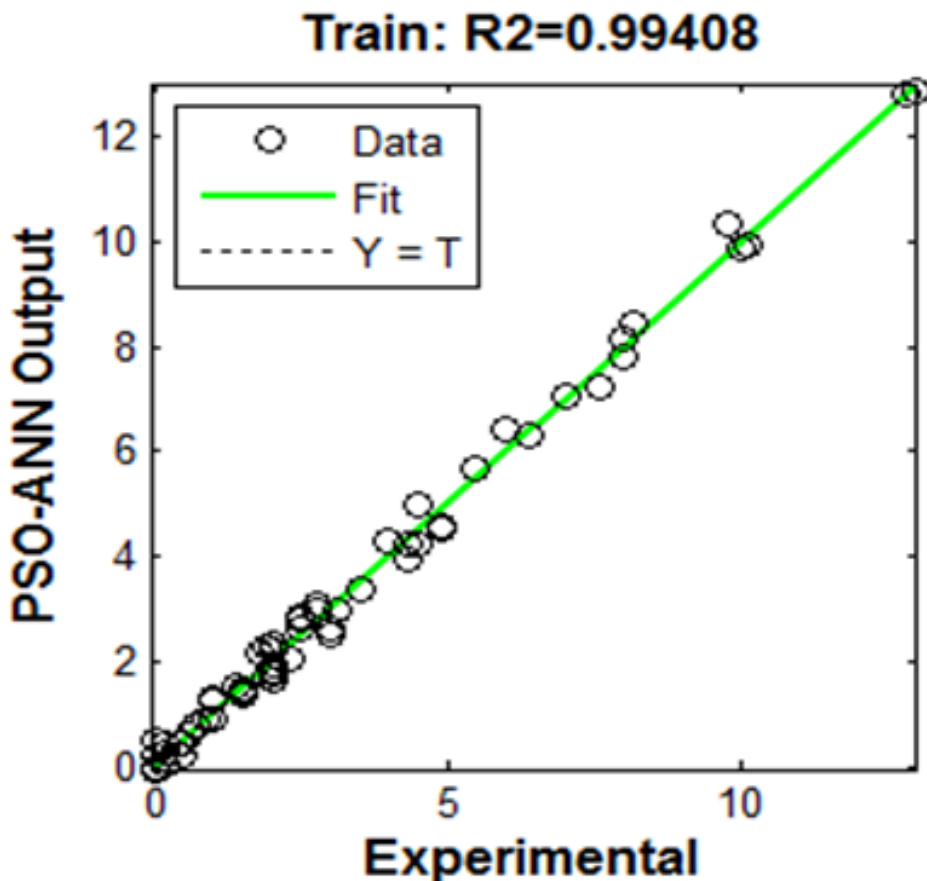


Figure 4. Network performance in data training.

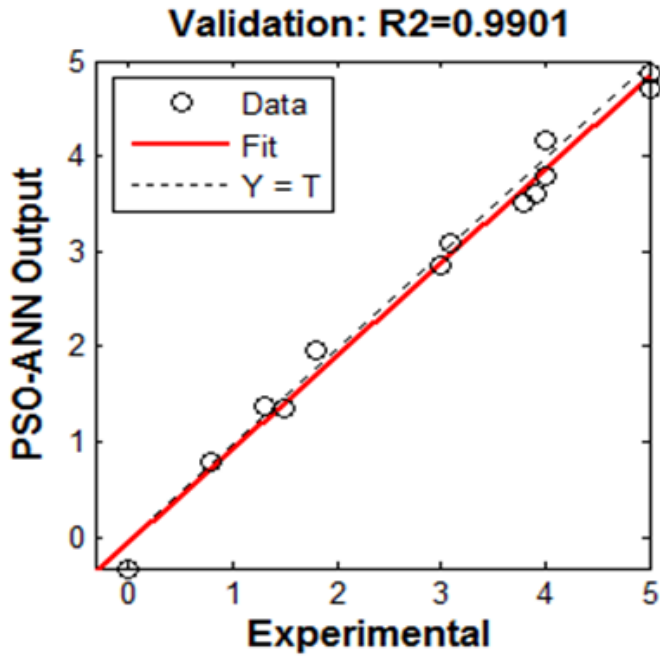


Figure 5. Network performance in data validating.

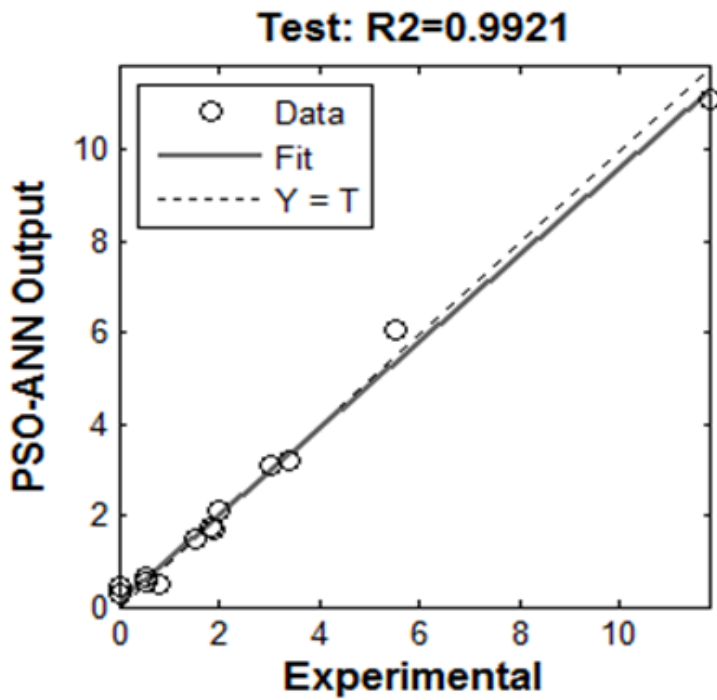


Figure 6. Network performance in data testing.

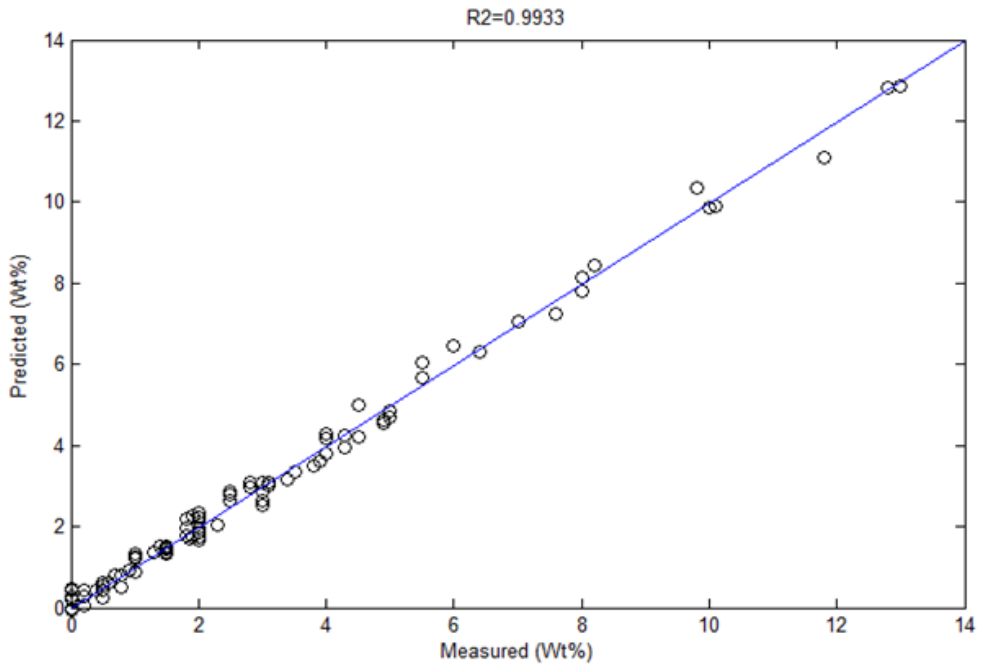


Figure 7. Scatter plot of the model prediction values versus the measured value.

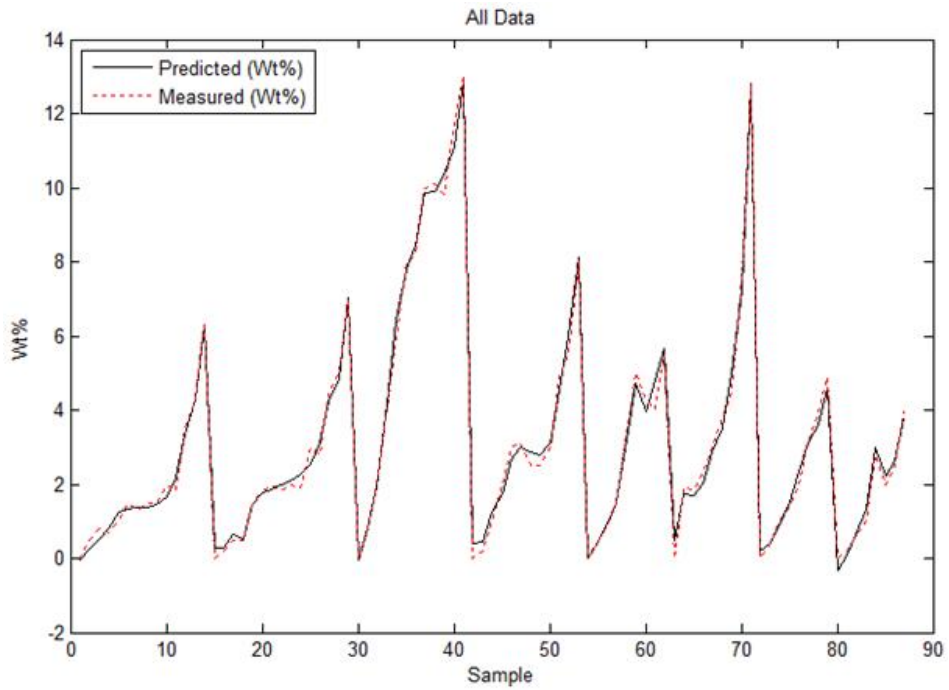


Figure 8. Comparison of the model prediction values with the measured values.

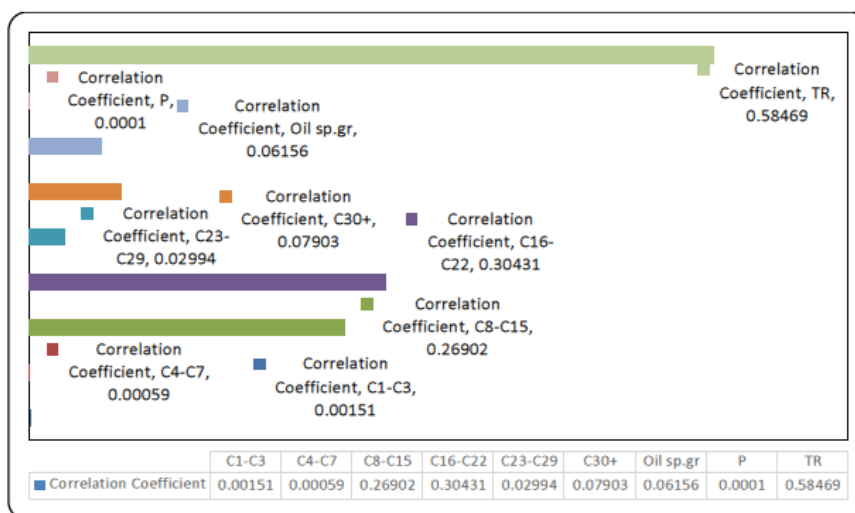


Figure 9. Impact of input variables on wax deposition amount.

Table 1. Crude oil samples characterization information

Information	Minimum	Maximum
Wax deposition (Wt%)	0	13
Temperature (K)	230	313.15
Pressure (bar)	1	1
Specific gravity	0.872	0.963
Composition (mole%)		
C ₁ -C ₃	0.218	2.127
C ₄ -C ₇	3.057	30.952
C ₈ -C ₁₅	33.468	49.791
C ₁₆ -C ₂₂	16.029	57.335
C ₂₃ -C ₂₉	6.974	10
C ₃₀₊	8.177	13.23

CONCLUSION

In this study, we have developed a feed forward artificial neural network model optimized by particle swarm optimization algorithm (namely PSO-based ANN model) for estimating wax deposition amount in crude oil system. This model is based on 94 experimental data sets of 8 different crude oil samples. The model uses 9 input parameters (mole percentage of (C1- C3), mole percentage of (C4-C7), mole percentage of (C8- C15), mole percentage of (C16- C22), mole percentage of (C23- C29), mole percentage of (C30+), oil specific gravity, temperature, pressure) and wax deposition amount is regarded as its output. It has been shown that the model is more accurate in comparison with multi-solid thermodynamic model and GPNN model for estimation of wax deposition amount.

REFERENCES

- [1] Coto, B., et al.: "A new method for the determination of wax deposition from non-diluted crude oils by fractional deposition." *Fuel*, 87(10): p. 2090-2094, 2008.
- [2] Bhat, N.V. and A.K. Mehrotra: "Measurement and Prediction of the Phase Behavior of Wax-Solvent Mixtures: Significance of the Wax Dis appearance Temperature" *Industrial and engineering chemistry research*, 43(13): p. 3451-3461, 2004.
- [3] Dalirsefat, R.; Feyzi, F.: "A thermodynamic model for wax deposition phenomena." *Fuel*, 86, (10), 1402-1408, 2007.
- [4] Zuo, J. Y.; Zhang, D. D.; Ng, H.-J.: "An improved thermodynamic model for wax deposition from petroleum fluids", *Chemical engineering science* 56, (24), 6941-6947, 2001.
- [5] Khaksar Manshad, A.; Ashoori, S.; Khaksar Manshad, M.; Omidvar, P.: "The Prediction of Wax Deposition by Neural Network and Genetic Algorithm and Comparison with a Multisolid Model in Crude Oil Systems", *Petroleum Science and Technology* 30, (13), 1369-1378, 2012.
- [6] Ekeh, M.K., S.A.-S. Hikmat, and S. Ahmmed, "Prediction of Wax Deposition Problems of Hydrocarbon Production System." *Journal of Petroleum Science and Engineering*, 2012.
- [7] Zhu, T., J.A. Walker, and J. Liang, "Evaluation of Wax Deposition and Its Control During Production of Alaska North Slope Oils." University of Alaska, 2008.
- [8] Sadeghazad, A. and R. Chrisriansen, "The effect of cloud point temperature on wax deposition" *SPE Paper*, 49467, 1998.
- [9] Hsu, J., M. Santamaria, and J. Brubaker.: "Wax deposition of waxy live crudes under turbulent flow conditions" in *SPE Annual Technical Conference and Exhibition*. 1994.
- [10] Jessen, F. and J. N. Howell, "Effect of flow rate on paraffin accumulation in plastic, steel, and coated pipe." *Pet. Trans. AIME*, 213: p. 80-84. 1958.
- [11] Tronov, V., "Effect of Flowrate and other Factors on the Formation of Paraffin Deposits." *Trans. Tator. Neft. Nauch-Issled Inst.*, 13: p. 207-30, 1969.
- [12] Haq, M. A., "Deposition of Paraffin Wax from Its Solutions with Hydrocarbons." SPE Paper, 1981. 10541-MS , Unpublished but included in SPE e-library with Permission of and Transfer of Copyright from the Author.
- [13] Jessen, F. and J. N. Howell, "Effect of flow rate on paraffin accumulation in plastic, steel, and coated pipe." *Pet. Trans. AIME*, 213: p. 80-84, 1958.
- [14] Jorda, R., "Paraffin deposition and prevention in oil wells." *Journal of Petroleum Technology*, 18(12): p. 1605-1612, 1966.
- [15] Hunt JR, E., "Laboratory study of paraffin deposition." *Journal of Petroleum Technology*, 14(11): p. 1259-1269, 1962.
- [16] Singh, A., et al. "Dilution Strategies for Wax Management and Control for Deepwater Development from a Flow Assurance Perspective": Part I-Current Practice and Perspective. in *SPE Annual Technical Conference and Exhibition*. 2004.
- [17] Kai, L., et al., "Phase Behavior of Highly Waxy Gas Condensate Systems" *SPE Middle East Oil Show*, 2001.

-
- [18] Won, K., "Thermodynamic calculation of cloud point temperatures and wax phase compositions of refined hydrocarbon mixtures." *Fluid Phase Equilibria*, 53: p. 377-396, 1989.
- [19] Coutinho, J. A. and J.-L. Daridon, "Low-pressure modeling of wax formation in crude oils". *Energy and fuels*, 15(6): p. 1454-1460, 2001.
- [20] Lira- Galeana, C.; Firoozabadi, A.; Prausnitz, J. M., "Thermodynamics of wax, deposition in petroleum mixtures." *AIChE Journal*, 42 (1), 239-248, 1996.
- [21] Won, K., "Thermodynamics for solid solution-liquid-vapor equilibria: wax phase formation from heavy hydrocarbon mixtures", *Fluid Phase Equilibria*, 30: p. 265-279, 1986.
- [22] Burger, E.; Perkins, T.; Striegler, J., Studies of wax deposition in the trans Alaska pipeline. *Journal of Petroleum Technology* 33, (6), 1075-1086, 1981.
- [23] Valinejad, R., Solaimany Nazar, A. R., "An experimental design approach for investigating the effects of operating factors on the wax deposition in pipelines." *Fuel* 2012.
- [24] Ekeh, M. K.; Hikmat, S. A.-S.; Ahmmed, S., "Prediction of Wax Deposition Problems of Hydrocarbon Production System." *Journal of Petroleum Science and Engineering*, 2012.
- [25] Akbarzadeh, K.; Zougari, M., "Introduction to a novel approach for modeling wax deposition in fluid flows." 1. Taylor-Couette system. *Industrial and Engineering Chemistry Research* 47, (3), 953-963, 2008.
- [26] Manshad, A. K., M. K. Manshad, and S. Ashoori, "The Application of an Artificial Neural Network (ANN) and a Genetic Programming Neural Network (GPNN) for the Modeling of Experimental Data of Slim Tube Permeability Reduction by Asphaltene Deposition in Iranian Crude Oil Reservoirs." *Petroleum Science and Technology*, 30(23): p. 2450-2459, 2012.
- [27] Rajasekaran, S., VijayalakshmiPai, G. A., "Neural networks, fuzzy logic, and genetic algorithms synthesis and applications", Prentice-Hall, 2004.
- [28] Gharbi, R. "Estimating the isothermal compressibility coefficient of under saturated Middle East crudes using neural networks". *EnergyFuels*, 11, pp. 372-378, 1997.
- [29] Hornik K., Stinchcombe M., White H. "Multilayer feedforward networks are universal approximators" *Neural Networks*, pp359-66, 1989.
- [30] Brown M., Harris C. J. "*Neurofuzzy adaptive modelling and control*" 1994.
- [31] Sayyad, H., Khaksar Manshad, A., Rostami, H., "Application of hybrid neural particle swarm optimization algorithm for prediction of MMP" *Fuel*, pp 625-633, 2014.
- [32] Eberhart, R., Kennedy, J., "A new optimizer using particle swarm theory" IEEE1995 MHS'95, proceedings of the sixth international symposium on micro machine and human science, pp 39-43,1995.
- [33] Bertsimas, D., Nohadani, O., "Robust optimization with simulated annealing" *J. Global Optim.*, pp323-34, 2010.
- [34] Goldberg, D. E., "Genetic algorithms in search, optimization, and machine learning" 1989.
- [35] Kennedy, J., Eberhart, R., "Particle swarm optimization" Proceedings of the IEEE international conference on neural networks, vol 4, pp 1942-1948, 2002.

-
- [36] Liu D., Hou Z-G. In: Advances in neural networks-ISNN 2007: 4th international symposium on neural networks, ISNN 2007 Nanjing, China, June 3–7, Proceedings, Springer-Verlag, New York incorporated, 2007.
- [37] Eberhart R., Simpson P., Dobbins R. “*Computational intelligence PC tools*” Academic Press Professional, Inc, 1996.

Chapter 8

**EFFICIENT ESTIMATION OF WELL
TESTING PARAMETERS FOR NATURALLY
FRACTURED OIL RESERVOIRS:
APPLICATION IN RESERVOIR CHARACTERIZATION**

***Abbas Khaksar Manshad¹, Habib Rostami²,
Seyed-Moein Hosseini³ and Amir H Mohammadi^{4,5,6,*}***

¹Department of Petroleum Engineering,
Abadan Faculty of Petroleum Engineering,

Petroleum University of Technology (PUT), Abadan, Iran

²Department of Computer Engineering,
School of Engineering, Persian Gulf University, Bushehr, Iran

³Department of Petroleum Engineering,
Ahwaz Faculty of Petroleum Engineering,

Petroleum University of Technology (PUT), Ahwaz, Iran

⁴Discipline of Chemical Engineering, School of Engineering,
University of KwaZulu-Natal, Howard College Campus, King George V Avenue,
Durban, South Africa

⁵Département de Génie des Mines, de la Métallurgie et des Matériaux,
Faculté des Sciences et de Génie, Université Laval, Québec, Canada

⁶Institut de Recherche en Génie Chimique et Pétrolier (IRGCP), Paris Cedex, France

ABSTRACT

Many diverse methods are available to calculate reservoir or well related parameters for the purpose of reservoir characterization and management amongst of which ANNs have shown to be very promising. In this study, three different ANN models including MLP, MLP optimized with GA and MLP optimized with PSO have been developed to predict permeability, skin factor and reservoir initial pressure. Comparison of each model

* Corresponding Author E-mail: a.h.m@irgcp.fr and amir_h_mohammadi@yahoo.com.

with Horner method based on correlation coefficient (R) or mean square error (MSE) suggests MLP-PSO algorithm is more robust and efficient. Estimated aforementioned parameters based on MLP-PSO model are then compared with those evaluated based on Horner method. Acceptable error values illustrate that MLP-PSO can be used in the absence of enough buildup well testing data which is less costly and time consuming.

Keywords: well testing, reservoir characterization, permeability, initial reservoir pressure, skin factor

NOMENCLATURE

R	Correlation coefficient
MSE	Mean square error
ANNs	artificial neural networks
GA	Genetic Algorithm
PSO	Particle Swarm Optimization
K	Permeability, md
ϕ	Porosity, fraction
μ	Viscosity, cp
Δt	Shut-in pressure, hr
t_p	Producing time, hr
P^*	False pressure, psi
r_w	Well bore radius, ft
c_t	Total compressibility, psi^{-1}
h	Formation thickness, ft
B_o	Formation volume factor, RB/STB
q	Flow rate, STB/D
m	Slope of Linear Portion of Horner plot, Psi/Cycle

INTRODUCTION

One of the most challenging subjects in petroleum industry management is reservoir characterization owing to the fact that there may exist many restricted and unreliable data. The primary objectives of reservoir characterization are reservoir modeling and simulation, enhanced oil recovery techniques, predicting different reservoir scenarios and determination of remaining recoverable oil while the latter is the most significant one. Amongst the usual methods that reservoir characterization utilizes to obtain many different data are well logging, well testing, geology, core analysis, seismic and geostatistics by which four different overall components are specified including drive mechanism, architecture (such as permeability and porosity), fluid type and dominant flow direction [1-3].

Well testing is an interpretation technique during which pressure of a well is recorded with respect to time to estimate some reservoir and well parameters such as permeability, skin

effect, reservoir initial pressure and reservoir boundaries which are essential to reservoir characterization and management [4]. The most frequent approaches in well testing technique used in petroleum industry are draw-down and build-up tests. In a build-up test, downhole pressure increasingly tends to the reservoir average pressure for a certain shut-in period of well, whereas in a simplest form of a draw-down test in which flow rate is kept constant, the well is allowed to flow and the pressure falls [5-7].

Application of pressure build-up well tests was first introduced in 1937 by Muskat in which the pressure behavior with time was utilized by extrapolation technique to estimate initial reservoir pressure, however due to excluding fluid compressibility impacts, this method did not give appropriate answers [8]. Later on, effects of fluid compressibility was incorporated in well testing by Miller et al. in 1950 to predict permeability and reservoir pressure from build-up test data [9]. The first analytical equation for build-up tests investigation was proposed by Horner for completed wells in under saturated reservoirs. Having divided the pressure behavior into three main time regions namely, early time, middle time and late time regions, a graphical method was proposed by Horner which used only the middle time region and put the other two regions aside. In the middle time region (which begins 1.5 log cycles after the end of early time region), the semi log plot of (P_{ws}) versus ($\frac{t_p + \Delta t}{\Delta t}$) gives a straight line, where t_p , Δt and p_{ws} are producing time, shut-in period time and wellbore shut-in pressure [10]. The slope and the intercept of the line with the pressure axis are used to calculate the permeability and the skin effect.

Many diverse techniques have been utilized effectively by several petroleum engineers to work out petroleum complications including MRI, Micro-wave and ANNs (Artificial Neural Networks) [11, 12]. One of the modern approaches which incorporates input/output data in a parametric modeling way as opposed to systematic methods is to use ANNs [11, 13]. Different applications of ANNs in distinctive areas of oil and gas engineering includes well testing, well logging, PVT properties of crude oils, seismic interpretation and EOR processes [12-16]. As an example, an artificial intelligence network optimized by particle swarm optimization (PSO) has been recently developed which predicts asphaltene precipitation as a function of temperature, pressure, solvent molecular weight, oil composition, solvent mole percent, oil specific gravity, and asphaltene content. The developed model is more accurate in comparison with previous models [17].

Application of ANNs in well testing analysis involves data saving, noise filtering, optimization problems and estimation of sampled functions in which no analytical solution can be applied. In other words, these petroleum engineering problems for which conventional older methods did not have any adequate answer for can now be solved by ANNs [12]. Earliest incorporation of ANNs in well testing interpretation dates back to 1990 when model step of well-test interpretation was identified to determine reservoir model and its parameters by Artificial Intelligence based on the pressure-derivative data [18]. Al-Kaabi and Lee (1990) presented an Artificial Neural Network approach for recognition of well-test interpretation model adopted from derivative plot. In their model, existing of systematic noise in data resulted in poor results, however it was tolerable with random noise [19]. Allian and Houze (1992) implemented a practical AI (Artificial Intelligence) module coupled with a symbolic approach for identification of well testing models and estimation of its parameters by use of pressure data [20]. Later, Guyaguler et al. (2001) demonstrated a regression method along with Genetic Algorithm (GA) wherein inaccurate selection of reservoir model was reduced

which led to be robust and effective in noisy pressure transient tests [21]. Jeirani and Mohebbi (2006) recommended a model based on Artificial Neural Network to calculate reservoir parameters such as permeability, initial pressure and skin factor of reservoirs. Their method was cost-effective and was claimed to be applicable for a wide range of reservoirs [11]. Vaferi et al. (2011) suggested an automatic approach in line with Artificial Neural Network in order to recognize reservoir model from drawdown data applicable to both single and double porosity under different late time conditions. Utilizing MLP (feed-forward multi-layer perceptron) structure, real reservoir models were successfully detected based on noisy pressure derivative data [22]. Ghaffarian et al. (2014) worked out model identification of different types of gas condensate reservoirs including different boundary conditions based on two MLP structures incorporating buildup tests data [23].

As mentioned earlier, knowing permeability, skin factor and pressure of reservoirs are of utmost significance for petroleum engineers owing to the fact that they are vitally needed for conducting pressure maintenance programs, well efficiency determination, effects of formation damage on hydrocarbon production, different EOR processes and reserves estimation [23]. Buildup tests are expensive for petroleum companies since it requires the wells to be shut in for a certain period of time and therefore leads to production loss. As an example, carrying out buildup tests for reservoir characterization in Alaska by BP company in 1991 resulted in \$1.3 loss [24].

In this work, an ANN-based methodology composed of MLP, MLP optimized with GA and PSO were developed and results are compared with each other as well as actual results from Horner model. The overall objective of this study is therefore to utilize newly developed efficient and cost-effective approach based on ANN to predict permeability, skin factor and initial pressure of single porosity reservoir without having enough buildup tests.

OVERVIEW OF ARTIFICIAL INTELLIGENCE

Overview of MLP Artificial Neural Networks

Artificial neural networks have proven to be promising techniques through the estimation of nonlinear complex functions and extracting the best correlation among the parameters in many different branches of science and engineering fields [17, 25-29]. ANN models can be best described as mathematical structures comprising many simple processing units called neurons which are capable of mapping an input space into an output space by regression method [30-32]. In the view of accomplishing these tasks, some particular algorithms are utilized to train neural networks via modifying input weights so that calculated output values approach actual outputs adequately [31]. This workaround is simply called an optimization process. Outline of an optimization process includes network training, testing the quality of the learned network and extending this network to new data. For this purpose, data sets are categorized into training, validating and testing types [17, 33].

Many approaches have been suggested to design and optimize neural networks including multilayer perception (MLP) trained with back propagation algorithm [34, 35]. MLPs which are based on feed forward neural networks, involve three different types of vectors namely an input layer, at least one hidden layer and an output layer, each of which having a number of

neurons [36]. The number of neurons in output layer can be equal to the number of parameters required to be approximated and number of neurons in hidden layer may be specified according to a trial and error method during the learning process until the best solution is achieved [37, 38]. Since neurons of consecutive layers are connected to each other, a possible nonlinear relationship might exist between input and output layers. Training algorithms such as back propagation (BP) are normally utilized in MLPs so that a hidden correlation in the form of nonlinear function between several inputs and output are appropriately calculated. The mechanism under which BP algorithm works is error-correction which means weights are modified only when the error has already propagated backward, however, several issues have been reported associated with this algorithm including inefficiency and slow convergence. Therefore, a number of modifications such as Marguardt-Levenberg which is a combination of Gauss-Newton nonlinear regression and gradient descent methods have been suggested to overcome such aforementioned problems [39-41].

As part of this study, MLP ANN coupled with back propagation and Marguardt-Levenberg learning algorithms have been utilized in which network weights are adjusted in order to increase the rate of performance function reduction which is inverse of distribution of errors [42-44].

Overview of Genetic Algorithm (GA)

GAs are computational models which have been first proposed by Holland, and are based on Darwinian evolutionary theory, applicable to optimize complex functions. The basic evolution processes found in nature such as crossover, mutation, reproduction and survival of the fittest are the primary properties of GA algorithm behavior [40, 45].

In this algorithm, individual solutions are selected based on stochastic process with the aim of better overall performance. A fitness function is then used to evaluate each solution after which developed solutions will be estimated. Therefore, the search space will evolve in the direction in which the optimal solution is reached [46]. Genetic Operators which are based on probabilistic rules are utilized in order to adjust the genetic information until a new set of individual solutions (also referred to as population) is formed. This process continues until a final population is reached based on a stopping criteria, hence making it an iterative process [45].

Overview of PSO

PSO was first proposed by Eberhart and Kennedy as a population-based stochastic optimization process in which the overall objective is to find the global optimum of some multidimensional nonlinear functions [17, 47, 48]. This algorithm has been applied in various aspects of petroleum engineering and has been reported to be effective [33, 48-52].

The global optimum of a system is converged due to randomly distribution of different particles over the search space. For this goal of converging, two parameters of gBest and pBest were introduced by Eberhart and Kennedy which mean the best solution gained by global optimization and a best solution obtained by a particle respectively [17].

Assume “k” number of particles is used in this algorithm wherein k_{th} particle position is shown by the vector $X_k = \{X_{k1}, X_{k2}, X_{k3}, \dots, X_{kN}\}$. j_{th} coordinate value in the N dimensional space is shown by X_{kj} . The best visited position of the k_{th} particles and the best result of all existing particles are noted by vectors $P_k = \{P_{k1}, P_{k2}, \dots, P_{kN}\}$ and $G = \{G_1, G_2, \dots, G_N\}$, respectively. At every iteration, each particle changes its position according to its apparent velocity, $V_p = \{V_{p1}, V_{p2}, \dots, V_{pN}\}$ and the new position is obtained based on the following equation;

$$v_{NK}^{i+1} = \omega v_{NK}^i + A_1 rand(0,1)(P_{NK} - X_{NK}) + A_2 rand(0,1)(G_N - X_{NK}) \quad (1)$$

wherein ω is the inertia factor which controls and updates the new velocity based on the former velocity values. For the goal of particles acceleration toward the best coordination existing in the search space, positive learning factors including A_1 and A_2 have been introduced to the above equation. Rand (0,1) is a function which generates random numbers between 0 and 1 in the search space.

Mostly, as the iteration number increases, the inertia factor decreases which is mathematically represented as follows:

$$\omega_i = \omega_{max} - \left(\frac{\omega_{max} - \omega_{min}}{i_{max}} \right) * i \quad (2)$$

In which ω_{max} , ω_{min} , i and i_{max} are the maximum value of inertia factor, minimum value of inertia factor, current and maximum number of iterations used in the PSO, respectively. Empirical investigations suggest the appropriate values of 0.4 and 0.9 for ω_{min} and ω_{max} , respectively [17].

Case Study

This study was done on three different wells in a southern Iranian naturally fractured carbonate oil field. Three wells in the same reservoir and adequately spaced from each other were selected; other wells were very distant apart and were neglected for this study. Table 1 shows wells and reservoir parameters used in this study. The shut-in time and the cumulative production time were sorted as $\frac{t_p + \Delta p}{\Delta p}$ and used as the ANN input, and the shut-in pressures

(P_{ws}) corresponding to shut-in times were used as the output of the network. Figure 1 shows the Horner plot of the three wells for which the ANN has been run on.

Data Analysis

93, 85 and 95 build-up data sets were available with respect to the three wells. The data were normalized between 0 and 1 first, 70% of the data were used for learning, 15% for validation and 15% for testing. There was no noise in the pressure-time data for the three wells and therefore they had the required quality to be used in the ANN, with $\left(\frac{P - P_{ws}}{\Delta t}\right)$ as the input and P_{ws} as the output. Figure 2 shows the fitness functions for the three data sets presented in Figure 1. MLP was optimized by GA and PSO in order to minimize the errors. Figures 3 and 4 show the results of the network learning in which a good agreement exists with the pressure build-up data. The results of the best GA and PSO tests are shown in Figures 5 and 6.

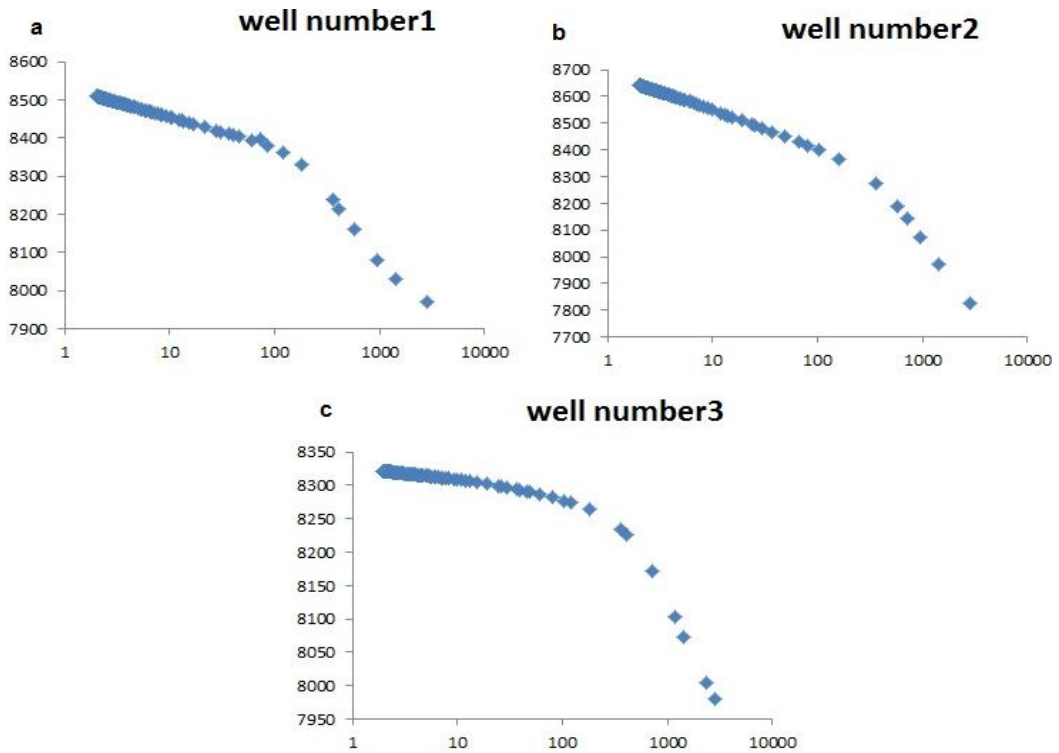


Figure 1. Horner plot of the data of the well 1 (a), well 2 (b), well 3 (c).

Table 1. Well and reservoir parameters

Well 3 Test	Well 2 Test	Well1 Test	Parameter
13	16.3	12	Matrix porosity (%)
2.94	2.136	3	(Well bore) in Radius
87	81.6	89	Average oil saturation (%)
128	137	327	(h net) Reservoir thickness
1.69	1.827	1.61	Oil formation volume factor (Bo)
0.312	0.32	0.22	Oil viscosity (cp)
1.362E-5	1.54E-5	1.362E-5	Oil compressibility Co (1/psi)

1.681E-5	1.567E-5	2.1579E-5	Total compressibility Ct (1/ psi)
----------	----------	-----------	-----------------------------------

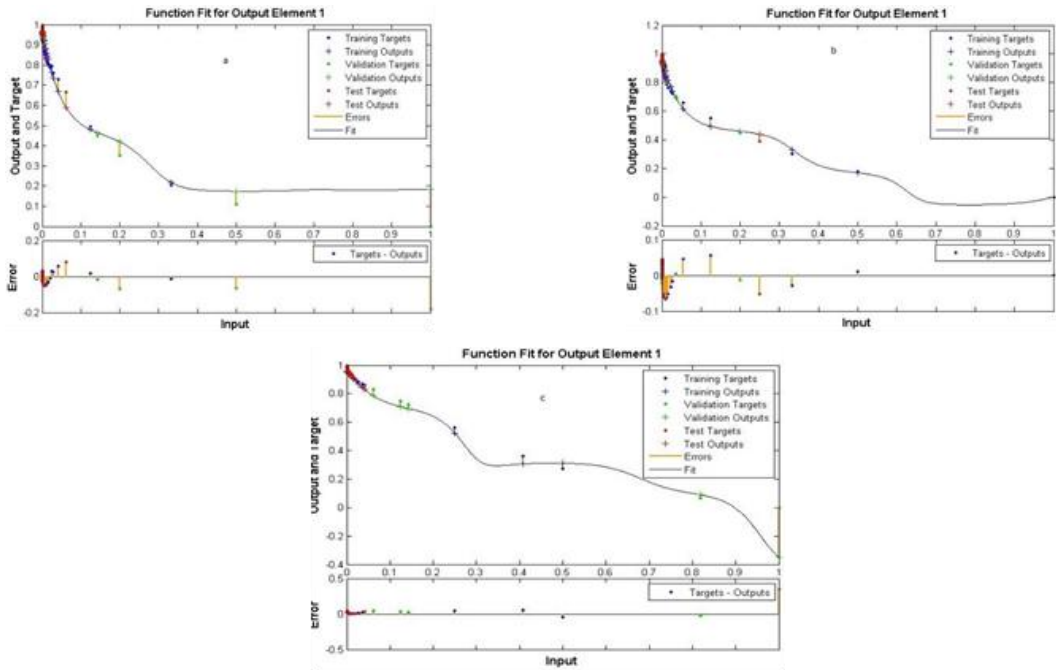


Figure 2. Fitness functions (input and output for learning, validation and test), with normalized MLP for (a) well 1, (b) well 2 and (c) well 3.

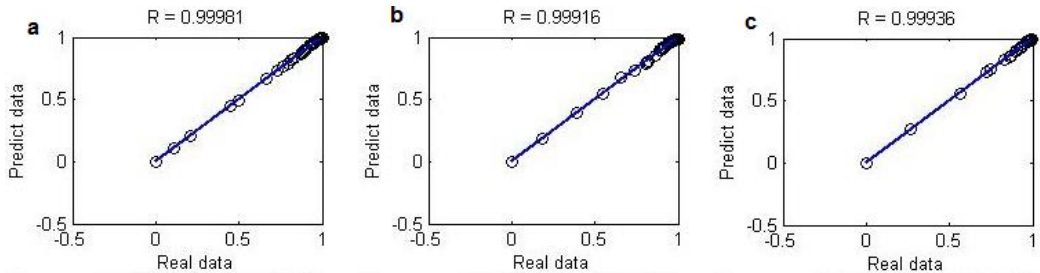


Figure 3. Results of learning, MLP optimized with GA for (a) well 1, (b) well 2 and (c) well 3.

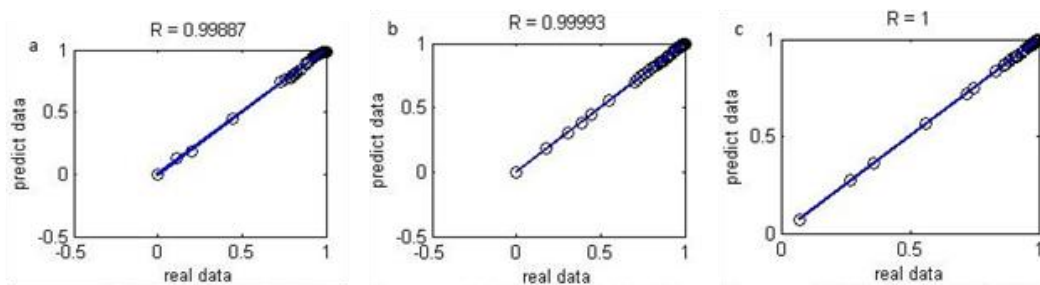


Figure 4. Results of learning, MLP optimized with PSO for (a) well 1, (b) well 2 and (c) well 3.

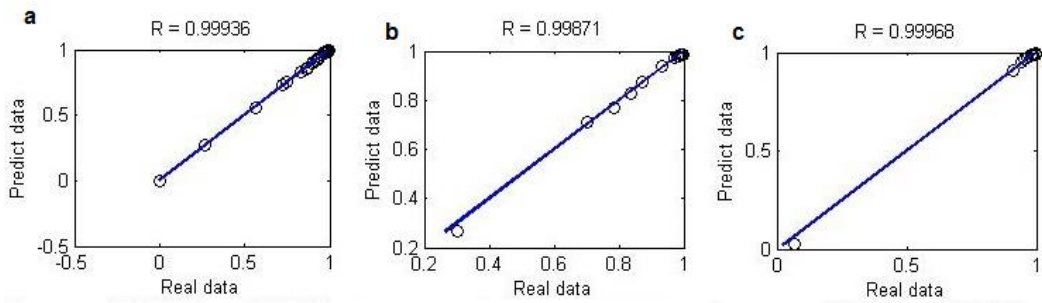


Figure 5. Results of testing the MLP optimized with GA for (a) well 1, (b) well 2 and (c) well 3.

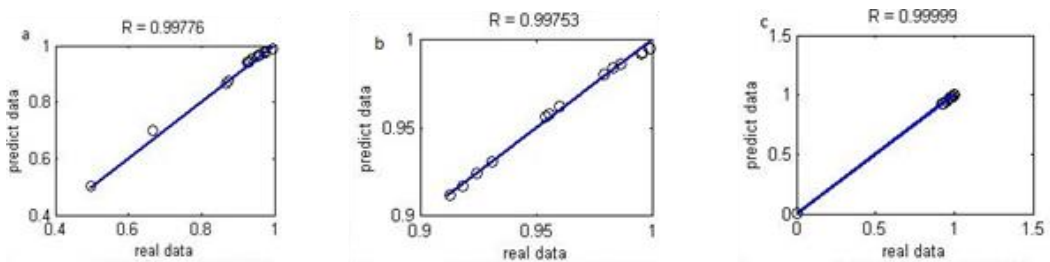


Figure 6. Results of testing the MLP optimized with PSO for (a) well 1, (b) well 2 and (c) well 3.

Methodology

Utilizing error back propagation algorithm, Horner time $\frac{t_p + \Delta p}{\Delta p}$ was used as the input to the ANN and the downhole shut-in pressure (P_{ws}) as the output. A two-layer hidden layer was used, which showed better results in comparison with single-layer and three-layer ones. Nevertheless, applying more than three layers decreases the performance of the network since in this case the networks tends to save he data. The program code was written in two files in order to analyze the learning process. The stages and methods of developing the ANNs include the following;

- a) Evaluating the effect of the input parameters as the first step in developing an efficient artificial intelligence. For instance, over-introducing data into the network caused an over-size of the network, and hence, decreased the rate of learning. To specify suitable input parameters, networks of different input configurations were tried and the input parameters with the most effect on the results were selected.
- b) In order to accelerate the learning process and assure that every parameter receives equal consideration from the network to improve the overall performance of the network, the data were preprocessed prior to introduction into the network. The input parameters had high values which decreased the recognition rate of the network, therefore the data were normalized between 0 and 1 using Equation 3 to cope with this problem.

$$X_n = \frac{X - X_{\min}}{X_{\max} - X_{\min}} \quad (3)$$

where X is the one dimensional data vector and X_n is he normalized value of X .

- c) Data categorization: 70% of the data were used as learning data, 15% as validation and 15% as network test data.
- d) Network structure design: the number of neurons in the input and output layers equals to the number of input and output data, respectively and the number of neurons in the intermediate layer was obtained by trial and error.
- e) Learning process: in three methods, the learning data were used to prevent the preprocessing problems, the number of cycles was unknown before execution, and the learning algorithm stopped as soon as the errors exceeded the limits.
- f) Validation: These sets of data were introduced after learning (MLP) and the results were compared with the actual data, consistency of these was used as a criterion of universalization. The network validity was verified in parallel with learning and as soon as the error on validation data rose, learning was stopped. Furthermore, if the mean square error reaches the determined value learning will again stop.
- g) Test: This step is specific to back propagation networks. In these networks, this error was controlled after each cycle by the test data in order to stop learning in case of error growth and to prevent the network from saving the learning data.

In this study, MLP ANNs and MLP optimized with GA and MLP optimized with PSO were used and the results were compared with each other using two indices; correlation coefficient (R , it should be mentioned that in some references it is shown as R^2) and mean square error (MSE) defined as follows [53-55]:

- a) Correlation coefficient is a dimensionless value ranging between 0 and 1, and is calculated through either of the following equations;

$$R = \frac{\sum_{n=1}^n \left[\left(E_n - \left(\sum_{n=1}^n E_n \right) / n \right) \left(R_n - \left(\sum_{n=1}^n R_n \right) / n \right) \right]}{\sqrt{\sum_{n=1}^n \left(E_n - \left(\sum_{n=1}^n E_n \right) / n \right)^2 \sum_{n=1}^n \left(R_n - \left(\sum_{n=1}^n R_n \right) / n \right)^2}} \quad (4)$$

$$R^2 = \frac{\sum_{n=1}^n \left[\left(E_n - \left(\sum_{n=1}^n R_n \right) / n \right) \right]^2}{\sum_{n=1}^n \left[\left(R_n - \left(\sum_{n=1}^n R_n \right) / n \right) \right]^2} \quad (5)$$

- b) The following equation represents MSE;

$$\varepsilon(n) = MSE = \frac{\sum_{n=1}^n (E_n - R_n)^2}{n} \quad (6)$$

where R_n is the actual observed value, E_n is the calculated value; n is the number of data to learn the network. The weights have to be varied to decrease the MSE or increase the R to reach the best fitness.

Table 2. Comparison of the best results for R and MSE using MLP and MLP optimized with GA and PSO in well 1

MLP optimized with PSO	MLP optimized with GA	MLP	Parameter
0.99837	0.99969	0.98432	Total R
0.00011245	2.1206E-5	0.001253	Total MSE
0.99887	0.99981	0.97541	Learning R
8.7187E-5	1.6138E-5	0.0076541	Learning MSE
0.99874	0.99971	0.99433	Validation R
0.00017974	4.0027E-5	0.0036888	Validation MSE
0.99776	0.99810	0.94405	Test R
0.00016242	2.5919E-5	0.0010808	Test MSE

Table 3. Comparison of the best results for R and MSE using MLP and MLP optimized with GA and PSO in well 2

MLP optimized with PSO	MLP optimized with GA	MLP	Parameter
0.99991	0.99887	0.98345	Total R
5.8971E-6	7.8534E-5	0.0011778	Total MSE
0.99993	0.99916	0.98533	Learning R
6.2575E-6	6.0757E-5	0.0011808	Learning MSE
0.99964	0.99899	0.98028	Validation R
5.5276E-6	5.3763E-5	0.00089797	Validation MSE
0.99753	0.99871	0.98126	Test R
4.63067E-6	0.00018399	0.0014442	Test MSE

Table 4. Comparison of the best results for R and MSE using MLP and MLP optimized with GA and PSO in well 3

MLP optimized with PSO	MLP optimized with GA	MLP	Parameter
0.99999	0.99916	0.98429	Total R
4.0444E-7	5.6924E-5	0.0021753	Total MSE
1.00000	0.99936	0.99449	Learning R
1.6975E-8	3.2802E-5	0.00094923	Learning MSE
0.99996	0.99923	0.98279	Validation R
2.2425E-5	4.0293E-5	0.0095191	Validation MSE
0.99999	0.99968	0.94922	Test R
2.6406E-6	0.00018899	0.00069919	Test MSE

Table 5. Comparison of actual Pi's by Horner and MLP-PSO models

Error %	Actual Horner Pi (psi)	ANN Pi (psi)	Well
0.18	8539.7	8524.40	Well 1
0.22	8690.5	8671.56	Well 2
-0.30	8328.3	8353.46	Well 3

Table 6. Comparison of Horner line slope (m) by actual and MLP-PSO models

Error %	Actual Horner Slope	ANN Horner Slope	Well
0.03	77.892	77.8654	Well 1
0.00	138.196	138.192	Well 2
-0.13	20.9041	20.931	Well 3

Table 7. Comparison of permeability's from Horner model by actual data and MLP-PSO results

Error %	Actual data Horner Permeability (k) (md)	ANN results Horner permeability (k) (md)	Well
-0.05	43.75	43.77	Well 1
-0.06	15.56	15.57	Well 2
0.12	165.8	165.6	Well 3

Correlation coefficient (R) and MSE were used to compare Horner method results and ANN results. R ranges between 0 and 1, whose best value is 1 and MSE best value is 0. The values of R and MSE obtained with MLP optimized by GA and PSO are listed in Tables 2 -4.

Horner model was used for estimating the initial pressure (Pi), permeability (K) and skin effect (s), that is for both actual and ANN, a straight line was passed through the data falling 1.5 cycles after the wellbore storage(early time) region on the semi-log plot of P_{ws} versus Horner time and this line was extended to intersect the P_{ws} axis, the intercept will be the Pi [18]. Table 5 shows a comparison of the actual initial pressures and those obtained from ANN.

Having obtained the slope of the line (m) in both actual Horner model and ANN model (Table 6), permeabilities were calculated by Equation 7, using the data provided in Table 1, the comparison of the results is shown in Table 7.

$$K = \frac{162.6q\mu B_o}{mh} \quad (7)$$

Skin factors were calculated by Equation 8 for both ANN models and Horner model again using the data from Table 1;

$$S = 1.1513 \left[\frac{P_{(\Delta t=0)} - P^*}{m} - \log\left(\frac{kt_p}{\phi\mu c_r r_w^2}\right) + 3.23 \right] \quad (8)$$

Table 8. Skin effects by Horner model for actual data and MLP-PSO

Error %	Skin factor by Actual data Horner model	Skin factor by ANN	Well
4.82	13.67	13.01	Well 1
4.67	11.644	11.10	Well 2
2.56	24.64	24.01	Well 3

In which P^* is obtained from the following equation.

$$P^* = P_{ws} - m \log\left(\frac{t_p + \Delta t}{\Delta t}\right) \quad (9)$$

RESULTS AND DISCUSSION

MLP, MLP optimized with GA and MLP optimized with PSO models have been separately developed using three different sets of pressure buildup tests for which Horner plots are represented in Figure 1. Figures 3-4 show the results of the network learning and according to fitness functions in Figure 2, there is a good agreement between actual pressure data and those obtained by ANN models which means presenting a good fitness with the pressure build-up data; hence, it can be concluded that the networks have been well learned enough to be used to estimate the initial pressure, permeability and the skin factor in a reservoir. The results of the best GA and PSO tests are shown in Figures 5-6.

Three different ANN models have been compared based on two indices namely R and MSE for all three wells, as mentioned earlier. Results of Table 2 suggest MLP optimized by GA is more accurate than two other developed ANNs for well number 1 owing to the fact it has a more acceptable R or MSE values. Nevertheless, MLP optimized with PSO is slightly different from MLP with GA in this well. For well numbers two and three, however, MLP optimized with PSO gives more adequate results compared to other ANNs based on values of R or MSE displayed in Tables 3-4. It can be seen that MLP optimized with PSO can be more effective compared to MLP and MLP optimized with GA.

Due to high performance of MLP optimized with PSO, its computed parameters of initial pressure, Horner line slope, permeability and skin factor have been judged against those of Horner model for all wells and results along with their error values are presented in Tables 5-8. Because of adequate error values, only a limited set of data by pressure buildup tests can be incorporated with MLP-PSO to extend more data needed to achieve reservoir well testing parameters which will lead to a less time and cost consuming tool.

CONCLUSION

In this study, ANN-based models of MLP, MLP-GA and MLP-PSO have been developed to predict reservoir well testing parameters including initial reservoir pressure, permeability and skin factor. Based on the obtained results for the case study, MLP-PSO algorithm is more efficient than the two other models. Buildup tests technique of well testing parameter calculation is both time consuming and costly; therefore, in the absence of sufficient buildup test data, MLP-PSO algorithm can be utilized to accurately estimate reservoir parameters which accelerates the calculation and reduces time and operating costs simultaneously.

REFERENCES

- [1] Mohaghegh, S., et al., Petroleum reservoir characterization with the aid of artificial neural networks. *Journal of Petroleum Science and Engineering*, 1996. 16(4): p. 263-274.
- [2] Baker, R. O., H. W. Yarranton, and J. Jensen, Practical Reservoir Engineering and Characterization. 2015: Elsevier Science.
- [3] Landa, J., et al. Reservoir Characterization Constrained to Well Test Data: A Field Example. in SPE Annual Technical Conference and Exhibition. 1996. Society of Petroleum Engineers.
- [4] Athichanagorn, S. and R. N. Horne. Automatic parameter estimation from well test data using artificial neural network. in *SPE Annual Technical Conference and Exhibition*. 1995. Society of Petroleum Engineers.
- [5] Lee, J., J. B. Rollins, and J. P. Spivey, Pressure transient testing. Vol. 9. 2003: Henry L. Doherty Memorial Fund of Aime Society of Petroleum.
- [6] Chaudhry, A., Oil well testing handbook. 2004: Elsevier.
- [7] Lee, J., Well testing. 1982: New York: Society of Petroleum Engineers.
- [8] Muskat, M., Use of Data Oil the Build-up of Bottom-hole Pressures. *Transactions of the AIME*, 1937. 123(01): p. 44-48.
- [9] Miller, C., A. B. Dyes, and C. Hutchinson Jr, The estimation of permeability and reservoir pressure from bottom hole pressure build-up characteristics. *Journal of Petroleum Technology*, 1950. 2(04): p. 91-104.
- [10] Horner, D. Pressure build-up in wells. in 3rd World Petroleum Congress. 1951. World Petroleum Congress.
- [11] Jeirani, Z. and A. Mohebbi, Estimating the initial pressure, permeability and skin factor of oil reservoirs using artificial neural networks. *Journal of petroleum science and engineering*, 2006. 50(1): p. 11-20.
- [12] Mohaghegh, S. and S. Ameri, Artificial neural network as a valuable tool for petroleum engineers. *Paper SPE*, 1995. 29220.
- [13] Adibifard, M., S. Tabatabaei-Nejad, and E. Khodapanah, Artificial Neural Network (ANN) to estimate reservoir parameters in Naturally Fractured Reservoirs using well test data. *Journal of Petroleum Science and Engineering*, 2014. 122: p. 585-594.
- [14] Rafiee-Taghanaki, S., et al. Implementation of SVM framework to estimate PVT properties of reservoir oil. *Fluid Phase Equilibria*, 2013. 346: p. 25-32.

-
- [15] Talebi, R., et al. Application of soft computing approaches for modeling saturation pressure of reservoir oils. *Journal of Natural Gas Science and Engineering*, 2014. 20: p. 8-15.
- [16] Ibatullin, R., et al. Application and method based on artificial intelligence for selection of structures and screening of technologies for enhanced oil recovery. in *SPE/DOE Improved Oil Recovery Symposium*. 2002. Society of Petroleum Engineers.
- [17] Manshad, A. K., et al. Application of Artificial Neural Network-Particle Swarm Optimization Algorithm for Prediction of Asphaltene Precipitation During Gas Injection Process and Comparison With Gaussian Process Algorithm. *Journal of Energy Resources Technology*, 2015. 137(6): p. 062904.
- [18] Allain, O. F. and R. N. Horne, Use of artificial intelligence in well-test interpretation. *Journal of Petroleum Technology*, 1990. 42(03): p. 342-349.
- [19] Al-Kaabi, A. and W. J. Lee, Using Artificial Neural Networks To Identify the Well Test Interpretation Model (includes associated papers 28151 and 28165). *SPE formation evaluation*, 1993. 8(03): p. 233-240.
- [20] Allain, O. and O. Houze. A practical artificial intelligence application in well test interpretation. in *European Petroleum Computer Conference*. 1992. Society of Petroleum Engineers.
- [21] Guyaguler, B., R. N. Horne, and E. Tazuin. Automated reservoir model selection in Well Test Interpretation. in *SPE Annual Technical Conference and Exhibition*. 2001. Society of Petroleum Engineers.
- [22] Vaferi, B., R. Eslamloueyan, and S. Ayatollahi, Automatic recognition of oil reservoir models from well testing data by using multi-layer perceptron networks. *Journal of Petroleum Science and Engineering*, 2011. 77(3): p. 254-262.
- [23] Ghaffarian, N., R. Eslamloueyan, and B. Vaferi, Model identification for gas condensate reservoirs by using ANN method based on well test data. *Journal of Petroleum Science and Engineering*, 2014. 123: p. 20-29.
- [24] Ahmed, U. Use of Transient Rate and Pressure Data To Determine Drainage Area Average Reservoir Pressure Without Shutting In the Well. in *European Production Operations Conference and Exhibition*. 1994. Society of Petroleum Engineers.
- [25] Manshad, A. K., M. K. Manshad, and S. Ashoori, The Application of an Artificial Neural Network (ANN) and a Genetic Programming Neural Network (GPNN) for the Modeling of Experimental Data of Slim Tube Permeability Reduction by Asphaltene Precipitation in Iranian Crude Oil Reservoirs. *Petroleum Science and Technology*, 2012. 30(23): p. 2450-2459.
- [26] Shokrollahi, A., et al. Intelligent model for prediction of CO₂ – reservoir oil minimum miscibility pressure. *Fuel*, 2013. 112: p. 375-384.
- [27] Chapoy, A., A. H. Mohammadi, and D. Richon, Predicting the hydrate stability zones of natural gases using artificial neural networks. *Oil and Gas Science and Technology- Revue de l'IFP*, 2007. 62(5): p. 701-706.
- [28] Gharagheizi, F., et al. Solubility parameters of nonelectrolyte organic compounds: determination using quantitative structure–property relationship strategy. *Industrial and Engineering Chemistry Research*, 2011. 50(19): p. 11382-11395.
- [29] Yang, C.-H., et al. Novel generating protective single nucleotide polymorphism barcode for breast cancer using particle swarm optimization. *Cancer epidemiology*, 2009. 33(2): p. 147-154.

-
- [30] Priddy, K. L. and P. E. Keller, Artificial neural networks: an introduction. Vol. 68. 2005: SPIE Press.
- [31] Gharbi, R., Estimating the isothermal compressibility coefficient of undersaturated Middle East crudes using neural networks. *Energy and fuels*, 1997. 11(2): p. 372-378.
- [32] Hsu, K. I., H. V. Gupta, and S. Sorooshian, Artificial Neural Network Modeling of the Rainfall-Runoff Process. *Water resources research*, 1995. 31(10): p. 2517-2530.
- [33] Sayyad, H., A. K. Manshad, and H. Rostami, Application of hybrid neural particle swarm optimization algorithm for prediction of MMP. *Fuel*, 2014. 116: p. 625-633.
- [34] Hornik, K., M. Stinchcombe, and H. White, Multilayer feedforward networks are universal approximators. *Neural networks*, 1989. 2(5): p. 359-366.
- [35] Andrews, R., J. Diederich, and A. B. Tickle, Survey and critique of techniques for extracting rules from trained artificial neural networks. *Knowledge-based systems*, 1995. 8(6): p. 373-389.
- [36] Javadian, S., et al. Determining fault's type and accurate location in distribution systems with DG using MLP neural networks. in *Clean Electrical Power*, 2009 International Conference on. 2009. IEEE.
- [37] Jayawardena, A. and D. A. K. Fernando, Use of radial basis function type artificial neural networks for runoff simulation. *Computer-Aided Civil and Infrastructure Engineering*, 1998. 13(2): p. 91-99.
- [38] Osowski, S. and T. H. Linh, ECG beat recognition using fuzzy hybrid neural network. *Biomedical Engineering, IEEE Transactions on*, 2001. 48(11): p. 1265-1271.
- [39] Asadisaghandi, J. and P. Tahmasebi, Comparative evaluation of back-propagation neural network learning algorithms and empirical correlations for prediction of oil PVT properties in Iran oilfields. *Journal of Petroleum Science and Engineering*, 2011. 78(2): p. 464-475.
- [40] Ghiasi-Freez, J., A. Hatampour, and P. Parvasi, Application of Optimized Neural Network Models for Prediction of Nuclear Magnetic Resonance Parameters in Carbonate Reservoir Rocks. *International Journal of Intelligent Systems and Applications (IJISA)*, 2015. 7(6): p. 21.
- [41] Haykin, S. and R. Lippmann, Neural Networks, A Comprehensive Foundation. *International Journal of Neural Systems*, 1994. 5(4): p. 363-364.
- [42] Natarajan, S. and R. R. Rhinehart. Automated stopping criteria for neural network training. in American Control Conference, 1997. *Proceedings of the 1997. 1997. IEEE*.
- [43] Poggio, T. and F. Girosi, Regularization algorithms for learning that are equivalent to multilayer networks. *Science*, 1990. 247(4945): p. 978-982.
- [44] Graupe, D., *Principles of artificial neural networks*. Vol. 6. 2007: World Scientific.
- [45] Romero, C., et al. A modified genetic algorithm for reservoir characterisation. in International Oil and Gas Conference and Exhibition in China. 2000. Society of Petroleum Engineers.
- [46] Holland, J. H., *Adaptation in natural and artificial systems: an introductory analysis with applications to biology, control, and artificial intelligence*. 1992: MIT press.
- [47] Eberhart, R. C. and J. Kennedy. A new optimizer using particle swarm theory. in *Proceedings of the sixth international symposium on micro machine and human science*. 1995. New York, NY.

-
- [48] Onwunalu, J. E. and L. J. Durlofsky, Application of a particle swarm optimization algorithm for determining optimum well location and type. *Computational Geosciences*, 2010. 14(1): p. 183-198.
- [49] Gorjaei, R. G., et al. A novel PSO-LSSVM model for predicting liquid rate of two phase flow through wellhead chokes. *Journal of Natural Gas Science and Engineering*, 2015. 24: p. 228-237.
- [50] Kamari, A., A. H. Mohammadi, and A. Bahadori, On the determination of breakthrough time for water coning phenomenon in oil reservoirs.
- [51] Ghiasi, M. M., et al. Rigorous models to optimise stripping gas rate in natural gas dehydration units. *Fuel*, 2015. 140: p. 421-428.
- [52] Nasimi, R., M. Shahbazian, and R. Irani, A hybrid particle swarm optimization–neural network strategy for permeability estimation of the reservoir, in *SPEEDAM 2010*. 2010.
- [53] Kurt, H. and M. Kayfeci, Prediction of thermal conductivity of ethylene glycol–water solutions by using artificial neural networks. *Applied energy*, 2009. 86(10): p. 2244-2248.
- [54] Durairaj, M. and P. Thamilselvan, Applications of artificial neural network for IVF data analysis and prediction. *Journal of Engineering Computers and Applied Sciences*, 2013. 2(9): p. 11-15.
- [55] Esfe, M. H., et al. Applicability of artificial neural network and nonlinear regression to predict thermal conductivity modeling of Al₂O₃–water nanofluids using experimental data. *International Communications in Heat and Mass Transfer*, 2015. 66: p. 246-249.

Chapter 9

ON THE PREDICTION OF WELL PRODUCTIVITY INDEX FOR HORIZONTAL OIL WELLS

*Abbas Khaksar Manshad¹, Habib Rostami²
and Amir H. Mohammadi^{3,4,5,*}*

¹Department of Petroleum Engineering, Abadan Faculty of Petroleum Engineering,
Petroleum University of Technology (PUT), Abadan, Iran

²Department of Computer Engineering, School of Engineering,
Persian Gulf University, Bushehr, Iran

³Discipline of Chemical Engineering, School of Engineering, University of KwaZulu-
Natal, Howard College Campus, Durban, South Africa

⁴Département de Génie des Mines, de la Métallurgie et des Matériaux, Faculté
des Sciences et de Génie, Université Laval, Québec, Canada

⁵Institut de Recherche en Génie Chimique et Pétrolier (IRGCP), Paris Cedex, France

ABSTRACT

For development and evaluation of oil fields, having enough information about hydrocarbon reservoirs is necessary, in other words, set various parameters in the evaluation of reservoir rock and fluid are important in hydrocarbon reservoirs. Reservoir productivity index (PI) of wells can be considered as one of the most important parameters in determining the economic value of a reservoir. Productivity index of wells accompanying with certain reservoir parameters plays an important role in the evaluation of oil reserves. The main objective of this study was to utilize a non-linear model called artificial neural networks to predict reservoir parameters. Data for the various stages of learning and assessment networks were divided into three categories of training, validation, and testing. After the data processing network, 70% of them were placed for education, 15% for validation, and 15% for the MLP experiments. The results show that neural network with two hidden layer simulators does best in terms of simulation.

Keywords: well productivity index, well testing, permeability, porosity, data mining, model

* Corresponding Author E-mail: amir_h_mohammadi@yahoo.com and a.h.m@irgcp.fr.

1. INTRODUCTION

Well testing is one of the most important branches of reservoir engineering which can play an essential role in studying the parameters of a reservoir. Determination of productivity index (PI) of reservoir is one of the main purposes of petroleum engineering. Data obtained from flow and pressure unsteady tests nearly at *in situ* reservoir conditions can be used to determine the productivity index [1-7].

The most important point to be considered is increasing production with a minimal cost in the exploitation of the reservoirs and productivity index is an effective factor to decide on the economical drilling [8]. Therefore, understanding the related phenomena and measuring the variables affecting productivity index are necessary [9]. Productivity index, j , represents the relation between different variables, mathematically illustrated in equation (1):

$$j = \frac{q}{p - p_{wf}} = \frac{kh}{\alpha_r \beta_\mu (p_D + s)} \quad (1)$$

This correlation expresses what imperative and possible is for a production engineer. At first, p_D (dimensionless pressure, where $p_D = \ln \frac{r_e}{r_w}$) depends on physical model that organizes well flow regime. A particular reservoir with special parameters and physical qualifications, permeability k , reservoir thickness h that their data can be obtained from balance wells [9], [10] and contains a fluid with B (formation volume factor) and μ (viscosity), s (skin factor) which is the only variable that can be adjusted. A positive value of skin factor (s) that is caused by damage and reduction of permeability around the wellbore [11] can be eliminated and decreased though matrix stimulation. On the other hand, a negatively skin factor is achieved, when the permeability of the formation, k , is less than that of around the well, k_{skin} , and it can be imposed by an effective hydraulic fracturing [10]. Therefore, productivity index can be improved by stimulation [9]. The skin factor is defined as;

$$s = \left[\frac{k}{k_{skin}} - 1 \right] \ln \left(\frac{r_{skin}}{r_w} \right) \quad (2)$$

where k = permeability of the formation, md. k_{skin} = permeability of the skin zone, md.

Production engineers are always interested in improving productivity index by optimization of flow rate from bottom hole to the surface. Well performance evaluation is a primary and essential goal of engineers. The three currently available major tools that are used for well performance are as follows:

1. Considering the flow path from bottom hole to the production unit and measure the rate-versus-pressure drop.

2. Well testing
3. Production logging

Petroleum engineers focus on flow system with available analytic data for optimization to enhance productivity. However, the estimation of productivity indices of reservoir is not accurate because the currently available models and tools are not very reliable and accurate [1], therefore, reservoir engineering experts are always trying to find appropriate and accurate tools for calculating accurately the horizontal and vertical well's productivity indices and organize industrial and economical possible studies before drilling the wells which is expensive. In traditional methods for estimating the parameters of the well and the reservoir, the relationship between the parameters, often with one or multiple linear regressions, or even sometimes non-linear multiple regressions (Like Gaussian process regression models) are examined and in most cases mathematical relationship is used to predict the parameters. Since the mathematical relationship between input parameters such as permeability and independent variables (i.e., data from various logs) are unknown, complex and often non-linear methods, using linear regression and non-linear approximation will lead to errors in results. The results of the nonlinear regression models depend on mathematical models, implemented processes, and the type of input variables, especially if they have a large variance [1]. To determine the parameters, a new approach is required with high accuracy and low time and money consuming. Hence, an alternative method to determine the parameters is to use artificial intelligence and machine learning approaches [2].

2. AN OVERVIEW OF ARTIFICIAL INTELLIGENCE METHODS

Artificial intelligence is the science of making intelligent machines and programs. In general, investigation of the requirements for computational tasks such as perception, reasoning, and learning systems for such acts is called artificial intelligence. Data mining is defined as a branch of artificial intelligence as a set of methods to get data from a data set into a meaningful outcome. Artificial neural network works as a data mining method inspired by a mammal, particularly a human brain [3]. The main similarities between artificial neural networks and human brains are as follows:

1. The data processing system using neural structures or neurons
2. Determination of both networks, connections between neurons
3. The formation of both behaviors from simple computational tools with high coherence

2.1. Multilayer Perceptron Networks (MLP)

Multi-layer perceptron networks are one of the most widely used types of networking forward artificial neural network models in modeling and prediction of productivity index for petroleum industry. In MLP, each neuron in each layer is connected to all neurons of the previous layer that are also called quite related networks. The framework of each neuron

network includes: inputs, weights, biases, the aggregator function activation function, and the output [4]. The network has three layers of input, middle or high (single or multi-layer), and the output. Neurons can use different stimulus functions to produce output that the most common of them are a logarithm sigmoid, tangent sigmoid function and linear actuator. The network that we have used has two layers, the first layer is the sigmoid, and the second layer is linear. This kind of two-layer network is used widely in Back propagation networks [4].

2.2. Method of Genetic Algorithm Optimization (GA) and Its Combination with Artificial Neural Network

GA method is a learning method based on biological evolution that was introduced in 1975 by John Holland. In this way, a large collection of possible solutions puts forward. Each solution is evaluated using a fitness function, and then the number of solutions produced is new solutions, which are developed solutions. Thus, the search space will evolve in the direction in which the optimal solution is reached [6] (If one selects the correct input parameters to this method will give a good answer). Using this algorithm, a lot of optimization problems that are not solved by standard algorithms optimization, can be solved. Among the issues, the objective function that is discontinuous, non-differentiable, stochastic, or highly nonlinear can be cited. The basic principles governing genetic algorithms can be expressed as follows [6]:

1. Form the initial population of random solutions and coding solutions as chromosomes.
2. Evaluate responses and select the appropriate response using a probabilistic rule selection, the selected solutions are called parents.
3. Create new solutions with law enforcement a couple of jumps on the parents for the next generation.

The generation process of gradual evolution and improvement of the solutions will continue.

2.3. Particle Swarm Optimization Algorithm (PSO) and Its Combination with Artificial Neural Network

PSO algorithm is a meta-heuristic optimization algorithm modeled by Aybrhart in 1995 based on a group of birds flying slow motion [7]. In general, we can say that an algorithm of particle swarm optimization algorithm mimicking the behavior of animal societies to process knowledge society. The algorithm is one of the most successful algorithms in the context of continuous and discrete optimization. In this algorithm, each answer of question is modeled like a particle that has proportion and amount. Normally, since a method based on the combined action of the population, there is no answer and there is rapid convergence. In general, the PSO works based on movement and intelligence of particle and uses the concept of intelligence and social interaction for solving optimization problems [7].

In the present work, the following criteria were used to select the best method:

1. The correlation coefficient is a dimensionless quantity, which varies from 0 to 1, where 1 is the best value; and it is determined through equation 1 or obtained from the coefficient of determination i.e., formula 2.

$$R = \frac{\sum_{n=1}^n [(E_n - (\sum_{n=1}^n E_n)/n)(R_n - (\sum_{n=1}^n R_n)/n)]}{\sqrt{\sum_{n=1}^n (E_n - (\sum_{n=1}^n E_n)/n)^2 \sum_{n=1}^n (R_n - (\sum_{n=1}^n R_n)/n)^2}} \quad (1)$$

$$R^2 = \frac{\sum_{n=1}^n [(E_n - (\sum_{n=1}^n E_n)/n)]^2}{\sum_{n=1}^n [(R_n - (\sum_{n=1}^n R_n)/n)]^2} \quad (2)$$

2. The error can be expressed using different methods of expression; one of these methods is mean square error (MSE), which is expressed by the formula (3). Its optimal value is zero.

$$\varepsilon(n) = \text{MSE} = \frac{\sum_{n=1}^n (E_n - R_n)^2}{n} \quad (3)$$

In the above equations, R_n and E_n are values of actual observations and estimated, respectively, and n is the number of data for network training.

3. RESULTS AND DISCUSSION

To obtain flow rate (the output of neural network used in this section), the pressure and temperature data of a well, located in South West of Iran were used. More information is available upon request to the authors.

3.1. Data Analyzing and Procedures and Methods of Creating Anns

To study the PI using ANNs (MLP), the data of flow rate and pressure of an oil field in the South West of Iran was used, as mentioned earlier. The data of pressure and flow rate are used, respectively, as input and output (with units used in Darcy's equation) of neural network [8]. Darcy's equation is expressed by equation 4.

$$\frac{q}{A} = \frac{K}{\mu} \frac{\Delta P}{L} \quad (4)$$

In this equation, q , A , K , μ , ΔP , and L are: rate, area, permeability, the pressure difference, and the length of the porous medium, respectively. The steps of ANN creation are given below in details:

- A) Knowing the effect of input parameters is the first step to create an artificial intelligence method. Introduction of numerous high numbers of inputs makes the site

of neural network larger and retards the speed of learning education. The determination of appropriate parameters was carried out through the different combination of networks and selection of inputs with high efficiency.

- B) Before entering data in ANNs, a pre – process has been implemented to investigate whether or not any parameter receives the same attention and works recognition speed between different numbers. Data have been normalized using the following relation (5):

$$XN = \frac{X - \text{Min}X}{(\text{Max}X - \text{Min}X)} \quad (5)$$

where X is a 1-dimensional vector, and XN is normalized X.

- C) From all available data, 70% for learning, 15% for validation, and 15% for (testing) were used in MLP method.
- D) In order to create network's structure, the number of hidden layers and existed neuron in each layer should be determined. The number of input and output neurons is the same number of input and output parameters. The general method of hidden or intermediate neurons is used by try and error.
- E) In order to prevent pre-processing defects, data of learning were used in all methods. The number of cycles in each network was unknown and as soon as errors in data of learning began to increase, learning algorithm was stopped.
- F) After learning, a set of data is presented to MLP network, and the produced results are compared with real data, then the match of these data was used as a criterion of extension. The validation of network was evaluated during education (learning) and the moment that error on validation data starts increasing, the network educating stops (If MSE reaches the predicted value, it will stop too).
- G) Examination: this step is just for back – propagating networks. In these networks, the errors are controlled after ending of each cycle.

3.2. Modeling Using MLP Network

In order to predict well productivity index, 326 data of a well located in South West of Iran (over a year) were used, that 228, 49, and 49 of the latter data were used in the training, validation, and testing steps, respectively. The best R and MSE normalized values obtained from MLP were optimized by PSO and GA algorithms that can be seen in Table 1. In each case, the total data, the training data, and the data used in the validation and test steps are given in Figure 1. The results of the test for all three modes MLP, MLP combined with PSO, and MLP with GA are shown in Figure 2. Combining weights and bias for prediction of flow properties of layers {1, 3, 4, 2} for the best MLP combined with GA are given in Tables 2 to 6.

Table 1. Comparison of the best R and MSE values for normalized PI by MLP and optimized MLP using different methods

Parameter	MLP	MLP optimized with GA	MLP optimized with PSO
R (Total data)	0.88026	0.95071	0.94744
MSE (Total data)	0.009808	0.001049	0.001152
R (Learning data)	0.904060	0.94552	0.94187
MSE (Learning data)	0.020598	0.001099	0.001107
R (Validation data)	0.87978	0.98094	0.95147
MSE (Validation data)	0.010056	0.000715	0.002009
R (Testing data)	0.92355	0.93132	0.96739
MSE (Testing data)	0.008892	0.001148	0.005042

Table 2. Weight for the best mode (MLP combined with GA) in the first layer

5.4107
-5.2398
-5.2308
3.4407

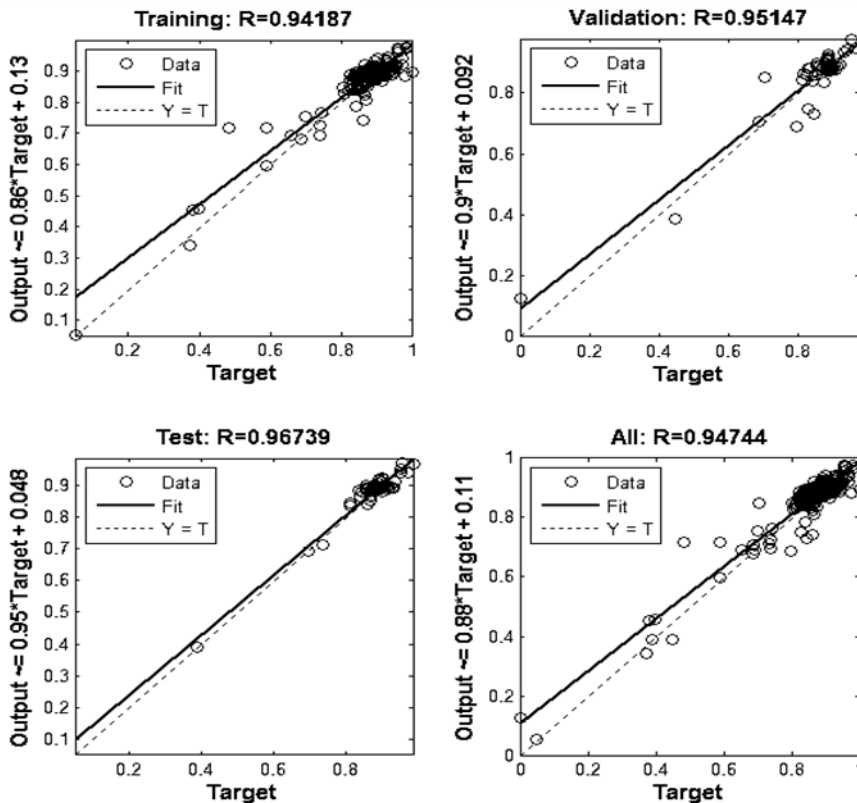


Figure 1. Comparison of Best R normalized rate (horizontal axis) and predicted normalized rate (vertical axis) MLP network with GA optimization method.

Table 3. Weights for the best case (MLP combined with GA) in the second layer

0.6124	1.6752	-0.2715	-0.0841
-0.1771	-1.8217	-0.7589	1.6952
-0.7206	2.5075	-0.7578	1.6019

Table 4. Weight for the best case (MLP combined with GA) in the output layer

-0.4304	0.5114	-0.674
---------	--------	--------

In addition, the output weight is 0.9169.

Table 5. Biasing for the best case (MLP combined with GA) in the first layer

-5.269
1.389
-3.186
7.777

Table 6. Bias for best case (MLP combined with GA) in the second layer

1.645
0.0262
1.269

In addition, the output bias is 0.5283.

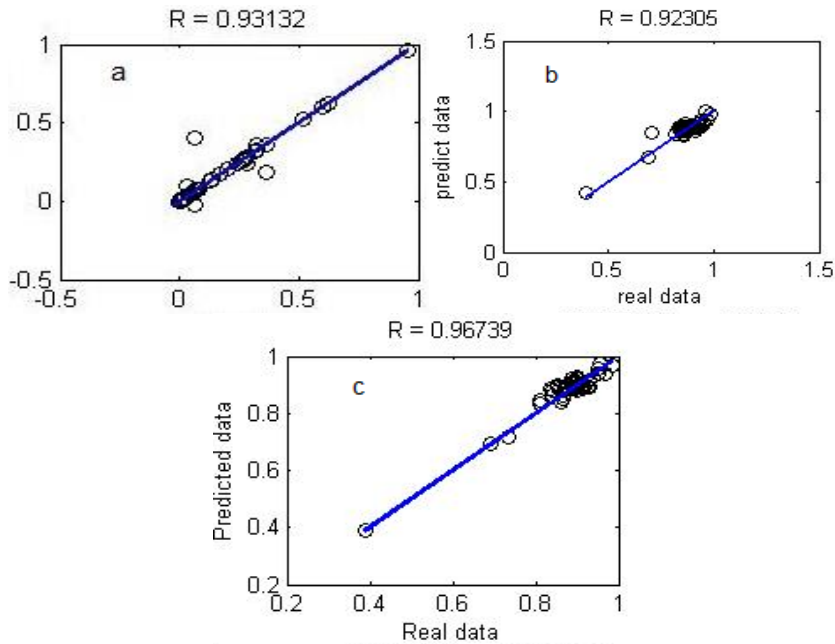


Figure 2. Results of the test of real data, the horizontal axis, the predicted data, vertical axis, MLP combined with PSO (a), using MLP (b) and MLP methods combined with GA (c), respectively.

It should be mentioned that as MLP back-propagation algorithm has been used in neural network modeling, we used two layers in the hidden layer (comparing with single- and three hidden layer; it shows better results). However, studies have shown that more than three layers of hidden layer cause a slight reduction in network performance, since in this case; the system will start to memorize the data.

CONCLUSION

Using artificial neural networks is an easy method for modeling reservoir parameters especially as it does not require sophisticated mathematical models. The most important issue in the use of these methods is the appropriate choice of learning algorithms. Also, the use of artificial neural network approach does not require any prior knowledge of the ingredients of the rocks or fluid filling cavities in rocks. Since in this method, input layer neurons are a function of the factors affecting output, the selection of input variables that need to be acted is the most influential factors on outputs. Using this method and integration with appropriate optimization algorithms of GA and PSO for predicting productivity index of well is a good practice. Also, significant savings in time and costs are created. In general, it can be said with regard to the application of neural networks in case of obtaining the proper relationship between the data is very difficult. The factors influencing the output of neural network are selecting the appropriate validation data sets training and testing the network. In case of distribution of data in these three categories, the modeling can be reached faster and with greater accuracy.

REFERENCES

- [1] Abdelgawad, A., Malekzadeh, D. (2001): Determination of the Drainage Area of Horizontal Wells in the Presence of Vertical Wells. Effect of Reservoir and Well Parameters. In: *Journal of Canadian Petroleum Technology* 40 (10), pp. 45-54. DOI: 10.2118/01-10-02.
- [2] Chaudhry, Amanat U. (2004): *Oil well testing handbook*. Burlington, MA: Gulf Professional Pub.
- [3] Earlougher, RC Jr. (1977). *Advances in Well Test Analysis*, Henry Doherty Memorial Fund of AIME, New York, p. 330.
- [4] Ehlig-Economides, C.A. and Ramey Jr, H.J., (1981). Pressure buildup for wells produced at a constant pressure. *Society of Petroleum Engineers Journal*, 21(01), pp. 105-114.
- [5] Fetkovich, M.J. and Vienot, M.E., (1985). Shape factor, CA, expressed as skin, SCA. *Journal of petroleum technology*, 37(02), pp. 321-322.
- [6] Peaceman, D.W., BABU, D. and ODEH, A., (1990). Discussion of productivity of a horizontal well. Reply. *SPE reservoir engineering*, 5(2), pp. 252-253.
- [7] Wan, J., Penmatcha, V.R., Arbabi, S., Aziz, K., (2000). Effects of grid systems on predicting horizontal-well productivity, *SPE J.*, 5 (3), pp. 309-314.

- [8] Ahmadi, M.A., Soleimani, R., Lee, M., Kashiwao, T., Bahadori, A., 2015. Determination of oil well production performance using artificial neural network (ANN) linked to the particle swarm optimization (PSO) tool, *Petroleum*, pp. 118-132.
- [9] Economides, M.J., Hill, A.D., Ehlig-Economides, C. and Zhu, D (1994): Petroleum production systems. Englewood Cliffs, N.J.: PTR Prentice Hall
- [10] Ibelegbu, C., (2004). (Productivity Index in Horizontal Well). *Journal of Scientific and Industrial Research*, 63, pp. 979-984.
- [11] Ahmed, T., (2006): *Reservoir engineering handbook*. 3rd ed. Burlington, MA: Elsevier/ Gulf Professional.
- [12] Poggio, T. and Girosi, F., (1990). Regularization algorithms for learning that are equivalent to multilayer networks. *Science*, 247(4945), pp. 978-982.
- [13] Demuth, H., Beale, M. and Hagan, M., (2000). *Neural Network Toolbox User's Guide*, Copyright 1992-2002, By The Math Works. Inc. Version 4, 480.
- [14] Han, J.; Kamber, M. (2006): *Data mining. Concepts and techniques*. 2nd ed. Amsterdam, Boston, San Francisco, CA: Elsevier; Morgan Kaufmann (The Morgan Kaufmann series in data management systems.
- [15] Menhaj, M.B., (2003). Principles of Artificial Neural Networks, Amirkabir University of Technology, *Computational Intelligence*, Vol. 1.
- [16] M Howard, (2006) Neural Network in Electrical Engineering. World Scientific Publishing Co. Pte. Ltd.
- [17] John Henry Holland, (1992). Adaptation in natural and artificial systems: an introductory analysis with applications to biology, control, and artificial intelligence. MIT press.
- [18] Kennedy, J., Eberhart, R., (2002). Particle swarm optimization. In: *Neural Networks Proceedings, IEEE International Conference on*, vol. 4, pp. 1942-1948.
- [19] Rezaee, M.R., Kadkhodaie-Ilkhchi, A. and Alizadeh, P.M., (2008). Intelligent approaches for the synthesis of petrophysical logs. *Journal of Geophysics and Engineering*, 5(1), pp. 12-26.

Chapter 10

EVALUATION OF PETRO-PHYSICAL PROPERTIES (POROSITY AND PERMEABILITY) OF CARBONATE OIL RESERVOIRS

***Abbas Khaksar Manshad,¹ Habib Rostami,²
Peyman Torabideh² and Amir H. Mohammadi^{3,4,5,*}***

¹Department of Petroleum Engineering, Abadan Faculty of Petroleum Engineering,
Petroleum University of Technology (PUT), Abadan, Iran

²Department of Computer Engineering, School of Engineering,
Persian Gulf University, Bushehr, Iran

³Discipline of Chemical Engineering, School of Engineering,
University of KwaZulu-Natal, Howard College Campus,
Durban, South Africa

⁴Département de Génie des Mines, de la Métallurgie et des Matériaux,
Faculté des Sciences et de Génie, Université Laval, Québec, QC, Canada

⁵Institut de Recherche en Génie Chimique et Pétrolier (IRGCP),
Paris Cedex, France

ABSTRACT

Petro-physical properties like porosity and permeability play an important role in petroleum reserves evaluation. Permeability indicates fluid flow ability in rock reservoir's pore spaces. The methods of core analysis, well testing and empirical correlations are normally used to measure/estimate petro-physical properties. The conventional methods of core analysis and well testing are time consuming and expensive. Furthermore, the latter data may not be provided for every well. On the other hand, empirical correlations are used for special cases and may not be accurate for every situation. Thus, developing a reliable method for estimating petro-physical properties based on well logging data could be significant as well logging data are provided almost for every well. An alternative method for evaluating petro-physical properties is data mining and artificial intelligence

* Corresponding Author's E-mail: amir_h_mohammadi@yahoo.com and a.h.m@irgcp.fr.

and machine learning techniques. In this communication, the method of data mining has been applied to estimate reservoir permeability and porosity using petro-physical data. First, the data were normalized and then horizontal and vertical permeabilities and porosities of an Iranian carbonate oil field were calculated using geophysical data and the methods of Multiple Layer Perceptron Neural Network (MLP-NN) and Radial Bias Function Neural Network (RBF-NN). Particle Swarm Optimization (PSO) and Genetic Algorithm (GA) were used for optimizing the NN parameters. Comparison of the results shows that combination of MLP and RBF with PSO or GA yields satisfactory results.

Keywords: porosity, permeability, MLP-NN, RBF-NN, Particle Swarm Optimization (PSO), Genetic Algorithm (GA)

1. INTRODUCTION

Hydrocarbon reservoirs are one of the main sources of energy in the world. Developing these reservoirs is important due to reduction of oil reserves. From reservoir properties, permeability is difficult to measure in comparison with water saturation and porosity [1-9]. Permeability and porosity are normally measured by direct costly experimental methods of core analysis and well tests, which are exact but not accurate to describe all the reservoir layering and heterogeneities [1-9]. So that, the results are limited to a special rock and layer and are not continuous plots for reservoir applications [1-9]. Therefore, development of precise, inexpensive, less time – consuming predictive methods for evaluation of permeability and porosity based on well logging data is of great interest [1-9]. The latter can be achieved by using artificial intelligence, machine learning and data mining methods [1-9]. Among them, Artificial Neural Networks (ANN) have been widely used in petroleum industry [2]. ANNs have been developed based on the neural system of the animals and human, and consists of units called neuron [10-18]. ANN has been inspired from the complicated structure of the mammals', human's, brain neural system where information is saved and processed to solve problems by a network of millions of interconnected neurons [10-18]. From mathematics point of view, ANNs are composed of multiple layers, through the first of which the information enters the network, then comes the intermediate layers (hidden layers) whose number may vary depending upon the nature of the problem, they take the role of processing the data and the connection between input and output [10-18]. Here, the data are analyzed, weighted, processed, coded, etc. and finally passed to the last layer, namely output layer [10-18]. Hence, one may say the output is a combination of inputs, weights, bias and the hidden layer elements [10-18].

In the present study, Multilayer Perceptron Networks (MLP) and Radial Basis Function (RBF) Neural Networks were applied for modeling purpose. The latter were used along with Genetic Algorithm (GA) and Particle Swarm Optimization (PSO) algorithms which are described briefly in the followings:

2. MODEL

2.1. Multilayer Perceptron Networks (MLP)

MPLs are of the most frequently applied feed-forward ANNs for modeling in petroleum industry [10-18]. In MLP, every neuron in every layer is connected to neurons in the preceding layer, such networks are known as completely interconnected layers [10-18]. Here, the network is first produced with one hidden layer and in case of malfunction the number of layer will be increased, however, the number of layers has to be the smallest possible since the system will be apt to over fitting oscillation if the number of layers is greater than a certain value and it will begin to preserve the data instead of analyzing them, thereby, errors high will rise. To prevent this cross, cross validation is used [1-18].

2.2. Radial Basis Function Neural Networks (RBF)

These networks need more neurons compared with standard feed-forward networks with error backpropagation, however, such networks can be learned in a shorter time than feed-forward networks. RBFs serve well when there is a great deal of input available, they are of the feed-forward type and their structure is like MLPs [10-18]. This network maps an N dimensional input pattern into a Z dimensional output patten using the adjacent layer nodes [10-18]. The inputs of each neuron are different from the others in RBFs, the inputs to the transfer function are equal to the distance vector between the weights and the inputs are multiplied by the bias [10-18].

2.3. Genetic Algorithm Optimization (GA)

This method provides a large set of possible solutions, each of which is analyzed with a crossover function, then a number of the solutions create new solutions that cause evolution of solutions, accordingly the process proceeds to the desired solution [10-18]. This method has shown to be effective since the input parameters are adequately selected [10-18].

2.4. Particle Swarm Optimization (PSO)

PSO is one of the most successful algorithms in discrete and continuous optimization where every solution is modeled as a particle of magnitude and correspondence (or similarity) [10-18]. Since it is a method population based and there is no solution combination in it, it normally converges fast [10-18]. In general, PSO operates based upon the intelligence and interaction of the particles and uses the concept of social interactions to solve optimization problems [10-18].

In the present work, correlation coefficient (R) and mean square error (MSE) have been used for the models evaluations:

- a. Correlation coefficient is a dimensionless value ranging between 0 and 1, and is calculated through either of the following equations (1), (2):

$$R = \frac{\sum_{n=1}^n [(E_n - (\sum_{n=1}^n E_n)/n)(R_n - (\sum_{n=1}^n R_n)/n)]}{\sqrt{\sum_{n=1}^n (E_n - (\sum_{n=1}^n E_n)/n)^2 \sum_{n=1}^n (R_n - (\sum_{n=1}^n R_n)/n)^2}} \quad (1)$$

$$R^2 = \frac{\sum_{n=1}^n [(E_n - (\sum_{n=1}^n R_n)/n)]^2}{\sum_{n=1}^n [(R_n - (\sum_{n=1}^n R_n)/n)]^2} \quad (2)$$

- b. The following equation denotes MSE (3):

$$\varepsilon(n) = MSE = \frac{\sum_{n=1}^n (E_n - R_n)^2}{n} \quad (3)$$

where R_n is the actual observed value, E_n is the calculated value, m is the number of data to learn the network. The weights have to be varied to decrease the error or increase the R to reach the best fitness [12].

3. CASE STUDY

One of the south-western Iranian oil fields was selected for this study. The data show that the reservoir is layered and heterogeneous. A great number of wells with an acceptable amount of data were available in this field whose most influential collection was used in this study. Four adequately spaced wells were selected from which vertical and horizontal cores were available, and other wells which were too far from these wells were neglected in this study.

For porosity modeling, the ANN inputs include the following logs: SGR, CGR, DT, ILD, Density, NPHI, Caliper and Depth. The outputs include the porosities of the vertical and horizontal cores.

For permeability modeling, the ANN inputs include:

- Spectral Gamma Ray (SGR) for lithology evaluation including shale regions.
- Electrical Resistivity (Rt) for determining water saturation.
- Water saturation data for indicating permeable zones.
- Effective or secondary porosity for finding the relation between porosity and permeability. Shale, Dolomite, Anhydrite and calcite are types of lithology. Caliper's data are used for showing well diameter: Depth logs are used for determining the effect of over burden pressure. The outputs include vertical and horizontal permeability.

3.1. Data Analysis and ANN Building Methods

The log and core data in the selected wells had good consistency, besides the cores had good quality to be used in ANN. The method and stages for building the ANNs are as follows [10-18]:

- a) The first step is to characterize the effect of the input parameters. Overpopulating the input data caused an oversize of the ANN and hence decelerated the learning process. Therefore, networks with different input configurations were used and those inputs of most influence on the efficiency of the results were selected.
- b) Before introducing the inputs into the network, preprocessing the data in order to assure that the input parameters receive equal attention from the network contributes to improving the overall efficiency of the network. The input values were mostly large, this reduced the recognition rate of the network, and therefore the data were normalized to fall in the interval between 0 and 1 using equation (4).

$$X_n = \frac{(x - \text{Min}X)}{(\text{Max}X - \text{Min}X)} \quad (4)$$

where X is the magnitude of the one dimensional vector of the data, X_n is the normalized value of X .

- c) Categorizing the data: Among all the data (petrophysical data, horizontal and vertical core data), 70% were used as training data, 15% as validation and 15% as test data in MLP, whereas in RBF 70% of the data were used as training data and the remaining 30% were used to test/verify the network.
- d) Network structure design: In order to build the network structure, the number of hidden layers as well as the number of neurons in each layer had to be determined. The number of neurons in the input and output layer were the number of input and output parameters respectively, the number of neurons in the intermediate layers was obtained by trial and error.
- e) Learning: To prevent preprocessing, the learning data set were used, the number of cycles in each network was unknown before execution and as soon as the error in the learning data grew the learning algorithm stopped.
- f) Validation: This series of data were introduced into the network after learning (only MLP) and the produced results were compared with the actual values of horizontal and vertical porosities and permeabilities, the consistency of these two sets of values was used as a criterion to universalizability of the network.
- g) Test/Verification: This stage is applicable to only back propagating networks, here the errors were controlled after each cycle ended and in order to stop the learning algorithm and prevent the data network to save the learning in case the error in learning grew beyond the required accuracy. Weka, Matlab, Excel and Neuro Solution softwares were used here.

4. RESULTS AND DISCUSSION

4.1. MLP Method for Porosity Prediction

Considering its applicability in prediction problems and its capability in generalizing the results, feed-forward MLP was used for vertical and horizontal porosity predictions. The MLP includes 8 inputs in the input layer, 2 hidden layers and finally the output layer which yield the results of the calculations. Different hidden layers with different neurons were tried and the best of which turned out to be those of greater R and smaller MSE in the two layers. Tangent sigmoid technique (Tansig) was used for introduction to the hidden layer and pure line (Purelin) was used to pass from the hidden layer to the output layer. For pure MLP, Levenberg-Marquardt back propagation was used due to its fast convergence in small to medium size networks. A number of 212 horizontal porosity data were available whose 148, 32 and 32 numbers were applied in training, validation and test, respectively. Besides, from the 190 vertical porosity data, 132, 29 and 29 numbers of them were accordingly used in testing, validation and test phases. The best R and MSE values and normalized values for horizontal and vertical porosity obtained from MLP and MLP optimized by GA and PSO are listed in Tables 1 and 2, respectively. Furthermore, Tables 3 and 4 show the best R and MSE obtained with MLP optimized by GA and normalized horizontal and vertical porosities for two layer MLP forms, respectively. It is worth mentioning that in single-layer and 3-layer perceptron the correlation coefficients were smaller and the MSE is greater compared with 2-layer perceptron, thus they were ignored to be presented here. Figure 1 presents a comparison of normalized actual and predicted vertical and horizontal values at R values (highest value) and MSE values (lowest) in the best prediction mode that is combination of MLP and GA, including the cases of total data, data used for learning, validation and test. Figure 2, for instance, shows the performance curve of the best normalized MLP network combined with GA for predicting porosities of horizontal and vertical cores. Figures 3 and 4 show comparisons of correlation coefficient (R) using (pure) MLP, MLP optimized by PSO and MLP optimized by GA for horizontal and vertical cores, respectively. As can be observed, satisfactory agreements are achieved when using MLP optimized by PSO and MLP optimized by GA.

Table 1. Comparison of the best R and MSE values for horizontal core porosities, normalized by pure MLP (Levenberg-Marquardt learning) and MLP optimized by GA and PSO

MLP optimized with PSO	MLP optimized with GA	MLP	Parameter
0.96912	0.99591	0.95715	R (Total data)
0.0038276	0.00038082	0.0039098	MSE (Total data)
0.98268	0.99689	0.96564	R (Learning data)
0.0012266	0.00031946	0.0035528	MSE (Learning data)
0.96386	0.99313	0.8652	R (Validation data)
0.0017712	0.00075073	0.0064069	MSE (Validation data)
0.98392	0.99023	0.9245	R (Testing data)
0.0019726	0.0002949	0.0030632	MSE (Testing data)

Table 2. Comparison of the best R and MSE values for vertical core porosities, normalized by pure MLP (Levenberg-Marquardt learning) and MLP optimized by GA and PSO

MLP optimized with PSO	MLP optimized with GA	MLP	Parameter
0.98813	0.99507	0.96262	R (Total data)
0.00050951	0.00021173	0.00076555	MSE (Total data)
0.99000	0.99496	0.96968	R (Learning data)
0.00037344	0.00018985	0.00055004	MSE (Learning data)
0.96707	0.99043	0.94108	R (Validation data)
0.00089356	0.00025433	0.001369	MSE (Validation data)
0.98136	0.9989	0.96693	R (Testing data)
0.00074352	0.0002687	0.01143	MSE (Testing data)

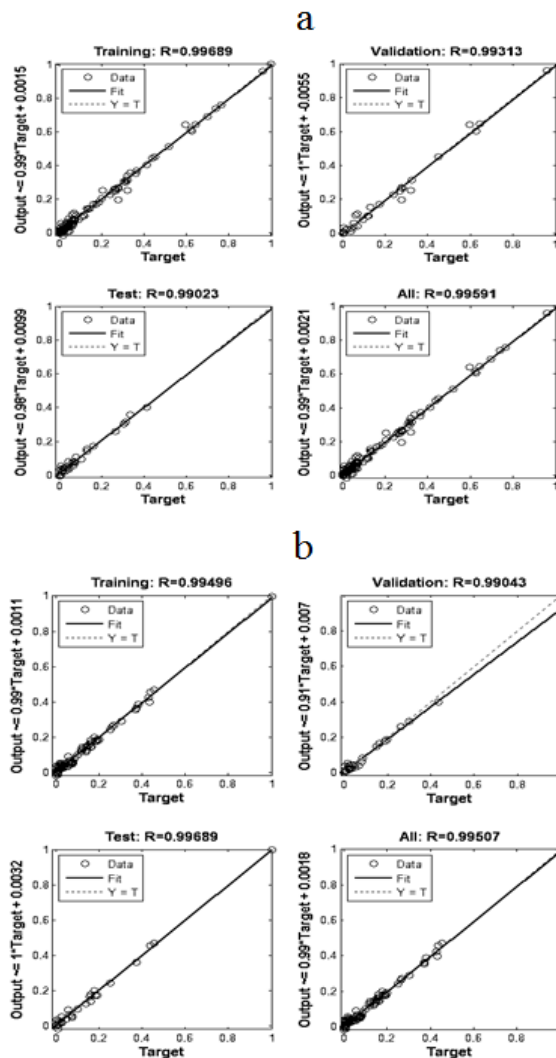


Figure 1. The best R in actual normalized porosity (Horizontal axis) vs. that in normalized porosity predicted by MLP optimized by GA (vertical axis). (a) Horizontal cores, (b) Vertical cores.

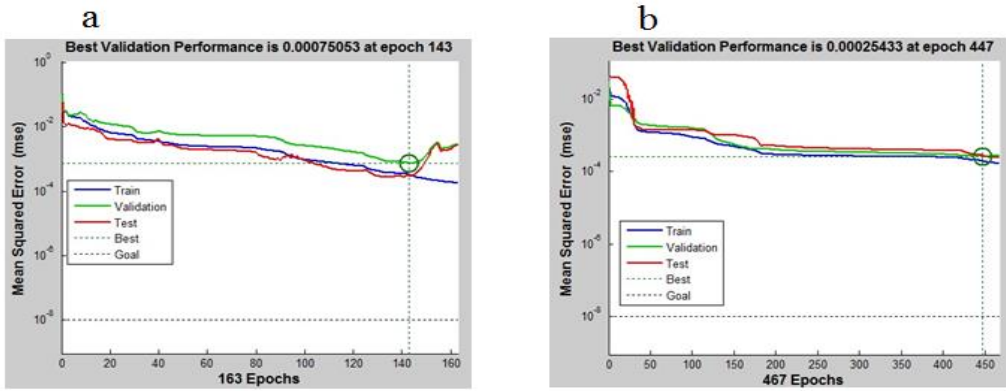


Figure 2. Performance curve for normalized MLP optimized by GA. (a) Horizontal core, (b) Vertical core.

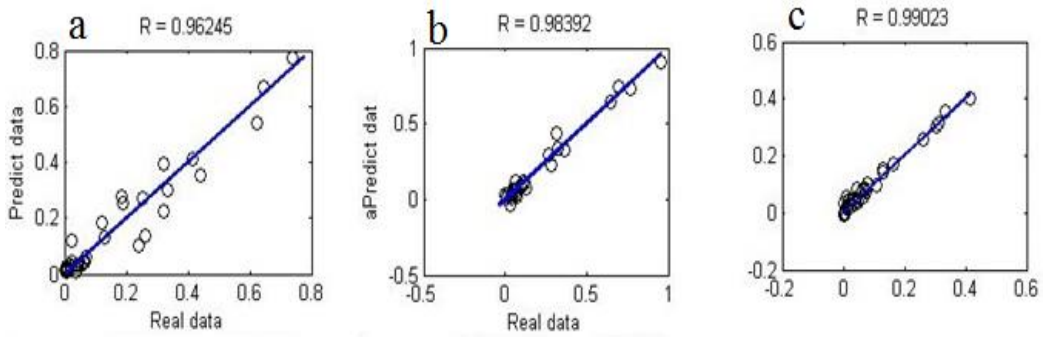


Figure 3. Comparison of correlation coefficient (R) in horizontal core. (a) MLP, (b) Optimized by PSO, (c) Optimized by GA.

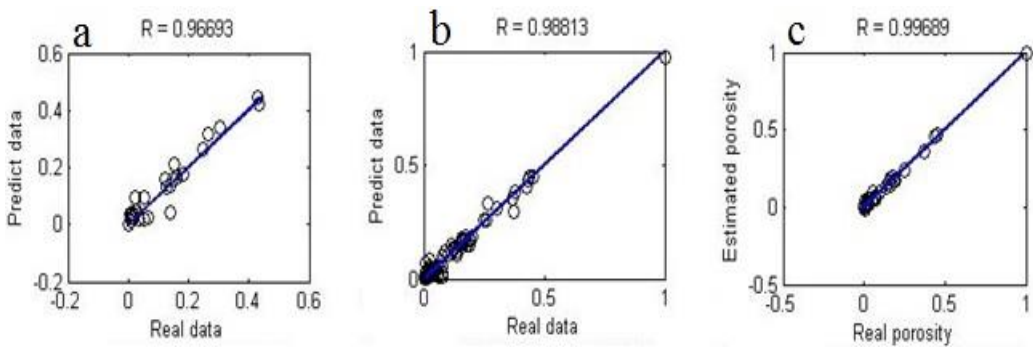


Figure 4. Comparison of correlation coefficient (R) in vertical core. (a) MLP, (b) Optimized by PSO, (c) Optimized by GA.

Table 3. The results of applications of different two-layer normalized perceptron configurations with GA optimization for horizontal core porosity prediction in test data (15 of the total data)

MSE	R	No. of neurons in two layer config.	No. of Networks
0.0012405	0.98901	[2 2]	1
0.00189204	0.98367	[4 3]	2
0.0002949	0.99023	[5 4]	3
0.00095807	0.89718	[8 6]	4
0.001659	0.90804	[10 11]	5
0.00091356	0.92315	[15 15]	6

4.2. RBF Method for Porosity Prediction

As mentioned earlier, these networks operate well when there is a large amount of input data. Since there is no validation stage in such networks in analogy with MLP networks, RBF uses a radial mechanism which enables it to have a better interpretation when there is large amount of input [16]. The same data as in MLP where used here: 212 horizontal core porosities of which 149 ones were used in learning stage and the rest were used for testing, as well as 190 vertical core porosities 133 of which were used in learning stage and the rest were used for testing. Tables 5 and 6 show the best normalized R and MSE values for horizontal and vertical porosities obtained by RBF and RBF optimized by different techniques. As can be seen, the combination of RBF and PSO yields the highest R and lowest MSE. Figure 5 presents a comparison of the best R values for actual porosities and those predicted in test data by normalized RBF and optimized by PSO for horizontal and vertical cores. As can be seen, satisfactory agreements are achieved.

Table 5. Comparison of the best R and MSE values for vertical core porosities, normalized by pure RBF (Levenberg-Marquardt learning) and RBF optimized by GA and PSO

RBF optimized by PSO	RBF Optimized by GA	RBF	Parameter
0.98388	0.96715	0.89976	R (Total data)
0.0015553	0.0039891	0.011355	MSE (Total data)
1.000	1.000	1.000	R (Learning data)
1.0104E-17	4.078E-17	9.58E-17	MSE (Learning data)
0.93132	0.92585	0.76411	R (Testing data)
0.005152	0.0091216	0.037547	MSE (Testing data)

4.3. MLP Method for Permeability Prediction

The method of MLP was used for vertical and horizontal permeability predictions due to its application and its high ability. Eleven inputs (for each permeability) were entered in input layer network. There were two hidden layers for getting data and one output (again for each permeability). We tested different hidden layers with different neurons and we found out that

the best architecture has two layers. The sigmoid tangent (Tansig) activation function for hidden layer inputs and linear (purelin) for hidden layer output were used. Back propagation (BP) and Levenberg-Marquardt algorithm were used for network learning with average to small size due to fair convergence. From 248 data, 174, 37, 37 of them were used in training, validation and examination. Average square error for the methods of single layer and three-layer perceptron were greater than two-layer perceptron (Correlation index was smaller) and thus, the result of two-layer were only considered here. The best values of R and MSE were obtained for (pure) MLP, and MLP optimized by PSO and GA algorithms which are reported in Tables 7 and 8 for horizontal and vertical permeabilities, respectively. In Tables 9 and 10, the results of employing different designs, two-layer perceptron normalized and optimized using GA to predict the horizontal and vertical permeabilities (for the 15% test) are shown. Figures 6 and 7 show comparisons of the actual permeability correlation coefficient and predicted permeability with normalized data using (pure) MLP and MLP optimized with PSO and GA for the horizontal and vertical permeabilities, respectively. Figure 8 illustrates comparisons of the normalized correlation coefficient of the real permeability and predicted permeability and normalized using MLP optimized by GA for horizontal and vertical permeabilities. Normalized MLP network efficiency plot at its best condition is given in Figure 9. Figure 10 shows the effect of the input parameters used in the training to estimate horizontal and vertical permeabilities. In overall, satisfactory agreements are achieved using this modeling approach.

Table 6. Comparison of the best R and MSE values for vertical core porosities, normalized by pure RBF (Levenberg-Marquardt learning) and RBF optimized by GA and PSO

RBF optimized by PSO	RBF Optimized by GA	RBF	Parameter
0.99507	0.98159	0.91203	R (Total data)
0.00026875	0.00089621	0.0017469	MSE (Total data)
1.000	1.000	1.000	R (Learning data)
2.8039E-18	7.6805E-18	9.996E-18	MSE (Learning data)
0.98184	0.9652	0.80169	R (Testing data)
0.00089582	0.0010366	0.0027804	MSE (Testing data)

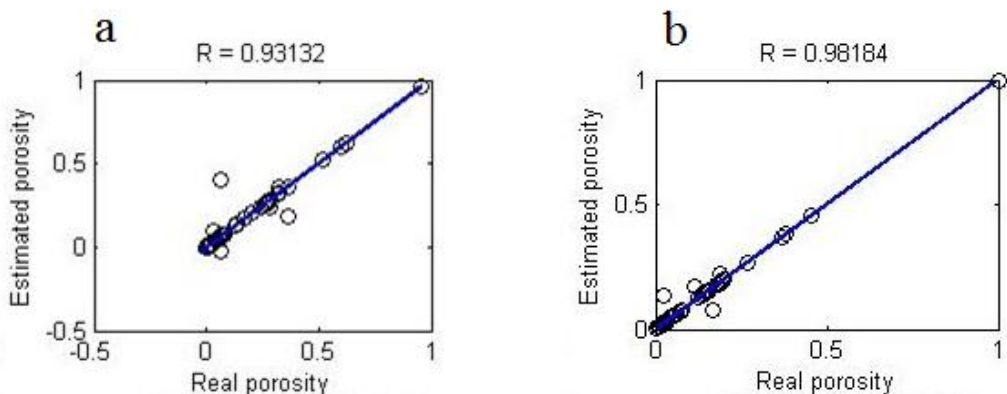


Figure 5. Comparison of R in normalized actual core porosities and those predicted by RBF optimized by PSO for test data. (a) Horizontal core, (b) Vertical core.

Table 7. Comparison of the best results for R and MSE using MLP optimized by GA and PSO for horizontal permeability

MLP optimized with PSO	MLP optimized with GA	MLP	Parameter
0.99449	0.99281	0.97002	R (Total data)
0.00032517	0.00042422	0.0017569	MSE (Total data)
0.99628	0.99185	0.97881	R (Learning data)
0.00020979	0.00045699	0.0011322	MSE (Learning data)
0.98389	0.99248	0.97501	R (Validation data)
0.00097193	0.0005864	0.0015745	MSE (Validation data)
0.99719	0.99808	0.94171	R (Testing data)
0.000221	0.000342	0.0048768	MSE (Testing data)

Table 8. Comparison of the best results for R and MSE using MLP optimized by GA and PSO for vertical permeability

MLP optimized with PSO	MLP optimized with GA	MLP	Parameter
0.98552	0.9976	0.94537	R (Total data)
0.00085198	0.000071422	0.0015893	MSE (Total data)
0.98672	0.99828	0.95251	R (Learning data)
0.00072373	0.000044505	0.0011938	MSE (Learning data)
0.98445	0.98832	0.94905	R (Validation data)
0.0015823	0.00016801	0.00044481	MSE (Validation data)
0.98162	0.99843	0.93273	R (Testing data)
0.00072477	0.000096852	0.0045932	MSE (Testing data)

Table 9. The results of employing different designs, two-layer perceptron normalized and optimized using GA (Education Network type Levenberg-Marquardt) to predict the horizontal permeability (for the 15% test)

MSE	R	No. of neurons in two layer config.	No. of Networks
0.003510	0.9318	[2 2]	1
0.0017312	0.97622	[3 3]	2
0.000342	0.99808	[4 3]	3
0.0073574	0.81939	[7 9]	4
0.003615	0.9289	[10 10]	5
0.50869	0.84072	[14 13]	6
0.0078198	0.903	[15 15]	7

Table 10. The results of employing different designs, two-layer perceptron normalized and optimized using GA (Education Network type Levenberg-Marquardt) to predict the vertical permeability (for the 15% test)

MSE	R	No. of neurons in two layer config.	No. of Networks
0.0015503	0.94678	[2 2]	1
0.00096852	0.99843	[3 3]	2
0.00098235	0.97037	[4 3]	3
0.0012449	0.93789	[7 9]	4
0.004963	0.9581	[10 10]	5
0.002528	0.85665	[14 13]	6
0.009444	0.95427	[15 15]	7
0.009444	0.95427	[15 15]	8

4.4. RBF Method for Permeability Prediction

As mentioned earlier, these networks works better when many input parameters are provided [16]. In this method, the validation part is omitted [16]. RBF uses a radial structure that has a beer consistency when number of inputs increases [16]. We used the same number of 248 data (174 for learning and 74 for examination for vertical and horizontal permeabilities. The best magnitudes (normalized) R, MSE from RBF (Levenberg-Marquardt) and RBF optimized with different methods are reported in Tables 11 and 12 for horizontal and vertical permeabilities, respectively. Comparison of the best R (higher) and MSE (smallest) for horizontal and vertical permeabilities and the predicted values using normalized MLP for test data are presented in Figure 11. The results show that the methods of MLP (optimized with PSO and GA) and RBF yield acceptable results. However, for RBF method, validation part has been omitted.

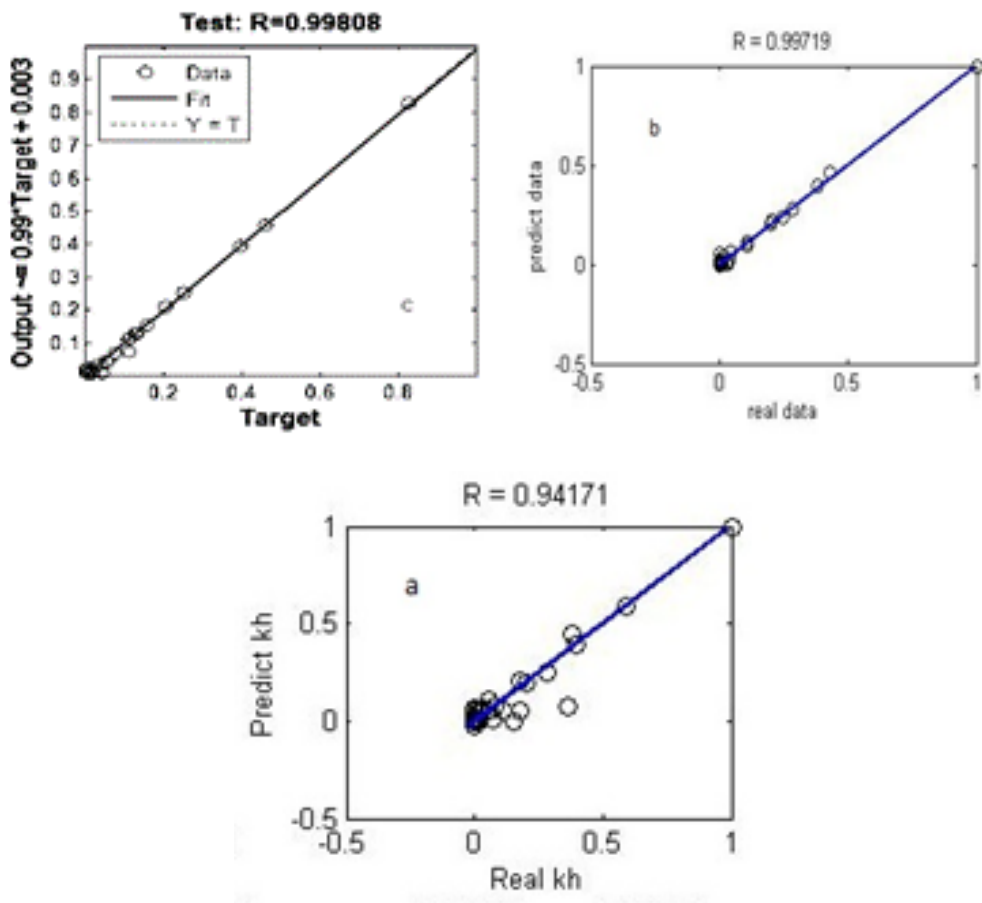


Figure 6. Comparison of the correlation coefficient and also the predicted permeability (vertical axis) with normalized data for horizontal permeability. (a) MLP, (b) MLP combined with PSO and (c) MLP combined with GA.

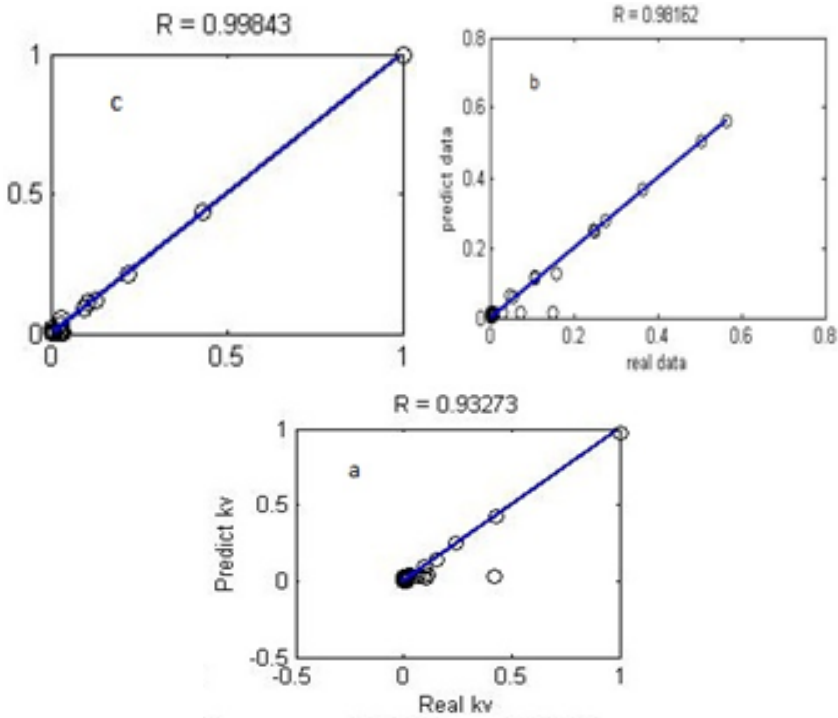


Figure 7. Comparison of the correlation coefficient and also the predicted permeability (vertical axis) with normalized data for vertical permeability. (a) MLP, (b) MLP combined with PSO and (c) MLP combined with GA.

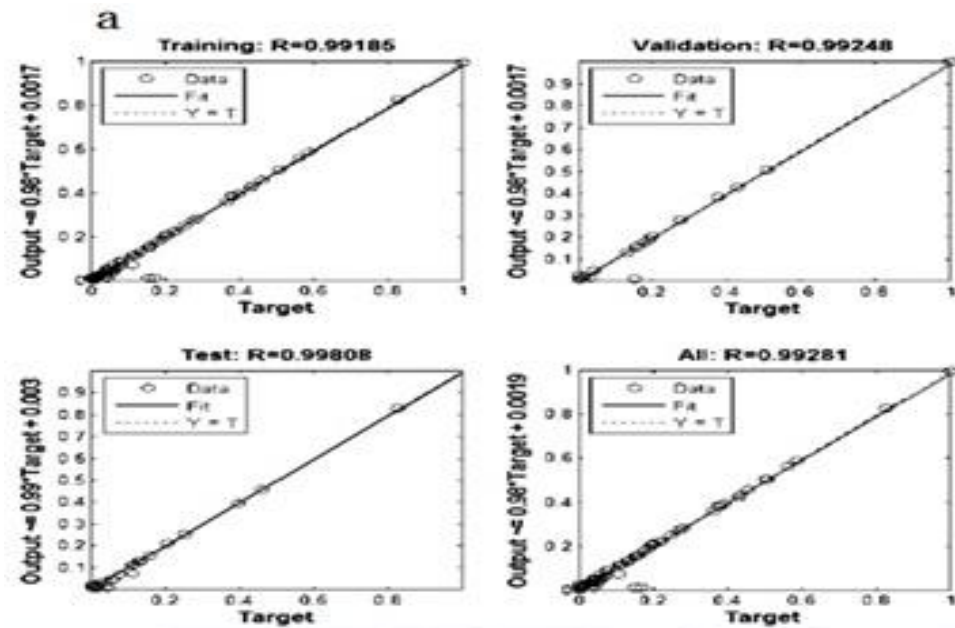


Figure 8. (Continued)

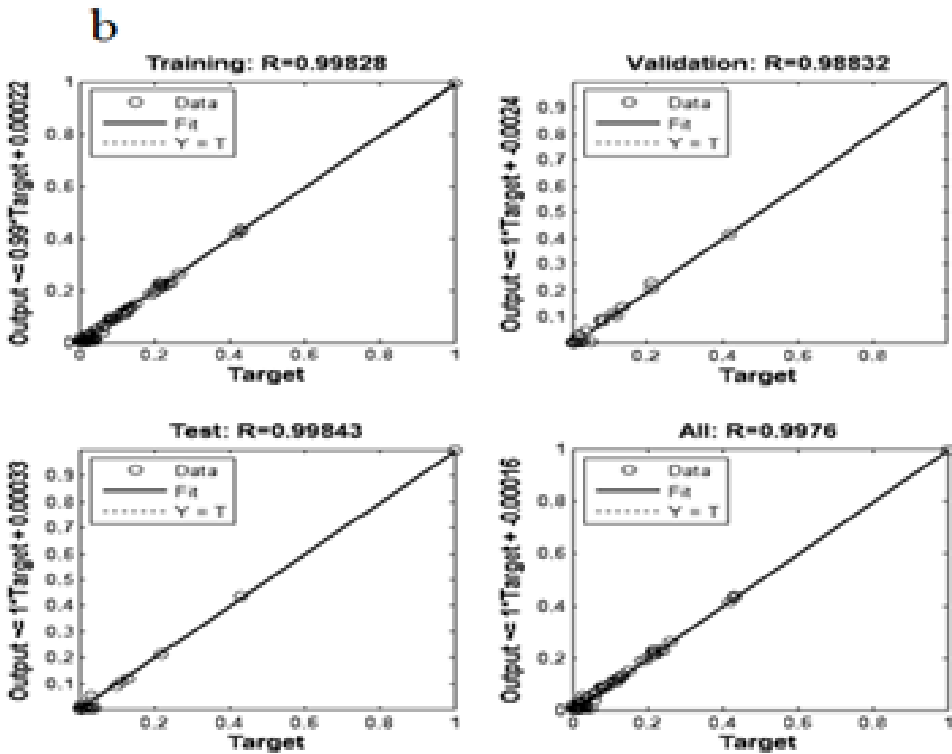


Figure 8. Comparison of the normalized correlation coefficient of the real permeability (horizontal axis) and predicted permeability and normalized (vertical axis) using MLP (optimized by GA) for (a) horizontal Permeability and (b) vertical permeability (where the network training Type Levenberg-Marquardt).

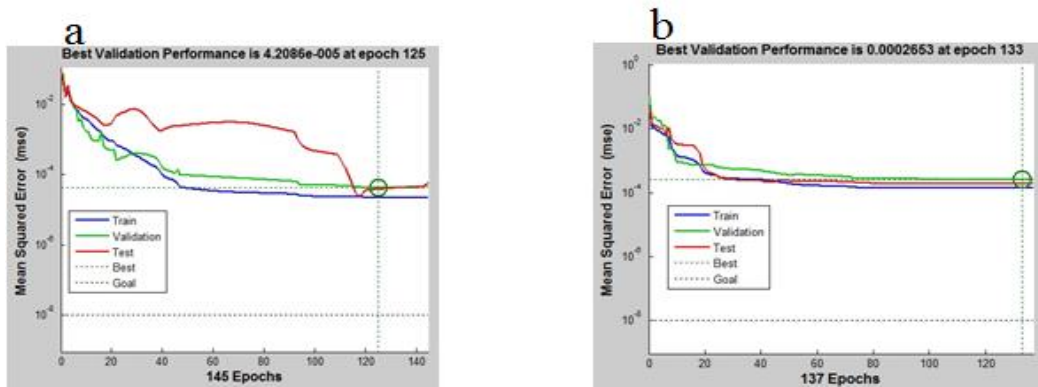


Figure 9. Plot of normalized MLP network performance for (a) horizontal permeability and (b) vertical permeability.

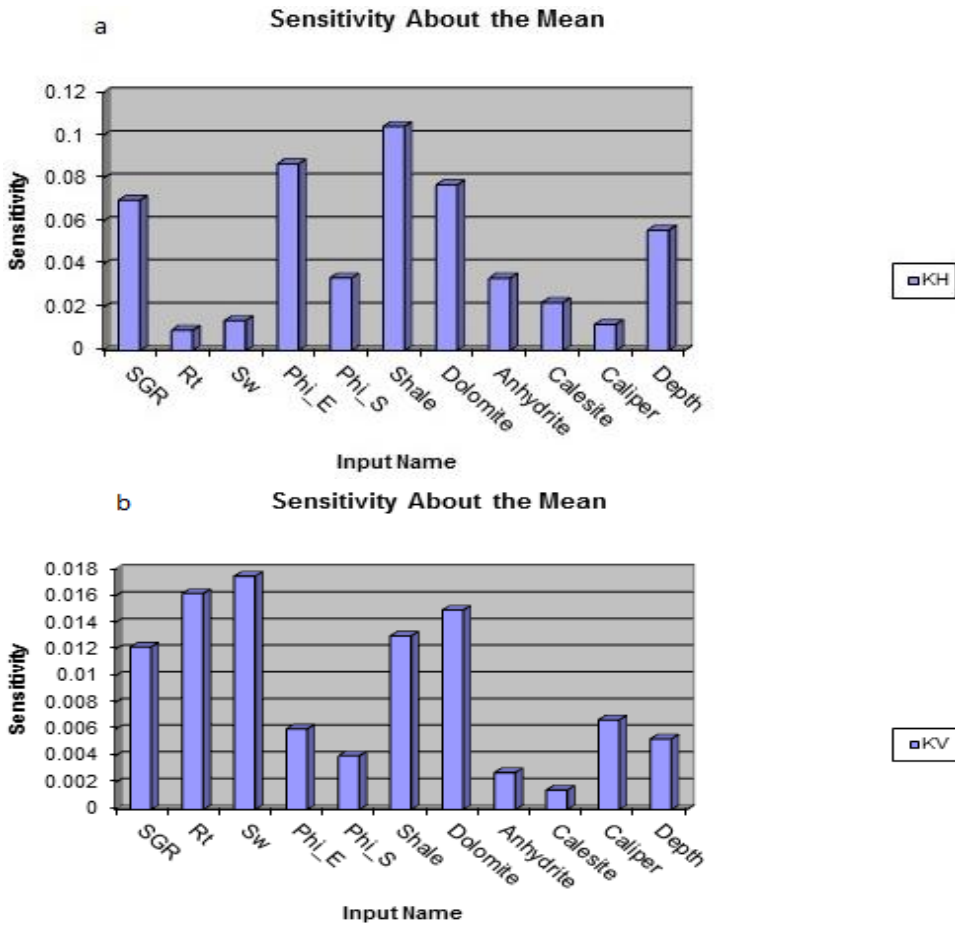


Figure 10. The effect of the input parameters used in the neural network training to estimate horizontal (a) permeability and (b) vertical permeability.

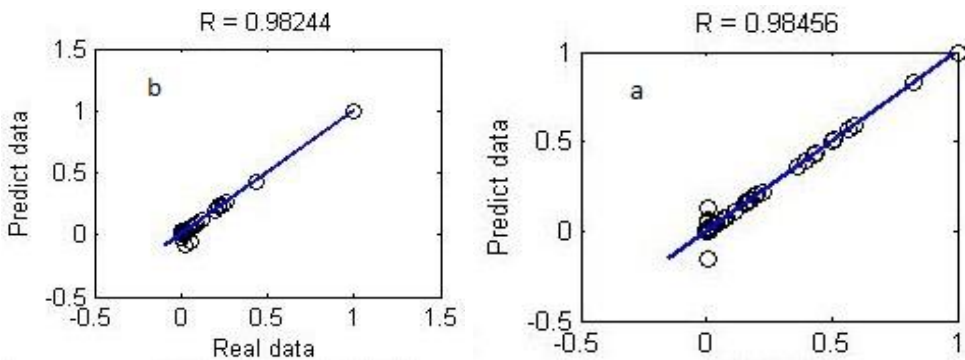


Figure 11. Comparison of the correlation coefficient and also the predicted permeability (vertical axis) using RBF method with normalized test data for (a) horizontal permeability and (b) vertical permeability.

Table 11. Comparison of the best values of R and MSE for normalized horizontal permeability data obtained from RBF (Education Network type Levenberg-Marquardt)

RBF	Parameter
0.99366	R (Total data)
0.00037785	MSE (Total data)
1.00	R (Learning data)
6.6118E-25	MSE (Learning data)
0.98456	R (Testing data)
0.0012663	MSE (Testing data)

Table 12. Comparison of the best values of R and MSE for normalized vertical permeability data obtained from RBF (Education Network type Levenberg-Marquardt)

RBF	Parameter
0.99247	R (Total data)
0.00023136	MSE (Total data)
1.00	R (Learning data)
2.96866E-25	MSE (Learning data)
0.98244	R (Testing data)
0.00077538	MSE (Testing data)

CONCLUSION

ANNs do not need complicated mathematical models, the important point is to select the adequate learning algorithm [10-18]. Furthermore, in ANN there is no need to know the rock lithology or the fluid filling the pores. Since the input layer neurons are functions of these parameters affecting the output, the input variables have to be selected so as to include the majority of parameters affecting the outputs, here the vertical and horizontal core porosities and permeabilities. ANN is a fast and effective technique to predict porosity and permeability in comparison with time consuming and costly laboratory techniques. The nonporous spots of the rock can be distinguished by logs and the results of this study to estimate horizontal and vertical porosity and permeability show that ANN can be an effective technique for prediction of reservoir parameters not only porosity and permeability but also its potential in reservoir studies. By both artificial intelligence techniques used in this work for normalized data, the best results were those obtained from MLP and RBF combined with GA and PSO optimization. Results show that MLP and RBF, if combined with optimization technique, deliver acceptable results for vertical and horizontal porosity and permeability predictions for the studied reservoir.

REFERENCES

- [1] Tahmasebi P, Hezarkhani A. A fast and independent architecture of artificial neural network for permeability prediction. *J of Petroleum Science and Engineering*; 2012, 86-87: 118-126.
- [2] Mohaghegh, S. Artificial Neural Networks as a Valuable Tool for Petroleum Engineers. *SPE J*: 29220; 1994.
- [3] Mohaghegh, S. Virtual intelligence and its application in petroleum engineering; 1. Artificial neural networks. *J Petrol. Technol*; 2000, 1–24 September.
- [4] Bean M, Jutten C. Neural networks in geophysical applications. *Geophysics* 2000, 65; 1032–1047.
- [5] Aminian K, Thomas B, Bilgesu HI, Ameri S, Oyerokun A. Permeability distribution prediction, *Proceeding of SPE Eastern Regional Conference*, October 2001.
- [6] Zuluaga E, Alvarez HD, Velasquez JD. Prediction of permeability reduction by external particles invasion using artificial neural networks and fuzzy models. *J. Can. Petrol. Technol*; 2002, 41 (6): 19–24.
- [7] Bhatt A, Helle HB. Committee neural networks for porosity and permeability prediction from well logs. *Geophys. Prospect*; 2002, 50: 645–660.
- [8] Rezaee, M. R., Nikjoo, M., Movahhed, B., Sabeti, N. Prediction of effective porosity and water saturation from wire line logs using artificial networks technique. *Journal of Geological Society of Iran*; 2006, Vol. 1: 21-27.
- [9] Rezaee, M. R., Kadkhodaie Ilkhchi, A. and Alizadeh, P. M. Intelligent approaches for the synthesis of Geophysics and Engineering, *Journal of Geophysics and Engineering*; 2008: 12-26.
- [10] Poggio, T., Girosi, F. Regularization algorithms for learning that are equivalent to multilayer networks, *Science* 1990, 247: 978–982.
- [11] Doyle, A.M., Schwaber, F.J., Show, J.S. A dynamic neural network approach to non-linear processing modeling. *Chem. Eng.* 1997: 385 – 371.
- [12] Han, J., Kamber, M. Data mining: concepts and techniques. *Morgan Kaufmann*, 2006.
- [13] Kennedy, J., Eberhart, R., “IEEE International Conference, vol. 4, pp. 1942{1948 (2002). DOI,” Particle swarm optimization. In: *Neural Networks Proceedings*, 1995.
- [14] Groupe, D. Principle of Artificial Neural Networks, Second ed. World Scientific Publishing Co Singapore; 2007.
- [15] Poggio T, Girosi F. Regularization algorithms for learning that are equivalent to multilayer networks. *J Science*; 1990, 247: 978-982.
- [16] Powell MJD. Radial Basis Functions for Multivariable Interpolation: A Review in IMA Conference on Algorithms for the Approximation of Functions and Data. RMCS, Shirvenham, UK, 1985: 143–167.
- [17] Demuth H, Beale M. Neural Network Toolbox User’s Guide, Copyright 1992-2002, By The Math Works, Inc, Version 4, 840 pp; 2000.
- [18] Holland, JH. Adaptation in Natural and Artificial Systems. University of Michigan Press, Ann Arbor, Michigan re-issued by MIT Press (1992); 1975.

Chapter 11

**PREDICTION AND ELIMINATION OF
DRILL STRING STICKING USING
ARTIFICIAL INTELLIGENCE TECHNIQUE**

***Hojat Toreifi¹, Abbas Khaksar Manshad², Habib Rostami³
and Amir H. Mohammadi^{4,5,6,*}***

¹Petroleum Engineering Department, School of Engineering,
Persian Gulf University, Bushehr, Iran

²Department of Petroleum Engineering, Abadan Faculty of Petroleum Engineering,
Petroleum University of Technology (PUT), Abadan, Iran

³Department of Computer Engineering, School of Engineering,
Persian Gulf University, Bushehr, Iran

⁴Discipline of Chemical Engineering, School of Engineering, University of KwaZulu-
Natal, Howard College Campus, King George V Avenue, Durban, South Africa

⁵Département de Génie des Mines, de la Métallurgie et des Matériaux, Faculté des
Sciences et de Génie, Université Laval, Québec, Canada

⁶Institut de Recherche en Génie Chimique et Pétrolier (IRGCP), Paris Cedex, France

ABSTRACT

Drill string stuck is a frequently occurring and risk-prone problem during drilling operation which imposes rises to the drilling cost of operations. Minimizing drill string stuck, today, is of priority in drilling engineering and has attracted attention as an important goal in drilling operation design. Currently, drilling engineers apply old and experimental methods and practices to prevent stuck drill string, by which it is hard to predict the nonlinear behavior of this challenge. Artificial neural networks are a new technique of solving engineering problems which are capable of simultaneous introduction of all effective parameters into account, nevertheless, they can learn and extend models directly from actual field data. In this work, two models have been designed using data from 33 wells in Maroun field. The first was developed to predict

* Corresponding Author E-mail: a.h.m@irgcp.fr and amir_h_mohammadi@yahoo.com.

stuck drill string (mechanical and pressure differential) by multilayer perceptron neural network optimized by open source development model algorithm (ODMA). The second model was developed using multilayer perceptron neural network optimized by particle swarm optimization algorithm, then to solve the differential pressure-stuck pipe the compound genetic-particle swarm algorithm was used. The high accuracy of these two models to predict stuck pipe motivates to utilize them both in well design and while operation. Analysis of the obtained models in conjunction with engineering judgments allows preventing stuck drill string by optimizing the influential parameters.

Keywords: drill string stuck, mechanical sticking, differential pressure sticking, drilling, artificial neural network (ANN)

NOMENCLATURE

Acronyms

ROP	rate of Penetration
ANN	annulus Diameter
WOB	Weight on Bit
MF Vis	mud filtrate viscosity
PV	plastic viscosity
YP	yield point
Initial Gel	initial gel strength
10 Min Gel	10 min gel strength
DC MT	drill collar metrage
RPN	rotation per minute

Variables

x_i	Position of ith particle
v_i	Velocity of ith particle
C_1, C_2	Trust factor
$rand$	Random number
R	Correlation coefficient
R^2	Coefficient of determination
MSE	Mean square error
RMSE	Rote mean square error

1. INTRODUCTION

Drill pipe sticking can be simply defined as downhole forces that prevent the pipe from rotation or pulling out of well. It is divided into two classes, mechanical and pressure differential sticking. In pressure differential sticking rotation and up and down movement of

the pipe is not possible but the mud can still circulate, whereas in mechanical sticking mud cannot circulate [1]. In case of a stuck drill pipe, immediate efforts should be put to free the pipe and drive the drilling operation ahead.

One of the conventional techniques to free the stuck pipe is to increase the tension upward and overload downward which is costly and time consuming, however in normal cases results in freeing the stuck pipe. In cases where not possible to free the pipe, the sticking problem is more stressed and the only way is to cut the drill string or to back-off the pipe by wireline free-point-indicator pack-off operations. In such severe cases, therefore, the drilled well usually has to be plugged up to the stuck point and deviated to continue the drilling operation, hence, the drilling plan has to be completely changed, thereby imposing additional cost and time consumption. In off-shore operations, stuck drill string can raise the costs of developing a well up to 30%, therefore a fundamental solution to predict and prevent this problem will be very requisite in terms of costs and time [2].

In the past, multivariable statistical analysis techniques and pipe sticking tests simulated with different drilling fluids were used to investigate and analyze pressure differential sticking conditions. Differentiating sticking types, the need to eliminating much data due to their dispersion and searching for the suitable technique were the essentials of most statistical correlations and techniques, much time and cost is required for pipe sticking simulation experiments on the other. Research on pipe sticking began in 1950. Kingsborough and Hempking worked on static analysis of pipe sticking based on drilling parameters, their work was based on comparison between wells in which stuck pipe occurred and those stuck-free (1985) [3]. That is they compared the parameters of the two classes and planned the drilling operations consistent with the parameters of stuck-free wells. They studied 121 parameters in 131 cases of stuck pipe in Mexico drilling operations and predicted the probability of stuck-pipe in nearby drilling operations. And, in 1994, Beigler and Kuhn investigated this problem by developing a data bank for 22 drilling parameters from 73 stuck-free wells and 54 wells experiencing stuck pipe in Gulf of Mexico [4]. They could not only predict the probability of pipe sticking, but could characterize its mechanism. These two works served as the basis for early analogical techniques. Howard and Glover, in 1994, could improve the pipe sticking prediction models by statistical techniques [5]. This work was conducted by testing 100 wells in Gulf of Mexico, the obtained models served for stuck-pipe prevention as well as for stuck-pipe freeing operations.

Application of artificial neural network for drill string sticking prediction was first tried by Halliburton in 2006 on pressure differential sticking in Gulf of Mexico [6]. Various parameters such as mud properties, downhole assembly configurations, formation properties, etc. play role in pipe sticking. Obtaining the interaction and correlation between the parameters contributing to pipe sticking takes a great deal of elaboration, artificial intelligence techniques are adequately capable of interpreting the complicated correlation of the multiple parameters in pipe sticking [7]. Using artificial intelligence methods in petroleum research becomes an emerging trend [21], [22]. In this study, a new model was developed for predicting and eliminating drill string sticking with artificial neural network and optimization algorithms. This method helps to predict and prevent pipe sticking by optimizing and improving the drilling parameters.

2. GEOGRAPHICAL LOCATION AND STRUCTURAL CHARACTERISTICS OF MAROUN OILFIELD

Maroun oilfield is located on the south of Northern Dezful syncline in line with Aghajari and Ramin anticlines. This large field was explored in 1963 by 2-D seismic survey and the presence of hydrocarbons in its Asmari reservoir was confirmed by drilling the first well. This field, in its Asmari reservoir, is 67km long and on average 5.5 km wide, the width ranges between 3.5 and 7 km. Geographically, this field is surrounded by Ramin field on the north, Koupal on the east, Shadegan and Ahwaz on the west and north-west and by Ramshir field on the south. Structurally, Maroun oil field is a long and narrow anticline with a northwest-southeast extension on the central and western part and northeast-southwest extension on its eastern end. Asmari formation is composed of deep marine sediments in the lowermost layer, semi-deep deposits in the mid layers and shallow sediments in the topmost layer. The altitude difference between the crest and the deepest water-oil contact in Asmari formation is 2000 meters. The dip of the flanks varies along the anticline, its symmetric on the eastern parts, asymmetric on the west to the central parts, steepest dip 70° . Figure 1 shows the geographical location of Maroun field. Figure 2 shows the well locations in Maroun field.

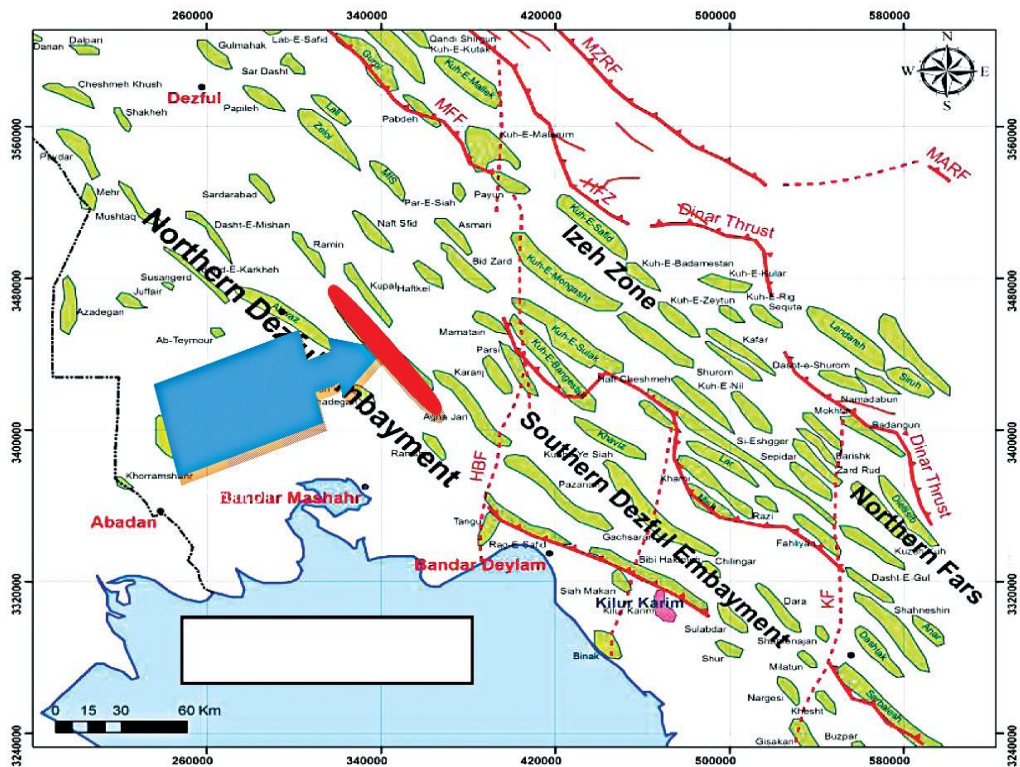


Figure 1. Maroun field geographical orientation in south west of Iran.

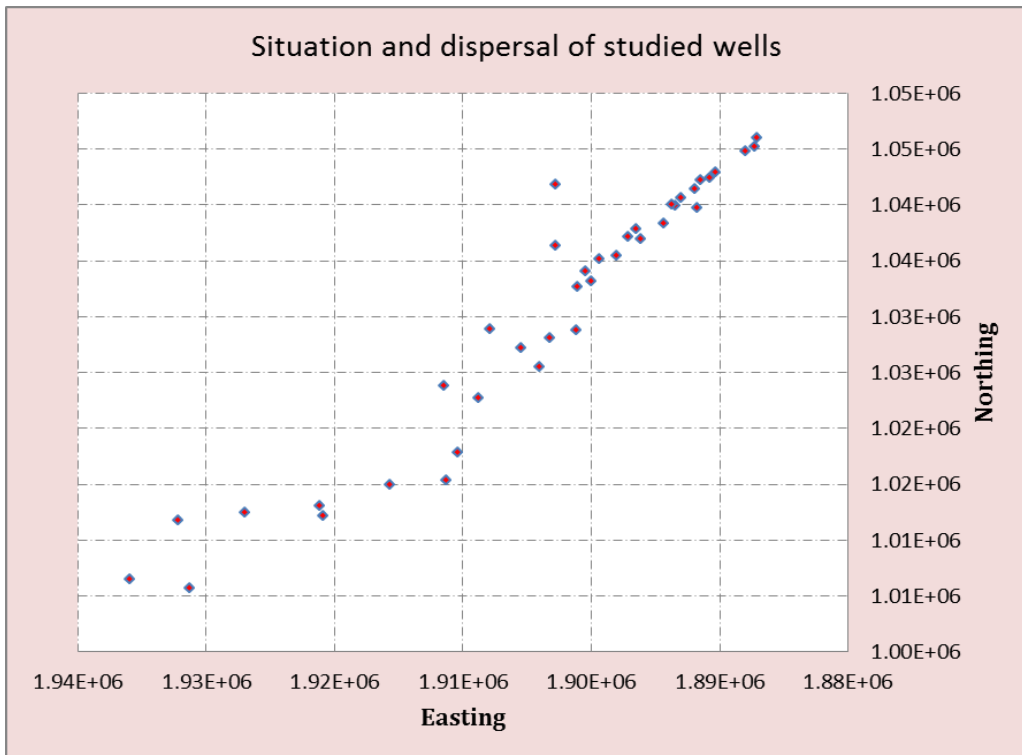


Figure 2. Wells locations in Maroun oil field.

3. ARTIFICIAL NEURAL NETWORK

Artificial neural networks are massively parallel distributed processing units known as neurons. These simple neurons have certain performance characteristics in common with biological neurons. Neural networks are capable of learning in order to recognize, classify, and generalize different systems. They are data-driven models that learn by examples presented to them. A typical neural network consists of three layers of neurons called input, hidden, and output layers. A neuron takes input values, which are multiplied by connection weights, from the proceeding neurons and adds them up with a value called bias and feeds them to its transfer function to produce results.

The majority of ANN's solutions have been trained with supervision. In this mode, the output of an ANN is compared to the desired output. Weights and biases, which are usually randomly set at the start, are then adjusted by a learning function in a manner such that the next iteration would result in a closer match between the desired and the network's output. The learning function works to minimize the current errors of all processing elements. During the training process, modifying the weights and biases continues by applying the same training data set until an acceptable network accuracy is reached [8].

4. METHAHEURISTIC OPTIMIZATION ALGORITHMS

In the last two decades, there has been a growing interest in evolutionary and swarm computing, which has inspired new ways for solving optimization problems. In contrast to traditional optimization methods, which emphasize accurate and exact computation, but may fall down on achieving the global optimum, evolutionary computation provides a more robust and efficient approach for solving complex real-world problems [9, 10]. Among existing evolutionary algorithms, the best-known branch is the genetic algorithm (GA). GA is a stochastic search procedure based on the mechanics of natural selection, genetics and evolution [11 - 13].

Compared with GA, PSO has some attractive characteristics. It has memory, so knowledge of good solutions is retained by all the particles; whereas in GA, previous knowledge of the problem is discarded once the population changes. It has constructive cooperation between particles; that is, particles in the swarm share information among themselves. To date, PSO has been successfully applied to optimizing various continuous nonlinear functions in practice [14].

Hybridization of evolutionary algorithms with local search has been investigated in many studies [15, 16]. Such a hybrid is often referred to as a mimetic algorithm. In the case at hand, we will combine two global optimization algorithms, i.e., GA and PSO, as PSO and GA both work with an initial population of solutions and combining the searching abilities of both methods seems to be a reasonable approach. Taking advantage of the compensatory property of GA and PSO, we propose a new algorithm that combines the evolutionary natures of both (denoted as GA-PSO).

Another swarm based optimization algorithm is Imperialist Competitive Algorithm (ICA) present in reference [20]. ICA is inspired by competition of imperialist countries to find global optima and solve the problems by simulation of the imperialist and colonies behaviors. Thus, it is a social inspired algorithm.

The most recent optimization algorithm is Open Source Development Model Algorithm (ODMA) [23]. It is a novel swarm-evolutionary metaheuristic optimizer inspired by open source development model and communities in such a way that each potential solution is considered as a software, and by evolution of the softwares, better solutions of the function that should be optimized are searched.

4.1. Genetic Algorithms (GA)

The discovery of genetic algorithms (GA) was dated to the 1960s by Holland and further described by Goldberg [11]. GA is a randomized global search technique that solves problems by imitating processes observed from natural evolution. Based on the survival and reproduction of the fittest, GA continually exploits new and better solutions without any pre-assumptions, such as continuity and unimodality. GA has been successfully adopted in many complex optimization problems and shows its merits over traditional optimization methods, especially when the system under study has multiple local optimum solutions.

GA evolves a population of candidate solutions. Each solution is normally coded as a binary string called a chromosome. The fitness of each chromosome is then evaluated using a

performance function after the chromosome has been decoded. Upon completion of the evaluation, a biased roulette wheel is used to randomly select pairs of better chromosomes to undergo such genetic operations as crossover and mutation that mimic nature. Should the newly produced chromosomes turn out to be stronger than the weaker ones from the previous generation, they will replace these weaker chromosomes. This evolution process continues until the stopping criteria are reached.

A real-coded GA uses a vector of floating-point numbers instead of 0's and 1's for implementing chromosome encoding. The crossover operator of a real-coded GA is constructed by borrowing the concept of linear combination of vectors from the area of convex set theory. The random mutation operator proposed for real-coded GA operates on the gene by introducing into it a perturbation that is a random number in the range of 0–1 in the feature's domain. With some modifications of the genetic operators, the real-coded GA has resulted in better performance than the binary coded GA for continuous problems [17].

4.2. Particle Swarm Optimization (PSO)

Particle swarm optimization (PSO) is one of the swarm optimization techniques developed by Eberhart and Kennedy [12]. PSO concept is based on a metaphor of social interaction such as bird flocking and fish schooling. The particles, which are potential solutions in the PSO algorithm, fly around in the multidimensional search space and the positions of individual particles are adjusted according to its previous best position, and the neighborhood best or the global best. Since all particles in PSO are kept as members of the population throughout the course of the searching process, PSO is the only evolutionary algorithm that does not implement survival of the fittest. As simple and economic in concept and computational cost, PSO has shown to successfully optimize a wide range of continuous optimization problems [18, 19].

4.3. Open Source Development Model Algorithm (ODMA)

Open source and proprietary closed are two kinds of software development methods [23]. Opening the source code enables a self-enhancing diversity of production plan, communication approach, and interactive communities. Generally, open source refers to a program in which the source code is available to the general public for use and/or modification from its original design. Open source code is normally created as a collaborative effort in which programmers improve the code and share the development within the community.

ODMA is presented according to analogy of open source software development [23]. As the most meta-heuristic algorithms, ODMA aims to search solution space of a given function.

In analogy to open source development model and community, ODMA considers each point in the solution space of the given function as open source software. Each considered software (point in the solution space) evolves over time by open source development mechanism such as employing features of leading softwares (point which have more optimum solutions) and forking from leading project. Over time, some softwares become leading or show to be promising and some of them can not develop enough; the latter ones are deleted

from the list of the softwares (the corresponding points in search space are deleted and do not processed any more).

The general steps of the ODMA algorithm are as follows:

- All softwares are initialized in random position in solution space.
- Each point in the solution space of a given function is considered as open source software.
- All softwares are evolved over time to get better position in the solution space according to the open source development mechanism (current top k softwares (points) are called leading softwares and the other points with the most progress are called promising softwares).
- The softwares with the least progress are removed after each iteration from the solution space and are not processed any longer.
- Some softwares are forked from leading softwares to exploit around them, and to explore the solution space. The forked softwares inherit some features of their base software.

4.4. Hybrid Genetic Algorithm and Particle Swarm Optimization

Figure 3 depicts the schematic representation of the hybrid GA-PSO. As can be seen, GA and PSO both work with the same initial population. When solving an N dimensional problem, the hybrid approach takes $4N$ individuals that are randomly generated. These individuals may be regarded as chromosomes in the case of GA, or as particles in the case of PSO. The $4N$ individuals are sorted by fitness, and the top $2N$ individuals are fed into the real-coded GA to create $2N$ new individuals by crossover and mutation operations, as shown in Figure 3. The crossover operator of the real-coded GA is implemented by borrowing the concept of linear combination of two vectors, which represent two individuals in our algorithm, with a 100% crossover probability. The random mutation operator proposed for the real-coded GA is to modify an individual with a random number in the problem's domain with a 20% probability. The effect of mutation rate is discussed in Section 4.1. The new $2N$ individuals created from real-coded GA are used to adjust the remaining $2N$ particles by the PSO method. The procedure of adjusting the $2N$ particles in the PSO method involves selection of the global best particle, selection of the neighborhood best particles, and finally velocity updates. The global best particle of the population is determined according to the sorted fitness values. The neighborhood best particles are selected by first evenly dividing the $2N$ particles into N neighborhoods and designating the particle with the better fitness value in each neighborhood as the neighborhood best particle. By Eqs. (5) and (6), velocity and position updates for each of the $2N$ particles are then carried out. The result is sorted in preparation for repeating the entire run. The hybrid algorithm, which is described in the four stages, terminates when it satisfies a convergence criterion that is based on the standard deviation of the objective function values of $N + 1$ best individuals of the population. It is defined as follows:

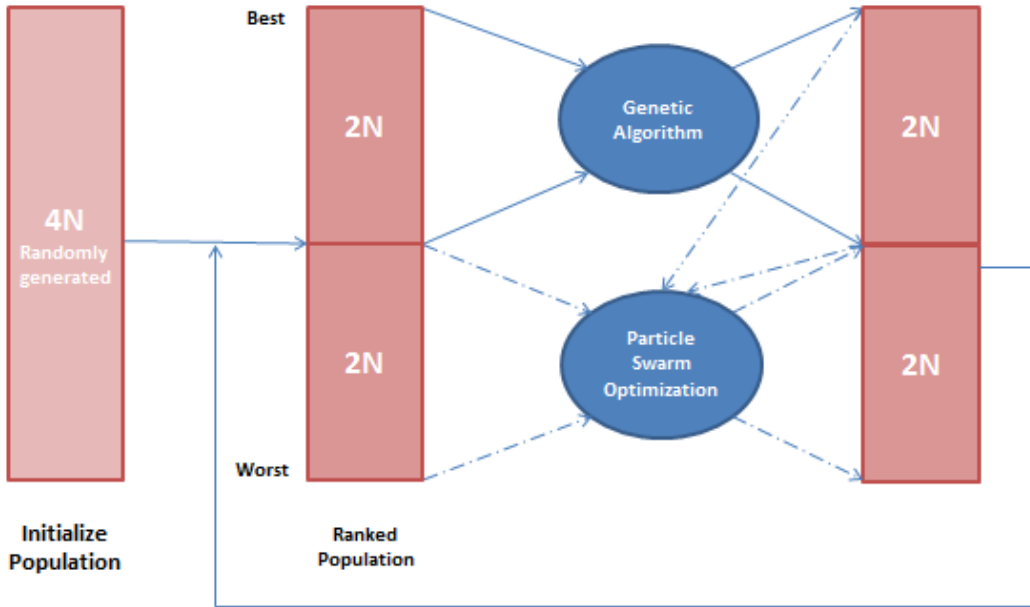


Figure 3. Schematic representation of the GA-PSO hybrid. (—>) Associated with the GA operation. (- ->) Associated with the PSO operation.

$$S_f = \left[\sum_{i=1}^{N+1} (f(x_i) - \bar{f})^2 / (N+1) \right]^{1/2} < v \tag{1}$$

where $\bar{f} = \sum_{i=1}^{N+1} f(x_i) / (N+1)$ and $v = 1 \times 10^{-4}$. Research regarding the parameter settings in the hybrid GA-PSO algorithm bears further scrutiny.

4.4.1. Initialization

Generate a population of size 4N for an N-dimensional problem. Repeat.

4.4.2. Evaluation and Ranking

Evaluate the fitness of each of the 4N individuals. Rank them on the basis of the fitness values.

4.4.3. GA Method

Apply real-coded GA operators (crossover and mutation) to the top 2N individuals and create other 2N individuals.

4.4.3.1. (Selection)

From the population, select the 2N best individuals according to fitness.

4.4.3.2. (100% Crossover)

Using the 2N best individuals, apply two-parent crossover to update the best 2N individuals by the following equations.

$$\mathbf{x}'_i = \text{Uniform}(0,1)\mathbf{x}_i + (1 - \text{Uniform}(0,1))\mathbf{x}_{i+1} \quad i = 1, 2, \dots, 2N + 1 \quad (2)$$

$$\mathbf{x}'_i = \text{Uniform}(0,1)\mathbf{x}_i + (1 - \text{Uniform}(0,1))\mathbf{x}_1 \quad i = 2N \quad (3)$$

4.4.3.3. (20% Mutation)

Apply mutation with a 20% mutation probability to the best 2N updated chromosomes according to the equation below:

$$\mathbf{x}'_k = \mathbf{x}_k + \text{rand} \times \mathbf{N}(0,1) \quad (4)$$

4.4.4. PSO method

Apply PSO operators (velocity and position updates) for updating the 2N individuals with worst fitness.

4.4.4.1. (Updates)

The particles velocities and positions are updated by the following equations:

$$\mathbf{v}_{id}^{\text{new}} = w \times \mathbf{v}_{id}^{\text{old}} + \mathbf{c}_1 \times \text{rand}(\mathbf{p}_{id} - \mathbf{x}_{id}^{\text{old}}) + \mathbf{c}_2 \times \text{rand}(\mathbf{p}_{gd} - \mathbf{x}_{id}^{\text{old}}) \quad (5)$$

$$\mathbf{x}_{id}^{\text{new}} = \mathbf{x}_{id}^{\text{old}} + \mathbf{v}_{id}^{\text{new}} \quad (6)$$

where \mathbf{c}_1 and $\mathbf{c}_2 = 2$ and $w = [0.5 + \text{rand}/2.0]$. Equation (5) illustrates that the new velocity for each individual particle is updated according to its previous velocity (\mathbf{v}_{id}), the best location in the neighborhood about the particle (\mathbf{p}_{id}) and the global best location (\mathbf{p}_{gd}). A particle's velocity in each dimension is clamped to a maximum velocity (\mathbf{v}_{\max}) and the maximum velocity \mathbf{v}_{\max} is set to a certain fraction of the range of the search space in each dimension. Equation (6) shows how each particle's position (\mathbf{x}_{id}) is updated during the search in the solution space. Until the termination criterion is reached.

4.5. Imperialist Competitive Algorithm (ICA)

ICA is another new and well-accepted metaheuristic algorithm. Like PSO and GA, ICA starts with an initial population (countries). Some of the most powerful (with the best fitness values) are selected as imperialists and the rest of countries and colonies of them. The

colonies are divided among imperialists in the initial population. Then these colonies move toward their corresponding imperialists [20].

Then the imperialistic competition is done among the empires. Any empire (Imperialist and the relevant colonies) which is not able to succeed in this competition (can not find good optimization points) will be eliminated. The competition gradually results in an increase in the power of powerful empires and a decrease in the power of weaker empires. By iteratively continuing the competition the most power full imperialist dominates all the countries. In the other words, the best solution in the solution space will be found.

5. METHODOLOGY AND RESULTS

Two models were developed using artificial neural networks in this work. In the first model, regarding that a considerable number of pipe sticking cases faced in Maroun field were of mechanical type, we decided to develop a model able to predict and solve both pipe sticking types first. In order to develop comprehensive model for predicting and diagnosing pipe sticking type, all the influential parameters had to be considered and taken into account. In this model, geographical coordinates (geographical east and north), present depth, rate of penetration, formation properties, open hole length, clearance between pipe and wellbore wall, weight on bit, drill string RPM, annular velocity of mud, mud pressure, mud cake viscosity, solid content of mud, mud salinity, mud plastic viscosity, mud yield point, initial mud resistance, mud resistance after 10 minutes and drill string length were considered as input parameters and sticking type was considered as output of the network (0, 0.5 and 1 for no sticking, pressure differential sticking and mechanical sticking respectively). We should note that layering and thickness of layers changes very slowly by geographical changes in the field (Figure 2). Thus, we can use geographical coordination of drilled wells as a feature to predict the behavior of other wells in the same field.

MLP optimized by ODMA has the best performance for the first problem. The neural network has a [8 4 1] structure (8 neurons in the first hidden layer, 4 in the second hidden layer and 1 neuron in the output layer), with Tansig and Poorline transfer function and Trainlim function.

The parameters of ODMA for optimizing the network are as follows: population size is 25, $k = 5$, $p = 10$, $\omega = 0.9$, $s = 3$ and 1000 iterations.

From 950 data sets (input and output), 874 sets associated with 33 wells, 86 sets of which represented sticking problem, were used in the modeling after eliminating the illogical data resulting from machine record error or human error. After normalizing, 60% of the data were used for learning, 15% for validation and remaining 25% for testing the network. The ranges of the parameters have been listed in Table 1.

We should note that by increasing the number of epochs, chance of memorization of the model increases. To control this phenomenon we use validation mechanism. The most accurate model is resulted using 1000 epochs. In this model, mean square error of training data and validation data are 0.00385 and 0.0051, respectively (Table 2). The remained 25% of data used as test data for evaluation of generalizability of the model. Table 3 and Figure 5 show the results. Mean square error of model on the test data is 0.00462. Figure 4 and Figure 5 show correlation of the predicted values with actual measured values. Correlation

coefficient and coefficient of determination of cross validation and test stages are 0.978, 0.958 and 0.992, 0.984, respectively.

Table 4 shows performance of MLP optimized by ODMA in comparison with the other methods. As it can be seen, MLP optimized by ODMA outperforms the others.

Table 1. The ranges of the parameters used in modeling

Range	Parameter
[1887105 – 1935965]	East
[1005701 – 1054298]	North
[164.04 – 17388.45]	Press Depth (ft)
[0 – 173.59]	Rate Of Penetration (ft/hr)
[10 – 95]	Formation
[1.64 – 8989.5]	Open Hole (ft)
[0.095 – 1.355]	Annulus (ft)
[0 - 80]	Weight On Bit (lb)
[0 - 208]	Annulus Velocity (ft/s)
[23.5 – 4523.7]	Mud Pressure (psi)
[0 - 100]	Mud Filtrate Viscosity (cp)
[0 - 490000]	Salt (ppm)
[0 - 62]	Ret Solid (%)
[0 - 120]	Plastic Viscosity (cp)
[0 - 105]	Yield Point (cp)
[0 - 18]	Initial Gel (lb/100ft ²)
[0 - 22]	10 Min Gel (lb/100ft ²)
[9 - 282]	Drill collar metrage (m)
[0 - 200]	RPM (rpm)
[0 - 1]	Stuck

Table 2. MLP&ODMA network learning and validation results

Best Network	Train	Cross Validation
Epoch	1000	1000
Minimum MSE	0.00385	0.0051
Final MSE	0.00385	0.0051

Table 3. MLP&ODMA network test results

Best Network	Test
MSE	0.00462
R	0.992

Table 4. Comparison of performance of the methods for the first problem (mechanical and pressure differential sticking)

Network	MSE	R	R ²
MLP and ODMA	0.00462	0.992	0.984
Support Vector Machine (SVM)	0.0362	0.978	0.956
MLP-PSO-GA	0.0052	0.96	0.92
MLP-PSO	0.048	0.91	0.83
MLP-GA	0.095	0.86	0.74

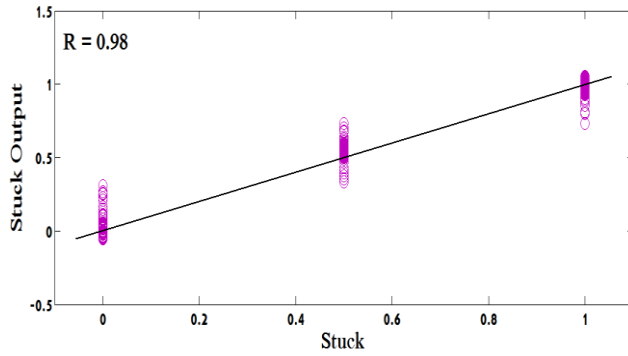


Figure 4. Correlation coefficient of MLP&ODMA network in the cross validation stage.

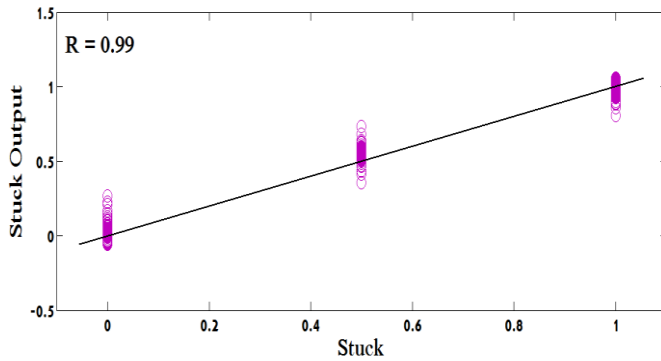


Figure 5. Correlation coefficient of MLP&ODMA network in the test stage.

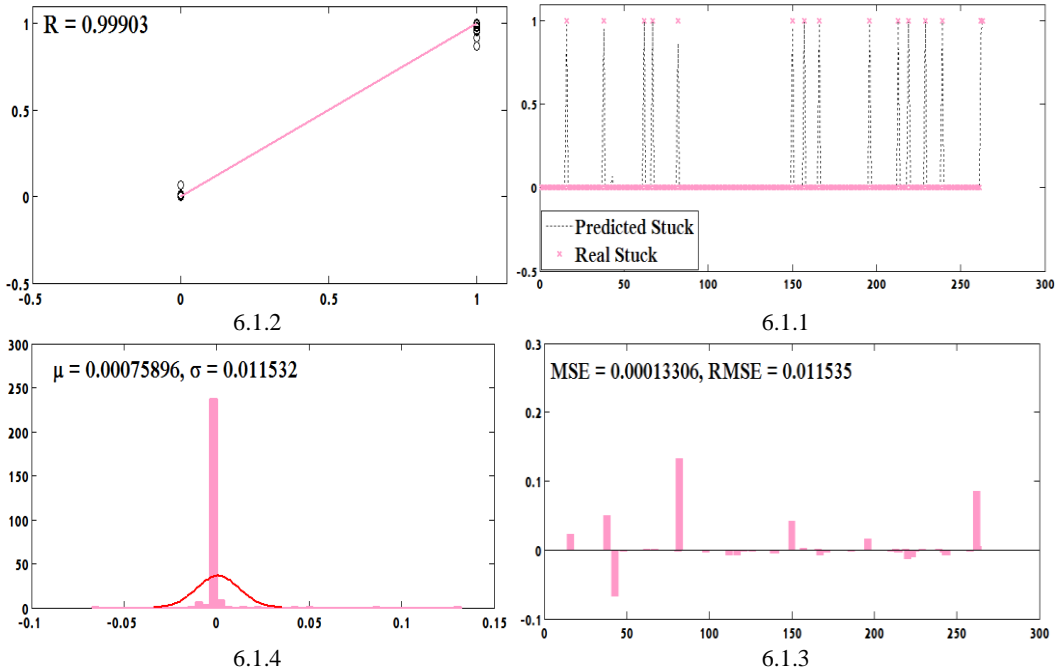


Figure 6.1. Results of multilayer perceptron neural network learning.
Figure 6. (Continued)

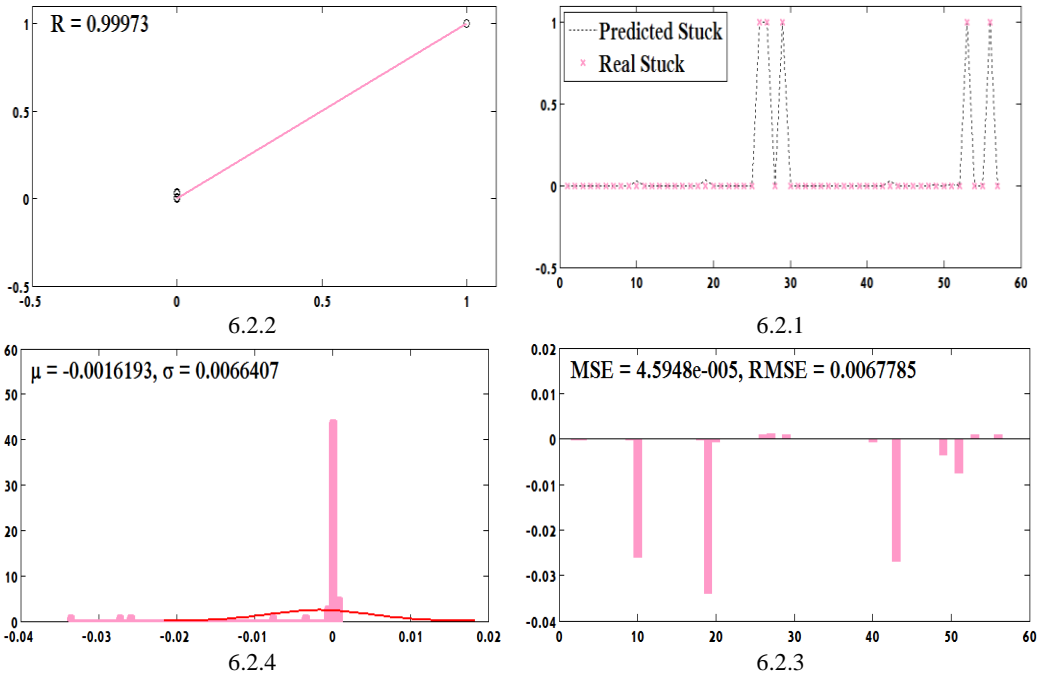


Figure 6.2. Results of multilayer perceptron neural network validation.

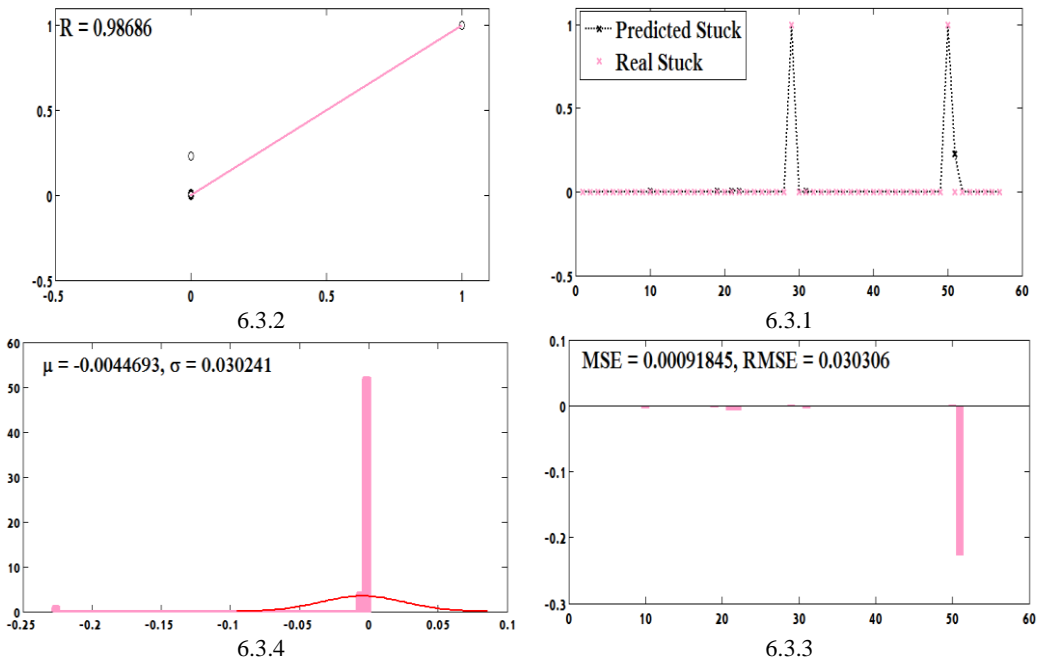


Figure 6.3. Results of multilayer perceptron neural network test.

Figure 6. Results of learning, validation and test of multilayer perceptron neural network optimized by PSO algorithm (on each sub-figure, the first figure compares the network output with the actual results, the second shows the correlation coefficient (R), the third shows the MSE and the forth presents the error distribution).

Table 5. The results of the multilayer perceptron neural network retest

	Network type				
	MLP	MLP-GA	MLP-PSO	MLP-GAPSO	MLP-ICA
Actual value	Predicted value				
0	0.2	0.12	0.069	0.15	0.02
1	0.79	0.66	0.996	0.99	0.59
1	0.83	0.91	0.951	0.89	0.67
0	0.36	0.09	0.004	0.66	0.05

The second model was developed to predict and solve pressure differential sticking; the mechanically stuck pipe data were not used in this model. Pressure differential sticking can be prevented and solved by improving the influential parameters. As the first step, a feed-forward multilayer perceptron neural network, optimized with particle swarm algorithm (PSO), was developed. The neural network has a [8 4 1] structure (8 neurons in the first hidden layer, 4 in the second hidden layer and 1 neuron in the output layer), with Tansig and Poorline transfer function and Trainlim function. In the PSO, the population size is 25 and the values of the parameters c_1 and c_2 equal 2. PSO was used to choose the optimized weight values and to increase the correlation coefficient of the neural network as a result. To improve the performance of the model the data were normalized in to fall in the interval of 0 to 1, here the pressure differential sticking data will be presented by 1 and sticking-free data by 0. The results associated with network learning, validation and test are shown, respectively, in Figures 6.1, 6.2 and 6.3.

Each figure presents four kinds of information. The first one is comparison of predicted values and actual measured values. The second results are correlation coefficient of the predicted and measured values. The third part shows mean square error and root mean square error of the predictions. The fourth subfigure shows distribution of errors. We should note that closer values of error distribution to zero shows better training of the neural network.

To verify the accuracy and performance of the model, it was again tested with the data not used in developing the model and the results of this test (retest) have been shown in Table 5. To build the model, we evaluated the ANN optimized with ICA, GA, PSO and GA-PSO. As it can be seen, MLP neural network optimized by GA-PSO shows the best performance (Table 5).

Compound GA-PSO was utilized to obtain the optimum values of the parameters, which is much more efficient than singular use of these algorithms. In the optimization, it is allowed to vary such parameters as weight on bit, drill string rotational speed (RPM), rate of penetration, open hole length, mud annular velocity and mud pressure, while formation type, geographical coordinates (orientation) and present depth have to be fixed. Using compound GA-PSO algorithm, network input parameter optimization was performed separately for each well in each formation having pipe sticking experience. The optimization results for parameters effective in pressure differential pipe sticking are presented in Table 6.

In order to ascertain the drill string sticking elimination, the optimized values and the fixed values of different points in the well were introduced into the network as input. The outputs are indicative of no sticking, that is sticking elimination. The optimized parameters test results are given in Table 7. As can be seen, the best way to eliminate differential pressure-stuck pipe is to use multilayer perceptron optimized by GA-PSO. It means that using this method we can prevent differential pressure-stuck pipe.

Table 6. The results of compound GA-PSO optimization of the parameters

Variable parameters															Fixed parameters		
SAIT	RPM	DC.MT	10 MIN Gel	Initial Gel	YP	PV	Ret.Solid	MF Vis	Mud Pressure	Annulus Velocity	WOB	ANN	Open Hole	ROP		Geographic coordinates and depth	Formation
305000	180	88	9	7	14	8	17	36	1331.7	85	30	0.5	7063	4.068	Present value	E = 1907895 N = 1028947 D = 2308	10
292142	397	610	25	10	26	72	36	60	2048	175.7	5	0.5	6683	32.5	Value optimized		
308000	80	88	6	5	11	9	18	36	1340	74	25	0.5	7109	3.084	Present value	E = 1907895 N = 1028947 D = 2322	10
308000	80	88	6	5	11	9	18	36	1340	74	25	0.5	7109	3.1	Value optimized		
315000	180	88	5	3	8	19	24	43	1774	78	30	0.5	8527	9.94	Present value	E = 1891929 N = 1041403 D = 2744	15
279921	187	446	14	15	26	103	48	38	1126	100.7	11	0.2	15.4	9.87	Value optimized		
320000	150	88	3	2	8	21	25	44	1859	65	45	0.5	8569	3.6	Present value	E = 1891929 N = 1041403 D = 2757	20
405574	617	492	18	18	31	95	8	75	1138	98.5	42	0.5	5055	26	Value optimized		
315000	180	88	5	4	15	25	27	43	1873	73	20	0.5	8182	7.9	Present value	E = 1897982 N = 1035439 D = 2641	20
167223	335	666	31	11	69	61	29	64	493	191.7	8	0.4	7828	20	Value optimized		
320000	180	190	7	5	20	59	40	58	2684	108	30	0.2	629	9.18	Present value	E = 1902807 N = 1036403 D = 2860	23
272414	408	482	21	7	30	44	42	59	403	192.6	18	0.6	8923	24.9	Value optimized		

Variable parameters															Fixed parameters		
SAIT	RPM	DCMT	10 MIN Gel	Initial Gel	YP	PV	Ret Solid	MF Vis	Mud Pressure	Annulus Velocity	WOB	ANN	Open Hole	ROP		Geographic coordinates and depth	Formation
330000	80	554	4	2	7	13	5	38	1584	180	15	0.2	287	13.8	Present value	E = 1907895 N = 1028947 D = 3863	45
262966	427	42	29	13	38	51	23	73	1099	208	5	0.5	5131	29	Value optimized		
343000	150	643	3	2	6	14	8	40	1592	179	20	0.2	1163	9.18	Present value	E = 1911491 N = 1023859 D = 3817	45
254883	333	465	23	13	12	80	27.5	72	2247	125	7	0.5	6847	27.9	Value optimized		
325000	0	184	4	3	11	30	12	60	1531	46	15	0.3	2431	4.9	Present value	E = 1915702 N = 1015000 D = 3103	55
219188	194	495	24	12	67	36	26	69	1848	172	13	0.5	8038	29.2	Value optimized		
415000	70	640	6	5	14	27	12	48	1808	93	20	0.1	739.8	4.9	Present value	E = 1908772 N = 1022719 D = 3663	65
183676	407	449	28	14	35	61	36	67	2011	150	11	0.4	8835	31.8	Value optimized		
440000	170	371	4	3	10	19	20	40	2371	117	30	0.3	6305	2.95	Present value	E = 1921140 N = 1013070 D = 4212	65
227992	358	462	22	16	36	62	32	56	1720	188	5	0.5	6397	25.6	Value optimized		
440000	75	643	8	7	12	40	37	48	4310	143	12	0.2	2534	5.6	Present value	E = 1920921 N = 1012193 D = 5166.5	85
43310	17	265	34	11	63	77	40	56	469	210	8	0.4	941	18	Value optimized		
300000	50	462	2	1	7	14	28	38	2531	172	15	0.2	12	4.26	Present value	E = 1905439 N = 1027193 D = 3310.7	95
244055	453	548	25	12	28	54	30	72	2114	141	8	0.4	656	29.5	Value optimized		

Table 7. Results of testing the optimization algorithm by the neural network

Input Parameters																			Output Parameter
Formation	Earth	North	Depth	ROP	Open Hole	ANN	WOB	ANN Velocity	Mud Pressure	MF Vis	Ret Solid	PV	YP	Initial Gel	10 Min Gel	DC Metrage	RPM	SALT	STUCK
10	1907895	1028947	7572	32.5	6683	0.54	5	175.7	2048	60	36	72	26	10	25	610	397	292142	0
10	1907895	1028947	7618	3.1	7109	0.57	25	74	1340	36	18	9	11	5	6	88	80	308000	0
15	1891929	1041403	9002	9.9	15	0.2	11	101	1126	38	48	103	26	15	14	446	187	279921	0
20	1891929	1041403	9045	26	5055	0.52	42	98	1138	75	8	95	31	18	18	492	617	405574	0
20	1897982	1035439	8664	20	7828	0.41	8	192	493	64	29	61	69	11	31	666	334	167222	0
23	1902807	1036403	9383	24.9	8923	0.67	18	193	403	59	42	44	30	7	21	482	408	272414	0
45	1907895	1028947	12673	29	5131	0.49	5	208	1099	73	23	51	38	13	29	42	427	262966	0
45	1911491	1023859	12522	28	6847	0.52	7	125	2247	72	27	79	12	13	23	465	333	254883	0
55	1915702	1015000	10180	29	8038	0.49	13	172	1848	69	26	36	67	11	24	495	194	219188	0
65	1908772	1022719	12017	32	8835	0.36	11	150	2011	67	36	61	35	14	28	449	407	183676	0
65	1921140	1013070	13818	26	6397	0.49	5	188	1720	56	32	62	36	16	22	462	358	227992	0
85	1920921	1012193	16948	18	941	0.36	8	210	469	56	40	40	63	11	34	265	17	43310	0
95	1905439	1027193	10859	29	656	0.44	8	141	2114	72	30	54	28	12	25	548	453	244055	0

Table 8. Comparison of the performance of the optimization algorithms

Optimization Algorithm	Present value	Model Output
ICA	1	0
	1	0.35
	1	0.55
PSO	1	0.79
	1	0.82
	1	0.65
GA	1	0.85
	1	0.99
	1	0.71
GA and PSO	1	0.93
	1	0.95
	1	1.06

CONCLUSION

1. The model presented for predicting and eliminating drill string sticking can predict mechanical and pressure differential pipe sticking both before and while drilling with very low costs.
2. In this method, by predicting the pipe sticking conditions, drilling engineers can eliminate the pressure differential sticking, hence, costs and operations associated with freeing the drill string can be eliminated which will in turn reduce rig costs and days.
3. MLP optimized by ODMA predicts mechanical and pressure differential sticking more accurate than the other methods.
4. Results show that Artificial Intelligence Techniques, ANNs and compound GA-PSO, are very efficient and accurate tools to predict stuck pipe and effective in drilling operation planning.
5. Besides, such conventional practices as avoiding long waiting while operation, continuous mud monitoring to check its properties and changes, trying to used the least possible mud solid content, using suitable wellbore stability additives and reducing drill string shakes to prevent key chain formation are also much recommended.
6. The developed model is based on Maroun oil field and to generalize the model to the other fields; we should retrain the model with the data of themselves with the same methodology explained in this study.

REFERENCES

- [1] R. Miri, J. Sampaio, M. Afshar, A. Lourenco. *Development of Artificial Neural Networks to Predict Differential Pipe Sticking in Iranian Offshore Oil Fields*. Mexico: SPE 108500, 2007. international Oil conference and Exhibition. pp. 27-30.

-
- [2] Helmick, W, R. and Longley, A. J. Pressure Differential Sticking of Drill Pipe and How It Can Be Avoided or Relieved. 1957, *Oil and Gas Jour.* 55, p. 132.
- [3] Hemphkins, W.B., Kingsborough, R.H., Lohec, W.E., Nini, C.J. *Multivariate Statistical Analysis of Stuck drill Pipe Situations*. September 1987, SPE Drilling Engineering.
- [4] Biegler, M.W. and Kuhn, G.R. *Advances in Prediction of Stuck Pipe Using Multivariate Statistical Analysis*. Dallas. Tx: SPE/IADC, February 1994. SPE/IADC Conference. pp. 15-18.
- [5] J.A. Howard, Enertech Engineering and Research Co., and S.S. Glover, Enertech Europe. *Tracking Stuck Pipe Probability While Drilling*. Dallas: SPE 27528, 1994. IADC/SPE Drilling conference.
- [6] C. Siruvuri, Halliburton Digital and Consulting Solutions, S. Nagarakanti, Nabors Industries and and R. Samuel, Halliburton Digital and Consulting Solutions. *Stuck Pipe Prediction and Avoidance: A Convolutional Neural Network Approach*. Dallas: SPE 98378, 1994. IADC/SPE Drilling conference.
- [7] Siruvuri, C., Nagarakanti, S., Samuel, R. *Stuck Pipe Prediction and Avoidance: A Convolutional Neural Network Approach*. Miami: SPE 98378, 2006. IADC/SPE Drilling Conference.
- [8] Demuth, H., Beale, M., and Hagan, M. *Artificial Neural Networks and Genetic Algorithms User's Guide. Revised for Matlab Programming v. 5.1*. s.l.: MathWorks, 2007.
- [9] Fogel, D.B. *Evolutionary Computation: Toward a New Philosophy of Machine Intelligence*, IEEE Press, Piscataway, NJ, 1995.1995.
- [10] (Ed.), X. Yao. *Evolutionary Computation: Theory and Applications*, World Scientific, Singapore. 1999.
- [11] Goldberg, D.E. *Genetic Algorithms in Search, Optimization and Machine learning*, Addison-Wesley, New York. 1998.
- [12] R.C. Eberhart, J. Kennedy. A new optimizer using particle swarm theory. Nagoya, Japan: s.n., 1995. Proceedings of the Sixth International Symposium on Micro Machine and Human Science. pp. 39–43.
- [13] J. Kennedy, R.C. Eberhart. Particle swarm optimization. Piscataway, NJ, USA: s.n., 1995. Proc. IEEE Int'l Conf. Neural Networks, Piscataway. pp. 1942-1948.
- [14] J. Kennedy, R.C. Eberhart, Y. Shi. *Swarm Intelligence*. San Francisco: Morgan Kaufmann, 2001.
- [15] R. Chelouah, P. Siarry. Genetic and Nelder–Mead algorithms hybridized for a more accurate global optimization of continuous multim minima functions. 2003, *Eur. J. Operat. Res.* 148, pp. 335–348.
- [16] S.F. Fan, E. Zahara. Hybrid simplex search and particle swarm optimization for unconstrained optimization problems. 2007, *Eur. J. Operat. Res.* 181, pp. 527–548.
- [17] C.Z. Janikow, Z. Michalewicz. An experimental comparison of binary and floating point representation in genetic algorithms. San Diego, CA, USA: s.n., 1991. Proceedings of the International Conference on Genetic Algorithms. pp. 31–36.
- [18] B. Brandstatter, U. Baumgartner. Particle swarm optimisation— mass-spring system analogon. 2002, *IEEE Trans. Magn.* 38, pp. 997-1000.
- [19] H. Yoshida, K. Kawata, Y. Fukuyama, S. Takayama, Y. Nakanishi. A particle swarm optimization for reactive power and voltage control considering voltage security assessment. 2000, *IEEE Trans. Power Syst.* 15, pp. 1232-1239.

-
- [20] E. Atashpaz-Gargari, C. Lucas. Imperialist Competitive Algorithm: An algorithm for optimization inspired by imperialistic competition. 2007, *IEEE Congress on Evolutionary Computation*. pp. 4661–4666.
 - [21] M. A. Ahmadi, M. Ebadi, A. Shokrollahi, S. M. J. Majidi. Evolving artificial neural network and imperialist competitive algorithm for prediction oil flow rate of the reservoir. 2013, *Applied Soft Computing*, 13 (2) pp. 1085-1098.
 - [22] S. O. Olatunji, A. Selamat, A. A. A. Raheem. Improved sensitivity based linear learning method for permeability prediction of carbonate reservoir using interval type-2 fuzzy logic system. 2014, *Applied Soft Computing*, 14, pp. 144-155.
 - [23] H. Hajipour, H. B. Khormuji, H. Rostami. ODMA: a novel swarm-evolutionary metaheuristic optimizer inspired by open source development model and communities. 2015, *Soft Computing*, DOI 10.1007/s00500-014-1536-x.

Chapter 12

INTEGRATED LOST CIRCULATION PREDICTION IN DRILLING OPERATION

*Abbas Khaksar Manshad¹, Habib Rostami²,
Hasan Niknafs³ and Amir H Mohammadi^{4,5,6,*}*

¹Department of Petroleum Engineering, Abadan Faculty of Petroleum Engineering,
Petroleum University of Technology (PUT), Abadan, Iran

²Department of Computer Engineering, School of Engineering,
Persian Gulf University, Bushehr, Iran

³Department of Petroleum Engineering,
Engineering and Basic Science Faculty, Khazar University, Baku, Azerbaijan

⁴Institut de Recherche en Génie Chimique et Pétrolier (IRGCP), Paris Cedex, France

⁵Département de Génie des Mines, de la Métallurgie et des Matériaux,
Faculté des Sciences et de Génie, Université Laval, Québec, Canada

⁶Discipline of Chemical Engineering, School of Engineering,
University of KwaZulu-Natal, Howard College Campus, King George V Avenue,
Durban, South Africa

ABSTRACT

Lost circulation is one of the most important issues that oil industry challenges with. Throughout drilling operation, cementing job or moving down the drilling pipes, great pressure of drilling fluid causes an over balance pressure on reservoir, so the drilling fluid penetrates the reservoir and is wasted. When the total loss happens, drilling pipes may stuck and make some incredible issues. One solution to this problem is under balance drilling. But many countries cannot drill with this method, because of financial problems or lack of technology. In this situation, it is better to know how drilling fluid moves and how much loss occurs, and then predict loss severity and add proper drilling fluid contents. Several obtainable factors affect circulation loss while drilling. This actually makes analytical modeling of loss circulation so complicated. Hereby, employing

* Corresponding Author E-mail: amir_h_mohammadi@yahoo.com AND a.h.m@irgcp.fr.

Support Vector Machine (SVM) can be a leeway with proven capability and accuracy. In this communication, operational parameters of one of the Middle Eastern oilfields were used to predict the mud loss severity along different sectors of this oilfield. Also, in this study cross validations and comparison with artificial neural network were applied.

Keywords: lost circulation, drilling, virtual intelligence, support vector machine, model

1. INTRODUCTION

Lost circulation is the most economical issue in drilling operation because of cost of mud losses and plugging in the throats. This phenomenon will have some consequences such as well instability, kick and blow out (Suyan et al., 2009). The amount of mud loss can vary from slow in consolidated formations to rapid in high permeable and fractured formations (Rojas et al., 1998). It will be much considerable when using heavy mud. Without adding plugging and bridging materials or loss circulation materials (LCMs) to drilling fluid, huge volume of mud may waste to the formation before it can be detected on surface, especially in fractured and unconsolidated formations (Moazzeni et al., 2013).

Circulation loss can be classified in different ways. One of these classifications has three groups with respect to the rate of loss: seepage loss (1-10 bbl/hr), partial loss (10-500 bbl/hr) and complete loss (500 bbl/hr) (Pilevari et al., 2002). In another classification, if the total loss is between 6 to 470 barrels or it takes less than 48hr to be treated by either increasing mud viscosity or increasing small amount of LCMs to the mud, it will be called minor loss. And when total loss is greater than 470 barrels or the time of treatment is greater than 48hr, it is called severe loss (Moazzeni et al., 2010).

In low rates, the loss will occur when dynamic bottom hole pressure exceeds minimum horizontal stress. When the bottom hole pressure goes up the horizontal stress will be increased (Economides et al., 1998, Charlez 1999). In the case of complete loss, the pressure of drilling fluid is enough to break down the wellbore wall. In this situation, rheological behavior of drilling fluid strongly affects the rate and the volume of loss (Majidi et al., 2008).

Parameters that affect loss circulation can be divided into two groups: formation parameters and operational parameters. Some parameters like formation pressure, fracture gradient and permeability distribution are formation parameters. Pump pressure, flow rate and drilling fluid properties are some examples of operational parameters. Some other effective parameters are wellbore and drill string geometry, mud rheology, sealing capacity of the drilling mud, hole cleaning efficiency (Burgoyne et al., 1991) and local stress field. These parameters have an interrelation with each other, so two big problems will occur. First, the analytical solution will be so difficult since we have more than one varying parameter, and second, the cost of investigations and removing the lost fluid will be too high. Thus, virtual intelligence machines are a good choice for predicting the loss circulation before drilling.

Previously, Sanfilippo et al., (1997), Lietard et al., (1999) and Majidi et al., (2008), each separately, developed models on drilling fluid circulation. Sanfilippo et al., (1997) developed a model in a non-deformable fracture of constant width with impermeable walls for Newtonian mud and then they modified their model for estimation of fracture aperture from drilling data. But there is a big problem in using this model. Most common drilling fluids are not Newtonian, so this model cannot be applied for them. Lietard et al., (1999) developed

their model for diffusion of drilling fluids to the single fracture. In this model, Darcy's law is combined with Bingham plastic model and the invaded zone radius is derived for different effective parameters versus time. Then, by curve fitting from results of real mud data, fracture aperture can be obtained (Moazzeni et al., 2009). Majidi et al., (2008) developed a theoretical model based on the work of Hemphill et al., (1993) on realistic rheological behavior of drilling fluids like Yield-Power-Law (YPL).

Above models explain the essential role of drilling fluid rheology on lost circulation in fractured reservoirs. These models cannot consider location of wells along the field. In the present work, according to Support Vector Machine (SVM) algorithm, a subset of above parameters is used for prediction of lost circulation. The parameters are selected using an attribute selection process.

2. MODELING APPROACH

Several models have been developed for prediction of drilling fluid invasion by combination of Darcy's law and drilling fluid properties. Mud rheology is the most important parameter on controlling drilling fluid invasion. Some models can predict mud rheology properties using bottom hole data. Another important parameter is intensity in addition to fracture aperture which must be considered to predict lost circulation. Unfortunately, recent models have not considered that. Therefore, in this paper, Maroun oilfield in Middle East is just selected because of presence of a highly fractured oil bearing zone which suffers from severe loss especially as oil production diminishes its pressure. Data from over 30 wells are used for evaluation of loss circulation. Since loss circulation is governed by very complicated and interrelated parameters, SVM modeling approach is used to predict the amount of mud loss quantitatively, and then interpretation of network-based mud loss is qualitatively done using neural network approach.

3. MODEL DEVELOPMENT

By developing computers and virtual machines lots of problems that cannot be solved by conventional analytical manner are solved. Recent machine learning and data mining tools are used to one or more attributes of "reason" such as generalization, discovery, association, and abstraction (Eberhart et al., 1996). To do this, support vector machine, artificial neural network, evolutionary programming and fuzzy logic are some useful examples of virtual machines. Integrating of these tools with conventional manners and of course with each other can be very useful in solving challenging problems perfectly (Mohaghegh et al., 2000).

3.1. Support Vector Machine

Support vector machines are based on training linear learning machines in the kernel-induced feature spaces, while respecting the insights provided by the generalization theory, and exploiting the optimization theory (Cristianini and Taylor 2000).

So drilling process must be classified to seepage, partial and complete lost circulation. But the problem is a ternary classification. Thus, a three class SVM is used. The basic support vector machines are binary classifiers which can categorize the target property (i.e., amount of lost circulation) into two classes. Hence, two classifiers should be generalized to three classifiers. The approach presented by Hastie and Tibshirani (1998) used to do this classification. The input of the model is the data from reservoir, drilling tools and drilling fluid materials, while the output is the prediction of the amount of loss circulation.

3.1.1. Linear Learning Machines

Binary classification using SVM is performed by using a real-valued function $f(X), f: R^n \rightarrow R$ in such a way that the input $X = (x_1, \dots, x_n)'$ is assigned to the positive class (+1) if $f(X) \geq 0$ and otherwise to the negative class. If $f(X)$ is a linear function, it can be written as

$$f(X) = \langle W, X \rangle + b = \sum_{i=1}^n w_i x_i + b \quad (1)$$

where $W \in R^n$ and $b \in R$. If the convention $\text{sgn}(0)$ is adjusted, then $\text{sgn}(f(X))$ is a decisive rule to determine the class (+1 or -1) of the input data. In this way, there is a hyper plane in $R^n \times R$ space, which separates instances of the two classes.

3.1.2. Kernel-Induced Feature Spaces

Computational power of linear learning machines is very limited (Minsky and Papert 1969). Kernel representation is a solution, which projects the data into a high dimensional feature space to increase the computational power of the linear learning machines. Therefore, the main idea of the kernel technique is to map input data to a higher dimensional space (feature space) in such a way that the projected data in the new space could be separated by a hyper plane (linearly) and then using a linear learning machine in the resulted space.

3.1.3. Generalization Theory

Another ingredient of support vector machines is generalization theory, which guides to control prediction error of the models. Some theoretical results give upper bounds for prediction error of unseen data in classification models. In this subsection, upper bounds will be reviewed.

As Vapnik and Chervonenkis presented the first bound, let H be a hypothesis space having VC dimension d . For any probability distribution on $P(X, y)$ on $X \times \{+1, -1\}$, with probability $1 - \delta$ over random training set S , any hypothesis $f \in H$ makes k errors on S no more than

$$\text{err}_p(f_s) \leq \frac{k}{l} + \frac{2}{l} \left(d \log \frac{2el}{d} + \log \frac{4}{\delta} \right) \quad (d \leq l), \quad (2)$$

In the mentioned error bound, l is number of training samples, e is base of the natural logarithm. VC dimension d is Vapnik and Chervonenkis dimension that for hyper planes is

at most equal to the dimensionality of the input space or number of attributes of the dataset (Vapnik and Chervonenkis 1964), (Vapnik and Chervonenkis 1971), (Cristianini and Taylor 2000). However, note that the presented bound usually is not tight and typically observed errors are much lower.

3.1.4. Optimization Theory

Optimization problem is finding the best separating surface in the feature space or finding maximum and minimum values of a function with given constraints, which is an ingredient of support vector machine.

In this section, soft margin support vector machine is used to find the best separating hyper plane. Thus, for solving optimization problem, $\min_{w,b,\xi} \frac{1}{2} w^T w + C \sum_{i=1}^l \xi_i$ subjects to $y_i (w^T \phi(x_i) + b) \geq 1 - \xi_i, \xi_i \geq 0, i = 1, \dots, l$. Therefore, optimization techniques can be applied to find the best separating hyperplane in the feature space.

3.1.5. Reducing Ternary SVM to Binary SVM

Several solutions have been proposed for using binary SVM classifiers to classify a multiclass problem (i.e., a problem with k classes, where k is more than two). Using lots of classes will reduce the multiclass problem to a set of binary problems. For instance, the simplest approach is to create one binary problem for each of the k classes. Hence, for each sample the given learning algorithm is applied to a binary problem. In this binary problem, all examples that were already labeled, are just considered as positive examples when all other examples considered negative ones, so k hypotheses must be combined. This is called the one-against-all approach (Allwein, Schapire and Singer, 2000).

Another approach that is used in the present work, was suggested by Hastie and Tibshirani (1998), and should be used as the given binary learning algorithm to distinguish each pair of k classes.

Therefore, for each sample, a classification using a binary SVM is applied to determine if it is categorized into seepage. Then, the same sample is tested against partial loss and finally against total loss. If the sample lies in only one class, then it is recognized as the member of that class, otherwise the class with highest margin will be selected.

3.2. Feature Selection

Feature selection is the process of finding a subset of features of the original data set with the most impact on target property (Hall 1999). For having a feature selection, all possible subsets of the mentioned features are incrementally searched. Then the relation between each subset and the target property is found by using:

$$r_{zc} = \frac{k \times r_{zi}}{\sqrt{k + k(k-1)r_{ii}}} \quad (3)$$

where r_{zc} is the relation between the features of the selected subset and the target property, k is the number of features of the selected subset, r_{zi} is the average of the correlations between features of selected subset and lost circulation and r_{ii} is the average inter-correlation between features of selected subset.

Now the subset with highest correlation should be selected as lost circulation class (Hall 1999).

Original data set includes the following features:

- Present driller depth of well in the day of study
- Present depth of well from sea level in the day of study
- Well trajectory (North and East direction in each data point of well path)
- Drilling time in the considered day
- Length of open hole section at the end of the day of study
- Asmari formation top from ground surface (Based on UGC data)
- Bit size (Exposure area)
- Average pump flow rate
- Average pump discharge pressure
- Mud weight
- Solid percent of drilling fluid obtained from retort solid equipment
- Achieved from rotational viscometer
- Mud filtrate loss gained from API filter press device
- Mud volume lost the day before the day of study
- Mud volume lost two days before the day of study
- Rock physical properties like porosity (Sonic log, Neutron porosity and bulk density),
- Rock type (Gamma Ray and Photo Electric Factor) and permeability of the interval
- Minimum horizontal stress profile

Based on the above feature selection algorithm, the following subset is selected as the results of the feature selection process:

- Well trajectory (North and East direction in each data point of well path)
- Mud volume lost in the day before the day of study
- Mud volume lost in two days before the day of study

The selected features show that previous behavior of the system is the best indicator of its current behavior.

4. RESULTS AND DISCUSSION

10 folds stratified classification selected to train and test the developed model. Furthermore, there are the following classes to determine the volume of lost circulations:

- Seepage loss when loss is less than 10 bbl/day (negligible).
- Partial loss when it is between 10 and 100 bbl/day.
- Complete loss when it is more than 100 bbl/day.

By using these classes, the model would be able to report the results qualitatively rather than quantitatively.

Radial Basis Function (RBF) kernel (Buhmann 2003) was used to map data to a feature space. RBF kernel was just used with the following equation for $k(x, x')$ to map input data to the feature space from training input (x) and test input (x'):

$$k(x, x') = e^{-(\alpha \langle x, x' \rangle - \|x - x'\|^2)}$$
(4)

where $\langle X, Y \rangle$ is dot product of X and Y . The different values of α influence the model accuracy. Figure 1 shows the effect of different values of α on accuracy of model in terms of correct classification.

Table 1. Classification performance of the model

Correctly Classified Instances	79.5%
Incorrectly Classified Instances	20.5%

Table 2. Confusion matrix of the model on test data

Class	True Positive Rate	False Positive Rate	Precision	Recall	ROC Area
Seepage	0.862	0.144	0.841	0.862	0.859
Partial loss	0.728	0.095	0.771	0.728	0.816
Complete loss	0.744	0.081	0.728	0.744	0.832
Weighted Avg.	0.795	0.115	0.794	0.795	0.84

Table 3. Comparison of the performance of the model with a previously published work (Moazzeni et al., 2009)

Correctly Classified Instances by our model	79.57%
Correctly Classified Instances by (Moazzeni et. al. 2009)	76%
Correctly Classified Instances by artificial neural network based on selected attributes.	78.3%

Table 4. Weights of connections between nodes of input layer and nodes of hidden layer in the developed neural network based on selected attributes

	Node 1	Node 2	Node 3	Node 4	Node 5
Easting	4.087	0.263	-3.846	-3.428	3.115
Northing	4.874	-0.571	2.912	-4.834	4.709
Last Day	-20.719	-21.161	-2.994	14.858	6.144
Two Last day	2.138	0.076	-7.534	-0.096	4.029
Bias	-9.959	-19.387	-11.358	7.155	-1.211

Table 5. Weights of connections between nodes of hidden layer and nodes output layer in developed neural network based on selected attributes

	Seepage	Partial Lost	Complete Lost
Node 1	3.255	1.620	-5.135
Node 2	4.196	-5.251	0.611
Node 3	1.851	-1.795	-1.688
Node 4	-6.561	-4.274	-0.617
Node 5	-6.022	-5.196	-3.854
Bias	-5.715	1.439	2.332

Table 1 shows the performance of the model. It seems that the model predicts loss circulation behavior correctly on about 80 percent of cases. Table 2 shows confusion matrix of the model. This table also confirms the performance of the model represented by Table 1.

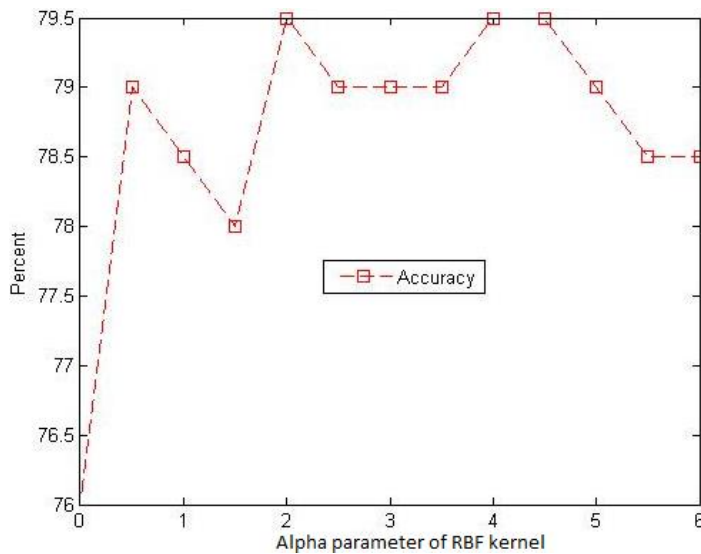


Figure 1. Effect of different α values on accuracy of the model.

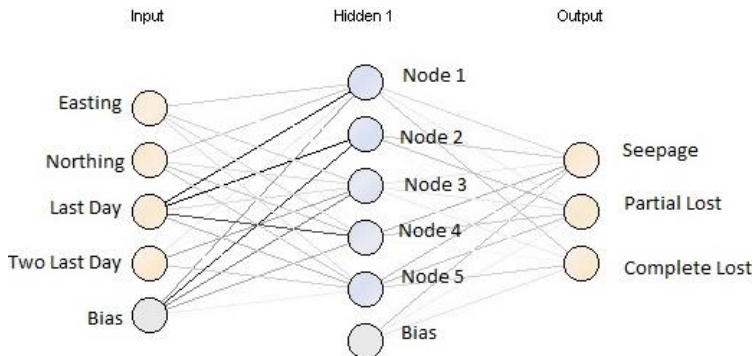


Figure 2. The topology of the developed neural network based on selected attributes. All nodes of hidden layer and outputs are sigmoid.

Table 3 compares the performance of the model with a work reported by (Moazzeni et al. 2009). They used a neural network based model to predict lost circulation. Besides, both models were tested using the same data set.

An artificial neural network model (Figure 2, Tables 4 and 5) was developed based on selected attributes. The performance of this model is reported in Table 3. As can be seen, using selected attributes increases performance of the neural network. Thus, results show that support vector machine based model outperforms the previous model as well as the trained neural network based on selected attributes, in term of classification precision.

CONCLUSION AND RECOMMENDATION

1. A methodology was proposed for prediction of lost circulation in any coordinates of field using operational and geological data.
2. Proposed methodology is based on multiclass support vector machine and its ability to solve complicated problems was proven.
3. Before developing the support vector machine model, we did some preprocessing on the dataset including feature selection. The results show that the best indicator for predicting lost circulation in a drilling operation is its previous behavior in previous days.
4. The most common drilling problem is lost circulation, especially in fractured formations.
5. Lost circulation is governed by numerous factors that make finding analytical solution with acceptable accuracy very difficult or impossible.
6. Support vector machine is recommended while dealing with different interrelated parameters (like lost circulation).
7. The results are just for the field under study and should not be used for another field even nearby ones.

REFERENCES

- Allwein, E. L., Schapire, R. E. and Singer, Y. (2000). Reducing Multiclass to Binary: A Unifying Approach for Margin Classifiers. *Journal of Machine Learning Research*, 1, 113-141.
- Buhmann, M. D. Radial Basis Functions: Theory and Implementations. Cambridge University Press, 2003.
- Burgoyne, A. T., Millheim, K. K., Chenevert, M. E., Young, F. S., Applied Drilling Engineering, *SPE Textbook Series*, Volume 2, 1991.
- Charlez, Ph. A.,: The Concept of Mud Weight Window Applied to Complex Drilling, SPE 56758, SPE Annual Technical Conference and Exhibition, Houston, Texas, 3 - 6 October 1999.

- Dupriest, F. E.: Fracture Closure Stress (FCS) and Lost Returns Practices, SPE 92192, SPE/IADC Drilling Conference, Amsterdam, Netherlands, 23-25 February 2005.
- Dyke, C. G., Wu, B., Milton-Taylor, D.: Advances in Characterizing Natural-Fracture Permeability from Mud-Log Data, SPE 25022, Europe Petroleum Conference, Cannes 1995.
- Eberhart, R., Simpson, P., and Dobbins, R.: Computational Intelligence PC Tools, Academic Press, Orlando, Florida, 1996.
- Economides, M. J., Watters, L. T. and Dunn-Norman, S.: Petroleum Well Construction, Chapter 5, pp. 135, John Wiley and Sons, New-York, 1998.
- Hall, M. A. (1999). Orrelation-based Feature Selection for Machine Learning. Ms. Thesis.
- Hastie, T. and Tibshirani, R. (1998). Classification by pairwise coupling. *The Annals of Statistics*, 26 (2), 451-471.
- Hemphill, T., Campos, W., Pilehvari, A.: Yield-Power Law Model More Accurately Predicts Mud Rheology, *Oil and Gas Journal* 91, no. 34 (August 23, 1993) 45-50.
- Hertz, J., Krogh, A., and Palmer, R. G.: Introduction to the Theory of Neural Computation, Addison-Wesley Publishing Co., Redwood City, California, 1991.
- Hopfield, J. J.: "Neural Networks and Physical Systems with Emergent Collective Computational Abilities," *Proc., Natl. Academy of Science* 79, 2554, 1982.
- Lietard, O., Unwin, T., Guillot, D. J., Hodder, M. H.: Fracture Width Logging While Drilling and Drilling Mud/Loss-Circulation-Material Selection Guidelines in Naturally Fractured Reservoirs," SPEDC (September 1999) 168-177.
- Majidi, R., Miska, S. Z., Yu, M., Thompson, L. G., Zhang, J.: Modeling of Drilling Fluid Losses in Naturally Fractured Formations, SPE 114630, SPE Annual Technical Conference and Exhibition, Denver, Colorado, USA, 21-24 September 2008.
- Majidi, R., S. Z., Miska, Yu, M., Thompson, L. G.: Quantitative Analysis of Mud Losses in Naturally Fractured Reservoirs: The Effect of Rheology, SPE 114130, *SPE Western Regional and Pacific Section AAPG Joint Meeting, Bakersfield*, California, USA, 31 March-2 April 2008.
- McCulloch, W. S. and Pitts, W.: A Logical Calculus of Ideas Immanent in Nervous Activity, *Bull. Mathematical Biophysics*, 1943.
- Minsky, M. L. and Papert, S. A.: Perceptrons, MIT Press, Cambridge, Massachusetts, 1969.
- Moazzeni A. R., Nabaei M., Ghadami jegarlooeei S.: Optimizing Size Distribution of Limestone Chips and Shellfish as Lost Circulation Materials, 6th International Chemical Engineering Conference (ICheC), 2009.
- Moazzeni, A., Nabaei, M.: Drilling Engineering, Kankash Publication, Vol. 2, Chapter 3, *Drilling Problems*, PP 321-322, 2010.
- Mohaghegh, S.: Virtual-Intelligence Applications in Petroleum Engineering: Part 1, Artificial Neural Networks, *JPT - Journal of Petroleum Technology*, October 2000.
- Pilehvari, A., Nyshadham, V. R.: Effect of Material Type and Size Distribution on Performance of Loss/Seepage Control Material, SPE 73791, Texas A&M University-Kingsville, p 13, 2002.
- Rojas, J. C., Bern, P. A., Fitzgerald, B. L., Modi, S., Bezant, P. N.; Minimizing Down Hole Mud Losses, IADC/SPE 39398, Presented at the IADC/SPE Drilling Conference, Dallas, 3 - 6 March, 1998.
- Rosenblatt, F.: "The Perceptron: Probabilistic Model for Information Storage and Organization in the Brain," *Psychol. Rev.* 65, 386, 1958.

-
- Rumelhart, D. E. and McClelland, J. L.: *Parallel Distributed Processing, Exploration in the Microstructure of Cognition*, Foundations, MIT Press, Cambridge, Massachusetts, 1986.
- Sanfillippo, F., Brignoli, M., Santarelli, F. J., Bezzola, C.,: *Characterization of Conductive Fractures While Drilling*, SPE 38177, SPE European Formation Damage Conference, The Hague, The Netherlands, 2–3 June, 1997.
- Stubbs, D.: “Neurocomputers,” *M. D. Computing* 5, No. 3, 14, 1988.
- Widrow, B.: “Generalization and Information Storage in Networks of Adeline Neurons,; Self-Organizing Systems, M. C. Yovitz, G. T. Jacobi, and G. D. Goldstein (eds.), Spartan Books, Washington, DC 435–61, 1962.

Chapter 13

OPTIMIZATION OF DRILLING PENETRATION RATE IN OIL FIELDS USING ARTIFICIAL INTELLIGENCE TECHNIQUE

***Abbas Khaksar Manshad¹, Habib Rostami²,
Hojjat Toreifi² and Amir H. Mohammadi^{3,4,5,*}***

¹Department of Petroleum Engineering, Abadan Faculty of Petroleum Engineering,
Petroleum University of Technology (PUT), Abadan, Iran

²Department of Computer Engineering, School of Engineering,
Persian Gulf University, Bushehr, Iran

³Discipline of Chemical Engineering, School of Engineering,
University of KwaZulu-Natal, Howard College Campus,
King George V Avenue, Durban, South Africa

⁴Département de Génie des Mines, de la Métallurgie et des Matériaux, Faculté des
Sciences et de Génie, Université Laval, Québec, Canada

⁵Institut de Recherche en Génie Chimique et Pétrolier (IRGCP), Paris Cedex, France

ABSTRACT

In drilling operation, the penetration rate depends on the factors such as the type of bit, formation properties, weight on bit (*WOB*), rotation per minute (*RPM*), and mud properties. We have used multi-layer perception (MLP) neural networks for optimization of drilling operation. The two models using neural networks have been developed for determining the type of bit and rate of penetration (*ROP*), then the inputs of the second model were optimized by the genetic algorithm (GA) to access maximum rate of penetration. To predict the type of bit and penetration rate in testing phase, the correlation coefficients were obtained 0.98 and 0.96, respectively, which show the capability of the aforementioned model in optimizing drilling operation.

* Corresponding Author E-mail: amir_h_mohammadi@yahoo.com AND a.h.m@irgcp.fr.

Keywords: Drilling, optimization of penetration rate, Bit selection, Artificial neural network (ANN), Genetic Algorithm (GA)

NOMENCLATURE

C_{angle} = Angel correction factor

D_{50cut} = Average size of particles, in

ESV = Corrected speed

MW = Density of drilling mud, PPG

D_{enp} = Density of drilling particles, PPG

D_p = Diagonal of particles, in

θ_{angle} = Inclination angel of well from vertical position, degree

MSE = Mean Square Error

ρ_{mud} = Mud density, PPG

C_{mw} = Mud weight correction factor

D_{pipe} = Outside diagonal of the drilling pipe, in

μ_a = Outward viscosity, cp

C_{size} = Particle size correction factor

PV = Plastic viscosity, cp

ROP = Rate of penetration, ft/sec

D_{hole} = The diagonal of well, in

V_{min} = The minimum speed of needed mud, ft/sec

V_{cut} = The speed of retail transfer, ft/sec

V_{slip} = The speed of vibration, ft/sec

INTRODUCTION

Analysis of field data is the main element of cost reduction and the improvement of drilling operation as well as the development of the tools of field data analysis is considered as a way of developing and improving drilling operation.

The two approaches, mechanical specific energy and the models of drilling penetration speed are used for optimization. The mechanical specific energy is referred to the amount of work needed for a certain volume of rock to be drilled. The concept of specific energy was first introduced by Teale (1985).

$$SE = \frac{WOB \times RPM}{D \times ROP}, \quad (1)$$

where the *WOB* is the weight on the bit in pounds (lb), *RPM* is the rotation of drilling bit per minute (rev/min), *ROP* is rate of penetration in foot per hour (ft/hr), *D* is the diameter in foot (ft), and *SE* is the Specific Energy. Rabia et al. (1985) only used three drilling parameters for evaluating the *SE* in rock drilling. These parameters were the weight on bit, speed of drilling bit, and the torque of bit.

A drilling model includes equations for penetration rate and bit erosion. There are numerous models in this field that have been used to relate the various parameters involving in the process of drilling on penetration rate. These models use important drilling parameters such as weight on bit and the rotation speed of drillstring for evaluation and prediction of the performance.

The Bourgoyne and Young (1974) model excels among all introduced models, because it includes almost all the formation parameters and drilling variables.

One of the newest models of drilling is utilization of artificial neural networks. Bilgusue et al. (2000) used the neural network for choosing bit in which the drilling parameters were used, however, formation parameters which play an important role in choosing bit were not considered.

Yilmaze et al. (2002), developed this model using the compressive strength average of formation, however, he only worked on bit selection and did not investigate evaluation of the optimal values of drilling parameters and how to increase drilling penetration rate. Edalatkhah et al. (2010), determined appropriate drill bit and also improved drilling penetration rate. In this communication, a method is introduced using artificial neural networks and genetic algorithms.

Initially, in this method, the appropriate bit is chosen by comparing the performance of different bit in drilling the wells of an oil field, to access the maximum penetration rate. Then, to achieve the maximum drilling penetration rate, a model is first constructed to predict the penetration rate, and secondly, the optimal values of the drilling parameters are calculated using genetic algorithm. Using this method, the appropriate bit and other parameters can be determined in order to achieve the maximum penetration rate. Increasing the amount of penetration rate and determining mud properties, optimal values of the weight on bit, and the rotation speed of drill string result in decreasing the costs as well as the time of drilling operation.

In the present work, in addition to increasing the accuracy of the model (using and comparing optimization algorithms and different neural networks and using the best algorithm and neural network in optimizing and modeling), we have tried to develop a more comprehensive model that includes all the effective parameters on drilling operations.

MODEL

Neural networks are parallel processing systems used for recognizing very complicated patterns among data. An artificial neural network is an information processing system that has some features common to biologic neural networks. Therefore, each network has been formed

from a collection of neurons that are arranged in particular. The main part of a neural network is the neurons and the connection lines between them (Demuth et al., 2007). One type of neural network is perception which is available as a single-layer perception and multi-layer perception (MLP). Perception neural networks are categorized within feed forward neural networks. Single-layer perception can classify separated linear problems and for complicated matters, it is necessary to use a greater number of layers (Demuth et al., 2007). MLP network consists of an input layer, one or more hidden layers and an output layer. In this structure, the neurons in one layer are connected to all neurons of the next layer which will finally form a network with complete connections (Demuth et al., 2007).

To reduce computational burden and determine suitable value of variables (weights and biases), optimization algorithms that have specific ability in this domain should be applied. For optimizing, the Genetic Algorithms (GA) has been used in this study. Genetic Algorithm is a population based algorithm that has proven to be successful in solving difficult optimization problems. A genetic algorithm for solving a problem, produces a large collection of possible methods. Each of these methods is evaluated using a coordination function. Then, a few numbers of the best solutions result in making new solutions. Thus, the search space will evolve in direction that reaches the optimal solution. If selection of parameters is correct, this method can perform effective (Demuth et al., 2007).

Oil Field

Ahwaz oil field is in Khuzestan province in southwest of Iran. This field includes anticline with the length of 67 and width of 6 square kilometers that is nearby Ramin (from the north), Maroom (field from the east), Shadegan and Mansoori (from the south) and Ab Teymour and Sousangerd (from the west). This field that contains the trend of north-west south-east is parallel to the Zagros mountain range. This field consists of three reservoirs namely Asmari, Bangestan, and Khami. Asmari reservoir contains the section of sandstone of Ahwaz. Bangestan reservoir is made of limestone, shale and anhydrite with less porosity than the Asmari and Khami reservoirs. From the reservoirs of Asmari and Bangestan, almost 800 thousand barrels are extracted per day. The amount of the residual oil in Bangestan reservoir is 31 billion barrels and the amount of the extractable oil is 4.3 billion barrels. Also, the amount of cumulative production has been announced 935 million barrels. The Bangestan reservoir consists of two major reservoirs named Ilam and Sarvak. At this moment in time, the production rate of Ilam and Sarvak reservoirs are 12 and 88 percent, respectively.

METHODOLOGY AND RESULTS

To have a comprehensive and pervasive model in choosing bit and determining the penetration rate, it is needed to consider all the parameters affecting drilling operations. With regard to the effect of the drilling mud on the penetration rate, drilling mud characteristics have also been considered as input parameters of the neural networks. In current studies, two models were developed using neural network.

The first model, since the drilling bit has a significant effect on the rate of penetration and can be, the main parameter for improving the penetration rate, a separated model has been made for choosing the drilling bit. In this model, size of bit, total flow area (*TFA*), drilling interval, depth in, depth out, weight on bit, rotation per minute of drilling string, rate of penetration, mud circulation rate, pressure, mud plastic viscosity, and average unconfined compressive strength of formation (*UCS*) are inputs for *ANN* and the output is the type of drilling bit based on *IADC* code.

The best developed neural network for the first model is the feed forward multi-layer perception neural network with the instruction of [4 1] (4-hidden layers and an output layer) and the transporting functions of tansig and poorlinand and the educating function of trainlim. Among 332 collections of data (input/output) and after removing illogical data which were the indicator of machines or human error, 299 data collection related to 10 different wells were used in training, cross validation and network testing. 70 percent of data put into work for training, 15 percent for cross validation and 15 percent for network testing. The range of the used parameters is listed in Table. 1. Figure 1 illustrates the correlation coefficient neural network model to predict the drill bit.

Table 1. The range of the parameters used in modeling

Parameter	Range
Weight on bit (<i>1000lb</i>)	10-80
Rotation speed of drill string (<i>rev/min</i>)	20-220
Total flow area (<i>in²</i>)	0.3-1.533
Plastic viscosity (<i>cp</i>)	2.5-75.93
Pump pressure (<i>psi</i>)	312.5-3328.57
Mud circulation rate (<i>gpm</i>)	116.7-1000
Input depth (<i>ft</i>)	187-10657
Bit size (<i>in</i>)	8.5-17.5
Drilling interval (<i>ft</i>)	3.28-4706.8
Rate of penetration (<i>ft/hr</i>)	0.95-86.56
Unconfined compressive strength (<i>psi</i>)	826.72-25969.66

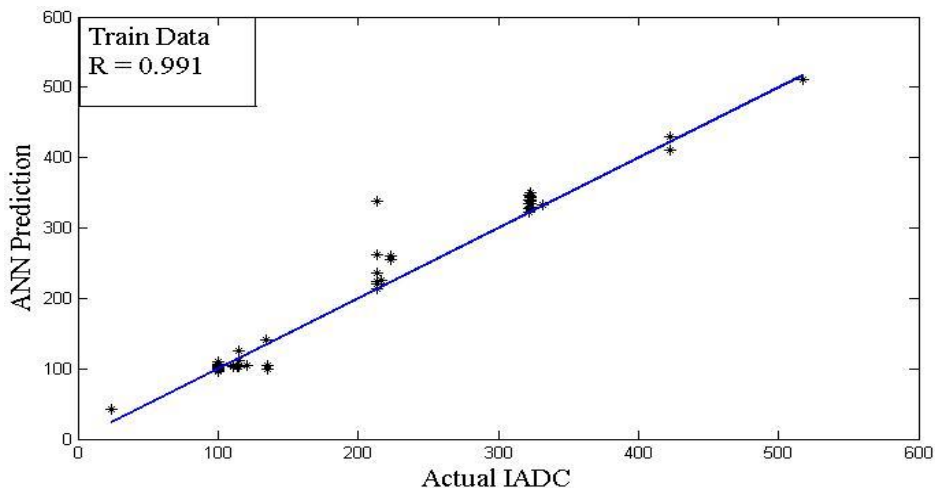


Figure 1a. Result of training the neural network model to forecast the drill bit.

Eventually, to ensure the accuracy and punctuality of the main network constructed, we have tested the model by unused data in which the results support the high accuracy of the model. These results are illustrated in Table. 2. Therefore, to assess the usability of the model in choosing the bit for the other oil fields, it has been tested by the drilling data of Maroon, Mansouri and Koopal fields. However, the results were not good. Using this model, we can predict an appropriate drilling bit, which is providing the desired penetration rate. This model can only be used for the Ahwaz oil field.

All the parameters were derived during drilling operations, except unconfined compressive strength of formation that is calculated using experimental correlation and logging operation. Based on statistical analysis on laboratory data, below equations were derived with acceptable accuracy for carbonate rocks:

$$UCS = 292.047e^{-9.541\phi}, \dots \tag{2}$$

$$UCS = 292.047e^{-9.541\phi}, \dots \tag{3}$$

where UCS is rock strength (MPa) and Δt_c is sonic wave travel time ($\mu s/ft$) and ϕ is porosity. Nabaei et al. (2010).

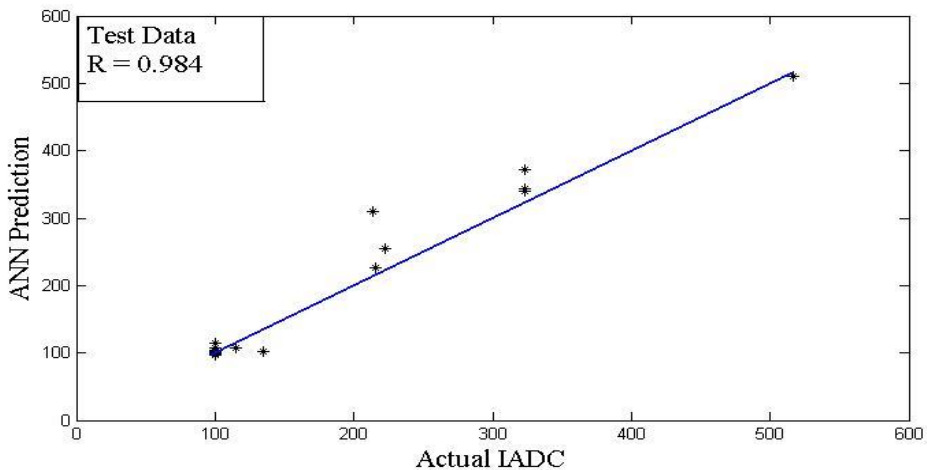


Figure 1b. Result of testing the neural network model to forecast the drill bit.

Table 2. Three test samples of the model for determining the type of the drilling bit, using the unused data in modeling

The nearest <i>IADC</i> code	Predict code	Bit Type (<i>IADC</i> code)
3.2.2	3.2.0	3.2.2
2.2.3	2.4.6	2.2.3
1.1.1	1.0.9	1.1.1

The second model, for predicting and achieving to the maximum drilling penetration rate, the second model is made. To begin with, the feed forward multilayer perception neural

network with the instruction of [11 1] (11 hidden layers and one output layer) is developed with the transition functions of tansig and poorlin and the training function of trainlim. In this model, the type of bit is the input parameter and the penetration rate is the target and the output of the model for predicting and optimizing. The results of training and test of the neural network model are illustrated in the Figures 2a and 2b, respectively. For assessing the accuracy and validity of the model, it was tested by Ahvaz field data, which had not been used in modeling. The results illustrated in Table. 3 showing the high accuracy of the model. Then to evaluate the usability of the model for the oil fields, it was tested by the drilling data of Maroon, Mansoori, and Koopal fields in which the accuracy of the model for these fields are 0.603, 0.848, and 0.898, respectively.

Table 3. Three test samples of the model for determining the type of the drilling bit using the unused data in modeling

<i>MSE</i>	Predict <i>ROP</i> (<i>ft/hr</i>)	Real <i>ROP</i> (<i>ft/hr</i>)	Filed
7.39	52.9	61.83	Ahvaz
0.005	34.5	34.6	Ahvaz
0.11	9.28	10.36	Ahvaz

Table 4. Value and the range of the fixed and valuable parameters in different parts of well

Variable parameters ranges	Fixed parameter	Bit size (in)
Bit Type: [1,18-27] <i>WOB</i> (1000 <i>Ib</i>) = [15-80] <i>RPM</i> (rev/min) = [100-200] <i>TFA</i> (<i>in</i> ²) = [0.589-1.553] <i>PV</i> (<i>cp</i>) = [2.5-29] Pump pressure (<i>Psi</i>) = [312.5-2900] Pump output (<i>gpm</i>) = [332.86-1000]	: 187) <i>ft</i> (Depth in : 4982) <i>ft</i> (Drill interval Unconfined compressive strength (<i>psi</i>) : 6381.7	17.5
Bit Type : [1,8,11-17] <i>WOB</i> (1000 <i>Ib</i>) = [10-45] <i>RPM</i> (rev/min) = [40-220] <i>TFA</i> (<i>in</i> ²) = [0.3-1.203] <i>PV</i> (<i>cp</i>) = [20.5-75.93] Pump pressure (<i>Psi</i>) = [491.67-3327.57] Pump output (<i>gpm</i>) = [225-650]	: 5169) <i>ft</i> (Depth in : 3608) <i>ft</i> (Drill interval Unconfined compressive strength (<i>psi</i>) : 12460.3	12.25
Bit Type : [1-10,12] <i>WOB</i> (1000 <i>Ib</i>) = [10-50] <i>RPM</i> (rev/min) = [20-190] <i>TFA</i> (<i>in</i> ²) = [0.451-1.491] <i>PV</i> (<i>cp</i>) = [4.25-64] Pump pressure (<i>Psi</i>) = [450-1633.33] Pump output (<i>gpm</i>) = [116.67-515]	: 8777) <i>ft</i> (Depth in : 3352) <i>ft</i> (Drill interval Unconfined compressive strength (<i>psi</i>) : 13549.54	8.5

Table 5. The values of the optimized parameters in different parts of well

Pump output (gpm)	Pump pressure (Psi)	PV (cp)	TFA (in ²)	RPM (rev/min)	WOB (1000lb)	ROP (ft/hr)	Bit Type	Bit Type (IADC)	Hole size
451	1225	15	0.88	198	22	93.8	HC606	M323	17.5
346	1550	40	1.15	170	35	45	DSX819	M422	12.25
480	1730	28	0.81	180	40	40.24	G536XL	M323	8.5

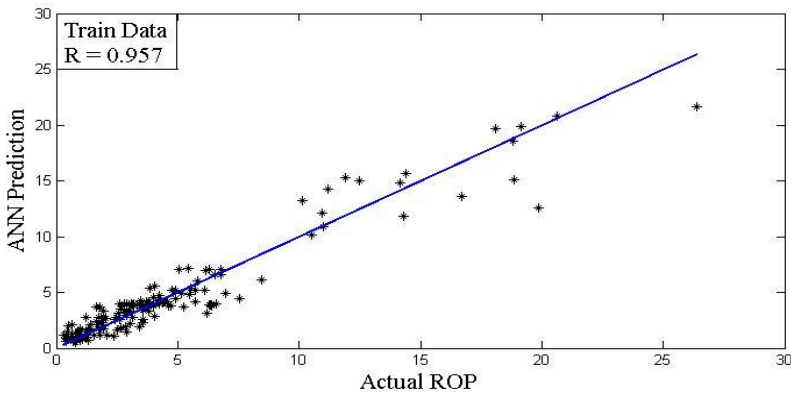


Figure 2a. Result of training the neural network model to predict the penetration rate of drilling.

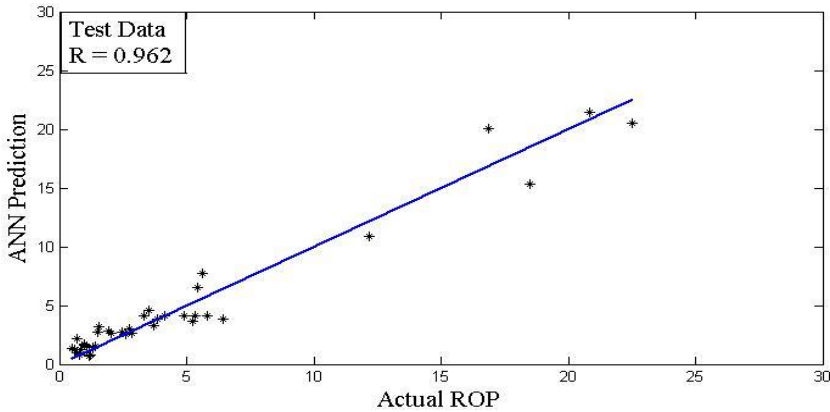


Figure 2b. Result of testing the neural network model to estimate the penetration rate of drilling.

According to well profile, the optimizing of bit selection and the other input parameters must be done in three different well intervals. For the process of optimization, changes are allowed in the parameters such as the weight on the bit, drilling string rotation, total flow area, mud circulation rate, and in the pressure while, the size of the bit and the unconfined compressive strength of the formation must be kept fixed. The range of the variable parameter and the fixed parameter values in different parts of the well are illustrated in Table. 4. For optimizing the penetration rate function, we have used the genetic algorithm as satisfactory results are obtained. Using the genetic algorithm as a powerful tool, optimization of the penetration rate in each part of the well for each individual bit is performed separately. As

illustrated in Table 4, the domain of the variable input and fixed parameters are changed in different parts of the well. This difference is due to the difference in the well geometry and limitation in mud circulation flow for cleaning and, prevention from pipe sticking. Optimizing the penetration rate function takes place via the genetic algorithm in the population size of 20, the scale function of rank, the selection function of stochastic uniform, mutation function of Gaussian and the crossover function of scattered. The results taken from optimizing parameters for reading to the maximum penetration rate are illustrated in Table. 5 and Figure 3.

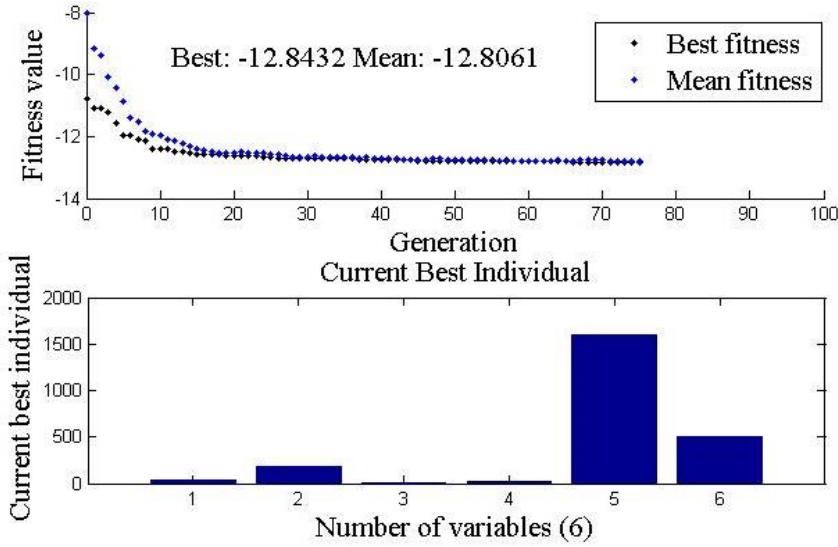


Figure 3a. Optimized results are drilling parameters by genetic algorithms in size17.5.

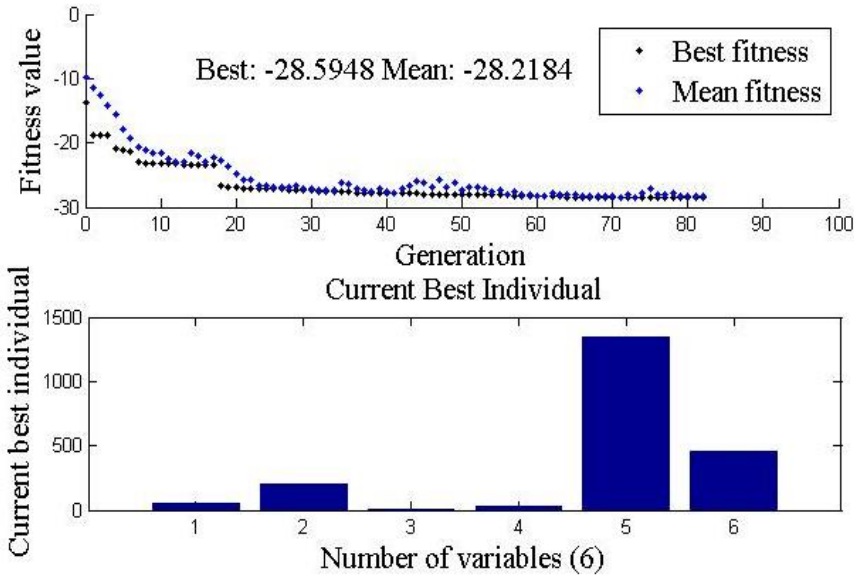


Figure 3b. Optimized results are drilling parameters by genetic algorithms in size 12.25.

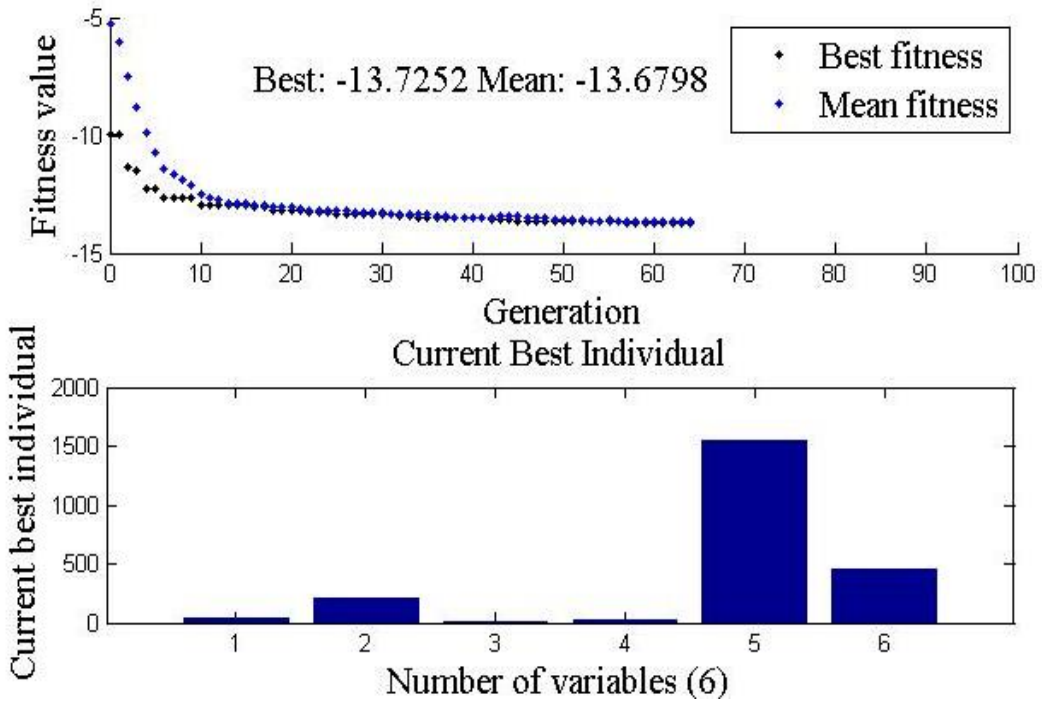


Figure 3c. Optimized results are drilling parameters by genetic algorithms in size 8.5.

DISCUSSION

The general observed trend in all well sections represent a decrease in *ROP* verses depth. This is due to the fact that the average compressive strength grows while depth increases. Comparing the optimized penetration rate with the maximum actual penetration rate shows its significant increase. The cause of low penetration rate in the size 8.5 inches well, is using of inappropriate bits, that out of the eleven bit used, 6 types are useable for the soft formation and 4 types for the soft-to-average formations. According to the unconfined compressive strength of the formation (13549.054psi), the formation are the average ones that only one type of bit, and that in average range, exists among the used bits. Now, the result of optimizing must be operationally assessed whether they are usable in operation or not.

1. Drilling Bit

The selected bit in each size must have the ability to drilling formation, for this reason, we put the bits under assessment for unconfined compressive strength. The results are illustrated in Table. 6.

Table 6. Assessment of the selected drilling bit

Unconfined compressive strength of the proposed bit (<i>psi</i>)	Unconfined compressive strength of formation (<i>psi</i>)	Bit type	Selected bit	Bit Size
14000	6381.7	<i>HC606</i>	<i>M323</i>	17.5
24000	12460.3	<i>DSX819</i>	<i>M422</i>	12.25
14000	13549.54	<i>G536XL</i>	<i>M323</i>	8.5

2. Rate of Penetration and Mud Circulation Rate

Using the optimum penetration rate may cause some problems. One of the predictable problems is drilling bit sticking caused by inappropriate well cleaning. For an appropriate cleaning; the speed of mud flow in annulus must be in a level that takes over the speed of mud vibration. For calculations of mud velocity in annulus and mud slippage velocity, the following formulas are used.

Mud velocity in Annulus

$$V_{ann} = \frac{24.5 \times Q}{D_{hole}^2 - D_{pipe}^2}, \dots \tag{3}$$

Mud slippage velocity in vertical and mostly –vertical. Lapeyrouse and Nortoned (2002).

$$V_s = 0.45 \left(\frac{PV}{MW \times D_p} \right) \left[\sqrt{\frac{36800}{\left(\frac{PV}{MW \times D_p} \right)^2} \times D_p \times \left(\frac{D_{enp}}{MW} - 1 \right) + 1} - 1 \right], \tag{4}$$

Mud slippage velocity in pointed wells Mirhaj et al. (2007).

$$V_{min} = V_{cut} + V_{slip}, \dots \tag{5}$$

$$V_{cut} = \frac{1}{\left[1 - \left(\frac{D_{pipe}}{D_{hole}} \right)^2 \right] \times \left(0.685 + \frac{17.82}{ROP} \right)}, \dots \tag{6}$$

$$V_{slip} = ESV \times C_{angle} \times C_{size} \times C_{mw}, \dots \tag{7}$$

$$C_{angle} = 0.0052 \times \theta_{angle} - 0.0002 \theta_{angle}^2 - 0.2, \dots \tag{8}$$

$$C_{size} = -1.02 \times D_{50cut} + 1.27, \quad (9)$$

$$C_{mw} = 1 - 0.333 \times (\rho_{mud} - 8.65), \quad (10)$$

$$ESV = 0.0052 \times \mu_a + 3.1, \quad (11)$$

Table 7. The results of calculations

Annulus velocity (ft/sec)	Slip velocity (ft/sec)	Average flow rate (gpm)	Optimal flow rate operation (gpm)	Maximum ROP (ft/hr)	ROP (ft/hr)	Bit Size
3.89	1.8	868.5	450	86.56	93.8	17.5
2.99	1.01	519.69	446	21.58	45	12.25
4.15	2.66	329.8	500	21.06	40.24	8.5

The results of calculations are illustrated in Table 7. As can be seen in Table 7, the velocity of the optimized mud is faster than the slippage velocity in each of three parts of well, therefore, well cleaning is well done. On the other hand, using this amount of the mud flow causes lower energy consumption by the pump. We can observe this energy reduction by comparing optimal flow rate with mud flow rate average in operations. These results show that even though the penetration rate of drilling has got a significant growth in new conditions, the optimal flow rate is less than the amount of the rate used in drilling conditions.

3. Pump Pressure and Total Flow Area

Outlet pump pressure is another parameter that appropriate determination of it causes boost to drilling operation and reduction of the costs. Low pump pressure cannot dominate the pressure drop produced through the drill string and result in inappropriate bottom hole cleaning. On the other hand, too much high pump pressure causes consumption of more fuel and correspondingly results in going up the costs of drilling. For assessing pressure drop through the length of drillstring, we used Hydraulic Calculator software. The results are shown in Table. 8. As can be seen, the range of pressure drop is less than the amount of the pump optimal pressure and also, the optimal pump pressure is less than the average amount of the pump operational pressure.

It is certain that the more hydraulic ability of the bit, the higher weight on the bit can be applied that result in increasing the penetration rate. As can be seen, the most pressure drop and as a result the most hydraulic power is produced among drilling string in the proposed bits with the optimized total flow area that indicates an appropriate choice in bit and total flow area. As shown in Table. 8, the ratio of the bit hydraulic power to the pump hydraulic power in the 12.25 size of well is low and it can be considered as one reason of drilling penetration rate reduction in this size.

Table 8. Assessment of mud pump pressure and the optimized cross- flow

$\frac{HP_b}{HP_p} \geq 50$	Hydraulic power bit (HP)	Hydraulic power pump (HP)	TFA (in^2)	Pressure drop during the drill string (psi)	Optimal pump pressure (psi)	Average pump pressure (psi)	Hole Size (in)
0.63	122	193.6	0.88	735.8	1225	1994.14	17.5
0.18	30.18	171.59	1.15	850	1550	1961	12.25
0.508	231	455	0.81	1626	1730	967	8.5

4. Weight on Bit and the Rotation Speed of the Drill String

The more weight on the bit and the rotation speed of drill string, the more penetration rate occurs. Of course, they must be chosen in a way that cause increasing of the penetration rate and also not make any problem for the drilling operation. Too much increase of the weight on the bit and the rotation speed of the drill string, in addition to a damage and shorten the life of bit, may cause a drilling bit sticking. However, as observed in the assessing part of the penetration rate, the problem of bottom hole cleaning won't be made. On the other hand, the maximum weight on the bit and the rotation speed of drilling bit which chosen bits can resist are illustrated in Table 9.

It Shows that the drilling bits have no problem regarding this and also, with using the optimal total flow area of the pumps, the bit hydraulic power includes more than half of the hydraulic power of total mud. Then application of the maximum weight on the bit in operations is possible. The amount of the weight and the tolerable rotation speed of the selected bits are illustrated in Table 9.

Table 9. Assessment of the weight on the bit and the optimized rotation of the drill string

Tolerable RPM (rev/min)	Optimal RPM (rev/min)	Tolerable WOB	Optimal WOB (1000lb)	Bit Type	Bit Type IADC Code	Hole Size (in)
60-260	198	25-180	22	HC606	M323	17.5
60-260	170	30-140	35	DSX819	M422	12.25
60-260	180	25-100	40	G536XL	M323	8.5

5. Mud Viscosity

The amount of the drilling mud viscosity must be in a level that can suspend large solid particles if there are any. On the other hand, too much amount of viscosity lessen the operation of the bottom hole cleaning. Due to increasing hydraulic pressure drop among pipes path and decreasing the bit hydraulic power. Increasing the bottom hole pressure and the formation damage cause loss circulation. Therefore, we should select the appropriate viscosity according to the characteristics of the formation, bit and optimizing the drilling

parameters like weight on bit, the rotation speed of the drillstring, and the hydraulic system of the bit.

CONCLUSION

- 1) The observations and results show that the artificial neural network methods are applicable and safe. Testing the models of bit selection and optimizing the penetration rate using unused data in modeling show that this method has high accuracy.
- 2) Assessment of the optimization results using software and the experimented formulas show that the values of the optimized parameters are in fact usable and won't make any problem in drilling operation and using the optimal parameters result cost savings and minimizing time overruns on drilling projects.
- 3) Since the drilling bit has a significant effect on rate of penetration, a separated model providing the appropriate bit based on the penetration rate, was produced.
- 4) The application of bit selection model and predicting the penetration rate of Ahwaz oil field result high errors even for adjacent fields. Therefore, these models may not be recommended for the other oil fields.
- 5) The advantage of this model than the other drilling improvement methods is consideration of all effective parameters on drilling operation and being accurate, comprehensive, and easy application.

METRIC CONVERSION FACTORS

$$\text{Cp} \times 1.0 \text{ E} - 03 = \text{Pa} \cdot \text{s}$$

$$\text{Ft} \times 3.048 \text{ E} - 01 = \text{m}$$

$$\text{In.} \times 2.54 \text{ E} + 00 = \text{cm}$$

$$\text{In}^2 \times 6.451 \text{ 6 E} + 00 = \text{cm}^2$$

$$\text{Ibm} \times 4.535 \text{ 924 E} - 01 = \text{kg}$$

$$\text{Hp} \times 7.460 \text{ 43 E} - 01 = \text{Kw}$$

$$\text{Psi} \times 6.894 \text{ 757 E} + 00 = \text{kPa}$$

$$\text{Degree (angle)} \times 1.745 \text{ 329 E} - 02 = \text{radian (rad)}$$

$$\text{Ibm/gal (U.S. liquid)} \times 1.198 \text{ 264 E} + 02 = \text{kilogram per metel}^3 \text{ (kg/m}^3\text{)}$$

$$\text{Ft/s} \times 3.048 \text{ E} - 01 = \text{meter per second (m/s)}$$

$$\text{Ft/hr} \times 8.466 \text{ 667 E} - 05 = \text{meter per second (m/s)}$$

$$\text{Gal (U.S. liquid)/min} \times 6.309020 \text{ E} - 05 = \text{meter}^3 \text{ per second (m}^3\text{/s)}$$

REFERENCES

Bilgesu, H. I.; Al-Rashidi, A. F.; Aminian, K.; Ameri, S. (2000). A new approach for drill bit selection. *SPE Eastern Regional Meeting*, Morgantown, WV, October, pp. 17–19.

-
- Bourgoyne, T.; Young, F. S. (1974). A multiple regression approach to optimal drilling and abnormal pressure detection. *SPE J.* 14, pp. 371–384.
- Demuth, H.; Beale, M.; Hagan, M. (2007). *Artificial Neural Networks and Genetic Algorithms User's Guide*. Revised for Matlab Programming v. 5.1. The MathWorks.
- Lapeyrouse; Nortoned, J. (2002). *Formulas and Calculations for Drilling Production and Workover*. s.l. : Gulf Professional Publishing is an imprint of Elsevier Science.
- Mirhaj, S. A.; Shadizadeh, S. R.; Fazaelizadeh, M. (2007). Cutting removal simulation for deviated and horizontal wellbores. Paper No. 105442, *SPE Middle Oil and Gas Show*, Bahrain, March, pp. 11–14.
- Nabaei, M.; Shahbazi; Khalil. (2010). A New Approach for Pre-Drilling Unconfined Rock Compressive Strength Prediction. *Petroleum Science and Technology*, LPET-2010-0072.
- Rabia, H.; Farrelly, M.; Barr, M. V. (1985). A new approach to drill bit selection. Paper No. 15894, *SPE European Petroleum Conference*, London, October, pp. 20–22.
- Edalatkhah, S.; Rasoul, R.; Hashemi, A. (2010). Bit Selection Optimization Using Artificial Intelligence Systems. *Petroleum Science and Technology*, 28:18, pp. 1946-1956.
- Teale, R. (1965). The concept of specific energy in rock drilling. s.l. : *Int. J. Rock Mech. Min. Sci.* 2:57–73.
- Yilmaz, S.; Demircioglu, C.; and Akin, S. (2002). Application of artificial neural networks to optimum bit selection. *Comput. Geosci.* 28, pp. 261–269.

Chapter 14

IMPROVEMENT OF DRILLING PENETRATION RATE IN OIL FIELDS USING A PSO - GA - MLP HYBRID NETWORK

***Abbas Khaksar Manshad¹, Habib Rostami²,
Hojjat Toreifi² and Amir H. Mohammadi^{3,4,5,*}***

¹Department of Petroleum Engineering, Abadan Faculty of Petroleum Engineering,
Petroleum University of Technology (PUT), Abadan, Iran

²Department of Computer Engineering,
School of Engineering, Persian Gulf University, Bushehr, Iran

³Discipline of Chemical Engineering, School of Engineering,
University of KwaZulu-Natal, Howard College Campus, Durban, South Africa

⁴Département de Génie des Mines, de la Métallurgie et des Matériaux,
Faculté des Sciences et de Génie, Université Laval, Québec, Canada

⁵Institut de Recherche en Génie Chimique et Pétrolier (IRGCP), Paris Cedex, France

ABSTRACT

One of the main challenges in drilling operations is optimizing and improving rate of penetration (ROP). Low values of the rate of penetration result in loss of rig time and increase the drilling cost. There are too many parameters intervening in rate of penetration. Therefore, developing a logical relationship between them to assist in rate of penetration prediction is necessary. In such a case, artificial neural networks have proven to be helpful in recognizing the complex relationship between variables. In this communication, a multilayer perceptron (MLP) neural network and optimized multilayer perceptron neural networks with differential algorithms were used to predict the penetration rate. The best performance is corresponding to the optimized multilayer perceptron neural network by a hybrid of particle swarm optimization (PSA) and genetic algorithm (GA) with a correlation coefficient of 0.98. Optimization process is achieved by using controllable and affecting parameters on penetration rate, such as weight on bit, rotation per minute, bit type, hydraulics and drilling fluid properties. The optimum values

* Corresponding Author E-mail: amir_h_mohammadi@yahoo.com AND a.h.m@irgcp.fr.

of effecting parameters for increasing the penetration rate were calculated. Review of optimum results show that the proposed method is efficient and can be used for saving drilling costs.

Keywords: drilling, penetration rate, ROP, MLP neural network, Genetic Algorithm (GA), Particle Swarm Optimization (PSA)

1. INTRODUCTION

Analysis of field data is the main element of cost reduction and the improvement of drilling operation. The development of the tools of field data analysis is considered as a way of developing and improving drilling operation. The two approaches, mechanical specific energy (SE) and the models of rate of penetration (ROP) are typically used for optimization. The mechanical specific energy is referred to the amount of work needed for a certain volume of rock to be drilled. The concept of specific energy was first introduced by Teale [1].

$$SE = \frac{WOB \times RPM}{D \times ROP} \quad (1)$$

where the *WOB* is the weight on the bit (*Ib*), *RPM* is the rotation of drilling bit per minute (*rev/min*), *ROP* is rate of penetration (*ft/hr*) and *D* is the diameter (*ft*). Rabia only used three drilling parameters for evaluating the SE in rock drilling. These parameters were the *WOB*, *RPM*, and the torque of bit [2]. A drilling model includes equations for *ROP* and bit erosion. There are numerous models in this field that have been used to relate the various parameters involving in the process of drilling on *ROP*. These models use important drilling parameters such as *WOB* and the *RPM* for evaluation and prediction of the performance. The Bourgoyne and Young model excels among all introduced models, because it includes almost all the formation parameters and drilling variables [3].

$$ROP = f_1 \times f_2 \times f_3 \times f_4 \times f_5 \times f_6 \times f_7 \times f_8 \quad (2)$$

The f_1 and f_8 express operations relationship between the *ROP* and effective variables. One of the newest models of drilling is utilization of artificial neural networks (ANNs). Bilguse used the ANN for choosing bit in which the drilling parameters were used, however, formation parameters which play an important role in choosing bit were not considered [4]. Yilmaze et al. developed a model using the compressive strength average of formation, however, they only worked on bit selection and did not investigate evaluation of the optimal values of drilling parameters and how to increase *ROP* [5]. In the present work, a method is presented to predict and improve the penetration rate by ANN and particle swarm optimization (PSO) and genetic (GA) algorithms.

2. MULTILAYER PERCEPTRON (MLP) NEURAL NETWORK

One of the simplest, yet most effective arrangements proposed for use in real nerves modeling is MLP neural network that consists of an input layer, one or more hidden layers and an output layer. In MLP ANN, all the neurons in one layer are connected to all neurons of the next layer. This arrangement will form a network with a complete connection. A schematic description of this architecture is presented in Figure 1. In a MLP neural network, the next m -dimensional input vector x is related to n -dimensional output vector y as follows:

$$y = f_l(w_l \times f_{l-1}(w_{l-1} \times f_{l-2}(\dots f_o(w_o \times x + b_o))\dots + b_{l-1}) + b_l) \quad (3)$$

In this regard, l represents the number of hidden layers of the network, w_l , the weights coefficients matrices corresponding to l layer, b_l the bias vector of l layer and f_l shows the transfer function of l layer and o variables are shown with subtitles in the output layer is corresponds to output layer.

Basically, there are two types of supervised and unsupervised learning. It is clear that a supervised learning approach, desired output for each training inputs is presented, while the output of the unsupervised learning methods, is not presented. MLP neural network is a kind of supervised learning method [6].

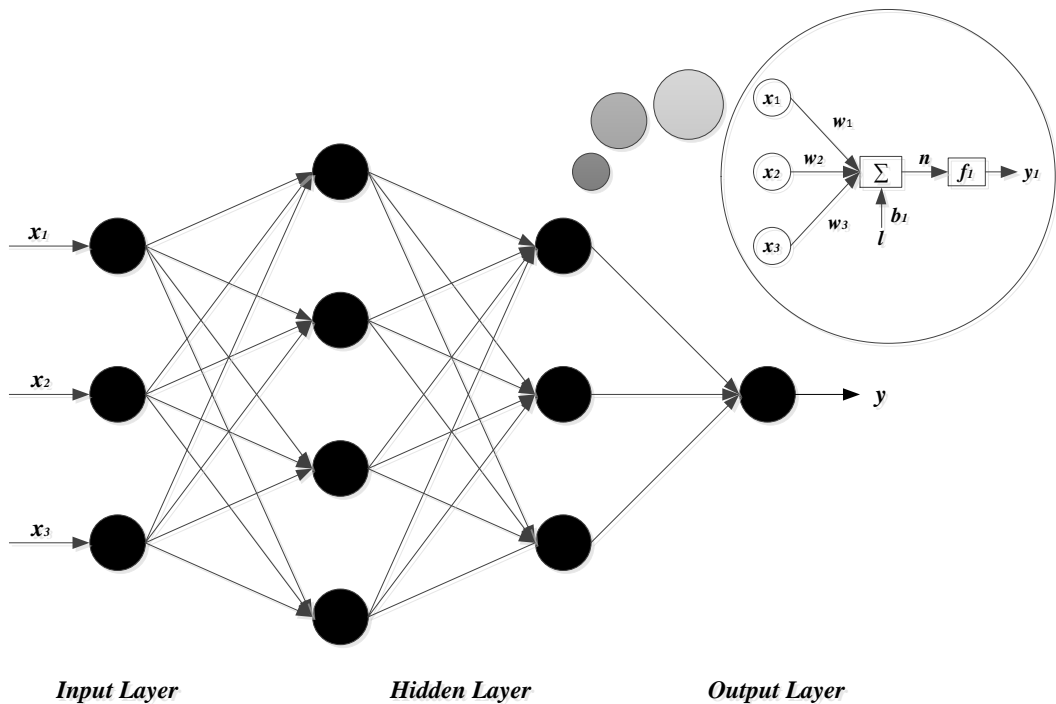


Figure 1. A schematic description of MLP network with two hidden layers.

According to both Figure 1 and the above formulation, it is obvious that there is a huge computational burden in MLP neural network. Therefore, very likely the network is trapped in the local minima if a lot of noisy data and local learning algorithm are available. Hence, to reduce computational burden and determine suitable value of variables (weights and biases), optimization algorithms that have specific ability in this domain can be applied. One of these algorithms is PSO-GA which is explained below.

3. PSO-GA HYBRID ALGORITHM

GA and PSO are both population based algorithms that have proven to be successful in solving very difficult optimization problems [7]. However, both models have strengths and weaknesses. The PSO algorithm is conceptually simple and can be implemented in a few lines of code. PSOs also have memory, whereas in a GA if an individual is not selected the information contained by that individual is lost. In PSO, the collaborative group interactions enhance the search for an optimal solution, whereas GAs have trouble finding an exact solution and are best at reaching a global region. However, without a selection operator PSOs may waste resources on a poor individual that is stuck in a poor region of the search space. Comparisons between GA and PSOs have been performed by both Eberhart [8] and Angeline et al. [9] and both studies suggested that a hybrid of the standard GA and PSO models would lead to a very effective search strategy. The standard PSO algorithm may not be flexible enough for practical applications particularly when the problem to be tackled is complicated, conflicting and multitasking. Means for modifying the PSO structure, fitness function, and PSO operators are sought in order to meet the design requirements. In the present work, we propose a hybrid PSO-GA algorithm combining the strengths of PSO and GA to enhance the search process in the QoS multicast problem. The hybrid algorithm combines the standard velocity and position update rules of PSOs with the ideas of selection, crossover and mutation from GAs. The population update concept can be easily understood thinking that a part of the individuals are the same of the previous generation but moved on the solution space by PSO. The remaining individuals are substituted by new generated ones by means of GA operators. This kind of updating results in a more natural evolution, where individuals not only improve their scores for natural selection of the fitness, or for good-knowledge sharing, but for both of them at the same time.

The main objective of the proposed algorithm is to design an adjustable technique that makes it possible to optimize the performance of the PSO-GA hybrid. Two driving parameters are added in the hybrid algorithm to give preference to either PSO or GA. The PSO velocity vector is multiplied by an influence term $\lambda \in [0: 1.0]$. When this term is set to 0 the PSO has no effect on the population, when set to 1 the PSO runs as the standard PSO. For intermediate values the PSO functions normally, but the size of the steps taken by the particles is reduced. The GAs selection operator has a replacement term $\psi \in [0: 1.0]$ which determines how many individuals in the population get replaced and crossed over in the current generation. When the $\psi = 0$ no individuals/particles are selected for crossover or mutation and the GA has no effect on the population. When the $\psi = 1$ the entire population is replaced in the generation. First, the hybrid algorithm performs the standard velocity and position update rules, with the influence term. The top (population size $\times (1 - \psi)$) individuals,

based on fitness, are copied into the new population. Selection, crossover and mutation then occur on the appropriate number of individuals determined by the replacement term to fill the remainder of the population. The flowchart of the proposed PSO-GA algorithm is shown in Figure 2.

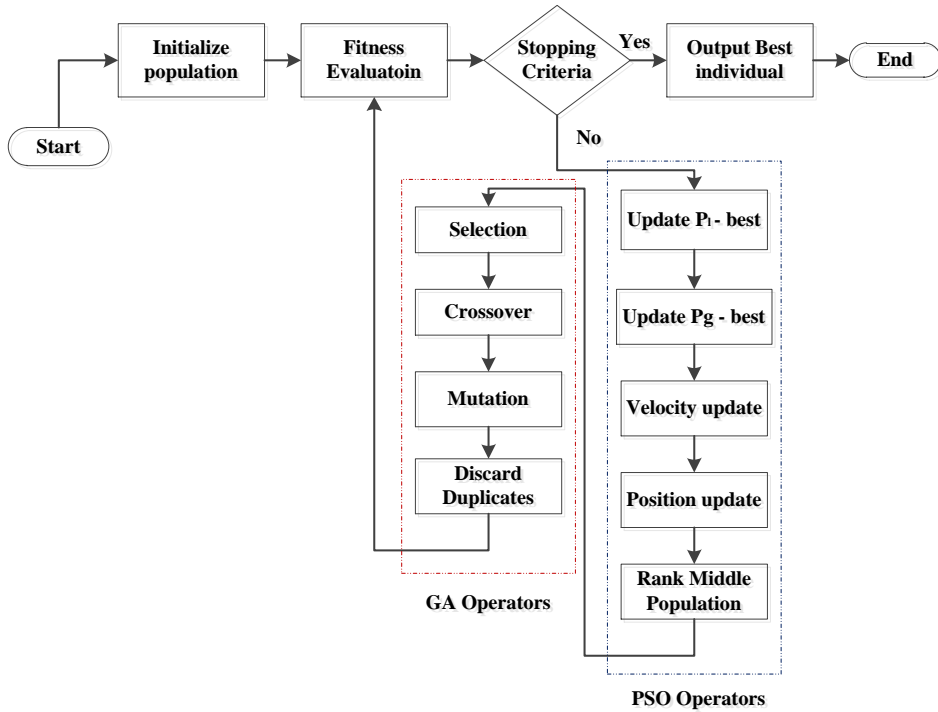


Figure 2. Flow-chart of the PSO-GA Hybrid Algorithm.

Table 1. Statistical description of the used data in this study for both input and output

Parameter	Unit	Min.	Max.	St. Dev	Median	Average	Q (1)	Q (2)	Q (3)
WOB	1000lb	10	80	13.6	30	31.11	22	30	40
RPM	Rev/min	20	220	53.64	160	136.56	80	160	180
TFA	in^2	0.3	1.55	0.256	0.72	0.782	0.59	0.72	0.97
MW	Pcf	54.83	147.33	28.26	74	88.54	67.5	74	113.33
PV	Cp	2.5	75.9	18.65	21.33	24.76	7.36	21.33	37.5
P_p	Psi	312.5	3328.6	757.22	1528.95	1506.3	866.67	1528.95	2137.5
Q_p	Gpm	116.7	1000	258.91	490	532.01	310	490	826.67
D_{in}	Ft	0	10650	2591	6360	6216.32	4943	6360	8357.44
D_{out}	Ft	1378	12129.4	2348	7086.44	7352.45	5550.25	7086.4	8880
Bit Type	IADC Code	100	423	112.27	100	151.3	100	100	114
Bit Size	In	8.5	17.5	3.83	12.25	12.25	8.5	12.25	17.5
UCS	Psi	5407	34128	2416.35	16012.3	15107.26	14659	16018	16142.8
ROP	ft/hr	0.95	86.56	14.17	9.5	13	4.03	9.54	15

In later evolution stage of PSO algorithm, the convergence speed becomes significantly slower. At the same time, after the algorithm converges to a certain precision, it cannot optimize anymore. In order to maintain the algorithm diversity, improve the search performance and avoid PSO algorithm plunged into local optimum, we propose to join the crossover and mutation operator together.

This algorithm was used to optimize in two parts. In part of prediction, the ROP was used to improve the performance of MLP neural network, and in optimizing part the ROP was applied to obtain the optimum values of effective parameters on the ROP. Optimizing the MLP neural network and ROP functions takes place via the PSO-GA in the population size of 50, Maximum Number of Iteration of 50, Maximum Number of sub-Iteration for PSO of 10, Maximum Number of Sub-Iteration for GA of 5. PSO Parameters: $\phi_1 = 2.05$, $\phi_2 = 2.05$, $\phi = \phi_1 + \phi_2$, $\chi = 2/(\phi_1 - 2 + \sqrt{\phi^2 - 4 * \phi})$, $\omega = \chi$, $c_1 = \phi_1 * \chi$, $c_2 = \phi_2 * \chi$. GA Parameters: Crossover Percentage = 0.7, Number of Parents = 36, Mutation Percentage = 0.2, Number of Mutants = 10.

4. CASE STUDY

The studied oil field is located in the southwest of Iran. This field has an anticline structure and nearly considered as the last part of Zagros folding region. According to the obtained geological setting and the available data, this field can be classified as a structural and heterogonous field. Survey data show that due to the high heterogeneity in this field, traditional and conventional methods cannot predict the ROP well. Generally, for accurate predicting and improving the drilling ROP, one should consider all impact parameters. In this study, drilling bit, formation properties, drilling parameters and drilling mud properties as effective parameters are considered. Statistical analysis of the parameters values is given in Table 1.

5. METHODOLOGY AND RESULTS

For predicting the drilling ROP, we have used MLP neural network and optimized MLP neural network by different algorithms. Since MLP neural network is the most commonly used ANN in petroleum engineering, its performance by GA, PSO and PSO-GA hybrid algorithms was studied and the best combination was used to predict the penetration rate.

In this model, size of bit, bit type, total flow area (TFA), depth in (D_{in}), depth out (D_{out}), WOB, RPM, pump output rate (Q_p), pump pressure (P_p), plastic viscosity (PV), mud weight (MW) and average unconfined compressive strength (UCS) of formation are considered the inputs for ANN and the output is the ROP. Among 308 data sets (input and output), after removal of suspicious data, 299 data sets for 10 wells were used to construct a neural network.

The datasets were divided randomly into three distinct subsets consisting of training, validation and testing. The proportions of each of these subsets were 70%, 15% and 15% of whole of the data. In this study, two criteria were used to stop the training phase, minimum

mean square error (MSE) and validation data. In the first criterion, the training will be stopped if its MSE reaches a predefined MSE. Also, based on the second criterion (validation dataset) and for preventing from overfitting, when the error of validation dataset was increased, then the training will be stopped. In other words, the validation dataset is given to network along with its training to ensure that the network is not memorizing the training data (generalizing) and is able to predict the other data finely. Therefore, anywhere in training phase when validation error is increased, there is no need to continue the training. Due to intrinsic dispersion of dataset and in order to help the network to be converged faster, the available data was normalized into [0: 1.0] [10].

5.1. Modeling

5.1.1. MLP

Multilayer perceptron is one of the most well studied architectures with several advantages in ANN, as mentioned earlier [11]. Therefore, in this study, we have employed this architecture to model ROP problem. Normally, finding an appropriate network in this architecture is based on a trial and error method. In other words, one should test different neurons with different layers. Then, based on the training and testing error, it is possible to reach a good enough structure.

The best architecture for MLP was found to be [8 5 1] (8 neurons in the first hidden layer, 5 neurons in the second hidden layer, and a neuron in the outer layer). Actually, this architecture yields the minimum MSE and maximum correlation coefficient. In this study, we have used Tansig and Purelin transfer functions for hidden layers and output layer of neural network, respectively. The MSE and correlation coefficient for testing dataset were 0.0033 and 0.89, respectively. The results of MLP networks performance are presented in Figure 3 and 4 and Table 2.

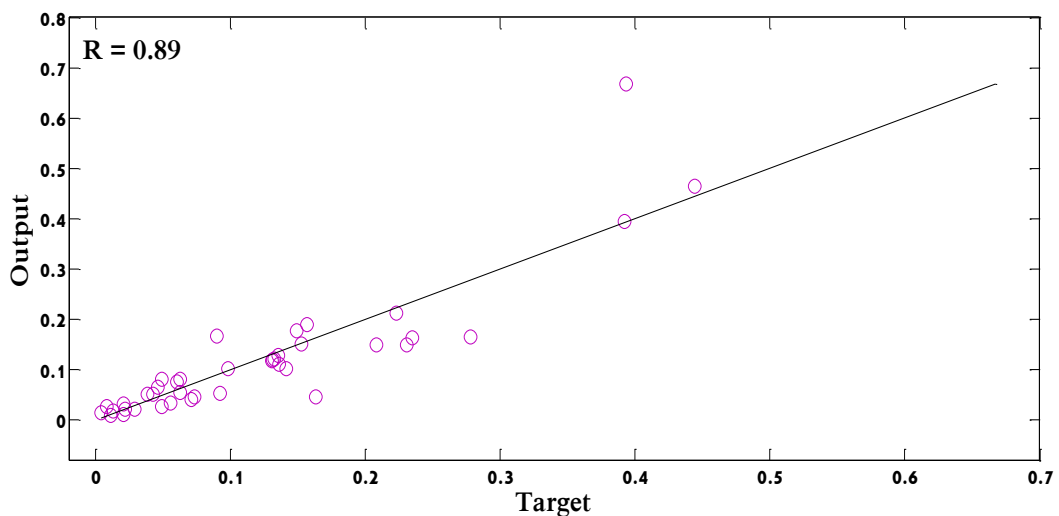


Figure 3. Correlation coefficient of MLP network in the test stage.

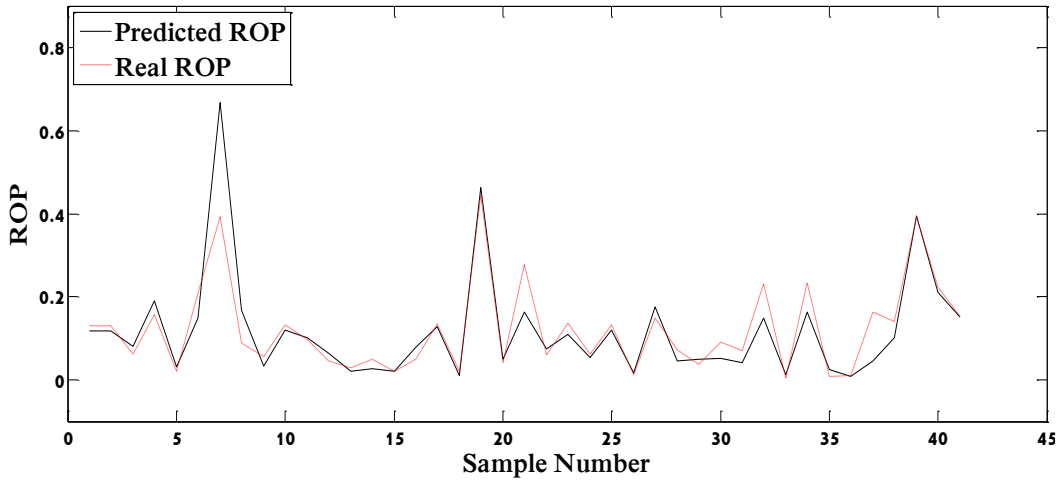


Figure 4. Comparison of the estimated values by MLP and the real ROP.

Table 2. Comparison of MLP and optimized MLP neural networks with different optimization algorithm

Network	MSE	R	R^2
MLP	0.0033	0.89	0.79
MLP-GA	0.00325	0.93	0.86
MLP-PSO	0.00307	0.96	0.92
MLP-PSO-GA	0.00027	0.98	0.96

The ROP can be predicted with good accuracy using perceptron neural network. However, for high values, the accuracy of network is not satisfactory. Therefore, optimization algorithms can be used to improve the applicability of neural networks.

5.1.2. Training of MLP with PSO-GA (MLP-PSO-GA)

One of the major problems in neural networks, especially MLP, is time demanding computations of multilayer weights. One of the useful and new methods for finding optimum value in a search space is optimization algorithms. In this section, GA, PSO and PSO-GA algorithms were used for network training and the best performance was found due with PSO-GA hybrid algorithm. PSO-GA hybrid algorithm has wide application areas, which is more useful in problems where the search space is large, complex or poorly understood, also when traditional search methods fail or no mathematical analysis is available. The steps of the method used to train the MLP using PSO-GA hybrid algorithm is described in Figure 5. The error and correction coefficient for calculating ROP are 0.00027 and 0.98, respectively. Figure 6 and 7 and Table 2 show the performance of this model.

It is clear that PSO-GA-MLP network has a performance much higher than other neural networks.

Table 3. Value and the range of the fixed and valuable parameters in different parts of well

Bit size (in)	Fixed parameter	Variable parameters ranges
17.5	: 0) ft (D_{in}) : 7140.56) ft (D_{out}) UCS (psi) : 6381.7	Bit Type : [111 - 323] WOB (1000lb) = [15 - 80] RPM (rev/min) = [100 - 200] TFA(in^2) = [0.589 - 1.55] MW (pcf) = [54.83 - 96.67] PV (cp) = [2.5 - 29] P_p (Psi) = [312.5 - 2900] Q_p (gpm) = [332.86 - 1000]
12.25	: 4711.72) ft (D_{in}) : 8796.96) ft (D_{out}) UCS (psi) : 12460.3	Bit Type : [214 - 423] WOB (1000lb) = [10 - 45] RPM (rev/min) = [40 - 220] TFA(in^2) = [0.3 - 1.203] MW (pcf) = [102.5 - 147.33] PV (cp) = [20.5 - 75.9] P_p (Psi) = [491.67 - 3328.6] Q_p (gpm) = [225 - 650]
8.5	: 7727.68) ft (D_{in}) : 12129.44) ft (D_{out}) UCS (psi) : 13549.54	Bit Type : [135 - 323] WOB (1000lb) = [10 - 50] RPM (rev/min) = [20 - 190] TFA(in^2) = [0.451 - 1.491] MW (pcf) = [63 - 113.33] PV (cp) = [4.25 - 64] P_p (Psi) = [450 - 1633.33] Q_p (gpm) = [116.7 - 515]

6. OPTIMIZATION OF DRILLING ROP

According to well profile, optimization of the input parameters must be done in three different well sizes. For the process of optimization, changes are allowed in the parameters such as WOB, RPM, TFA, Q_p and P_p while, the size of the bit and the UCS must be kept fixed. The range of the variable parameter and the fixed parameter values in different parts of the well are reported in Table 3.

To obtain optimal values for the parameters, the PSO-GA hybrid algorithm was used. Using this algorithm as a powerful tool, optimization of the ROP in each part of the well is performed separately. As illustrated in Table 3, the domain of the variable input and fixed parameters are changed in different parts of the well. This difference is due to the difference in the well geometry and limitation in mud circulation flow for cleaning and, prevention from pipe sticking. The results taken from optimizing parameters for reaching to the maximum penetration rate are illustrated in Table 4.

Table 4. The values of the optimized parameters in three parts of well

Fixed Parameters				Variable parameters (Optimized Value)								
Bit Size	D_{in}	D_{out}	UCS	WOB	RPM	TFA	MW	PV	P_p	Q_p	Bit Type	ROP
17.5	0	7140.56	63817	22	198	0.88	68.82	15	1225	451	M 323	93.8
12.25	5169	8779	12460.3	35	170	1.15	109.51	40	1550	346	M 422	45
8.5	6970	12129.4	13549.54	40	180	0.81	74.08	28	1730	480	M 323	40.24

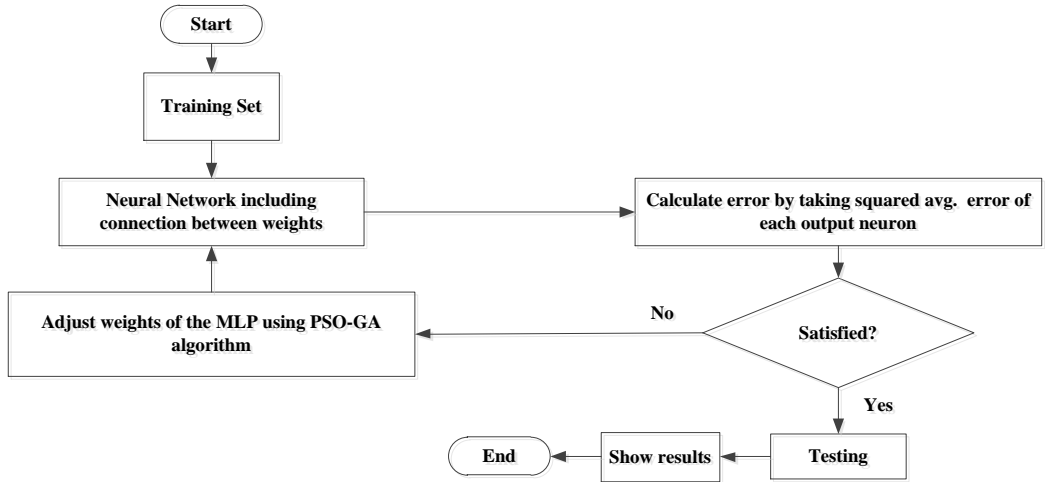


Figure 5. Flowchart of the MLP neural network training by particle swarm optimization and genetic hybrid algorithm.

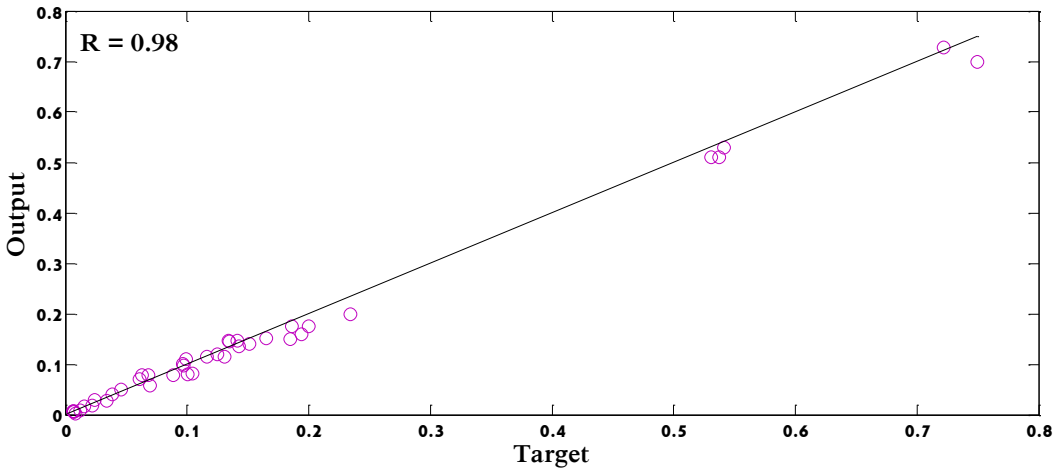


Figure 6. Correlation coefficient of MLP-PSO-GA network in the test stage.

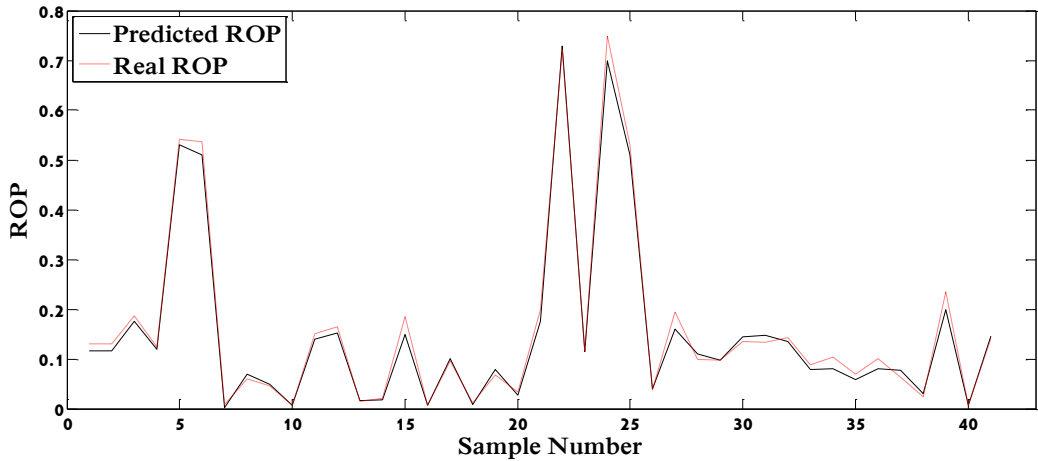


Figure 7. Comparison of the estimated values by MLP-PSO-GA and the real ROP.

7. DISCUSSION ON THE RESULTS

The general observed trend in all well sections represent a decrease in ROP verses depth. This is due to the fact that the average compressive strength grows while depth increases. Comparing the optimized penetration rate with the maximum actual penetration rate shows its significant increase. The cause of low ROP in the size 8.5 inches well is because of using inappropriate bits that out of the eleven bit used, 6 types are useable for the soft formation and 4 types for the soft-to-average formations. According to the UCS of the formation (13549.054psi), the formation is the average ones that only one type of bit, and that in average range, exists among the used bits. Now, the result of optimizing must be operationally assessed whether they are usable in operation or not.

7.1. Drilling Bit

The selected bit in each size must have the ability to drilling formation, for this reason, we put the bits under assessment for UCS. The results are illustrated in Table 5.

Table 5. Assessment of the selected drilling bit in the three hole sizes

Bit Size	Selected bit	Bit type	Unconfined compressive strength of formation (<i>psi</i>)	Unconfined compressive strength of the proposed bit (<i>psi</i>)
17.5	M323	HC606	6381.7	14000
12.25	M422	DSX819	12460.3	24000
8.5	M323	G536XL	13549.54	14000

Table 6. Assessment of the optimized ROP in the three hole sizes

Hole Size	ROP (ft/hr)	Maximum ROP (ft/hr)	Slip velocity (ft/sec)	Annulus velocity (ft/sec)
17.5	93.8	86.56	1.8	3.89
12.25	45	21.58	1.01	2.99
8.5	40.24	21.06	2.66	4.15

7.2. Drilling ROP

Using the optimum penetration rate may cause some problems. One of the predictable problems is drilling bit sticking caused by inappropriate well cleaning. For an appropriate cleaning; the speed of mud flow in annulus must be in a level that takes over the speed of mud vibration. For calculations of mud velocity in annulus and mud slippage velocity, the following formulas are used:

Mud velocity in Annulus:

$$V_{ann} = \frac{24.5 \times Q}{D_{hole}^2 - D_{pipe}^2} \quad (4)$$

Mud slippage velocity in vertical and mostly – vertical [12]:

$$V_s = 0.45 \left(\frac{PV}{MW \times D_p} \right) \left[\sqrt{\frac{36800}{\left(\frac{PV}{MW \times D_p} \right)^2} \times D_p \times \left(\frac{D_{enp}}{MW} - 1 \right) + 1} - 1 \right] \quad (5)$$

Mud slippage velocity in pointed wells [13]:

$$V_{min} = V_{cut} + V_{slip} \quad (6)$$

$$V_{cut} = \frac{1}{\left[\left(1 - \left(\frac{D_{pipe}}{D_{hole}} \right)^2 \right) \times \left(0.685 + \frac{17.82}{ROP} \right) \right]} \quad (7)$$

$$V_{slip} = ESV \times C_{angle} \times C_{size} \times C_{mw} \quad (8)$$

$$C_{angle} = 0.0052 \times \theta_{angle} - 0.0002 \theta_{angle}^2 - 0.2 \quad (9)$$

$$C_{size} = -1.02 \times D_{50cut} + 1.27 \quad (10)$$

$$C_{mw} = 1 - 0.333 \times (\rho_{mud} - 8.65) \quad (11)$$

$$ESV = 0.0052 \times \mu_a + 3.1 \quad (12)$$

where the V_{min} is minimum speed of needed mud (*ft/sec*), V_{cut} is speed of retail transfer (*ft/sec*), V_{slip} is speed of vibration (*ft/sec*), C_{angle} is angel correction factor, C_{size} is particle size correction factor, C_{mw} is mud weight correction factor, ESV is corrected speed, D_{pipe} is outside diagonal of the drilling pipe (*in*), D_{hole} is the diagonal of well (*in*), θ_{angle} is inclination angel of well from vertical position (*degree*), D_{50cut} is average size of particles (*in*), ρ_{mud} is mud density (*PPG*), μ_a is outward viscosity (*cp*), D_{enp} is density of drilling particles (*PPG*), D_p is diagonal of particles (*in*) and MW is density of drilling mud (*PPG*).

The results of calculations are illustrated in Table 6. As can be seen, the velocity of the optimized mud is faster than the slippage velocity in each of three parts of well, therefore, well cleaning is well done. As a result, there will not be bit floundering in the three sections by using the ROP and flow rate recommended by optimization results.

CONCLUSION

1. A methodology was proposed for prediction of ROP in any depth of field using operational and geological data.
2. ROP is governed by numerous factors that make finding analytical solution with acceptable accuracy very difficult or impossible.
3. A new method was carried out for prediction and optimization of ROP using hybrid PSO and GA algorithm and MLP network.
4. Results show that MLP ANN optimized with PSO-GA hybrid algorithm is a very efficient and accurate tool to predict ROP and is effective in drilling operation planning.
5. Assessment of the optimization results shows that the values of the optimized parameters are in fact usable and will not make any problem in drilling operation and using the optimal parameters results in cost savings and minimizing time for drilling projects.
6. The advantage of this model over other drilling improvement methods is consideration of all effective parameters on drilling operation and being accurate, comprehensive, and easy application.

REFERENCES

- [1] Teale R. The concept of specific energy in rock drilling. s. l.: *Int. J. Rock Mech. Min. Sci.* 2:57–73., 1965.
- [2] Rabia H, Farrelly M and Barr M. V. A new approach to drill bit selection. 1985, Paper No. 15894, *SPE European Petroleum Conference*, London, October, pp. 20–22.
- [3] Bourgoyne T and Young F. S. A. multiple regression approach to optimal drilling and abnormal pressure detection. 1974, *SPE J.* 14, pp. 371–384.
- [4] Bilgesu H. I, Al-Rashidi A. F, Aminian K and Ameri S. A new approach for drill bit selection. SPE Eastern Regional Meeting, Morgantown, WV, October 2000, pp. 17–19.
- [5] Yilmaz S, Demircioglu C and Akin S. Application of artificial neural networks to optimum bit selection. *Comput. Geosci.* 28, pp. 261–269.
- [6] Rumelhart D. E, Hinton G. E and Williams R. J. Learning representations by back propagating errors. *Nature* 323 (6088) 1986; 533–536. doi: 10.1038/323533a0.
- [7] Kennedy J and Eberhart R. Particle Swarm Optimization, *IEEE International Conf. on Neural Networks*, Vol. 4, pp. 1942-1948, 1995.
- [8] Angeline P. J. Evolutionary Optimization versus Particle Swarm Optimization: Philosophy and Performance Differences, Evolutionary Programming VII, *Lecture Notes in Computer Science*, Vol. 1447, pp. 601-611, 1998.
- [9] Eberhart R. C and Shi Y. Comparison between Genetic Algorithms and Particle Swarm Optimization, Evolutionary Programming VII, *Lecture Notes in Computer Science*, Vol. 1447, pp. 611-616, 1998.
- [10] Asadisaghadi J, Tahmasebi P. Comparative evaluation of back-propagation neural network learning algorithms and empirical correlations for prediction of oil PVT properties in Iran oilfields. *J. Petrol. Sci. Eng.* 2011; 78 (2), 464–475.
- [11] Bishop C. Neural Network for Pattern Recognition. *Clarendon Press*, Oxford 1995.
- [12] Lapeyrouse and Nortoned J. Formulas and Calculations for Drilling Production and Workover. S. l.: Gulf Professional Publishing is an imprint of Elsevier Science, 2002.
- [13] Mirhaj S. A, Shadizadeh S. R and Fazaelizadeh M. Cutting removal simulation for deviated and horizontal wellbores. Paper No. 105442, *SPE Middle Oil and Gas Show*, Bahrain, March, 2007, pp. 11–14.

Chapter 15

ESTIMATING THE DRILLING FLUID DENSITY IN THE MUD TECHNOLOGY: APPLICATION IN HIGH TEMPERATURE AND HIGH PRESSURE PETROLEUM WELLS

*Arash Kamari¹, Farhad Gharagheizi², Amin Shokrollahi³,
Milad Arabloo³ and Amir H. Mohammadi^{1,4,5,*}*

¹Thermodynamics Research Unit, School of Engineering,
University of KwaZulu-Natal, Durban, South Africa

²Department of Chemical Engineering, Texas Tech University, Lubbock, Texas, US

³Department of Chemical and Petroleum Engineering,
Sharif University of Technology, Tehran, Iran

⁴Institut de Recherche en Génie Chimique et Pétrolier (IRGCP), Paris Cedex, France

⁵Département de Génie des Mines, de la Métallurgie et des Matériaux, Faculté
des Sciences et de Génie, Université Laval, Québec (QC), G1V, Canada

ABSTRACT

Appropriate execution of drilling operation, in particular for high pressure and high temperature wells, requires accurate knowledge of behavior of the drilling fluid density as a function of pressure and temperature. In this communication, a novel mathematical-based approach is presented to develop a reliable model for predict the density of four drilling fluid including water-based, oil-based, Colloidal Gas Aphron (CGA) and synthetic. To pursue our objective, a predictive model is proposed using a robust soft computing approach namely least square support vector machine (LSSVM) modeling optimized with coupled simulated annealing (CSA) optimization tool. Moreover, leverage approach, in which the statistical Hat matrix, Williams plot, and the residuals of the model results lead to identification of the probable outliers, has been applied. It is found that all of the experimental data seem to be reliable and only a few percent of them are out of applicability domain of the developed models for drilling fluid density. The

* Corresponding Author E-mail: amir_h_mohammadi@yahoo.com and a.h.m@irgcp.fr.

obtained results demonstrate that the developed CSA-LSSVM model is rapid, reliable, and efficient to estimate the density of four aforementioned drilling fluids.

Keywords: density prediction, drilling fluid, least square support vector machine, coupled simulated annealing, crude oil

1. INTRODUCTION

In general, drilling fluids are complex heterogeneous mixtures of various types of chemical additives and base fluids that must remain stable over a range of pressure and temperature conditions. The drilling fluid density is a fundamental parameter for calculating wellbore pressure, and also is of crucial importance for the success of drilling and completion operations (Wang et al., 2012). Moreover, the effective drilling fluid density is directly concerned with the downhole variations in temperature and pressure and thus, is a very important part of drilling engineering (Karstad and Aadnoy, 1998). By the reducing in exploitable reserves from shallow horizons, deeper exploration activity is increasing (Ram Babu, 1998). In high temperature and high pressure (HTHP) wells, as drilling operation progresses for deep wells and thus the total vertical depth (TVD) increases, the density of drilling fluid will be changed with increasing temperature and pressure (Babu, 1996; Isambourg et al., 1996; Karstad and Aadnoy, 1998).

As mentioned above, as the TVD increases, there is an increase in the bottom-hole temperature, as well as the hydrostatic head of the mud column in the HTHP wells. These two factors have opposing influences on equivalent circulating density (ECD). The increased hydrostatic head causes increase in the ECD due to compression. On the other hand, the increase in temperature causes a decrease in the ECD due to thermal expansion. It is most often assumed that these two impacts cancel each other out (Harris, 2004). This is not always the case, especially in HTHP wells.

The accurate density behavior of a drilling fluid at HTHP can be obtained only through actual measurements (Wang et al., 2012). Consequently, these measurements require special equipment along with expensive, difficult and time-consuming procedures. Moreover, it is difficult to obtain a large data set that covers the entire range of pressure and temperature under bottom-hole conditions in order to achieve an accurate estimation. Therefore, introducing a rapid, robust and accurate technique than the aforementioned measurements is necessary. Recently, intelligent techniques such as Support Vector Machines (SVMs) have increasingly gained attention in solving complex classification and regression problems. The SVM strategy has been successfully utilized to several different applications in petroleum and natural engineering such as PVT properties estimation, gas properties prediction, porosity and permeability determination, etc. (Kamari et al., 2014a; Kamari et al., 2015a; Kamari et al., 2014b; Kamari et al., 2015b). Least Square Support Vector Machine (LSSVM) is a variant and modified version of SVM (Suykens and Vandewalle, 1999), which implements the equality constraints to replace the original convex quadratic programming problem (Wang et al., 2010).

In this work, more than 880 datasets including various types of mud, initial density, pressure and temperature have been gathered from the literatures (Demirdal and Cunha, 2007; McMordie et al., 1982; Osman and Aggour, 2003). In the next step, to obtain the most

efficient model the data points including inputs and their corresponding outputs randomly split in to three sub-sets: 80% have been utilized for developing the new model and the 10% and 10% have been used for validating and testing phases, respectively. The proposed strategy utilizes LSSVM to construct nonlinear modeling. Besides, a novel feature selection mechanism based on Coupled Simulated Annealing (CSA) optimization for tuning the optimal parameter has been applied. Moreover, statistical and graphical error analyses are conducted to establish the adequacy and accuracy of CSA-LSSVM model.

2. MODEL DEVELOPMENT

2.1. Data Gathering

The applicability, reliability and accuracy of any model normally associated to the comprehensiveness and validity of the employed data set for their development (Gharagheizi, 2009; Gharagheizi et al., 2008; Mohammadi and Richon, 2008; Scalabrin et al., 2006; Taghanaki et al., 2013). As previously mentioned, to estimate drilling fluid density, it is important to take into account the effects of temperature and pressure on fluid. Moreover, unlike the empirical methods which ignore the impact of drilling fluid type on the density at HTHP, to an accurate estimation type of mud is selected as input parameter in this work. Therefore, in this study, density of drilling fluid will be estimated based on experimental data reported in the literatures (Demirdal and Cunha, 2007; McMordie et al., 1982; Osman and Aggour, 2003) at various types of mud with different initial surface densities, temperatures and pressures. Statistical distributions of the data are summarized in Table 1 for water-based and oil-based, Colloidal Gas Aphron (CGA) and synthetic drilling fluids. As it is clearly seen in in Table 1 the data points cover a large and comprehensive range of densities at pressure and temperature for four types of drilling fluids. Moreover, as can be seen in Table 1, the oil-based mud has more density than water-based mud in same temperature and pressure.

2.2. Support Vector Machine Strategy

The Support Vector Machine (SVM) has been identified as a consistent and effective strategy proposed from the machine-learning community (Eslamimanesh et al., 2012; Suykens and Vandewalle, 1999). A SVM is a tool for a set of related supervised learning techniques which analyze data and recognize patterns and also are utilized for regression analysis. On the basis of SVM primary formulations any function $f(x)$ can be regressed as follow(Suykens et al., 2002):

$$f(x) = w^T \varphi(x) + b \quad (1)$$

where w^T is transposed output layer vector, $\varphi(x)$ represents the kernel function, and b stands for the bias. The input of the model, x , is of a dimension $N \times n$ in which N and n express the number of data points and number of input parameters, respectively (In case of

training set, N may be regarded as the number of training set data points). Vapnik proposed minimization of the following cost function in order to calculate w and b (Suykens et al., 2002):

$$Cost\ function = \frac{1}{2} w^T + c \sum_{k=1}^N (\xi_k - \xi_k^*) \tag{2}$$

Table 1. Descriptive statistics of data set for water-based, oil-based, CGA, and synthetic drilling fluids

Parameter	Unit	Min.	Avg.	Max
<i>Water-Based Drilling Fluid</i>				
Initial Density	g/cm ³	1.318155	1.71	2.156980228
Pressure	Mpa	0.101325	34.38	96.601325
Temperature	K	294.2611	392.55	477.5944444
Density at Pressure and Temperature	g/cm ³	1.149191	1.63	2.19892151
<i>Oil-Based Drilling Fluid</i>				
Initial Density	g/cm ³	1.318155	1.71	2.156980228
Pressure	Mpa	0.101325	34.38	96.601325
Temperature	K	294.2611	392.55	477.5944444
Density at Pressure and Temperature	g/cm ³	1.1839425	1.67	2.212103056
<i>CGA Drilling Fluid</i>				
Initial Density	g/cm ³	0.85	1.00	1.15
Pressure	Mpa	1	10.50	20
Temperature	K	303.15	353.15	403.15
Density at Pressure and Temperature	g/cm ³	0.780282	1.07	1.37571
<i>Synthetic Drilling Fluid</i>				
Initial Density	g/cm ³	0.7520671	0.76	0.781905333
Pressure	Mpa	0.020252	48.64	96.98939286
Temperature	K	298.15	373.15	448.15
Density at Pressure and Temperature	g/cm ³	0.6292642	0.74	0.834601558

To satisfy constraints:

$$\begin{cases} y_k - w^T \varphi(x_k) - b \leq \varepsilon + \xi_k, & k = 1, 2, \dots, N \\ w^T \varphi(x_k) + b - y_k \leq \varepsilon + \xi_k^*, & k = 1, 2, \dots, N \\ \xi_k, \xi_k^* \geq 0, & k = 1, 2, \dots, N \end{cases} \tag{3}$$

where x_k and y_k stand for k^{th} data point input, and k^{th} data point output, respectively. The ε denotes the fixed precision of the function approximation. The ξ_k and ξ_k^* are slack

variables. It should be considered that if we choose a small ε to develop a very accurate model, some data points may be outside of the ε precision. Consequently, this issue may result in infeasible solution. As a result, one should use slack parameters to determine the allowed margin of error. The $c > 0$ in Eq. (2) is considered as the tuning parameter of the SVM which determines the amount of the deviation from the desired ε . In other word, one of the tuning parameters of the SVM is c . To minimize the cost function illustrated in Eq. (2) along with its constraints defined in Eq. (3), one should use the Lagrangian for this problem as follows (Suykens et al., 2002):

$$L(a, a^*) = -\frac{1}{2} \sum_{k,l=1}^N (a_k - a_k^*)(a_l - a_l^*) K(x_k, x_l) - \varepsilon \sum_{k=1}^N (a_k - a_k^*) + \sum_{k=1}^N y_k (a_k - a_k^*) \quad (4)$$

$$\sum_{k=1}^N (a_k - a_k^*) = 0, a_k, a_k^* \in [0, c] \quad (4a)$$

$$K(x_k, x_l) = \varphi(x_k)^T \varphi(x_l), \quad k = 1, 2, \dots, N \quad (4b)$$

where a_k and a_k^* denote Lagrangin multipliers. Eventually, the final form of the SVM is obtained as follows:

$$f(x) = \sum_{k,l=1}^N (a_k - a_k^*) K(x, x_k) + b \quad (5)$$

To solve the problem and find a_k, a_k^* , and b , one should solve a quadratic programming problem which is immensely difficult. Later, Suykens and Vandewalle (Pelckmans et al., 2002; Suykens and Vandewalle, 1999) developed the least square modification of the SVM (LSSVM) to facilitate the original SVM method. In the proposed LSSVM approach, Suykens and Vandewalle (Pelckmans et al., 2002; Suykens and Vandewalle, 1999) reformulated the SVM as follows (Suykens et al., 2002):

$$\text{Cost function} = \frac{1}{2} w^T w + \frac{1}{2} \gamma \sum_{k=1}^N e_k^2 \quad (6)$$

Subjected to the following constraint:

$$y_k = w^T \varphi(x_k) + b + e_k \quad (7)$$

where γ is tuning parameter in LSSVM method and e_k represents the error variable. The Lagrangian for this problem is as follows:

$$L(w, b, e, a) = \frac{1}{2} w^T w + \frac{1}{2} \gamma \sum_{k=1}^N e_k^2 - \sum_{k=1}^N a_k (w^T \varphi(x_k) + b + e_k - y_k) \quad (8)$$

where a_k are Lagrangian multipliers. The derivatives of Eq. (8) should be equated to zero in order to solve the problem. Thus, the following equations are obtained:

$$\begin{cases} \frac{\partial L}{\partial w} = 0 \Rightarrow w = \sum_{k=1}^N a_k \varphi(x_k) \\ \frac{\partial L}{\partial b} = 0 \Rightarrow \sum_{k=1}^N a_k = 0 \\ \frac{\partial L}{\partial e_k} = 0 \Rightarrow a_k = \gamma e_k, \quad k = 1, 2, \dots, N \\ \frac{\partial L}{\partial a_k} = 0 \Rightarrow w^T \varphi(x_k) + b + e_k - y_k = 0 \quad k = 1, 2, \dots, N \end{cases} \quad (9)$$

Eq. (9) indicates that there are $2N + 2$ equations and $2N + 2$ unknown parameters (a_k, e_k, w , and b). Thus, the parameters of LSSVM can be obtained by solving the system of equations defined in Eq. (9) (Suykens et al., 2002).

As stated earlier, the LSSVM has a tuning parameter γ . Since, either of the LSSVM and SVM are kernel-based technique, we should consider the parameters of the kernel functions as other tuning parameters. In case of RBF kernel function:

$$K(x, x_k) = \exp(-\|x_k - x\|^2 / \sigma^2) \quad (10)$$

The other tuning parameter is σ^2 . Therefore, in LSSVM algorithm with RBF kernel function, there is two tuning parameters which should be achieved by minimization of the deviation of the LSSVM model from experimental values (Suykens et al., 2002).

4. RESULTS AND DISCUSSION

Drilling fluid type, initial density, temperature and pressure have been considered as correlating parameters of density of drilling fluid. As previously mentioned, the optimum values of the LSSVM parameters consist of γ and σ^2 have been evaluated using CSA. The optimized values of CSA-LSSVM models are 102.4870 and 9115303629.8906 for σ^2 and γ , respectively. The numbers of reported digits of the two aforementioned parameters are normally obtained through sensitivity analysis of the overall error of the optimization procedure (Gharagheizi, 2007).

Table 5 summaries the statistical parameters of the developed model involving squared correlation coefficients (R^2), average absolute relative deviations (AARDs), standard deviation errors STD, and root mean square errors (RMSEs). A comparison between the

represented/predicted drilling fluid density values and the experimental values are illustrated in Figures 1 and 2. Figure 1 illustrates the scatter diagram that compares experimental density versus CSA-LSSVM model outputs. A tight cloud of points about 45° line for training, validation and testing data sets show the robustness of the developed model. The obtained results indicate that excellent agreement exists between the prediction of CSA-LSSVM and the experimental data. Moreover, Figure 2 represents the error distribution of the developed CSA-LSSVM model for prediction of drilling fluid density. This figure confirms that the proposed CSA-LSSVM model has the small error range and the low scatter around the zero error. These results display that the major advantage of CSA-LSSVM method is appropriate capability for modeling nonlinear properties.

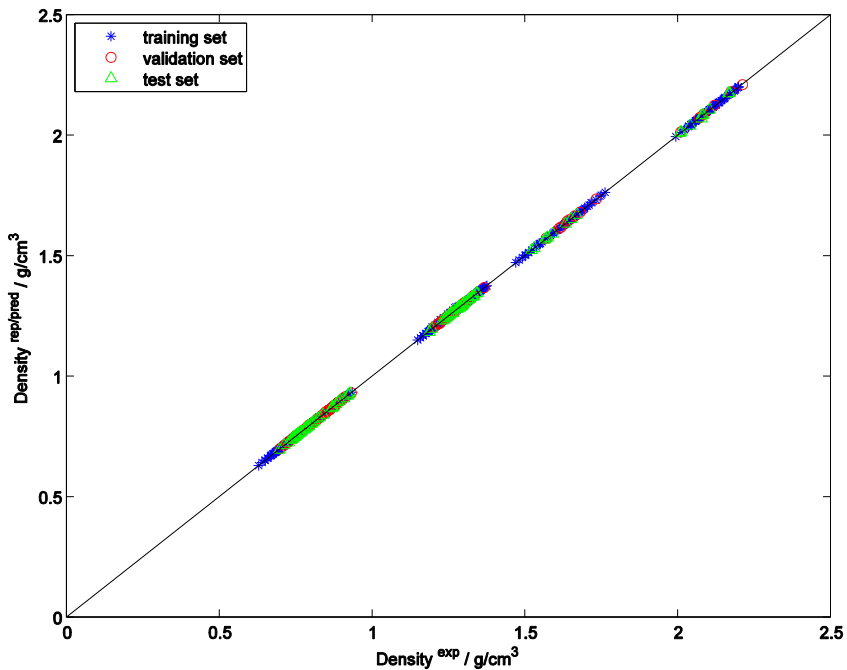


Figure 1. Comparison between the results of the developed model and the data base values.

Table 2. Statistical Parameters of the developed CSA-LSSVM model to determine the drilling fluid density

Statistical Parameter	Value
	<i>Training Set</i>
R ²	0.999
Average absolute relative deviation	0.1
Standard deviation error	0.002
Root mean square error	0.002
N	708
	<i>Validation Set</i>
R ²	0.999
Average absolute relative deviation	0.1
Standard deviation error	0.002

Table 2. (Continued)

Statistical Parameter	Value
Root mean square error	0.002
N	88
	<i>Test Set</i>
R ²	0.999
Average absolute relative deviation	0.1
Standard deviation error	0.002
Root mean square error	0.002
N	88
	<i>Total</i>
R ²	0.999
Average absolute relative deviation	0.1
Standard deviation error	0.002
Root mean square error	0.002
N ^e	88

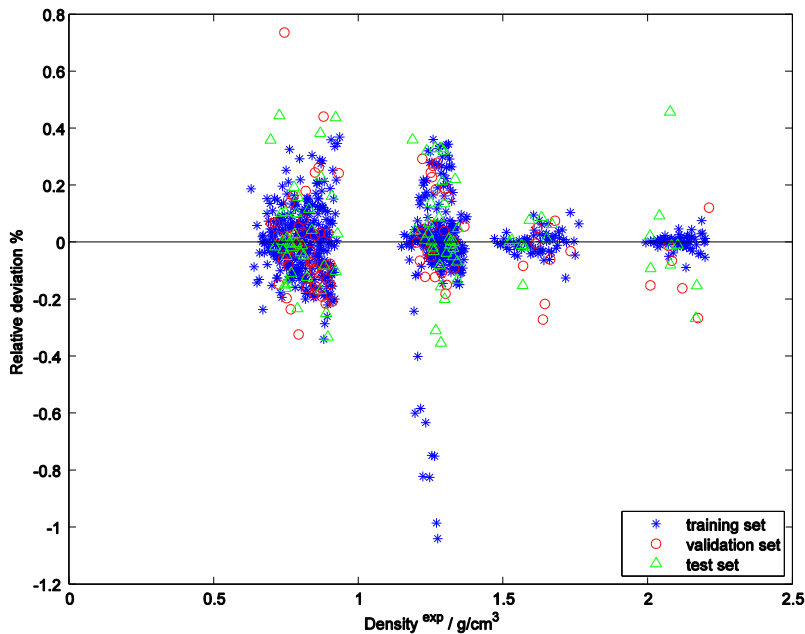


Figure 2. Relative deviations of the drilling fluid density values obtained by the proposed model from data base values.

Outlier detection (or diagnostics) is of much importance in proposing the mathematical models (Mohammadi et al., 2012a; Mohammadi et al., 2012b). Detection of outlier is to recognize of individual datum (or groups of data) that may differ from the bulk of the data present in a databank (Gramatica, 2007; Mohammadi et al., 2012a; Mohammadi et al., 2012b; Rousseeuw and Leroy, 2005). Consequently, there is indeed a necessity to evaluate the available experimental data for drilling fluid density data, since uncertainties affect the estimation capability of the proposed CSA-LSSVM model. Therefore, we have implemented the Leverage Value Statistics technique (Goodall, 1993; Gramatica, 2007). The Graphical

detection of the suspended data or outliers is undertaken through sketching the Williams plot on the basis of the calculated H values (Mohammadi et al., 2012a; Mohammadi et al., 2012b). A detailed definition of computational procedure and equations of this technique can be found elsewhere (Mohammadi et al., 2012a; Mohammadi et al., 2012b). The Williams plot has been sketched in Figure 3 for the obtained results using the CSA-LSSVM model. Existence of the majority of data points in the ranges $0 \leq H \leq 0.01696$ and $-3 \leq P \leq 3$ displays that the implemented models are statistically valid and correct. Moreover, it indicates that the whole data except one in the dataset are located within the applicability domains of the implemented models. Therefore, there are only a few points in the datasets which is within this domain and consequently we can state it as probable doubtful datum.

CONCLUSION

In this study, least square support vector machine technique as a supervised learning method based on coupled simulated annealing has been proposed in order to predict the density of various types of drilling fluids. In actuality, the method employed a hybrid CSA-LSSVM approach for optimizing the model parameters. The results illustrated that SVM-based (LSSVM) method with the CSA-based parameters tuning approach, introduced in this work, can result in excellent generalization and can be advantageously used for prediction of drilling fluid density. Furthermore, the CSA-LSSVM model can easily be utilized in any reservoir simulation software and provides superior accuracy and performance for drilling fluid density estimation than previous correlations and analytical methods.

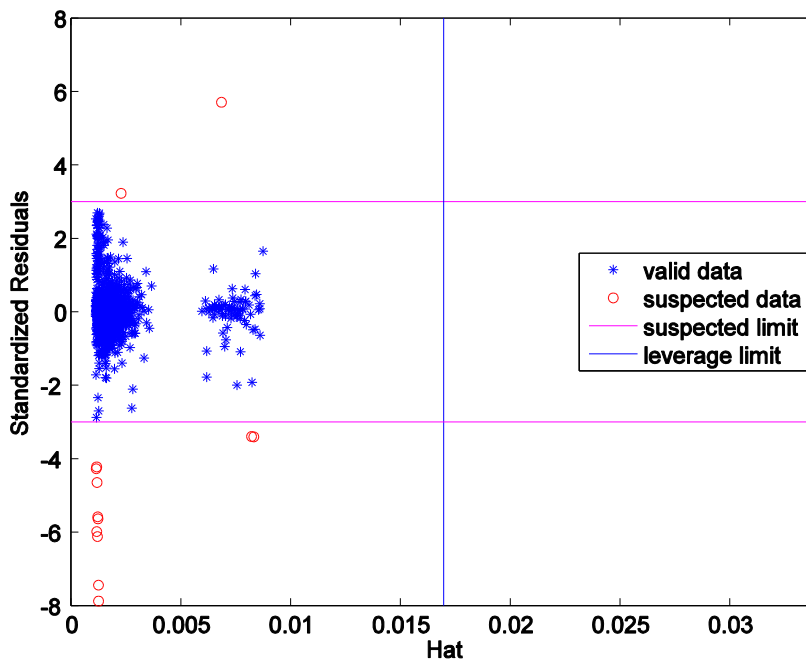


Figure 3. Detection of the probable doubtful data and the applicability domain of the developed CSA-LSSVM model.

REFERENCES

- Babu, D., 1996. Effects of PpT Behaviour of Muds on Static Pressures during Deep Well Drilling-Part 2: Static Pressures. *SPE Drilling and Completion*, 11(2): 91-97.
- Demirdal, B. and Cunha, J., 2007. Olefin Based Synthetic Drilling Fluids' Volumetric Behavior Under Downhole Conditions, Rocky Mountain Oil and Gas Technology Symposium.
- Eslamimanesh, A. et al., 2012. Phase equilibrium modeling of clathrate hydrates of methane, carbon dioxide, nitrogen, and hydrogen + water soluble organic promoters using Support Vector Machine algorithm. *Fluid Phase Equilibria*, 316: 34-45.
- Gharagheizi, F., 2007. QSPR analysis for intrinsic viscosity of polymer solutions by means of GA-MLR and RBFNN. *Computational materials science*, 40(1): 159-167.
- Gharagheizi, F., 2009. Prediction of the standard enthalpy of formation of pure compounds using molecular structure. *Australian Journal of Chemistry*, 62(4): 376-381.
- Gharagheizi, F., Alamdari, R.F. and Angaji, M.T., 2008. A new neural network – group contribution method for estimation of flash point temperature of pure components. *Energy and Fuels*, 22(3): 1628-1635.
- Goodall, C.R., 1993. 13 Computation using the QR decomposition. *Handbook of Statistics*, 9: 467-508.
- Gramatica, P., 2007. Principles of QSAR models validation: internal and external. *QSAR and combinatorial science*, 26(5): 694-701.
- Harris, O., 2004. Evaluation Of Equivalent Circulating Density Of Drilling Fluids Under High Pressure-High Temperature Conditions, University of Oklahoma.
- Isambourg, P., Anfinson, B. and Marken, C., 1996. Volumetric behavior of drilling muds at high pressure and high temperature, European Petroleum Conference.
- Kamari, A., Bahadori, A., Mohammadi, A.H. and Zendehboudi, S., 2014a. Evaluating the Unloading Gradient Pressure in Continuous Gas-lift Systems During Petroleum Production Operations. *Petroleum Science and Technology*, 32(24): 2961-2968.
- Kamari, A., Bahadori, A., Mohammadi, A.H. and Zendehboudi, S., 2015a. New tools predict monoethylene glycol injection rate for natural gas hydrate inhibition. *Journal of Loss Prevention in the Process Industries*, 33: 222-231.
- Kamari, A., Gharagheizi, F., Bahadori, A. and Mohammadi, A.H., 2014b. Determination of the equilibrated calcium carbonate (calcite) scaling in aqueous phase using a reliable approach. *Journal of the Taiwan Institute of Chemical Engineers*, 45: 1307-1313.
- Kamari, A., Safirri, A. and Mohammadi, A.H., 2015b. Compositional Model for Estimating Asphaltene Precipitation Conditions in Live Reservoir Oil Systems. *Journal of Dispersion Science and Technology* 36: 301-309.
- Karstad, E. and Aadnoy, B., 1998. Density behavior of drilling fluids during high pressure high temperature drilling operations. IADC/SPE Asia Pacific Drilling Technology.
- McMordie, W., Bland, R. and Hauser, J., 1982. Effect of temperature and pressure on the density of drilling fluids, SPE Annual Technical Conference and Exhibition.
- Mohammadi, A.H., Eslamimanesh, A., Gharagheizi, F. and Richon, D., 2012a. A novel method for evaluation of asphaltene precipitation titration data. *Chemical Engineering Science*, 78: 181-185.

- Mohammadi, A.H., Gharagheizi, F., Eslamimanesh, A. and Richon, D., 2012b. Evaluation of experimental data for wax and diamondoids solubility in gaseous systems. *Chemical Engineering Science*.
- Mohammadi, A.H. and Richon, D., 2008. A mathematical model based on artificial neural network technique for estimating liquid water - hydrate equilibrium of water - hydrocarbon System. *Industrial and Engineering Chemistry Research*, 47(14): 4966-4970.
- Osman, E. and Aggour, M., 2003. Determination of drilling mud density change with pressure and temperature made simple and accurate by ANN. *Middle East Oil Show*.
- Pelckmans, K. et al., 2002. LS-SVMLab: a Matlab/c toolbox for least squares support vector machines. Tutorial. KULeuven-ESAT. Leuven.
- Ram Babu, D., 1998. Effect of P - ρ - T behavior of muds on loss/gain during high-temperature deep-well drilling. *Journal of Petroleum Science and Engineering*, 20(1): 49-62.
- Rousseeuw, P.J. and Leroy, A.M., 2005. *Robust regression and outlier detection*, 589. Wiley. com.
- Scalabrin, G., Marchi, P., Bettio, L. and Richon, D., 2006. Enhancement of the extended corresponding states techniques for thermodynamic modeling. II. Mixtures. *International journal of refrigeration*, 29(7): 1195-1207.
- Suykens, J.A. and Vandewalle, J., 1999. Least squares support vector machine classifiers. *Neural processing letters*, 9(3): 293-300.
- Suykens, J.A.K., Van Gestel, T., De Brabanter, J., De Moor, B. and Vandewalle, J., 2002. *Least Squares Support Vector Machines*. World Scientific Publishing Company.
- Taghanaki, S.R. et al., 2013. Implementation of SVM framework to estimate PVT properties of reservoir oil. *Fluid Phase Equilibria*.
- Wang, G., Pu, X.-L. and Tao, H.-Z., 2012. A Support Vector Machine Approach for the Prediction of Drilling Fluid Density at High Temperature and High Pressure. *Petroleum Science and Technology*, 30(5): 435-442.
- Wang, X., Chen, J., Liu, C. and Pan, F., 2010. Hybrid modeling of penicillin fermentation process based on least square support vector machine. *Chemical Engineering Research and Design*, 88(4): 415-420.

INDEX

#

10 min gel strength (10 Min Gel), 222, 232, 238

A

abstraction, 245

access, 255, 257

acetone, 162

acid, 17, 19, 95

activation energy, 5, 71

active site, 104

actual output, 178

actuality, 293

additives, 77, 239, 286

adhesion strength, 85

adsorption, 90, 97, 101, 120

advancement, 75

aggregation, 117, 141

Alaska, 171, 172, 178

alcohols, 82, 85, 88

algorithm, 44, 133, 136, 139, 143, 150, 152, 153,

155, 156, 158, 162, 163, 164, 165, 167, 170, 172,

176, 178, 179, 180, 183, 184, 187, 190, 196, 198,

201, 207, 212, 218, 222, 226, 227, 228, 229, 230,

234, 235, 238, 241, 245, 247, 248, 255, 257, 258,

262, 271, 274, 276, 278, 279, 280, 283, 290, 294

alkane, 112, 130, 131, 132, 143, 155, 156, 157

aluminum oxide, 101, 103, 104

American Petroleum Institute (API), 6, 70, 71, 72,

77, 98, 99, 100, 107, 248

amines, 107

amino, 94

amphoteric or zwitterionic surfactants, 81

Anionic surfactants, 81, 91

anisotropy, 40, 41

annealing, 143, 164, 172, 285, 286, 293

Annulus Diameter, 118, 139, 140, 162, 163, 165,

166, 170, 172, 175, 178, 179, 180, 181, 183, 186,

187, 188, 189, 197, 202, 204, 206, 207, 218, 219,

222, 225, 231, 235, 236, 237, 238, 259, 272, 273,

276, 277, 283, 295

aqueous solutions, 90

aromatic compounds, 107

aromatic hydrocarbons, 104

aromatics, 73, 95, 101, 104, 105, 116, 120, 121

Arrhenius equation, 5, 71

artificial intelligence, 177, 183, 188, 189, 190, 195,

197, 202, 203, 204, 218, 223

artificial lift, 53, 54

artificial neural network (ANN), 118, 129, 138, 139,

140, 161, 162, 163, 165, 166, 170, 172, 175, 176,

177, 178, 179, 180, 181, 183, 186, 187, 188, 189,

190, 191, 193, 195, 196, 197, 201, 202, 204, 206,

207, 218, 219, 221, 222, 223, 225, 231, 235, 236,

237, 238, 239, 240, 241, 244, 245, 249, 251, 252,

256, 257, 259, 268, 269, 271, 272, 273, 276, 277,

283, 284, 295

Asia, 294

Asphaltene molecules, 73, 97, 104, 107, 110

asphaltene phase behavior, 94, 112, 114, 115, 116,

119, 123, 124, 157

asphaltene precipitation, 94, 95, 97, 98, 105, 106,

112, 115, 116, 117, 118, 119, 121, 122, 123, 124,

125, 127, 128, 129, 130, 131, 132, 133, 134, 137,

139, 140, 142, 143, 144, 145, 147, 149, 150, 152,

153, 155, 156, 157, 158, 159, 177, 189, 294

assessment, 35, 44, 128, 159, 193, 240, 264, 265,

267, 268, 281, 282, 283

association theory, 157

atmospheric pressure, 135

atoms, 82, 84, 107

Azerbaijan, 161, 243

B

Bahrain, 19, 269, 284
 banks, 153
 base, 25, 44, 95, 116, 228, 246, 286, 291, 292
 behaviors, 92, 114, 195, 226
 Belgium, 158
 benefits, 15, 85
 benzene, 95, 100, 101
 bias, 138, 198, 200, 204, 205, 225, 273, 287
 biocompatibility, 85
 biodegradability, 85
 biomolecules, 94
 birds, 196
 Bit selection, 256, 257, 262, 268, 269, 272, 284
 bitumen, 23, 24, 68, 69, 70, 71, 72, 74, 78, 87, 88, 89, 90, 91, 92, 94, 98, 120, 121
 bituminous sand, 70
 blend films, 89
 bonding, 104, 111
 boreholes, 24
 bounds, 41, 246
 butadiene, 86
 by-products, 97

C

Ca²⁺, 2, 5, 7, 9, 10, 11, 12, 15, 16, 17, 19
 calcium carbonate, 294
 calibration, 102, 121
 capillary, 32, 88
 carbon, 70, 94, 95, 96, 97, 104, 106, 107, 108, 112, 294
 carbon dioxide (CO₂), 95, 112, 116, 145, 156, 189, 294
 carboxylic acids, 107
 Caribbean, 156
 cationic surfactants, 2, 81
 chain molecules, 113, 124
 challenges, 26, 69, 76, 119, 243, 271
 chemical, 2, 5, 49, 68, 70, 73, 77, 80, 81, 82, 83, 85, 86, 88, 93, 94, 95, 97, 100, 104, 108, 111, 115, 117, 120, 128, 286
 chemical nature of the crude oil, 70
 chemical properties, 82, 85, 86, 88, 94
 chemical reactions, 77
 chemical structure, 83, 93, 94, 104, 108
 China, 173, 190
 chitosan, 90
 chloroform, 95

cholesterol, 95, 106, 119
 chromatography, 100, 101, 102, 111, 119, 120, 121
 chromosome, 133, 226, 227
 circulation, 24, 243, 244, 245, 246, 248, 250, 251, 259, 262, 267, 279
 classes, 81, 100, 112, 222, 223, 246, 247, 248, 249
 classification, 92, 94, 97, 112, 244, 246, 247, 248, 249, 251, 286
 cleaning, 244, 263, 265, 266, 267, 279, 282, 283
 cluster model, 110
 coal, 94, 122
 Colombia, 19
 combustion, 97
 common law, 25
 communication, 24, 227
 communities, 226, 227, 241, 287
 compatibility, 76, 85, 86
 competition, 226, 231, 241
 complications, 177
 composition, 2, 3, 5, 7, 70, 78, 91, 95, 98, 100, 105, 106, 112, 113, 117, 128, 130, 161, 162, 163, 165, 177
 compounds, 70, 72, 73, 84, 85, 94, 100, 108, 115, 294
 comprehension, 158
 compressibility, 172, 176, 177, 181, 189
 compression, 58, 286
 computing, 30, 40, 123, 188, 226, 285
 condensation, 87
 conduction, 11, 12, 14, 22, 24, 26, 27, 29, 31, 36, 38, 39, 40, 50, 191
 conference, 172, 239, 240
 configuration, 147
 confinement, 32
 Congress, 89, 92, 188, 241
 conserving, 76
 constituents, 73, 100, 104, 113, 116, 117
 construction, 163, 165, 167
 consumption, 5, 68, 74, 223, 266
 contact time, 97, 98, 100
 contamination, 101
 Continental, 109, 110
 controversial, 2, 93, 117
 convention, 246
 convergence, 138, 164, 179, 196, 208, 212, 228, 276
 cooperation, 226
 coordination, 120, 180, 231, 258
 copolymer, 86
 correlation coefficient, 133, 134, 137, 142, 150, 151, 152, 156, 167, 176, 184, 197, 205, 208, 210, 212,

214, 215, 216, 217, 234, 235, 255, 259, 271, 277, 290
 corrosion, 70, 76, 85
 cost, 1, 54, 58, 62, 63, 64, 65, 69, 76, 85, 86, 103, 178, 187, 194, 221, 223, 227, 244, 256, 268, 271, 272, 283, 288, 289
 coupled simulated annealing (CSA), 143, 153, 285, 286, 287, 290, 291, 292, 293
 CPT, 105
 crude oil, 2, 68, 69, 70, 71, 72, 73, 74, 75, 76, 77, 78, 80, 86, 87, 88, 89, 90, 91, 92, 94, 95, 97, 98, 99, 100, 101, 103, 104, 105, 108, 112, 114, 115, 116, 117, 118, 119, 120, 121, 122, 123, 124, 125, 128, 129, 130, 131, 132, 135, 143, 145, 150, 156, 157, 158, 159, 161, 162, 165, 166, 170, 171, 172, 177, 189, 286
 crystals, 105
 CSS, 76
 cycles, 177, 184, 186, 198, 207

D

Darwinian evolutionary theory, 179
 data analysis, 191, 256, 272
 data collection, 259
 data gathering, 163
 data mining, 193, 195, 202, 203, 204, 219, 245
 data processing, 193, 195
 data set, 118, 130, 137, 143, 145, 153, 162, 163, 165, 167, 170, 178, 180, 195, 201, 207, 225, 231, 247, 248, 251, 276, 286, 287, 288, 291
 database, 61
 decomposition, 89, 120, 122, 294
 deficiencies, 147
 deformation, 42
 degree of hydrolysis (DH), 85
 degree of polymerization (DP), 85
 dehydration, 191
 Denmark, 157
 density prediction, 286
 density values, 291
 Department of Energy, 88
 depolarization, 111
 deposition, 95, 105, 106, 119, 120, 121, 123, 124, 128, 145, 157, 158, 161, 162, 163, 165, 166, 167, 170, 171, 172
 deposits, 122, 224
 depressants, 85
 depression, 111
 depth, 23, 29, 30, 39, 58, 60, 98, 231, 235, 236, 237, 248, 259, 264, 276, 281, 283, 286

derivatives, 39, 101, 290
 detection, 120, 121, 153, 156, 269, 284, 292, 295
 deviation, 139, 140, 144, 149, 289, 290, 291, 292
 dielectric constant, 120
 diesel fuel, 90
 differential pressure sticking, 222
 diffusion, 49, 162, 245
 diffusivity, 14, 23, 41
 diluent, 76
 dimension number, 164
 dimensionality, 246
 direct cost, 204
 dispersion, 49, 77, 85, 122, 223, 277
 displacement, 7, 25, 88
 dissociation, 81
 distillation, 71, 159
 distribution, 12, 26, 27, 28, 31, 34, 39, 40, 48, 70, 78, 79, 90, 111, 113, 115, 137, 179, 190, 201, 219, 234, 235, 244, 291
 distribution function, 111
 divergence, 113
 diversity, 227, 276
 DOI, 87, 90, 201, 219, 241
 drainage, 1, 22, 23, 24, 26, 28, 30, 31, 32, 33, 35, 36, 37, 44, 45, 46, 48, 49, 50, 53, 54, 69, 76, 90
 drill collar metrage (DC MT), 222, 232, 236, 237
 drill string stuck, 221, 222
 drilling, 194, 195, 221, 222, 223, 224, 239, 240, 243, 244, 245, 246, 248, 251, 252, 253, 255, 256, 257, 258, 259, 260, 261, 262, 263, 264, 265, 266, 267, 268, 269, 271, 272, 276, 279, 281, 282, 283, 284, 285, 286, 287, 288, 290, 291, 292, 293, 294, 295
 drilling fluid, 223, 243, 244, 245, 246, 248, 252, 271, 285, 286, 287, 288, 290, 291, 292, 293, 294, 295

E

ECG, 190
 electric submersible pump (ESP), 54, 61, 62, 63, 64, 65
 electricity, 65
 electrolyte, 123
 electron, 82, 83, 84, 104, 111
 electron density distribution, 83
 electrons, 83, 84
 emergency, 76
 empirical methods, 287
 Emulsification, 67, 69, 73, 74, 75, 76, 77, 78, 79, 85, 86, 87, 90, 92
 encoding, 227

energy, 2, 3, 11, 17, 19, 22, 32, 53, 54, 67, 68, 69, 74, 76, 78, 83, 84, 88, 93, 113, 115, 117, 191, 204, 256, 266, 269, 272, 284
 energy consumption, 68, 266
 energy density, 74
 energy input, 74, 78
 energy supply, 67, 68
 engineering, 26, 49, 85, 88, 91, 93, 111, 121, 122, 123, 124, 133, 163, 171, 177, 178, 179, 188, 194, 195, 201, 202, 219, 221, 276, 286
 England, 89
 Enhanced Oil Recovery (EOR), 1, 2, 22, 23, 26, 49, 74, 77, 82, 86, 88, 91, 95, 100, 106, 118, 152, 159, 176, 177, 178, 188
 entropy, 113
 environment, 80, 81, 98
 epidemiology, 189
 equality, 113, 286
 equilibrium, 3, 4, 5, 41, 43, 114, 115, 124, 294, 295
 equipment, 54, 128, 248, 286
 erosion, 257, 272
 ESR spectroscopy, 108
 ethylene glycol, 191
 Europe, 240, 252
 evaporation, 90
 evidence, 104
 evolution, 158, 179, 196, 205, 226, 227, 276
 evolutionary computation, 226
 execution, 184, 207, 285
 experimental design, 172
 exploitation, 93, 100, 194
 extra heavy oil, 19, 51, 68, 71, 75

F

families, 73
 feature selection, 247, 248, 251, 287
 feedstock, 102, 119
 fermentation, 295
 films, 92
 financial, 243
 fish, 227
 fitness, 133, 150, 165, 179, 181, 185, 187, 196, 206, 226, 228, 229, 230, 274, 275
 flame, 102, 103, 120, 121
 flocculation, 78, 117, 120, 122, 123, 124, 156, 157, 158
 flooding, 49, 76, 77, 88, 90, 91, 128
 Flory-Huggins equation, 128
 fluid, 2, 3, 38, 40, 43, 53, 54, 59, 60, 69, 74, 77, 78, 114, 116, 124, 157, 162, 172, 176, 177, 193, 194,

201, 203, 218, 243, 244, 245, 246, 248, 271, 285, 286, 287, 290, 291, 292, 293
 force, 7, 15, 42, 74, 77, 101
 formation, 5, 6, 7, 22, 23, 24, 25, 32, 35, 38, 44, 48, 67, 70, 73, 74, 76, 77, 78, 85, 87, 88, 90, 92, 106, 110, 111, 113, 119, 122, 162, 172, 178, 181, 189, 194, 195, 223, 224, 231, 235, 239, 244, 248, 255, 257, 259, 260, 262, 264, 265, 267, 272, 276, 281, 294
 formula, 35, 37, 40, 41, 46, 136, 197
 fouling, 85
 fractures, 24
 France, 21, 53, 93, 127, 161, 175, 193, 203, 221, 243, 255, 271, 285
 free energy, 3, 80, 115, 117
 free volume, 114
 freezing, 111
 function values, 228

G

gas lift, 53, 54, 56, 58, 59, 60, 61, 62, 63, 65
 gel, 101, 103, 111, 222, 232, 238
 gel permeation chromatography, 111
 Genetic Algorithm (GA), 133, 134, 136, 150, 152, 153, 155, 156, 158, 164, 171, 172, 175, 176, 177, 178, 179, 181, 182, 183, 184, 185, 186, 187, 190, 196, 198, 199, 200, 201, 204, 205, 208, 209, 210, 211, 212, 213, 214, 215, 216, 218, 226, 227, 228, 229, 230, 232, 235, 236, 239, 240, 255, 256, 257, 258, 262, 263, 264, 269, 271, 272, 274, 275, 276, 278, 279, 280, 281, 283, 284, 294
 genetic information, 179
 Genetic Programming Neural Network, 162, 163, 167, 172, 189
 geology, 176
 geometrical parameters, 36
 geometry, 26, 32, 35, 37, 45, 46, 47, 48, 49, 50, 244, 263, 279
 Gibbs energy, 113
 global demand, 100
 global economy, 68
 glycol, 294
 GPC, 108, 111
 gravitational force, 78
 gravity, 7, 23, 24, 25, 38, 48, 49, 50, 55, 58, 69, 70, 71, 72, 76, 77, 90, 98, 99, 100, 101, 107, 166, 170
 group interactions, 274
 growth, 24, 46, 124, 158, 184, 266
 Gulf of Mexico, 6, 223

H

halogen, 81
 harmony, 158
 heat capacity, 14, 22, 43
 heat loss, 10, 11, 12, 13, 15, 19, 38, 48
 heat transfer, 24, 26, 31, 38, 39, 40
 heavy oil, 1, 2, 6, 9, 10, 11, 15, 18, 23, 24, 25, 49, 50, 51, 67, 68, 69, 70, 71, 72, 74, 75, 76, 77, 78, 80, 81, 82, 84, 85, 86, 88, 89, 90, 91, 92, 93, 95, 101, 110, 120, 122, 123, 157, 158
 height, 25, 40, 44, 45, 48, 49
 heptane, 100, 101, 104, 108
 heterogeneity, 1, 40, 41, 48, 276
 history, 6, 7, 9, 15, 21, 46, 47
 House, 91
 HTHP, 286, 287
 hybrid, 2, 124, 133, 134, 150, 156, 158, 172, 190, 191, 226, 228, 229, 271, 274, 276, 278, 279, 280, 283, 293
 hydrocarbon media, 156
 hydrocarbons, 68, 70, 110, 224
 hydrogen, 84, 94, 95, 104, 107, 108, 111, 122, 294
 hydrogen bonds, 84
 hydrolysis, 82, 85
 hydroxyl, 82
 hypothesis, 246

I

identification, 73, 121, 177, 189, 285
 IMA, 219
 imbibition, 2, 6
 incompatibility, 122
 independent variable, 167, 195
 individuals, 228, 229, 230, 274
 industry, 26, 69, 73, 74, 91, 102, 103, 114, 119, 162, 176, 177, 195, 204, 205, 243
 inefficiency, 179
 inertia, 164, 180
 information processing, 257
 ingredients, 128, 201
 inhibition, 124, 156, 294
 initial gel strength, 222
 initial reservoir pressure, 176, 177, 187
 injections, 10, 11, 158
 integration, 28, 133, 201
 intelligence, 173, 195, 196, 205, 219, 223, 244
 interface, 21, 22, 23, 25, 26, 27, 28, 29, 30, 31, 32, 33, 34, 35, 36, 38, 39, 40, 42, 46, 77, 89, 102

intermolecular interactions, 113
 intrinsic viscosity, 294
 ionization, 84, 102, 103, 120, 121
 IPR, 55
 Iran, 21, 53, 54, 93, 121, 127, 135, 161, 175, 190, 193, 197, 198, 203, 219, 221, 224, 243, 255, 258, 271, 276, 284, 285
 iron, 107
 issues, 179, 196, 243
 Italy, 65
 iteration, 164, 165, 180, 225, 228

J

Japan, 67, 240
 Jordan, 91

K

K^+ , 7, 81
 kerogen, 94
 ketones, 107
 kinetics, 122
 Korea, 1

L

laminar, 162
 Latin America, 51, 156
 lattices, 86
 law enforcement, 196
 layering, 204, 231
 learning, 138, 139, 158, 163, 164, 179, 180, 182, 183, 184, 187, 190, 193, 195, 196, 198, 201, 202, 207, 208, 209, 211, 212, 214, 218, 219, 225, 231, 232, 233, 234, 235, 240, 241, 245, 246, 247, 273, 274, 284, 287, 293
 learning process, 179, 183, 207
 least square support vector machine, 129, 143, 285, 286, 293, 295
 Least squares, 158, 295
 light, 71, 72, 95, 101, 105, 110, 111, 112, 116
 limestone, 6, 258
 linear function, 246
 linear model, 193
 lipids, 94
 liquid chromatography, 102, 103, 120, 121
 liquid phase, 74, 114, 115, 117, 162
 lithology, 206, 218
 logging, 176, 177, 195, 203, 204, 260

lognormal probability density function (PDF), 79, 88, 89
 lost circulation, 243, 244, 245, 246, 248, 251, 252
 Louisiana, 19
 Luo, 159

M

machine learning, 172, 195, 204, 245
 macromolecules, 128
 magnitude, 34, 63, 205, 207
 majority, 70, 218, 225, 293
 mammal, 195, 204
 management, 54, 122, 175, 176, 177, 202
 Mandela, President Nelson, 67
 manipulation, 31
 mass, 32, 77, 108, 240
 materials, 70, 80, 85, 93, 103, 104, 113, 114, 244, 246, 294
 materials science, 294
 mathematics, 204
 matrix, 153, 156, 194, 249, 250, 285
 measurements, 54, 55, 97, 111, 120, 122, 128, 158, 162, 286
 mechanical properties, 85
 mechanical sticking, 222, 223, 231
 media, 117
 medical science, 85
 medicine, 85, 103
 mercury, 88
 methodology, 178, 239, 251, 283
 Mexico, 223, 239
 Mg²⁺, 2, 5, 7
 Miami, 240
 microcrystalline, 106
 microparticles, 90
 Middle East, 19, 118, 119, 171, 172, 189, 244, 245, 295
 mixing, 73, 74, 78, 80, 86, 95, 113
 MLP neural network (MLP-NN), 190, 204, 235, 272, 273, 274, 276, 278, 280
 MMP, 172, 190
 modifications, 6, 21, 26, 44, 45, 48, 114, 179, 227
 molar volume, 130
 mole, 113, 114, 115, 144, 165, 166, 170, 177
 molecular modelling, 82
 molecular structure, 294
 molecular weight, 72, 81, 85, 86, 93, 94, 96, 98, 104, 110, 111, 114, 116, 122, 129, 130, 139, 144, 145, 150, 153, 157, 158, 177

molecules, 70, 73, 74, 80, 82, 84, 97, 101, 104, 106, 107, 110, 112, 114, 116, 117, 118
 moment means, 78
 monomers, 117
 Montana, 19
 morphology, 78
 MRI, 177
 mud filtrate viscosity (MF Vis), 222, 232, 236, 237, 238
 multi solid thermodynamic model, 162
 multidimensional, 103, 179, 227
 multiple regression, 195, 269, 284
 mutation, 179, 227, 228, 229, 230, 263, 274, 276

N

Na⁺, 7, 81
 naphthalene, 101
 natural evolution, 226, 274
 natural gas, 112, 189, 191, 294
 natural selection, 226, 274
 net present values, 54
 Netherlands, 251, 253
 networking, 195
 neural network, 118, 124, 129, 138, 139, 140, 150, 151, 156, 158, 159, 161, 162, 163, 165, 166, 170, 172, 173, 175, 176, 177, 178, 179, 180, 181, 183, 186, 187, 188, 189, 190, 191, 193, 195, 196, 197, 198, 201, 202, 204, 206, 207, 217, 218, 219, 221, 222, 223, 225, 231, 233, 234, 235, 236, 237, 238, 239, 240, 241, 244, 245, 249, 250, 251, 252, 255, 256, 257, 258, 259, 260, 261, 262, 268, 269, 271, 272, 273, 274, 276, 277, 278, 280, 283, 284, 294, 295
 Neural Network Model, 138, 189, 190
 neural system, 204
 neurons, 165, 178, 179, 184, 195, 198, 201, 204, 205, 207, 208, 211, 213, 218, 225, 231, 235, 258, 273, 277
 nickel, 73, 94, 107
 Nigeria, 67, 68
 nitrogen, 70, 89, 94, 107, 145, 146, 294
 nodes, 205, 249, 250
 non-ionic surfactants, 81
 nonlinear systems, 164
 non-polar, 80, 111, 116
 Norway, 121
 NPC, 88
 Nuclear Magnetic Resonance (NMR), 5, 108, 190
 nucleophilicity, 84

O

oil prices, 69
oil production, 3, 6, 7, 8, 11, 14, 15, 19, 26, 27, 28, 31, 32, 46, 48, 49, 54, 58, 65, 74, 75, 100, 123, 124, 161, 162, 245
oil samples, 99, 153, 162, 166, 170
oil sands, 92
oil-in-water (O/W), 67, 70, 74, 76, 77, 80, 81, 86, 87, 88, 90, 91
oil-steam interface, 22, 32, 34, 35, 39, 46
Oklahoma, 65, 125, 294
olefins, 101
one dimension, 73, 184, 207
operating costs, 63, 65, 188
operating range, 61
operations, 76, 121, 221, 223, 227, 228, 239, 257, 258, 260, 266, 267, 271, 272, 286, 294
optimization, 50, 53, 84, 87, 133, 136, 161, 162, 164, 170, 172, 177, 178, 179, 189, 190, 191, 194, 195, 196, 199, 201, 202, 205, 211, 218, 219, 222, 223, 226, 227, 231, 235, 236, 238, 239, 240, 241, 245, 247, 255, 256, 257, 258, 262, 268, 271, 272, 274, 278, 279, 280, 283, 285, 287, 290
optimization method, 161, 199, 226
optimization of penetration rate, 256
optimum production, 53, 54
organic compounds, 158, 189
organic matter, 94
organic solvents, 73
oscillation, 205
Ostwald ripening, 78, 92
oxidation, 98
oxygen, 70, 94, 102, 107

P

Pacific, 252, 294
paraffin, 96, 162, 171
parallel, 23, 38, 138, 184, 225, 257, 258
parameter estimation, 188
particle morphology, 78
particle size, 78, 79, 86, 90, 91, 283
particle swarm optimization (PSO), 161, 162, 164, 165, 166, 170, 172, 175, 176, 177, 178, 179, 180, 181, 182, 183, 184, 185, 186, 187, 189, 190, 191, 196, 198, 199, 200, 201, 202, 204, 205, 208, 209, 210, 211, 212, 213, 214, 215, 218, 219, 222, 226, 227, 228, 229, 230, 232, 234, 235, 236, 239, 240,

271, 272, 274, 275, 276, 278, 279, 280, 281, 283, 284
penetration rate, 255, 256, 257, 258, 259, 260, 262, 264, 265, 266, 267, 268, 271, 272, 276, 279, 281, 282
penicillin, 295
perforation, 23
permeability, 6, 7, 9, 14, 22, 40, 41, 43, 44, 45, 48, 49, 172, 175, 176, 177, 178, 186, 187, 188, 189, 191, 193, 194, 195, 197, 203, 204, 206, 211, 213, 214, 215, 216, 217, 218, 219, 241, 244, 248, 252, 286
Persian Gulf, 161, 175, 193, 203, 221, 243, 255, 271
petroleum, 21, 23, 26, 48, 49, 50, 51, 53, 65, 67, 70, 71, 72, 73, 74, 77, 81, 87, 88, 89, 90, 91, 92, 93, 94, 95, 100, 101, 104, 105, 106, 119, 120, 121, 122, 123, 124, 125, 127, 156, 157, 158, 159, 161, 162, 171, 172, 175, 176, 177, 178, 179, 188, 189, 190, 193, 194, 195, 201, 202, 203, 204, 205, 219, 221, 223, 243, 252, 255, 269, 271, 276, 284, 285, 286, 294, 295
pH, 7, 16, 18, 19, 81, 85, 86, 92, 122
pharmaceutical, 73, 85
phase diagram, 106, 112, 115
phase inversion, 78
phenol, 82, 84, 88
physical interaction, 115
physical properties, 78, 84, 128, 203, 248
physics, 40
pipeline, 70, 74, 75, 76, 77, 86, 87, 89, 90, 162, 172
Pipeline transportation, 70, 74, 75, 76, 77, 86, 87, 89, 91
plastic viscosity (PV), 12, 222, 231, 232, 236, 237, 238, 256, 259, 261, 262, 275, 276, 279, 280
PNA, 100
polar, 73, 80, 84, 85, 101, 104, 105, 111, 115, 116
Poly vinyl alcohol (PVA), 67, 81, 82, 83, 84, 85, 86, 87, 90
polydispersity, 111
polymer chain, 113, 114
polymer solutions, 113, 294
polymeric surfactants, 81, 91
polymerization, 82, 85, 118, 121
polymorphism, 189
polystyrene, 73, 86
polyvinyl acetate, 82
polyvinyl alcohol, 67, 82, 83, 84, 90, 92
population, 165, 179, 196, 205, 226, 227, 228, 229, 230, 231, 235, 258, 263, 274, 276
porosity, 7, 14, 23, 41, 43, 44, 176, 178, 181, 193, 203, 204, 206, 208, 209, 211, 218, 219, 248, 258, 260, 286

porous media, 88, 106
 porphyrins, 107
 precipitation, 2, 3, 4, 5, 94, 95, 97, 98, 100, 105, 108, 112, 115, 116, 117, 118, 119, 121, 122, 123, 124, 127, 128, 129, 130, 131, 132, 133, 134, 137, 139, 140, 142, 143, 144, 145, 147, 149, 150, 152, 153, 155, 156, 157, 158, 159, 177, 294
 prediction, 48, 49, 112, 114, 118, 119, 123, 124, 127, 128, 137, 147, 157, 158, 161, 162, 163, 167, 169, 171, 172, 189, 190, 191, 193, 195, 198, 208, 211, 214, 218, 219, 221, 223, 240, 241, 243, 245, 246, 251, 257, 269, 271, 272, 276, 283, 284, 286, 291, 293, 294, 295
 prediction models, 223
 preparation, 86, 103, 228
 present value, 54, 63, 65
 prevention, 89, 119, 171, 223, 263, 279
 principles, 91, 196
 prior knowledge, 201
 probability, 79, 223, 228, 230, 246
 probability density function, 79
 probability distribution, 246
 procurement, 65
 profitability, 63
 programming, 245
 propagation, 138, 163, 178, 179, 183, 184, 190, 196, 201, 208, 212, 284
 propagators, 104
 propane, 104
 PSA, 271, 272
 pumps, 267
 pure line, 208
 PVAc, 82
 PVP, 82, 84

Q

QoS, 274
 quadratic programming, 286, 289
 quantification, 101, 103, 120, 121, 194
 quaternary ammonium, 81

R

radius, 22, 36, 38, 40, 176, 245
 random numbers, 180
 rate of penetration (ROP), 222, 231, 232, 235, 236, 237, 238, 255, 256, 257, 259, 261, 262, 264, 266, 268, 271, 272, 275, 276, 277, 278, 279, 280, 281, 282, 283

RBF-NN, 204
 reaction rate, 5
 recognition, 122, 158, 177, 183, 189, 190, 198, 207
 recovery, 1, 2, 3, 9, 10, 11, 12, 15, 23, 27, 48, 49, 50, 67, 68, 70, 75, 82, 87, 88, 90, 91, 92, 95, 100, 106, 112, 118, 176, 188
 reference system, 115, 116
 refractive index, 102, 118
 regression, 55, 131, 132, 137, 158, 177, 178, 179, 191, 195, 286, 287, 295
 regression analysis, 287
 regression method, 177, 178
 regression model, 195
 reliability, 128, 287
 reproduction, 179, 226
 requirements, 61, 93, 127, 155, 195, 274
 researchers, 25, 26, 40, 93, 97, 108, 113, 119, 127
 reserves, 68, 69, 92, 178, 193, 203, 204, 286
 reservoir characterization, 175, 176, 177, 178, 188
 residuals, 153, 155, 156, 285
 residues, 70, 95, 101, 104, 115, 121, 122
 resin molecules, 101, 117, 122
 resins, 73, 74, 77, 80, 94, 97, 100, 101, 102, 104, 105, 108, 112, 116, 117, 118, 120, 121, 122, 148, 149, 150
 resistance, 23, 25, 85, 231
 resolution, 67
 resources, 67, 68, 92, 93, 189, 274
 response, 103, 196
 reusability, 85
 rheology, 87, 89, 90, 244, 245
 ROC, 249
 rotation per minute (RPN), 222, 255, 259, 271
 roughness, 162
 rules, 141, 179, 190, 274

S

SAGD process, 21, 22, 24, 25, 26, 32, 35, 37, 40, 46, 48, 49, 50
 salinity, 1, 2, 3, 7, 9, 81, 85, 86, 87, 90, 231
 salt concentration, 92
 SAR, 104
 SARA, 73, 100, 101, 102, 103, 106, 118, 119, 120, 121, 123, 125, 158
 saturated hydrocarbons, 101
 saturation, 1, 7, 9, 12, 22, 41, 148, 181, 188, 204, 206, 219
 savings, 201

- scaling, 118, 124, 127, 128, 129, 130, 133, 134, 135, 136, 139, 140, 141, 142, 144, 145, 147, 148, 149, 150, 151, 152, 153, 155, 156, 157, 158, 159, 294
- scaling equation, 118, 124, 127, 128, 129, 130, 133, 134, 135, 136, 140, 141, 142, 144, 145, 147, 149, 151, 152, 153, 155, 156, 157, 158, 159
- scaling law, 128, 129
- scatter, 167, 291
- schooling, 227
- science, 73, 91, 119, 120, 122, 123, 133, 163, 171, 172, 178, 188, 190, 195, 294
- sea level, 248
- search space, 179, 180, 196, 227, 228, 230, 258, 274, 278
- security, 240
- sedimentation, 78, 98
- sediments, 224
- selectivity, 5, 6, 90
- semi-analytical models, 21, 22, 27, 48
- sensitivity, 1, 3, 9, 11, 14, 150, 167, 241, 290
- set theory, 227
- showing, 26, 72, 84, 134, 137, 142, 151, 153, 206, 261
- silica, 92, 101, 103, 104
- simulation, 2, 6, 11, 15, 17, 21, 25, 26, 40, 41, 45, 48, 50, 54, 87, 176, 190, 193, 223, 226, 269, 284, 293
- Singapore, 219, 240
- skin, 175, 176, 177, 178, 186, 187, 188, 194, 201
- SO42, 2, 5, 7
- social interaction, 196, 205, 227
- sodium, 77
- sodium hydroxide, 77
- software, 26, 54, 55, 61, 82, 167, 226, 227, 228, 266, 268, 293
- solid phase, 5, 114, 162
- solubility, 5, 73, 84, 85, 95, 97, 100, 108, 112, 114, 119, 123, 130, 162, 295
- solution, 3, 4, 11, 21, 38, 40, 42, 44, 46, 67, 77, 81, 85, 86, 100, 112, 113, 114, 128, 162, 164, 165, 172, 177, 179, 196, 205, 223, 226, 227, 228, 230, 231, 243, 244, 246, 251, 258, 274, 283, 289
- solution space, 164, 165, 227, 228, 230, 231, 274
- solvation, 117
- solvents, 77, 95, 97, 108, 111, 112, 116, 117, 119, 129, 143, 156
- South Africa, 21, 53, 67, 93, 127, 161, 175, 193, 203, 221, 243, 255, 271, 285
- species, 3, 5, 84, 102, 108
- specific gravity, 55, 58, 59, 70, 162, 163, 165, 170, 177
- spectroscopy, 108
- speed of light, 118
- stability, 60, 77, 80, 82, 83, 85, 86, 89, 92, 100, 104, 105, 112, 114, 118, 119, 125, 145, 189, 239
- stabilization, 77, 88, 117
- standard deviation, 133, 136, 138, 141, 156, 228, 290
- standardization, 103, 121
- state, 3, 21, 26, 27, 28, 29, 38, 39, 91, 114, 115, 116, 117, 119, 122, 123, 124, 128, 145, 157, 293, 295
- statistics, 288
- steam chamber, 22, 23, 24, 25, 26, 27, 28, 30, 32, 33, 36, 40, 41, 45, 46, 48, 49
- stimulation, 50, 70, 76, 88, 95, 194
- stimulus, 196
- STM, 101
- stoichiometry, 3
- storage, 86, 186
- stress, 42, 244, 248
- structure, 70, 72, 82, 83, 90, 94, 108, 120, 122, 165, 178, 184, 189, 198, 204, 205, 207, 214, 231, 235, 258, 274, 276, 277
- substitution, 93
- sulfate, 2
- sulfonamide, 89
- sulfur, 70, 72, 76, 94, 102, 107, 120
- supervision, 225
- support vector machine, 129, 137, 143, 155, 158, 232, 244, 245, 246, 247, 251, 285, 286, 287, 293, 294, 295
- surface area, 5
- surface tension, 80, 84, 85
- surface-active materials, 80
- surfactants, 2, 49, 70, 74, 75, 77, 78, 79, 80, 81, 82, 85, 86, 87, 88, 89, 91, 122
- survival, 179, 226, 227
- synthesis, 82, 172, 202, 219
- system analysis, 56

T

- Taiwan, 294
- tar, 49, 50, 71
- techniques, 54, 76, 88, 100, 102, 111, 133, 155, 176, 177, 178, 190, 202, 204, 211, 218, 219, 223, 227, 247, 286, 287, 295
- technological advancement, 81
- temperature, 1, 2, 3, 4, 5, 6, 7, 8, 10, 11, 12, 15, 22, 23, 26, 27, 28, 29, 30, 34, 37, 39, 40, 41, 42, 43, 55, 71, 76, 78, 87, 95, 97, 103, 105, 106, 111, 112, 114, 115, 117, 118, 122, 128, 130, 139, 144, 145, 156,

157, 161, 162, 163, 165, 167, 170, 171, 177, 197, 285, 286, 287, 290, 294, 295

temporal variation, 1

tension, 73, 77, 80, 85, 91, 122, 223

test data, 55, 60, 177, 184, 188, 189, 207, 211, 212, 214, 217, 231, 249

testing, 118, 139, 140, 150, 163, 168, 176, 177, 178, 181, 183, 187, 188, 189, 193, 194, 195, 198, 201, 203, 208, 211, 223, 231, 238, 255, 259, 260, 262, 276, 277, 287, 291

thermal energy, 3, 11, 12, 15, 18, 77

Thermal EOR (TEOR), 76

thermal expansion, 43, 286

thermal method, 2, 22, 23

thermal properties, 12

thermal stability, 90

thermal stimulation, 70, 88

thermodynamic equilibrium, 3, 116

thermodynamic model, 94, 112, 119, 123, 128, 147, 150, 156, 157, 162, 163, 167, 170, 171, 295

thermodynamic properties, 87

thermodynamics, 121, 157, 161, 162

toluene, 70, 73, 95, 100, 115, 117

topology, 250

total energy, 46, 68

total product, 63, 65

training, 118, 137, 138, 139, 140, 150, 163, 164, 165, 167, 178, 190, 193, 197, 198, 201, 207, 208, 212, 216, 217, 225, 231, 235, 245, 246, 249, 259, 261, 262, 273, 276, 277, 278, 280, 288, 291

trajectory, 248

transformation, 94, 120

transport, 2, 3, 4, 6, 75, 76, 91, 162

transportation, 67, 70, 74, 75, 76, 77, 86, 87, 89, 90, 91, 105, 106, 161, 162

treatment, 91, 244

trial, 179, 184, 207, 277

turbulence, 74

types of emulsion, 74, 75

U

unconventional hydrocarbons, 68

uniform, 103, 114, 263

United States (USA), 19, 20, 50, 92, 120, 121, 122, 156, 240, 252

universal gas constant, 71

universality, 129, 130

updating, 230, 274

V

vacuum, 70, 101

validation, 137, 150, 181, 182, 184, 193, 198, 201, 205, 207, 208, 211, 212, 214, 231, 232, 233, 234, 235, 259, 276, 291, 294

valuation, 63

valve, 62

vanadium, 73, 94, 107

vapor, 108, 111, 115, 116, 122, 162, 172

vapor-liquid-solid, 162

variables, 39, 40, 78, 118, 129, 139, 145, 152, 170, 194, 195, 201, 218, 257, 258, 271, 272, 273, 274, 289

variations, 46, 286

varieties, 106

vector, 129, 137, 143, 155, 158, 180, 184, 198, 205, 207, 227, 232, 244, 245, 246, 247, 251, 273, 274, 285, 286, 287, 293, 294, 295

vegetable oil, 85

velocity, 22, 23, 26, 27, 28, 30, 33, 34, 36, 40, 41, 164, 165, 180, 228, 230, 231, 235, 265, 266, 274, 282, 283

Venezuela, 76

vibration, 256, 265, 282, 283

vinyl chloride, 86

virtual intelligence, 219, 244

viscosity, 6, 7, 8, 10, 11, 12, 15, 16, 18, 22, 23, 25, 26, 27, 41, 55, 57, 67, 68, 69, 70, 71, 72, 74, 75, 76, 77, 81, 82, 85, 86, 89, 90, 92, 176, 181, 194, 222, 231, 232, 244, 256, 259, 267, 276, 283, 294

volatility, 70

volumetric changes, 43

W

Washington, 88, 89, 91, 120, 121, 253

waste, 244, 274

water, 2, 6, 7, 9, 12, 15, 16, 23, 43, 67, 70, 74, 75, 76, 77, 78, 80, 81, 82, 85, 86, 87, 88, 89, 90, 91, 92, 106, 190, 191, 204, 206, 219, 224, 285, 287, 288, 294, 295

water-in-oil (W/O), 74, 77, 80, 92

wax deposition, 105, 161, 162, 163, 165, 166, 167, 170, 171, 172

weakness, 26

Weight on Bit (WOB), 222, 231, 232, 235, 236, 237, 238, 255, 257, 259, 261, 262, 267, 268, 271, 272, 275, 276, 279, 280

well productivity index, 193, 198

well testing, 176, 177, 187, 188, 189, 193, 194, 195, 201, 203

wells, 23, 24, 26, 32, 48, 50, 54, 55, 56, 61, 63, 65, 106, 171, 177, 178, 180, 187, 188, 193, 194, 195, 201, 206, 207, 221, 223, 231, 245, 257, 259, 265, 276, 282, 285, 286

wettability, 1, 2, 3, 6, 9, 11, 12, 15, 18, 84, 106

wetting, 80

worldwide, 68

world energy consumption, 68

X

X-ray diffraction, 108

Y

yield point (YP), 222, 231, 232, 236, 237, 238